



Single Molecule Characterisation of ATP Synthase

Wei Meng Ho

St Cross College, Oxford

The Life Science Interface Doctoral Training Centre

and

The Department of Physics

Trinity 2010

A thesis submitted for the degree of

Doctor of Philosophy

Single Molecule Characterisation of ATP Synthase

Wei Meng Ho
St Cross College, Oxford

A thesis submitted for the degree of
Doctor of Philosophy
at the University of Oxford, Trinity 2010

Abstract

ATP synthase (or F-ATPase) is a ubiquitous enzyme that catalyses the synthesis and hydrolysis of adenosine triphosphate (ATP). The enzyme is divided into two functional portions. The water soluble portion contains the enzymatic sites and is also known as F₁-ATPase, while the membrane embedded portion controls the flow of ions and is known as F_o. One of the most remarkable features of this enzyme is the incorporation of mechanical rotation in its catalytic cycle. Both portions are able to rotate independently, but interact in tandem during *in vivo* catalysis of ATP. Although rotation of F₁-ATPase has been well characterised, coupled rotation of the complete enzyme is still not well understood. The main bottleneck is the difficulty in inducing and observing rotation of F-ATPase in a stable energised bilayer environment.

This thesis is about designing an experimental setup for high resolution imaging of F-ATPase rotation in an energisable bilayer. F-ATPases are first purified and reconstituted back into vesicles. An agarose supported planar lipid bilayer is formed using an aqueous droplet immersed in lipid/hexadecane. F-ATPases in vesicles are then reconstituted into the planar bilayer via vesicle fusion. To observe rotation, F_o is immobilised to the agarose beneath the bilayer and F₁-ATPase attached to a gold nanoparticle. ATP is added to induce rotation and the movement of the gold nanoparticle tracked using a dark-field microscope. Although no unidirectional rotation is observed, F-ATPase tethered gold nano-particles are found to dwell preferentially at three distinct angles of their ellipsoidal trajectory. The observation is attributed to the presence of an opposing proton motive force, formed by accumulation of protons, which make ATP hydrolysis (i.e. rotation) unfavourable and trap the orientation of the enzyme at energy minima. Improvements will be made to overcome this problem, in the hope that rotation of F-ATPase on planar bilayers can finally be observed.

Acknowledgements

Spending an extended amount of time abroad to do a PhD is not easy. I am not a brilliant person and am still overawed by the esteemed academic environment of the University. Fortunately, this also means that I am able to meet and learn from some of the brightest minds in the business. David Gavaghan was the first “big name” I met when I first arrived. He is also the person who has made my DPhil in Oxford possible. I still remember the butterflies in my stomach during the phone interview for admission into the DPhil programme. It wasn't the best interview I have had but I was fortunate to be accepted by the Doctoral Training Centre despite that. I would like to thank him for accepting me and having confidence in my completion of this course.

If David is the person who opens the door to my DPhil, then Richard would be the guiding light in the dark realms of the DPhil sojourn. Honestly, I found myself needing to be at my best to just stay in tune with Richard's intellectual prowess during our discussions, but it was also through these exchanges that I've learnt the most. Richard is a supervisor with many ideas and is ever so sharp to see through my numerous straw-man arguments. My meeting with him therefore requires me to make extensive preparation and be constantly on my toes. Admittedly, I still break a dab of cold sweat before stepping into his office, but to be constantly prepared before a supervisory meeting is probably the best training a graduate student can receive from his supervisor.

Helping Richard with the supervision of his students is the band of post docs in the lab. Bradley is probably the person who I have pestered the most. Behind the deceptively soft-spoken and gentle appearance is actually a man who is as dependable as steel. His oracle like ability in providing answers to perplexing technical questions is probably why his desk is never quite free from other people's problem. Nowadays, my mantra is that if an argument can get past him, it will probably convince Richard as well. Bradley is also one of the proof readers to have bore through the atrocities of my poor language in the draft thesis.

The other post docs have also helped me tremendously during the course of my DPhil. Teuta is the person who guided me through the early days of F-ATPase reconstitution and purification. Tom is the main person who has worked with me through the long hours of purification, making flash freezing of F-ATPase at 2 am slightly more bearable. I must also confess to have infected him with some of my OCDⁱ predisposition. Also, big thank-you to Mostyn for the YFP mutants and stimulating discussions in the wet-lab, as well as Lo, Yoshi and Bai Fan for dispensing advices and encouragements when things were not working.

i. Obsessive Compulsive Disorder

Not to be left out are the peer supports from the fellow graduate students working in the lab. Special thanks go to Matt for being in the proof reading team that has made my thesis many times more readable. I have always been amazed by how he can perform comedy gigs, vie for a place in the Olympics, volunteer for a prison reform charity and do a PhD all at the same time. Branch is another fellow DTC classmate who has dispensed many words of encouragement and advice. He is the final proof reader for the thesis and has graciously agreed to help me despite his busy work in Harvard. Finally, to all others in the lab that have helped in one way or another, a big thank-you to you all.

Beyond the Berry group, I would especially like to thank Mark (Wallace) and Andy for lending their expertise in the bilayer setup. This thesis would have taken a very different route if not for the help they have given. My gratitude also goes to Achilles for his advice, technical help and encouragement during my short stint in his lab and beyond. His permission for me to use his apparatus (despite numerous hours of usage and a misalignment accident) has allowed me to show some results which I would otherwise not be able to show. Finally, I must also thank the people in the various other labs, whom I have worked with or have provided me with either equipment or work space to use. They include the colleagues from the Watts lab, Armitage lab, Tucker lab, Turberfield lab and Leake lab.

Moving closer to home, this DPhil would not have been possible if not for the generous funding from my company: DSO National Laboratories, Singapore. Their full funding of my five years stay in Oxford is unprecedented.

Most importantly, I would like to thank my wife, Wan Ying, for first encouraging me to pursue a PhD and then supporting me throughout the long and arduous journey. There were many moments of frustration and disappointment, which would have been impossible to bear if not for her support and understanding. Now that my work here is almost done, it is my turn to help her with her PhD. The reversal of role will be a big shoe for me to fill.

Finally, I would like to dedicate this thesis to my parents and family. Thank you for the trust and confidence. I hope I have made you proud.

Wei Meng

Sept 2010

Abbreviations

ACMA – 9-amino-6-Chloro-2-MethoxyAcridine.

ADP – Adenosine DiPhosphate

ALEX – Alternating Laser Excitation

AMP – Adenosine MonoPhosphate

AMP-PNP - Adenosine-5'-(β,γ -imino)-triphosphate. This is an unhydrolysable analogue to ATP

APD – Avalanche PhotoDiode

ATP – Adenosine TriPhosphate

CCD – Charged Coupled Device

CDI - Carbonyldiimidazole

CF₁ - F₁ from Chloroplast

CMOS – Complementary Metal Oxide Semiconductor

DCCD – DiCyclohexylCarboDiimide

DDW – Double Distilled Water

DHB – Droplet on Hydrogel Bilayer

DPhPC – 1,2-diphytanoyl-*sn*-glycero-3-phosphocholine

DLS – Dynamic Light Scattering

E. coli - Escherichia coli

EDTA - EthyleneDiamineTetraAcetate

EF₁(F_o) - F₁(F_o) from *e. coli*

FCS – Fluorescence Correlation Spectroscopy

Fm – Flipping Mirrors

FRET – Fluorescence Resonance Energy Transfer

GNP – Gold Nano Particles

HWP – Half Wave Plate

HCl – Hydrochloric Acid

K_d – Equilibrium Dissociation Constant

LDM – Laser DarkField Microscope

MF₁ – F₁ from Mitochondria

MSD – Mean square displacement

NAD(H) – (Reduced) Nicotinamide Adenine DiNucleotide

NEM – N-Ethyl maleimide

NMR – Nuclear Magnetic Resonance

NTA – NitriloTriAcetic Acid

OD – Optical Density

OSCP – Oligomycin Sensitivity Conferring Protein

PA – Phosphatidic Acid

PBS – Polarising Beam Splitter

PC – Phosphatidylcholine

PDDF – Pairwise Difference Distribution Function

PE – PhosphatidylEthanolamine

PEP – Phospho(enol)pyruvic acid monopotassium salt

PG – PhosphatidylGlycerol

PMF – Proton Motive force

PMMA - PolyMethyMethaAcrylate

POPC - 1-palmitoyl-2-oleoyl-*sn*-glycero-3-phosphocholine

POPE - 1-palmitoyl-2-oleoyl-*sn*-glycero-3-phosphoethanolamine

PSF – Point Spread Function

QFD – Quadrant Photo Diode

QWP – Quarter Wave Plate

TCEP – Tris (2-carboxyethyl) phosphine

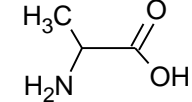
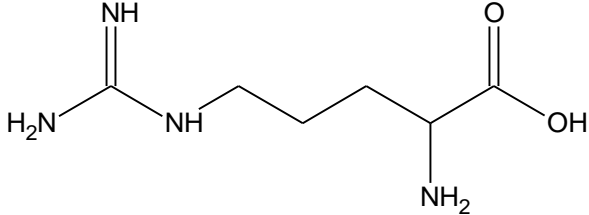
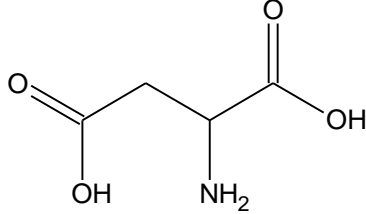
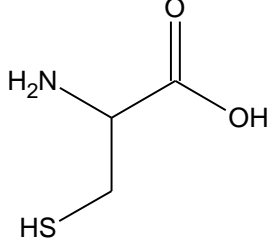
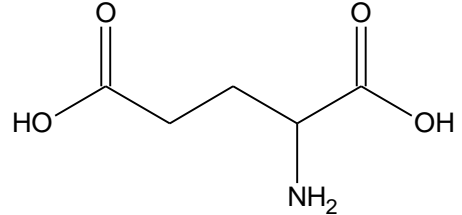
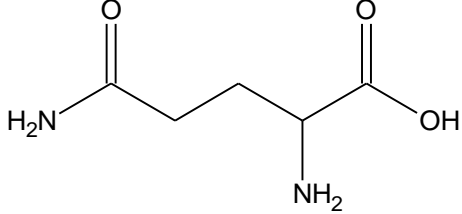
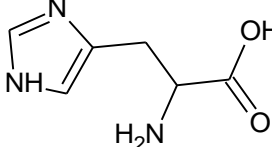
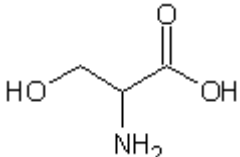
TIRFM – Total Internal Reflection Fluorescence Microscopy

TF₁ - F₁ from Thermophilic Bacteria PS3

TMH1/5 – Transmembrane Helix 1 / 5 of the a-subunit.

YF₁ - F₁ from Yeast Mitochondria

Amino Acids Mentioned in Text and their Structures

Alanine (Aln)	
Arginine (Arg)	
Aspartic Acid (Asp)	
Cysteine (Cys)	
Glutamic Acid (Glu)	
Glutamine (Gln)	
Histidine (His)	
Serine (Ser)	

Contents

1 Introduction.....	4
1.1 Types of ATPase	6
1.1.1 P-ATPases.....	7
1.1.2 V-ATPases	8
1.1.3 F-ATPase	11
1.1.4 Summary of this Section	12
1.2 Historical Perspective of ATP Synthase	13
1.2.1 Early Days.....	13
1.2.2 Finding the Currency of Energy – Discovery of ATP	14
1.2.3 Discovery of Oxidative Phosphorylation and its Relation to Respiration	15
1.2.4. Discovery of the Electron Transport Chain and Chemiosmotic Coupling – The Energy Source for ATP production	17
1.2.5 Elucidation of F-ATPase – Early Model of ATP Turnover.....	19
1.2.6 Elucidation of F-ATPase – Composition of F-ATPase	21
1.2.7 Elucidation of F ATPase – Structure and Morphology of F-ATPase....	23
1.2.8 Summary for this section	24
1.3 Further Research Questions	26
1.4 Summary of Thesis.....	27
1.3.1 Structure of Thesis	30
2 Review of F-ATPase.....	33
2.1 Overall structure of F ₁ ATPase	33
2.1.1 The $\alpha_3\beta_3$ Hexameric Head Piece	34
2.1.2 The γ subunit.....	38
2.1.3 The ϵ subunit.....	39
2.1.4 The δ -subunit (<i>E. Coli</i>)	41
2.2 Overall Structure of F _o ATPase.....	42
2.2.1 The b-subunit	43
2.2.2 The c-subunit	47
2.2.3 The a-subunit	51
2.3 Summary of the Structure of F-ATPase.....	53

2.4	Current Understanding of F-ATPase – Mechanism of F ₁ and F _o ATPase	56
2.4.1	Binding Change Mechanism – F ₁ rotation	56
2.4.2	Chemo-Mechanical coupling of F ₁ rotation	58
2.4.3	Theoretical Model of Torque Generation in F ₁	61
2.4.4	Inhibited state of the F ₁	63
2.5	Mechanism of F _o Rotation	63
2.6	Summary of Mechanism of F-ATPase	70
2.7	Current Understanding of F-ATPase – Combined Rotation of F-ATPase	72
3	Preparation of F-ATPase	77
3.1	Introduction	77
3.2	Materials and Instruments	79
3.2.1	Chemicals	79
3.2.2	Equipment	79
3.2.3	Bacteria	80
3.3	Methods & Results	81
3.3.1	F-ATPase Purification	81
3.3.2	Reconstitution of F ₁ F _o ATP Synthase into Vesicles and Testing its Activity	88
3.3.3	Estimating the number of F-ATPases per Vesicle	107
3.4	Conclusion and Summary	122
4	Preparing Planar Bilayer and Incorporating F-ATPase	124
4.1	Introduction	124
4.2	About this Chapter	126
4.3	Material	128
4.4	Methods & Results	129
4.4.1	Preparing Droplet On Hydrogel Bilayers	129
4.4.2	Estimating the Thickness and Hydration of Substrate Agarose	133
4.4.3	F ₁ F _o ATPase in Bilayers	143
4.4.4	Studying diffusion of F-ATPase on Bilayers	153
4.5	Summary of Chapter	157
5	Functionalising Agarose and Gold Nano-Particles	159
5.1	Introduction	159
5.2	Material	160
5.3	Method & Results	160
5.3.1	Modification of Agarose with NitriloTriAcetic Acid	160
5.3.2	Characterisation of the Interaction between Histag YFP and NTA Agarose	163

5.3.3	Finding the Dissociation Constant (K_d) of NTA – Histag bond using DNA substrate.....	166
5.3.5	Characterising the Number of Streptavidin per GNP	172
5.4	Summary of Chapter	181
6	Rotation Studies of <i>E. coli</i> F-ATPase in an Energisable Lipid Bilayer.....	182
6.1	Introduction	182
6.2	Material and Instrument	183
6.2.1	Laser Dark-field Microscope	183
6.3	Methods & Results	186
6.3.1	Preparation of Samples	186
6.3.2	Images from Laser DarkField Microscopy	187
6.3.3	Analysing Movement of Immobilised GNPs.....	189
6.4	Discussion	196
6.5	Summary of chapter	203
7	Summary, Future Work and Conclusion	204
7.1	Summary	204
7.2	Future Work	206
7.3	Conclusion.....	207
	Reference	209

Appendix 1 – Protocols for experiments

Appendix 2 – Derivations and Calculations

1

Introduction

Nature has produced many marvellous systems. Arguably, the crown jewel among them is the creation of life itself. However, an unequivocal definition of life has remained elusive, despite us having unprecedented understanding and knowledge. On one hand, life is so diversified that no single definition can be unambiguously assigned to it. Yet, on the other hand, it is tangible enough for us to easily see, touch or even feel its presence, without needing a proper definition. A further conundrum arises if one probes deeper into the mechanisms of life from a reductionist's perspective. At the nano-meter length scale, life is nothing but a cascade of chemical reactions. All processes are undirected and constrained only by the laws of nature. Yet they can orchestrate themselves to perform the most complicated of tasks. Each of which can build upon another to ultimately create what is known to us as life. It is indeed mind boggling, to even start imagining how a countless number of carbon, nitrogen and oxygen atoms can be strung together to create sentient beings capable of movement, thoughts and thesis writing.

To say that life is a self ordered system is probably an understatement, but nonetheless a good starting point. We know from thermodynamics that any system¹

¹ We assume in this case that the system contains internal cyclic processes that constantly generate entropy.

capable of continuously maintaining its orderliness (reducing entropy), can only do so with the input of energy (Just imagine the constant amount of work we have to do to keep our desk tidy!). In fact, one of the premises of life is its ability to metabolise chemicals and derive useful energy out of these reactions. Nature's answer to such energy harvesting is the cyclic production and consumption of energy rich molecules called adenosine tri-phosphate (ATP), using externally derived energy sources. This mode of energy conversion is well conserved from bacteria to human beings. A normal human has been estimated to consume 40 kg of ATP everyday [1]. This is equivalent to $\sim 5 \times 10^{20}$ molecules of ATP per second. ATP is in turn regenerated by a distinctive complex of proteins called the ATP synthase, which transforms electrical energy to mechanical energy and finally to chemical energy (and *vice versa*). Furthermore, ATP synthase is the only known enzyme found in nature that incorporates physical rotation into its catalytic cycle [2]. It is also one of the two known rotating motors² that nature has produced. The other one is the bacterial flagellar motor (BFM), which is an ion driven motor and used primarily for locomotion in bacteria. Both ATP synthase and the BFM are studied in Berry's group.

This thesis contains the work which I have done during my four years with the laboratory. Coming from an engineering background, I was tasked to build a system that would allow one to visualise the rotation of F_1F_0 ATPase in a planar bilayer. It is a project filled with many technical challenges, which explains why scientists have been trying for many years to design such systems. Fortunately, the maturation of several techniques has helped to make this attempt possible. Preliminary results appear promising, but the setup still requires further improvements. Details of these is

² We regard the other homologous ATPase (A-ATPase / V-ATPase) to be in the same family of rotating motors

given in chapter three to six. In this chapter, I will briefly introduce what ATPases are and the different types of ATPases present in nature. This is followed by a short history of ATPase research in the last century. Finally, I will end this chapter with the motivations and overview of the thesis.

1.1 Types of ATPase

Adenosine tri-phosphate (ATP) has been called the basic “currency” of energy in living organisms [3]. Just as real currency provides the impetus for the activities in modern society, this high energy molecule is often the prime mover for various biochemical processes taking place in living organisms. There are many ways in which the body can utilise energy stored in ATP to do useful work [4]. One of these is the direct hydrolysis of ATP into ADP (adenosine di-phosphate) and free phosphate. In such a reaction, ATP acts as the donor of the phosphoryl group and water molecule, the acceptor. Catalysis of this sort is usually brought about by a class of enzymes called ATPases. The energy derived from the action of ATPases is normally used to perform some useful physiological functions. Among the essential functions performed by the body is the pumping of ions across membranes. In fact, the ATPases involved in pumping of Ca^{2+} , Na^+ and K^+ alone, account for about a third of the energy used in humans [5].

1.1.1 P-ATPases

Ion pumping ATPase can generally be categorised into three major types – the P-ATPase, V-ATPase and F-ATPase [6]. P-ATPases are membrane bound proteins and function primarily as cation transporters. They are named P-ATPases, because of the formation of a phosphorylated intermediate during the process of ATP hydrolysis [6, 7]. The cations that can be transported by P-ATPase include, but are not limited to, H^+ , K^+ , Mg^{2+} , Ca^{2+} , Na^+ , Cu^{2+} [6]. One of the more widely studied P-ATPases is the Ca^{2+} -ATPase from the sarcoplasmic reticulum³. This protein has a molecular weight of ~ 110 kDa and is involved in pumping Ca^{2+} back into the sarcoplasmic reticulum during muscle relaxation. The crystal structure for this protein shows a membrane domain comprising 10 alpha helices and a hydrophilic head piece of three distinctive domains (called N, P and A) [6, 8]. These hydrophilic domains are actually the cytoplasmic loops of the transmembrane helices and are responsible for the binding and hydrolysis of the ATP [6], while four of the transmembrane helices form the binding site for the Ca^{2+} cargo [6].

The mechanism of the Ca^{2+} -ATPase can briefly be described as follows [9]: The binding of two Ca^{2+} ions on the ATPase results in a protein conformation that favours the hydrolysis of the ATP. Upon hydrolysis of ATP, a large conformational change occurs, causing the channel to open at the other side of the membrane and lowering the affinity of the Ca^{2+} at the same time. This results in the release of Ca^{2+} to the other side, in exchange for H^+ . ADP is then replaced with a fresh ATP and the state now favours the closure of the channel again. Finally the phosphate from the hydrolysed

³ Sarcoplasmic reticulum is a specialised organelle of the muscle cell that is responsible for storing Ca^{2+} ions.

ATP leaves the enzyme and restores it back to its original start state, ready for the next cycle. Figure 1-1 shows a schematic of the mechanism of Ca^{2+} -ATPase. In comparison with V and F type ATPase, the P type ATPases are very different, both from a structural and mechanistic point of view.

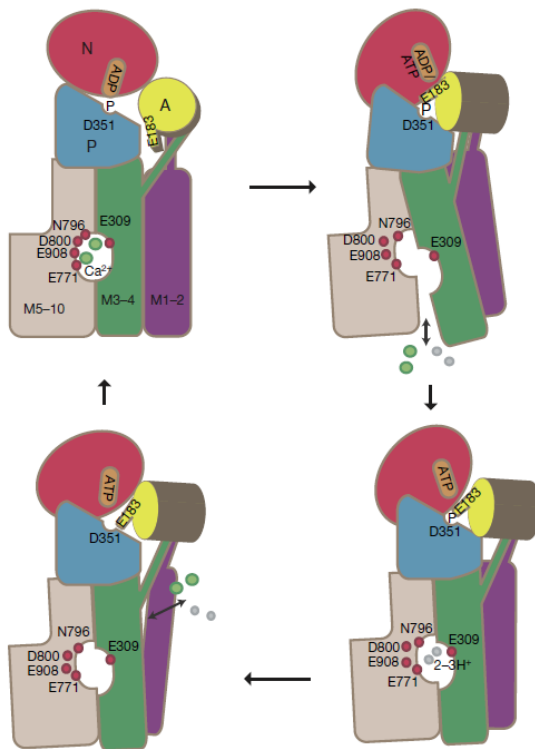


Figure 1-1. Cartoon showing the mechanism of the Ca^{2+} -ATPase. Diagram is obtained from [9]. M1 to M10 represents the ten transmembrane helices. N, A and P represent the three domains of the hydrophilic headgroup.

1.1.2 V-ATPases

The second type of ATPase is the V-type ATPase. This class of ATPase is similar to F-ATPase in terms of its structure and mechanism, but is sufficiently different, in physiological functions and locality, to be classified as a separate type of ATPase. V-ATPase is the protein responsible for the acidification of vacuoles⁴ in plant cells (thus

⁴ Vacuoles are vesicles inside plant cells that can be used as storage for nutrients and waste products or simply as proton buffer.

the name V-ATPase), and many other specialised intracellular compartments like the lysosomes⁵, secretory vesicles⁶ etc [6, 10]. It is found on the plasma membrane of macrophages and osteoclasts, for regulation of pH and resorption of bone respectively [11]. In fact, V-ATPases are thought to be present in virtually all eukaryotic cells, ensuring proper physiological functions via a careful control of both the pH and membrane potential [10]. Beside H⁺ V-ATPase, Na⁺ V-ATPases have also been discovered, but so far only in prokaryotes [12].

Structurally speaking, V-ATPase is similar to, albeit more complicated than, F-ATPase [6]. It consists of a soluble portion called V₁ that is responsible for the hydrolysis of ATP and a membrane portion V_o, for proton translocation. The V₁ of the yeast V-ATPase is about 640kDa and is made up of eight different subunits while V_o has a molecular mass of 260kDa and is composed of six different subunits [13]. One of the main differences between F-ATPase and the V-ATPase is the characteristics of the subunits in the membrane portion. Both the F-type and V-type ATPase have a ring like structure in the membrane portion called the c-ring. In F-ATPase, this c-ring comprises 10 to 15 identical c-subunits [14, 15] (see also later for details). The equivalent c-ring in V_o typically has fewer subunits. In yeast, the number of c-subunits is found to be ~ 4 to 5 [6]. Furthermore, yeast V_o has two additional “c” like subunits – c’ and c’’, which are encoded by separate genes [6]. Each of the c and c’ subunits in yeast V_o is a protein with four transmembrane helices, while the c’’ contains five helices [13, 16]. In comparison, the c-subunit of F_o comprises only two transmembrane helices. Figure 1-2 shows a schematic of the yeast V-ATPase. Sequence homology suggests that the mechanism of V-ATPase is similar to that of F-

⁵ Lysosomes are organelles in cells that are responsible for the controlled digestion of macromolecules

⁶ Vesicles containing proteins designated for secretion by cells.

ATPase [6, 13]. Indeed, this idea was vindicated when V_1 ATPase from *Thermus thermophilus* was shown to rotate and hydrolyse three ATPs per revolution [17].

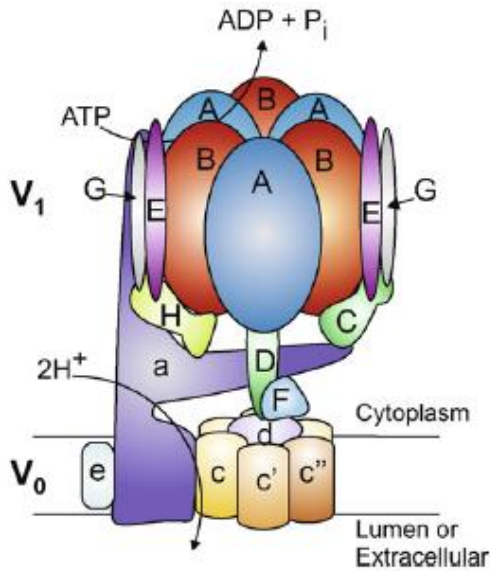


Figure 1-2. Schematic of the V_1V_0 ATPase. Diagram is taken from [13]. Letters in upper case represent the V_1 portion while the letters in lower case represent the V_0 portion. In another model [18], a three peripheral stalk model is proposed, although only two interact with the c-subunits.

As the role of V-ATPase is intimately tied to the physiological processes inside the cell, one would expect some form of control mechanism to be in place for quick regulation of its activity. It was discovered that yeast and tobacco horn worms, when under unfavourable conditions, are able to swiftly inhibit the activity of their V-ATPase by reversibly dissociating the V_1 portion from V_0 [10]. When this happens, both the V_1 and V_0 become inactive (i.e. they do not hydrolyse ATP or allow protons to pass) [10, 11]. This unique mode of inhibition has not been reported in F-ATPases.

1.1.3 F-ATPase

The final group of ATPases to be discussed is the F-ATPase. This group of ATPases is distinguished by its ability to synthesise ATP using energy generated from respiration [19] (They are hence also called the ATP synthase). Prokaryotic F-ATPases can also function in reverse, consuming ATP while producing an ion flow across the membrane [20]. In eukaryotic cells, F-ATPases are located at the inner membrane of the mitochondria for animal cells, or the chloroplasts in plant cells. Energy harvested at these organelles, either from respiration or the absorption of light, is utilised by the F-ATPase to synthesise ATP. The ATP can then be transported to other parts of the body. In bacteria, the F-ATPase is located on the cytoplasmic membrane.

F-ATPases from various different sources are remarkably similar in morphology and functions. Crystal structures of the soluble part of F-ATPase (also known as F_1 ATPase) from bovine mitochondria [21], yeast [22, 23], *E. coli* [24, 25] and chloroplast [26] are similar in both structure and the arrangement of their major subunits. Furthermore, single-molecule experiments have shown that F_1 ATPases from thermophilic bacteria PS3 [27], *E. coli* [28, 29], chloroplast [30] and yeast⁷ all move in a rotary manner as they hydrolyse ATP. The common morphology and working mechanism of F-ATPase across various organisms have thus been verified. More details on the structures and functions of the F-ATPase are described in Chapter 2. For ease of differentiation, I will now adopt the following nomenclature for F_1 from various sources: TF_1 – thermophilic bacteria, MF_1 – beef mitochondria, CF_1 – chloroplast, EF_1 – *E. coli* and YF_1 – yeast F_1 .

⁷ Unpublished results from the Berry group

Finally, as an extension to the F-ATPase, it is interesting to also mention the ATPase derived from Archaea⁸ (also known as A-ATPase). Genetic comparison of the ATPases has revealed that the A-ATPase is closer to V-ATPase than F-ATPase [31]. However, unlike V-ATPase⁹, A-ATPase is able to both synthesise and hydrolyse ATP. The ability to make ATP may explain why most of the A-ATPases found so far have c-subunits that are structurally similar to F-ATPase i.e. each c-subunit has only two transmembrane helices [32]. Nonetheless, A-ATPases with c-subunits that comprise more than two transmembrane helices have also been found, some of which resemble the c-subunits of the V-ATPases [32]. As expected, the A-ATPase is morphologically similar to both the V-ATPase and F-ATPase [33].

1.1.4 Summary of this Section

This section gives a brief coverage of the different types of ion pumping ATPases that occur in nature. The P-type ATPase is able to move myriad kinds of cations, but is structurally and mechanically different from the V-type and F-type ATPase. The latter two are differentiated mainly by their functions, locality and differences in their subunits. Finally, a fourth type of ATPase derived from Archaea, the A-ATPase, possesses features that can be found in both F-ATPase and V-ATPases.

⁸ Archaea are prokaryotes but differ from bacteria and have a distinct evolutionary history. Some of the notable differences include having unique membrane compositions and metabolic pathways.

⁹ It has however been found that V-ATPase from *Thermus thermophilus* is able to synthesise ATP from membrane potential.

1.2 Historical Perspective of ATP Synthase

1.2.1 Early Days

This section gives a historical overview of the research on energy conversion in living organisms. I initially wanted to give only a brief account of the notable historical events leading to our current appreciation of the F-ATPase. However, as I delved deeper into this subject, I found myself becoming overawed and inspired by the work of those who have made our current understanding possible. Every small piece of information is a culmination of relentless effort, coupled with the brilliance of crafting the right experiments to probe seemingly impossible research questions. Indeed, the now ‘textbook’ understanding of F-ATPase is a steady consolidation of many years of research and generations of diligence by some of the top minds in this area.

It will be incomplete to mention F-ATPase without discussing the role of adenosine tri-phosphate (ATP). The role of ATP is in turn fundamental to the wider context of how humans (or for that matter, most other organisms) obtain energy to do work, think or just simply maintain life. Thermodynamically speaking, a system without energy inputs will eventually disperse into chaos. Without the cascades of chemical interactions to provide energy, an ordered system such as life would never have existed.

One of the first ideas of energy utilisation in living things is the concept of heat production through respiration. Using a guinea pig trapped in a snow covered chamber and measuring the amount of snow melted, Lavoisier (1743 – 1794) was able to estimate the amount of heat produced by the animal. He proposed that the heat

came from respiration of the animal, through a slow combustion of oxygen and “organic matter” in the body [34, 35]. This “organic matter” found a more tangible form, when glycogen¹⁰ was discovered in the 1850s. The understanding then, was that oxidation and fermentation (non oxidative breaking down of glycogen to lactic acid) of glycogen was what gave muscles the energy to do work. There was however no knowledge about how glycogen could be broken down or converted into energy packets usable by the body.

1.2.2 Finding the Currency of Energy – Discovery of ATP

The first clue for this came from the work by Meyerhof in the early 20th century. Meyerhof found that when glycogen was consumed in muscles under anaerobic conditions, it was converted into lactic acid [35, 36]. With the availability of oxygen, part of this lactic acid became fully oxidised while the rest reverted back to glycogen. This finding was insightful because it was the first time energy conversion in living organisms was proposed to be a cyclic process [35, 36]. Meyerhof called it the lactic acid cycle. Later, together with Hill, he went on further to elucidate the metabolism of muscles *vis-à-vis* the energetics of the lactic acid cycle. For this work, Meyerhof and Hill were awarded the Nobel Prize in 1922.

It was soon realised that the mechanism for breaking down glycogen was more complicated than expected. The mechanism was found to involve many sub-steps, with each requiring different enzymes and chemical intermediates [37]. It was the endeavour to uncover the chemical intermediates that led to the discovery of creatine

¹⁰ Glycogen is a polymer of glucose stored as an energy reserve in the body

phosphate by Fiske and SubbaRow in 1927 [35, 38]. This was a notable discovery because it gave rise to the possibility that energy rich phosphates might play a role in energy conversion within muscle. It was not until three years later that the discovery of another energy rich phosphate – adenosine tri-phosphate, was independently reported by Lohmann [38] and then by Fiske and SubbaRow [39] two months later. By 1934, Lohmann was able to show that ATP is synthesised during glycolysis¹¹. He also found that creatine phosphate was in fact, an energy source for the regeneration of ATP in muscles [35, 38]. These findings, together with the discovery of myosin, eventually led Meyerhof to conclude that ATP is the immediate energy source for muscle contraction. Shortly after this, ATP as a bearer of an ‘energy rich phosphate bond’, was spelt out explicitly by Lipmann¹² in 1941 [40].

1.2.3 Discovery of Oxidative Phosphorylation and its Relation to Respiration

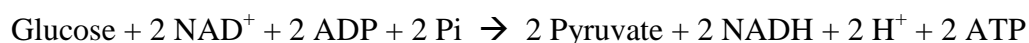
If ATP is the energy currency in organisms, then there must be an efficient mechanism for ATP to be synthesised. The active aerobic esterification of inorganic phosphate to produce ATP was first reported in 1932 by Engelhardt [41]. He noticed that the ATP content inside nucleated avian blood cells remained stable until anaerobic conditions were imposed. Thereupon, the amount of ATP inside the cells became depleted within an hour. It was then postulated that the consumption of ATP under normal aerobic conditions must be “*compensated for by a steadily proceeding reverse process*” [41]. This observation had provided a first glimpse of the oxidative

¹¹ Glycolysis is the process in which glucose derived from glycogen is broken down to pyruvate

¹² Fritz Lipmann was a co-worker of Meyerhof and winner of 1953 Nobel prize in physiology or medicine. He shared the prize with Hans Krebs.

phosphorylation metabolic pathway [42] – the process whereby ATP is produced via oxidation.

However, this still did not shed light on how ATP could be produced via respiration. To explain this, one must return to the work by Meyerhof on the breakdown of glucose derived from glycogen. By the end of the 1930s, the pathway for glycolysis had been broadly unravelled, mainly by Meyerhof and Embden [35, 36]. The overall reaction could be written as [43]:



Where NAD^+ is nicotinamide adenine di-nucleotide and NADH is the reduced form of NAD^+ .

The breakdown of glucose can thus directly yield ATP. However, this cannot explain the vast amount of ATP produced in the body. Besides ATP, glycolysis also produces two energy rich products (Pyruvate and NADH), which can potentially be tapped further. Indeed, Lipmann was able to show that ATP was produced when bacteria¹³ were incubated with pyruvate and AMP¹⁴ [44]. At about the same time (1937), Krebs¹⁵ had elucidated how pyruvate was broken in animal tissues [45, 46], resulting in the production of NADH [43]. This was later known as the Citric acid cycle or the Krebs' cycle. There was however no direct production of ATP. Moreover, the Krebs cycle, by itself, does not require the presence of oxygen to occur [43]. There must

¹³ *Lactobacillus delbrückii*

¹⁴ Adenosine monophosphate

¹⁵ Hans Krebs was the winner of the 1953 Nobel prize in physiology or medicine for his discovery of the citric acid cycle

therefore be a separate pathway in the respiratory chain for the use of NADH and consumption of free oxygen. Friedkin offered a clue to this in 1949, when he found that NADH enabled the production of ATP, via the “*transport of electrons from DPNH₂ (NADH) to oxygen*” [47]. It is through this reduction of free oxygen that more ATP can be produced. The respiratory mechanism was finally in sight.

1.2.4. Discovery of the Electron Transport Chain and Chemiosmotic Coupling – The Energy Source for ATP production

To appreciate the role of oxygen usage in the production of ATP, one must return again to 1925. This is the year when the role of cytochrome as an “intracellular respiratory catalyst” was reported by Keilin [48]. Cytochrome is a family of coloured proteins that participate in the respiratory mechanisms of disparate organisms ranging from animals and plants to aerobic bacteria [48]. Importantly, it was suggested that their role in respiration involved transferring electrons to oxygen molecules [48, 49], via a series of oxidation and reduction sub-steps. The multiple steps in the reduction of oxygen, to ultimately form water, allows a more regulated way to harvest the latent chemical energy, rather than through a single step reaction [43]. The cascade of reactions, involving cytochromes, is also known as the electron transport chain [49]. The link between the electron transfer chain and phosphorylation of ADP was suggested independently by Ochoa and Tsibakowa in 1939 – 1940 [49]. Indeed, if ATP is regarded as the end product of respiration, then the electron transfer chain would be the main process that provides the energy for ADP phosphorylation to take place.

It was not until 1961 that the role of the electron transport chain was formalised by Mitchell¹⁶ [50]. He proposed that ATP was produced by an “*ATPase system*” located on the surface of membranes. Furthermore, the energy for the production of ATP was derived from the chemical and electrical potential difference across the membranes. This chemical and electrical potential difference was in turn due to trans-membrane proton pumping by the electron transfer chain [50]. Mitchell called this a “*chemiosmotic type mechanism*”. The proposed mechanism was, at that time, seen as a paradigm shift from the more accepted model of ATP production via chemical reactions with high energy intermediates [50]. At this point, one can finally visualise the big picture of ATP production via respiration (Figure 1-3)

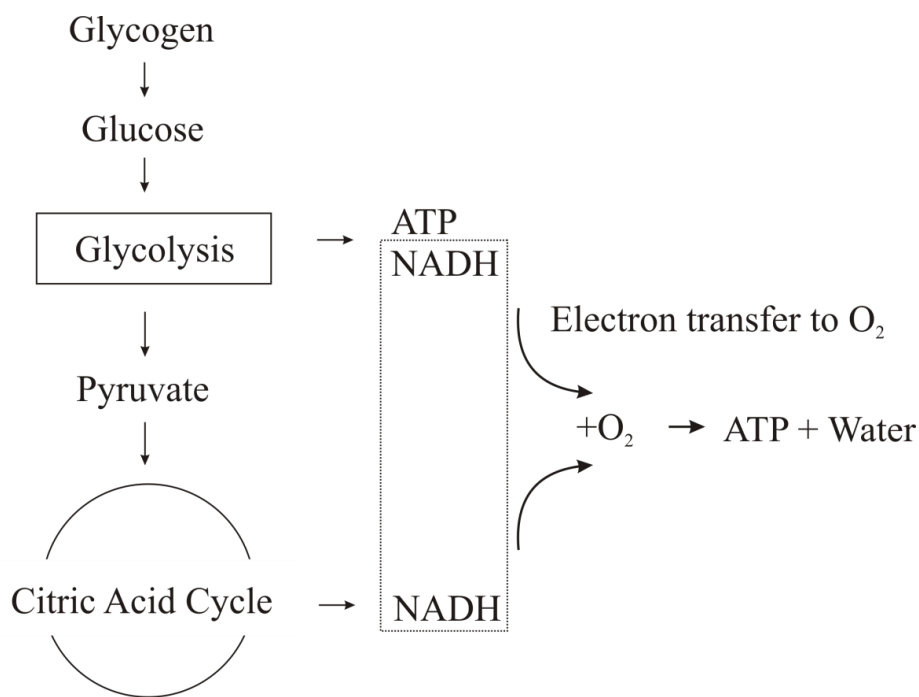


Figure 1-3. A simplified schematic showing the process in which glycogen is broken down to produce ATP.

¹⁶ Peter Mitchell was the winner of the Nobel prize for chemistry in 1978 for his discovery of chemiosmotic coupling in ATP production

1.2.5 Elucidation of F-ATPase – Early Model of ATP Turnover

As the big picture of oxidative phosphorylation began to settle, scientists started to shift their focus on the interactions that were happening at individual intermediate steps. One of the areas that attracted much interest was the study of how the “ATPase system”, as described by Mitchell, actually worked. Among the main contributors in this area was Paul Boyer¹⁷. By tracking the exchange of isotopes (P^{32} and O^{18}) on intact F-ATPase membranes¹⁸, Boyer was able to study the equilibrium reactions existing between different chemical entities participating in the synthesis and hydrolysis of ATP (i.e. ADP, ATP, phosphate ions, H_2O). For example, it was observed that the exchange of P^{32} between ATP and free phosphate (P^{32}) was inhibited when ADP was removed from the reaction buffer [51]. The reversible hydrolysis of ATP, as detected by the exchange of oxygen isotopes O^{18} on the ATP, was however still detected. This led to the postulation that, in the absence of ADP, ATP could still be transiently produced and hydrolysed by the enzyme but the products could not be released into the buffer. i.e. the release of ATP by the F-ATPase required the presence of ADP (Figure 1-4).

Furthermore, it was separately reported that each F-ATPase in beef heart mitochondria contained two binding sites for ADP, with one binding ADP more tightly than the other [52]. Together, these evidences suggested that a second catalytic site might be present for the binding of ADP and that it functioned in catalytic cooperativity with the first [51, 53]. Using this observation and other data from the isotope exchange studies, Boyer et. al. proposed a two site model in 1977, describing

¹⁷ Paul Boyer was the winner of 1997 Nobel prize for chemistry for his work on F ATPase

¹⁸ Beef heart submitochondrial particles were used. These contained intact F-ATPase on energisable membranes

the mechanism of ATP synthesis and hydrolysis [51] (See Figure 1-5). This model essentially explained how the action of the first catalytic site was dependent on the state of the second. It was remarkable because the model had had some features that were very similar to the current working model of F₁ ATPase, which was obtained using precise single molecule experiments (this is discussed in chapter two). Boyers' model was later refined to one that included three catalytic sites [54]. In addition, Boyer et. al. was also among the first to speculate that ATP production might proceed by the rotation of subunits in the enzyme [53, 55] – another radical idea that was conclusively proven fifteen years later [27].

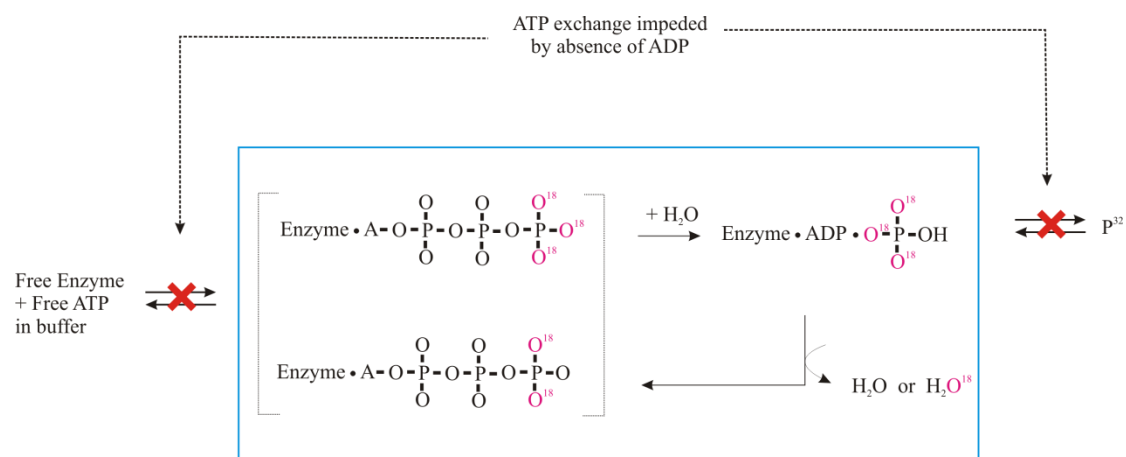


Figure 1-4. Schematic showing the exchange of phosphate and oxygen isotopes when ADP was removed from the buffer using an ATP regeneration solution to reduce the concentration of ADP. Most of the ATP detected at the end of incubation did not possess P³² from solution. On the contrary, some of the O¹⁸ in the ATP were exchanged with O¹⁶ from the reversible reaction with H₂O. This indicated that while the equilibrium in the blue box was active, the ones on the left or right had been impeded. The presence of O¹⁸ exchange meant that ADP at the catalytic site was not lost to the buffer. There must thus be another ADP dependent process that was preventing the exchange of ATP (on the left) and / or phosphate (on the right). This process was thought to be binding of ADP at an adjacent catalytic site.

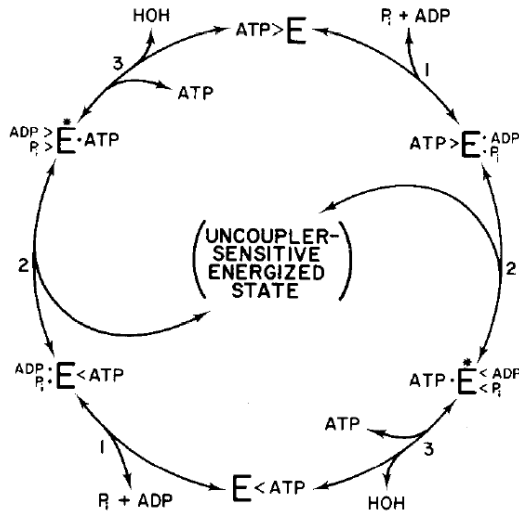


Figure 1-5. One of the first models by Boyer's group, depicting the turnover of ATP / ADP during synthesis and hydrolysis mode. In this model, there were two sites for ATP / ADP binding. Each site worked in catalytic cooperativity with another. For example, the binding of ATP on one site was necessary for the release of ADP and Pi at the other. Similarly, the release of ATP at the first catalytic site required ADP and Pi to be present at second. > represents strong affinity while • represents weak affinity. Diagram obtained from Kayalar [51].

1.2.6 Elucidation of F-ATPase – Composition of F-ATPase

Concomitantly, there had been much progress made on the structure and isolation of F-ATPase. One of the first revelations about the composition of the enzyme was that it comprised two portions. In 1960, Penefsky [56] found that both the water soluble fraction and membrane particulate of the beef heart mitochondria were mandatory for the production of ATP. In addition, the water soluble fraction possessed the enzymatic activity to hydrolyse ATP, while the membrane fraction partook in the electron transport mechanism via citrate / succinate oxidation¹⁹. In the same year, the water soluble fraction was purified by Pullman et. al. [57] and named 'Coupling Factor 1' or F₁ [58] – the coupling factor referred to the necessary coupling of F₁ in order to preserve the ability to synthesise ATP. Five years later, in 1965, a new coupling factor was obtained from the membrane particulate fraction of the beef heart mitochondria.

¹⁹ Citrate or succinate oxidation is part of the Krebs cycle that provides energy to translocate protons across the membrane.

This factor was found to make F_1 susceptible to oligomycin²⁰ [59] again. (F_1 , by itself, is not sensitive to oligomycin). The ‘Coupling Factor’ was later named F_o ²¹, with ‘o’ representing the oligomycin sensitive characteristic. F_o remained the descriptive name for the membrane portion, even though its suppression by oligomycin applies only strongly to mitochondrial F_1F_o (MF_1F_o). Oligomycin has only a weak effect on *E. coli* and chloroplast F-ATPase [21, 22]. The subunit responsible for the sensitivity of MF_1F_o was later called the oligomycin sensitivity conferring protein (OSCP).

By the early 1970s, it was realised that both F_1 and F_o were actually protein ensembles that comprised many other smaller subunits. It was a progress which, to some extent, was attributed to the introduction of SDS gel electrophoresis²² in 1965 [60]. F_1 from yeast [61], chloroplast [62], thermophilic bacteria [63], *E. coli* [64, 65] and beef heart mitochondria [66, 67] were all found to contain five subunits with a stoichiometry of 3:3:1:1:1 [63, 64, 68]. In addition, beef heart mitochondria contained an additional inhibitor protein, which was regarded as the sixth subunit [68].

It is more difficult to determine the number of subunits and their stoichiometry in the F_o portion. This is because the subunits in F_o were more difficult to purify [19]. Furthermore, some of these subunits respond poorly to staining and other polypeptide separation techniques like isoelectric focussing²³ does not work well with the hydrophobic subunits found in F_o [19]. Nonetheless, at least five subunits had been reported in yeast and beef mitochondria F_o [68], while thermophilic bacteria and *E.*

²⁰ Oligomycin is an antibiotics created by *Streptomyces*

²¹ Contrary to common belief, the ‘o’ in F_o actually refers to oligomycin and not the number zero

²² SDS gel electrophoresis is an electrophoresis technique which allows the separation of proteins according to their molecular sizes

²³ Isoelectric focussing is a method for separating polypeptide. It uses a gel with a pH gradient. Protein with a net charge will migrate in the gel until it reaches a pH that corresponds to its isoelectric point. At that point it will stop migrating.

coli had only three [63, 65]. The number of subunits in F_o for beef mitochondria was later revised to be between seven and nine [69, 70] and four subunits were reported in chloroplast [71]. A more detailed discussion on the subunits of F-ATPase is given in the next chapter.

1.2.7 Elucidation of F ATPase – Structure and Morphology of F-ATPase

On a separate front, scientists had also been trying to envisage the structure of F-ATPase and understand how the subunits were assembled. One way of visualising the F-ATPases was by direct observation of the mitochondrial particles using electron microscopes. This technique gave us some of the earliest high resolution images of F-ATPase. Using beef heart mitochondria as the specimen, Fernández-Morán et al. [72, 73] reported, in 1962, a series of ‘repeating particles’ lining the inner membrane. These repeating units had a general morphology comprising a head piece of diameter $\sim 80 \text{ \AA}$ to 100 \AA , a stalk $\sim 30 \text{ \AA}$ wide by 50 \AA long and a base piece that was embedded in the membrane (see Figure 1-6). It was postulated that the repeating particles were “elementary units” of a protein ensemble that were responsible for the electron transfer chain [72] during oxidative phosphorylation. Kagawa later corrected this in 1966 by attributing the head piece to be due to just the F_1 ATPase alone [74].

By combining the knowledge of subunit composition and morphology of F-ATPase, Senior [68] proposed a tentative model of F-ATPase in 1973 (See Figure 1-7). The idea that the OSCP resided at the central stalk came as early as 1968 [75] and persisted until the mid 1990s [76]. In 1996, Collinson [77] suggested the presence of a

separate stalk that extended up to the top of the α -subunit²⁴. This stalk was thought to consist of the OSCP and three other interacting proteins²⁵. A model of *E. coli* F₁F₀ ATPase, which explicitly contained the ‘new’ peripheral stalk, was introduced by Capaldi in 1997 [78, 79].

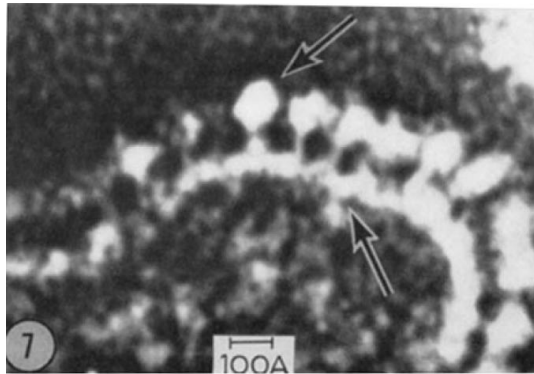


Figure 1-6. Electron micrograph extracted from Fernández-Morán et. al. [72]. A mitochondria sample was magnified by 600,000 x. The head piece, stalk and base piece can be clearly differentiated.

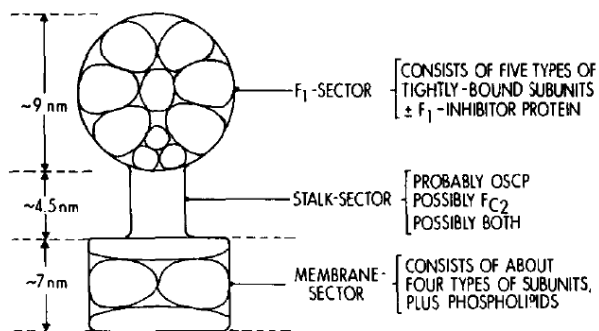


Figure 1-7 Historical morphology of the mitochondria F₁F₀ ATPase by Senior in 1973 [68]. The actual arrangement of the subunits was not known then. The head piece was attributed to F₁. F₀ was thought to comprise the membrane sector and stalk sector.

1.2.8 Summary for this section

The above is only a snapshot of the history of ATPase research. The constraints of time and space have restricted my account to only the more notable events. I have also

²⁴ The α -subunit is one of the two repeating subunits that form the hexameric head piece.

²⁵ Subunits b, d, and F₆ of the bovine F₁F₀ ATPase

chosen (with bias) to mention only those breakthroughs that led to a paradigm shift in our understanding of F_1F_0 ATPase. Needless to say, these ideas are results of many years of knowledge accumulation rather than a single stroke of genius. It is impossible to mention all those who have contributed to this extensive field.

Before progressing further, let us recapitulate the information that is presented thus far. This will serve as the premise for the next chapter. We now know that

- ATP is the basic energy currency.
- ATP is resynthesised by a process called oxidative phosphorylation.
- The energy for ATP production can be explained by glycolysis, the Krebs cycle and the electron transport chain.
- There is an enzyme directly responsible in the synthesis of ATP. It is now known as F-ATPase
- A potential difference across the membrane directly provides the energy for ATP production by the F-ATPase. This potential difference is produced by reactions occurring during the electron transport chain.
- The F-ATPase contains more than one catalytic site, each working in cooperativity with the others.
- The F-ATPase comprises two portions. A water soluble part called F_1 and a membrane part called F_0 .
- F_1 comprises 5 major subunits. F_0 contains a varied number of subunits that is dependent on the source of the protein.

- In their native state, the morphology of the F_1F_0 ATPase can be divided into four distinct structures. A head piece and main stalk which correspond to F_1 and a membrane base piece and peripheral stalk that correspond to F_0 .

In the next chapter, I will provide more details on the two aspects of F-ATPase that have seen much progress in the last twenty years. The first is the visualisation of the structure of the subunits and the prediction of their roles during the catalytic turnover. The second is the postulation of the mechanism of the F-ATPase using clever single-molecule techniques. Before delving into the detailed literature review, the overview and motivation of this thesis is presented.

1.3 Further Research Questions

The motivation of studying F_1F_0 ATPase in an energisable²⁶ membrane is clear. The synthesis mode is the only way in which eukaryotic F-ATPase operates *in vivo*, while the hydrolysis mode is also used by prokaryotic F-ATPase to maintain a stable cytoplasmic pH. Both these functions are fundamental to the sustainability of life. Scientists have so far been able to decipher the functions of individual subunits and rotation characteristics of F_1 and F_0 individually. However, the mechanisms of the coupled F_1F_0 ATPase rotation remain elusive. Despite making extensive progress in this area, scientists are only now starting to understand how F_1F_0 ATPase would behave as an ensemble protein. Ultimately, the overarching research questions needed to be answered include:

²⁶ Energisable membranes are defined as membranes which can sustain an a ion motive force

- What is the mechanism behind fully coupled F_1F_0 rotation?
- How does the synthesis mode differ from the hydrolysis mode, in terms of the ways energy is converted from one form to another, the efficiencies of such conversion and the mechanism of operation?
- How do the two modes of coupled rotations vary with different conditions e.g. availability of ATP, ADP, phosphate, ion motive force and inhibitors?
- What are the roles of the main and peripheral stalk in the combined motor, in terms of transient elastic energy storage and mediating the symmetry mismatch between the F_1 and F_0 ?
- How does the eukaryotic F-ATPase prevent the hydrolysis mode from taking place *in-vivo* and when does the prokaryotic F-ATPase switch from synthesis mode to hydrolysis mode (and *vice versa*).

The first step to answering these questions is to devise a way to observe rotation of intact F_1F_0 ATPase in an energisable membrane. This setup should ideally be robust and have high temporal and spatial resolution so that fast transient events can be detected and localised. This is definitely not an easy task judging by the limited literature available thus far. This project aims exactly to tackle the problem head on. Preliminary results appear promising. However, admittedly, more work is still needed to improve the setup and obtain conclusive coupled F-ATPase rotation.

1.4 Summary of Thesis

This project attempts to develop an experimental setup for the studying of F_1F_0 ATPase in an energisable membrane. Since this was a relatively new area for our

group, a lot of protocols had to be learnt, either from existing literature or through trial and error. Fortunately, help was available from more experienced hands / minds, locally and abroad. The mutant F-ATPases and purification protocol were obtained from our collaborators in Japan. The bilayer setup was obtained from Dr Mark Wallace and Dr Andrew Heron in the chemistry department, University of Oxford. Recent progress in laser darkfield microscopy in our group and the availability of commercial high speed data acquisition hardware, were also crucial to the development of this setup.

The objective of this project is straight forward. Our aim is to develop a setup that allows us to observe rotation of the F-ATPase at high spatial and temporal resolution. The conceptual framework is broadly summarised into four main steps. Figure 1-8 shows a pictorial representation of the project overview. The work includes

- Purifying functional F-ATPases from bacteria.
- Reconstituting the F-ATPases onto a planar bilayer set up
- Immobilising part of the F-ATPase (stator) using an agarose substrate, and attaching a gold nano-particle to the rotor.
- Detecting any rotation or interesting movement of the gold nano-particle, during hydrolysis / synthesis conditions, using a high speed laser dark-field microscope.

Below is a point by point summary of the main achievements for this project.

- *E. coli* F₁F₀ ATPase was purified, reconstituted into vesicles and tested for hydrolysis activity. This was an achievement for me because it involved an area of work that was completely different from my previous training. Furthermore, many of the protocols were not yet developed in this laboratory and had to be learnt the laborious way.
- A stable planar bilayer setup was adapted to support the insertion of F₁F₀ ATPase. Using total internal reflection fluorescent microscopy (TIRFM), the enzyme was found to adhere to the bilayer and able to diffuse freely along it. The behaviour of this diffusion was characterised.
- A substrate agarose with functionalised nitrilotriacetic acid (NTA) was made and characterised. This substrate was used to support the bilayer and also anchor the c-subunits of the F₁F₀ ATPase.
- Gold nano-particles (GNP) were modified with streptavidin molecules. These particles were used as probes to observe the rotation of F₁F₀ ATPase under laser dark-field microscopy. The efficiency of the streptavidin conjugation to GNP was estimated using a simple photo bleaching assay.
- Finally the F₁F₀ reconstituted bilayer was observed using a homemade dark-field microscope. Populations with three dwell angles were observed. Unidirectional rotation of the enzyme was however not observed.

The new planar bilayer setup developed for the observation of F-ATPase rotation has three main advantages compared to published systems (vesicles or suspended bilayer methods):

- This method allows direct observation of rotation under laser dark-field microscopy. The laser dark-field technique is able to provide enough photons to give very high temporal (up to 10 μ s) and spatial (max \sim 0.6 nm) resolution for analysing the rotation of F₁F_o ATPase. Unlike fluorescence techniques, it does not suffer from photobleaching / blinking events or generate free radicals that may denature F-ATPases. This setup is also amenable to other conventional microscopy like total internal reflection fluorescence microscopy (TIRFM) or confocal microscopy. In this thesis, both total internal reflection fluorescence microscopy (TIRFM) and laser dark-field microscopy (LDF) were used to visualise F-ATPases on bilayers.
- In the planar bilayer setup, both the *cis* and *trans* side of the bilayer can be assessed electrically. It is therefore a fully energisable membrane where a prescribed proton motive force (PMF) can be applied, and for a sustained period, using a pair of electrodes.
- The stator of the F-ATPase was immobilised so that only the movement of the rotor can be observed. This requires a substrate capable of holding on to part of the F-ATPase. The system developed here allows such immobilisation via an electrically conductive agarose substrate.

1.3.1 Structure of Thesis

The structure of this thesis is arranged in a chronological work flow, starting from F-ATPase purification to final observation of tethered enzymes. The first chapter gives a general overview of ATPases and the historical background behind the research of F-

ATPases. Chapter two expands further on the current understanding of F-ATPase. It mainly summarises the recent progress on the structure and mechanism on the F-ATPase. This chapter is not deliberately intended to be a laborious read, but probably ended up that way because of my obsessive attempt to make the section complete. Even for that, much information has to be left out. The third chapter deals mainly with the biochemistry of purifying and testing the activity of F_1F_0 ATPase. In that chapter, I have described the procedure for obtaining F-ATPases, reconstituting them into vesicles and testing their activity. Chapter four shows the characterisation of the planar bilayer setup and the results of F-ATPase reconstitution onto the bilayer. It describes how the purified F-ATPases were transferred onto the planar bilayer and how the presence of the enzymes was tested. In chapter five, work on GNP and the agarose substrate are described. The GNP was attached to the biotinylated β -subunits of F_1F_0 ATPase so that rotation could be picked up by the dark-field microscope – it thus needs to be efficiently coated with streptavidin molecules. The agarose substrate was used as a support for the planar bilayer and an anchor to hold the histagged c-subunit of F_0 . This is done so that the other subunits (comprising $\alpha_3\beta_3\delta ab_2$) can rotate with respect to it – it thus needs to be efficiently coated with nitrilotriacetic acid (NTA) functional groups. Chapter six contains the results with the GNP labelled F-ATPase observed under the laser dark-field microscope. This is a short chapter because the results are still preliminary and require more extensive tests to confirm (or refute) the findings. Finally, I will summarise the thesis and outline the future work for this project in Chapter 7.

Overview of Thesis

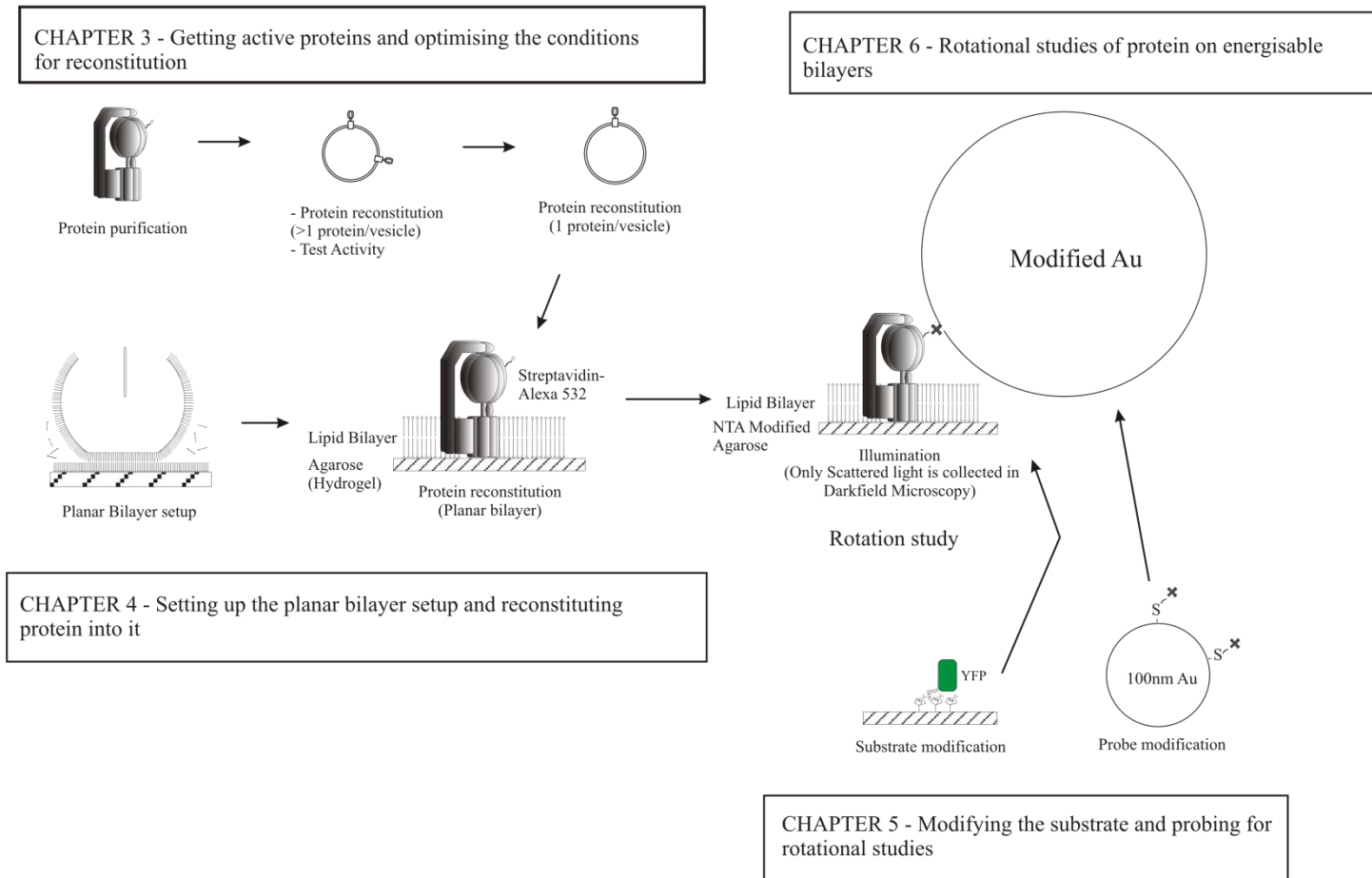


Figure 1-8. A pictorial representation of the overview of this thesis

2

Review of F-ATPase

2.1 Overall structure of F₁ ATPase

The first high resolution crystal structure of the soluble F₁ was obtained from beef heart mitochondria in 1994 [21]. Other structures of F₁ from *E. coli* ($\gamma + \epsilon$ only) [25], chloroplast [26], and yeast [22, 23] were obtained shortly after that. A comparison of these structures demonstrates remarkable similarities, despite the disparate sources from which they were obtained. The structure of F₁ described hereinafter is thus generally true, at least for all sources of F₁ that have been discovered so far. For ease of explanation, bovine MF₁ is as the model system for the description, since it has the most detailed crystal structures available [21, 80-82]. Nevertheless, where there are unique regions specific to the source of the F-ATPase, it will be explicitly stated.

The five subunits that make up the F₁ portion of the F-ATPase have been given the nomenclature α , β , γ , δ and ϵ . There are three copies of α and β per F₁ and one of each for the rest of the remaining subunits. Crystal structures of the bovine MF₁ ATPase show the α and β -subunits arranging alternately in a circular manner, forming a six-segmental head piece. There is a cavity through the middle of the head piece and a dimple at the top [21]. The cavity is occupied by the γ -subunit, which extends out of

the hexameric structure to form part of the main stalk. In *E. coli* F₁, the δ -subunit rests on the top of the head piece while the ϵ -subunit can be found at the base of the main stalk. The mitochondrial F₁ is similar to that of *E. coli*, except that the nomenclature of the subunits has been modified slightly. Figure 2-1 shows the cartoons of the *E. coli* F₁ ATPase and mitochondrial F₁.

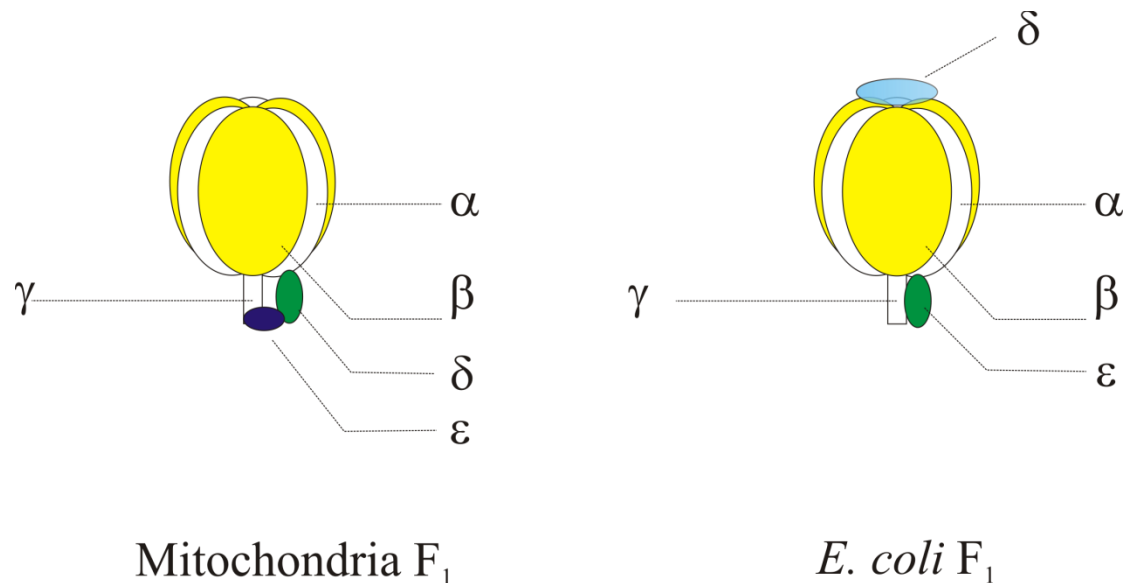


Figure 2-1. Cartoons of the overall structure of the *E. coli* and mitochondria F₁ ATPase and the positions of their various subunits.

2.1.1 The $\alpha_3\beta_3$ Hexameric Head Piece

Each α and β -subunit has a nucleotide binding domain, which is situated near the interface where the two subunits meet (see Figure 2-2a). This domain contains the phosphate binding P-loop, which bears the conserved GXXXXGKT/S nucleotide binding motif [21]. However, only β -subunits are able to catalyse the hydrolysis of ATP. This is because of the presence of a hydrogen-bonded water molecule, set in place by an amino acid on the β -subunit (β -Glu-188) [21]. The water molecule is thought to be able to react with the γ -phosphate of the ATP, cleaving it to form ADP

and phosphate. In the α -subunit, the equivalent β -Glu-188 (glutamic acid) has been replaced by α -Gln-208 (glutamine) [21]. Besides β -Glu-188, other important residues at the catalytic site include α -Arg373, β -Arg-189 and β -Lys-162. These residues are thought to stabilise the transition states during catalysis [21, 81].

The first structures of the β -subunits in F_1 were obtained in the presence of ADP and AMP-PNP²⁷ [21]. They existed in three different conformational states, corresponding to the type of nucleotides they bind to. While the first β site contained AMP-PNP, the second had an ADP and the last one was empty. These sites were denoted as β_{TP} , β_{DP} and β_E respectively. β_{DP} and β_{TP} were similar in structure and thought to be in a “closed” state. In this state, the nucleotide (ADP or ATP) was held relatively tightly by the β -subunit. In contrast, β_E represented an open state and was characterized by a large conformational change with respect to β_{TP} and β_{DP} [21]. This difference was thought to be mainly due to the interaction between the β_E and γ -subunit. From the crystal structure, hydrogen bonds between residues of the γ -subunit (γ -Arg 254, γ -Gln 255) and β_E subunit (β_E -Asp 316, β_E -Thr 318 and β_E -Asp 319) were evident. These hydrogen bonds were thought to form a “catch” that hold the conformation in place. The γ -subunit also obstructed the lower half of the β_E , preventing it from moving towards the central axis [21, 80] and disallowing the adoption of a nucleotide binding conformation. Figure 2-2b shows the partial structure of MF_1 with the salient domains.

²⁷ AMP-PNP is a non hydrolysable analogue of ATP

In another crystal structure obtained using $\text{ADP}\cdot\text{AlF}_4^-$ as inhibitor²⁸ [81], a new structural state of the F_1 was observed. As expected, β_{TP} and β_{DP} were bound to $\text{ADP}\cdot\text{AlF}_4^-$. However, instead of an absence of nucleotide seen in other structures, the β_{E} of the new structure contained an ADP and free sulphate ion (mimicking a phosphate ion). It was thought to represent an intermediate state that corresponded to post-ATP hydrolysis but pre-product release [81]. The next step of the catalytic cycle was suggested to be the release of ADP or phosphate, so that the β_{E} could become a fully open state. This structure also supported the tri-site assumption, where all the three catalytic sites could be occupied by nucleotides at some point during the catalytic cycle.

The crystal structures are in good agreement with the “binding change mechanism” proposed by Boyer et. al. [54, 83]. In this model, ATP turnover requires each catalytic binding site to adopt a different state, which has a descending order of affinity to nucleotides. As a binding site transits from one state to another, ATP is hydrolysed (or synthesised) and the products released into the environment. It has been postulated that the β_{TP} , β_{DP} and β_{E} from the crystal structure represent the different states stipulated in this model [21]. More information about the binding change mechanism is discussed further in section 2.4.

²⁸ $\text{ADP}\cdot\text{AlF}_4^-$ is an inhibitor that stabilises the catalytic transition state

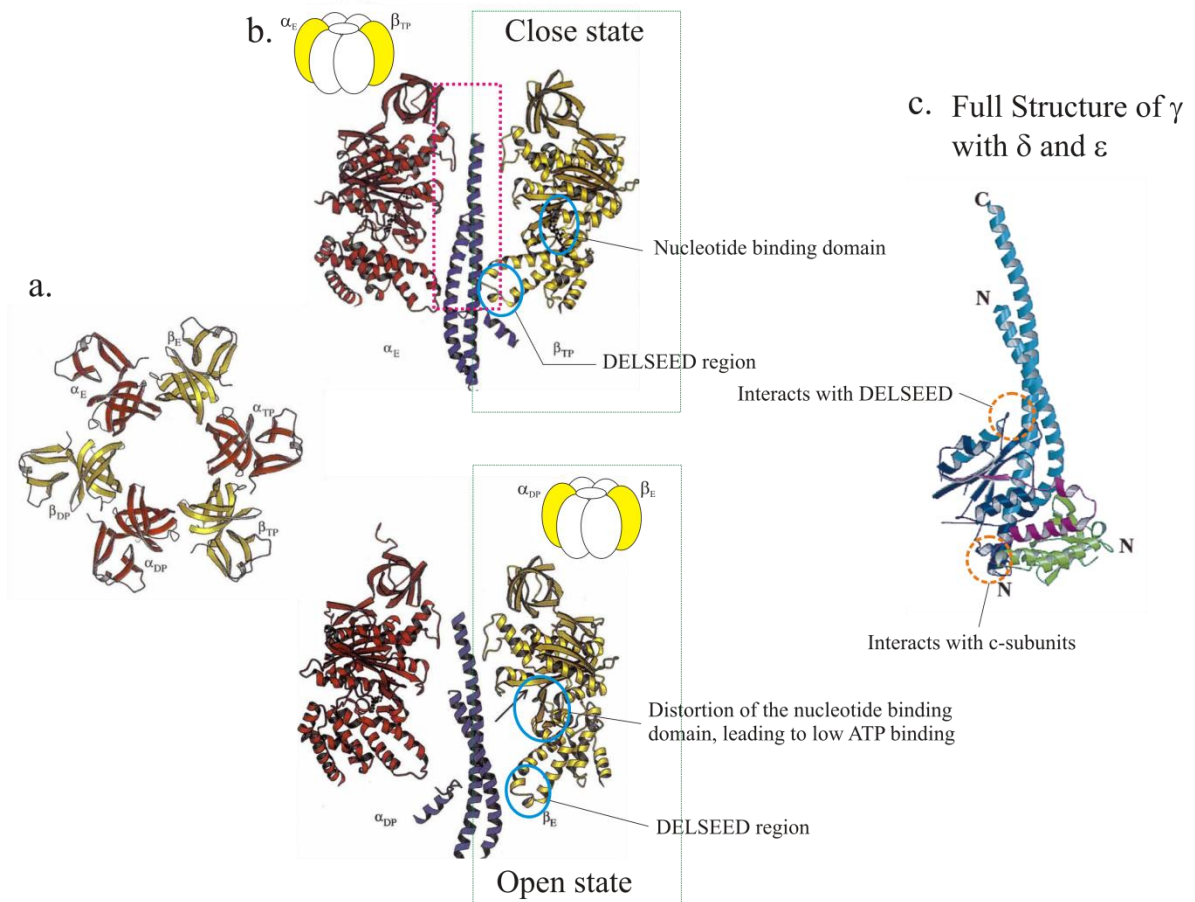


Figure 2-2. a) Arrangement of α and β -subunits to form a hexameric headpiece. Nucleotide binding pockets are denoted as β_{xx} or α_{xx} . β_{xx} in the β -subunits represents the different nucleotide binding states found on the crystal structure. α_{xx} represents the α -subunit that is adjacent to the β counterpart. For the structures in a) and b), α -subunits are coloured red and β -subunits are coloured yellow. b) Partial structures of the MF₁ showing one pair of α and β -subunits within the hexameric head piece. The pair of α and β chosen for display are indicated by the cartoons above the structures. The diagram also shows the partial coiled coil structure of the γ -subunit (in purple) relative to the α and β -subunits. The nucleotide binding domain and DELSEED region are highlighted in blue. The cavity inside the hexameric structure is shown by the pink box. The structure at the top shows the close configuration, where ATP is bound tightly to the β_{TP} subunit. Structure at the bottom shows the open configuration, where the nucleotide binding site in β_E is distorted and has low affinity to ATP. Structures in a) and b) are adapted from Abrahams [21]. c) shows the structure of the entire γ (blue), δ (green) and ϵ (magenta) subunits in MF₁. Orange circles show the location of residues that interact with the DELSEED motif and c-subunits. The diagram is obtained from [80]

2.1.2 The γ subunit

The γ -subunit is an asymmetric structure. It has a long C-terminal α -helix that passes through the centre of the hexameric $\alpha_3\beta_3$ structure, emerging into a dimple at the top [21]. The lower half of this helix meets a second helix (N-terminal helix of the γ -subunit), forming a coiled coil structure. This coiled coil structure extends out of the hexameric head piece and bears slightly away from the central axis, thus breaking the symmetry with respect to the central axis of the hexameric headpiece (see Figure 2-2c). Recently, it was demonstrated in TF_1 that part of the coiled coil axis inside the cavity could be deleted without a catastrophic loss of rotation, although the speed and torque generated were reduced [84]. This led to the postulation that part of the torque generation must come from the interaction between the γ -subunit and hexameric structure near the entrance of the cavity [84, 85]. Furthermore, it was also shown that the C-terminal helix of the coiled coil structure contributes partially to the torque generation, while the contribution of the N-terminal helix to torque generation is less apparent [85].

Once outside the hexameric headpiece, the γ -subunit assembles into a structure of five beta strands and six α -helices [80]. This structure was thought to provide stability to the coiled coil shaft [80]. Furthermore, a conserved residue γ -Arg75 at the protruding loop appears to interact with the carboxyl terminal domain of the β - subunits (β -Glu395) [80], which is part of the conserved DELSEED motif (DELSDED in TF_1) – see Figure 2-2b. The polar interaction between γ -Arg75 and β -Glu395 was believed to help stabilise the conformational states during rotation [80]. It might explain why mutation of the equivalent residue in TF_1 (β -Glu391) resulted in a five-fold decrease

in ATPase activity [86]. Also notable is the interaction between γ -Met23 (*E. coli*) with the same DELSEED motif. Mutation of γ -Met23 to lysine was reported to cause a loss in coupling efficiency between proton translocation and ATP hydrolysis [87]. Finally, three carboxyl groups of the γ -subunit (γ -Asp 194, γ -Asp 195 and γ -Asp 197) were found to extend downward at the foot of the stalk. These residues were thought to interact with the basic residues of the c-ring in F_o [80]. Crosslinking experiments also showed that residue γ -Tyr 205 is in close proximity with the c-subunits and N terminal domain of the ϵ -subunit of EF_1 [88].

2.1.3 The ϵ subunit

Before going on to explain the δ and ϵ -subunits, it is worth clarifying the confusing nomenclature of the subunits in F-ATPase of eukaryotes and bacteria. The δ -subunit in MF_1 is in fact homologous to the ϵ -subunit of EF_1 ; while OSCP of MF-ATPase is related to the δ -subunit of EF_1 . There is no equivalent of mitochondrial ϵ -subunit in bacteria (see Figure 2-1). To avoid ambiguity, I will use the suffix to represent the sources of the subunits, whenever δ and ϵ are mentioned (e.g. ϵ - MF_1 = ϵ -subunit from Mitochondria F_1).

From the crystal structure of MF_1 , it was found that δ - MF_1 and ϵ - MF_1 interacted with the γ -subunit at the foot of the main stalk [80]. A similar interaction was seen in EF_1 (*E. coli*), except that, instead of two subunits, only one subunit (ϵ - EF_1) was present. The ϵ - EF_1 was reported to comprise two domains – the C-terminal domain and N-terminal domain [89]. The N-terminal domain of ϵ - EF_1 was found to interact with the c-subunits [90, 91] and γ -subunit [80]. Interaction of the C-terminal domain is

however less straight forward. Structural studies revealed two possible conformations of the C-terminal domain of ϵ -EF₁. Gibbons [80] reported in his crystal structure that the δ -MF₁ was sufficiently far away from the α and β -subunits to prevent any interactions. However, experiments using zero-length crosslinkers had shown that the C-terminal domain of ϵ -EF₁ did interact with the α and β -subunits [92, 93]. At about the same time, a different structure of ϵ -EF₁ was reported by Rodgers [25] and later supported by Hausrath [94]. This alternative structure placed the C-terminus of ϵ -EF₁ sufficiently close to the α and β -subunits to allow interaction and was therefore in agreement with the results from the cross-linking experiments. By fixing the conformation of the ϵ -EF₁ using cross-linkers, Tsunoda was able to show that both the reported conformations existed and actually corresponded to the inhibited and non-inhibited state of the F-ATPase [95] (see Figure 2-3). In the ϵ -inhibited state, the C-terminal domain of the ϵ -EF₁, extends upward and interacts with the hexameric head piece. In that paper, the rate of ATP synthesis was said to remain unperturbed by ϵ -EF₁. This was however, countered later by Iino [96] who proved that synthesis mode is also affected by the extended ϵ -subunit. Iino also proposed that the inhibition is due to restricted rotation of the γ -“ ϵ -extended” stalk. Using mutagenesis experiments, Hara [97] demonstrated that the inhibition may be due to an electrostatic interaction between the C-terminal α -helix of ϵ -TF₁ and the DELSDED (or DELSEED in MF₁) motif of the β -subunit.

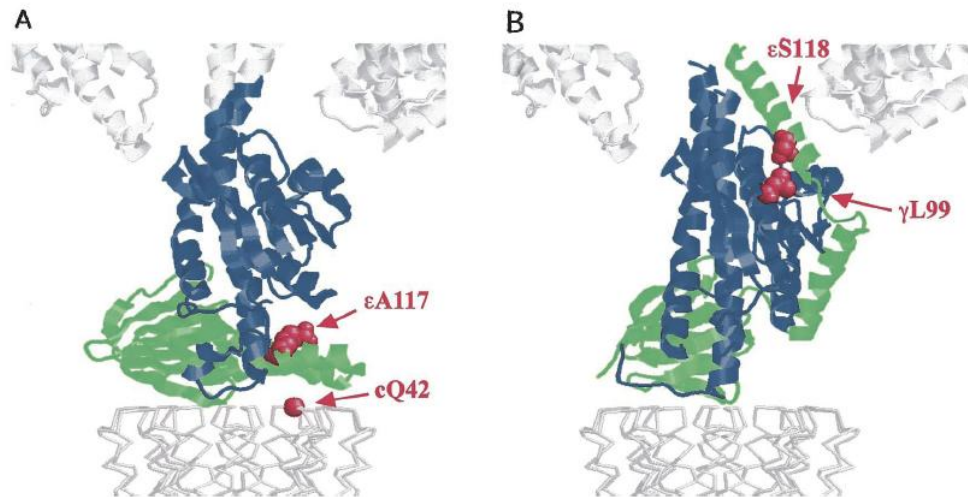


Figure 2-3. Comparison of the different conformational states of ϵ -EF₁ (δ -MF₁). A) shows the first conformational state of δ and γ obtained from the structure of MF₁. B) shows the second conformational state of the homologue ϵ -EF₁ obtained from structure of EF₁. ϵ -EF₁ (δ -MF₁) subunit is shown in green and part of the γ subunit is shown in blue. Other subunits are greyed out. Tsunoda [95] replaced residues in the c, γ and ϵ of *E. coli* with cysteine (as shown in red) so that ϵ -EF₁ could be “fixed” in its various *in-vivo* conformational states. The diagram shows two possible conformations which ϵ -EF₁ can adopt, notably at the C-terminal helices. The N-terminal domain of the ϵ -EF₁ remains relatively unchanged in these two conformations. The diagram above is obtained from Tsunoda [95].

Besides selective inhibition, ϵ -EF₁ / ϵ -TF₁ / ϵ -YF₁ are also found to be important for maintaining the structural integrity of the F-ATPase, without which F₁ cannot bind to F_o [98-100]. This is primarily due to the interactions at the N-terminus of the ϵ -EF₁ subunit [101]. The C-terminal domain, in contrast, is not crucial for F₁ binding [102]. Furthermore, ϵ -TF₁ was shown to affect the efficiency of ATP synthesis, as demonstrated by forced rotation of F₁ molecules [103]. Finally, it had also been suggested that the ϵ -EF₁ promotes coupling of F₁ to F_o during rotation, ensuring a tight connection between translocation of protons and ATP hydrolysis [104].

2.1.4 The δ -subunit (*E. Coli*)

Using electron microscopy and δ -EF₁ specific antibodies, δ -EF₁ was found to reside at the top of the hexameric structure [105]. From there, it is able to interact with both

the α -subunit [106] and b-subunits [107]. This further supported the current F-ATPase model [78, 79], which postulates that the δ -EF₁ extends from the top of F₁ to interact with the b-subunits, thus forming the peripheral stalk. The solution NMR²⁹ structure of isolated δ -EF₁ revealed a protein comprising two domains. The domain at the N-terminus is a six helix structure and is involved in binding with F₁ [79]. This domain was found to interact with the N-terminus of the α -subunit. NMR data by Wilkens [108] gave further structural details for this interaction. It revealed a previously undetermined part of the α subunit³⁰ (residues 8 to 18) forming a helix which interacts with helices I and V of the δ -EF₁.

The domain at the C-terminus was not defined in the structure of δ -EF₁ [79]. In fact, no high resolution structure is available for this domain thus far. However, deletion of just four or five terminal residues in δ -EF₁ [109] and OSCP (eukaryotic equivalent of δ -EF₁) [110] respectively, was to impede the coupling between F₁ and F_o. Later, it was shown that the δ -EF₁ interacts with the b-subunits via their respective C-termini [107]. Functionally, δ -EF₁ (or OSCP in MF-ATPase) has been demonstrated to be necessary for the binding of F₁ to F_o, in thermophilic bacteria, *E. coli* and yeast [98, 99, 110].

2.2 Overall Structure of F_o ATPase

The F_o portion of the F-ATPase is significantly more diverse in terms of its composition and stoichiometry. In MF_o, there are as many as seven to nine different

²⁹ Nuclear Magnetic Resonance

³⁰ The structure of the N-terminus of the α -subunit (residues 1 – 18) is not defined in the original crystal structure by Abrahams.

subunits [69, 70], while F_o of *E. coli* and thermophilic bacteria comprise only three subunits [63, 65]. As the subject of investigation in this thesis is F-ATPase from *E. coli*, I will therefore focus the discussion mainly on the F_o of this organism. Unless otherwise mentioned, description of F_o hereinafter will be of reference to *E. coli* F-ATPase.

The main subunits contain in the F_o portion are named “a”, “b”, and “c”. Both the a and c-subunits are membrane proteins [111] while the b-subunit possesses a trans-membrane section and a cytoplasmic section [112]. The b and δ -EF₁ subunits combine to form the peripheral stalk of the F-ATPase. At the base of the peripheral stalk are the a-subunit and the c-subunits. There are altogether ten identical c-subunits in *E. coli* [113]. Together, they form a ring-like structure. In our current understanding, proton translocation proceeds via the interface between the a-subunit and the c-ring [111, 114]. As each c-subunit can carry a proton, one complete rotation of the c-ring therefore corresponds to a translocation of ten ions across the membrane [15, 111].

2.2.1 The b-subunit

In *E. coli*, the b-subunit is an elongated homo-dimer [115] and interacts with the δ -subunit via its C-terminal domain [107]. It consists of four distinct domains, named according to their function (see Figure 2-4). They are: 1. trans-membrane domain, 2. tether domain, 3. dimerisation domain 4. δ -binding domain. The NMR structure of the trans-membrane domain of the b-subunit (residues 1 to 34) revealed two α -helices in close proximity [112]. A bend of $\sim 20^\circ$ occurs at the residue Lys-23, which coincides

with the interface of the bilayer membrane and the cytoplasm [112]. After emerging from the membrane, the b-dimer continues to extend upward by at least 110 Å to reach the top of the EF₁, placing its C-terminus in close proximity with the δ and α-subunits [116]. The crystal structure of the main part of the dimerisation domain (residues 62 – 122) had been solved, but only in the monomeric form [117]. Nonetheless, the result was used to predict the structure of the b-dimer, which was fitted to an extended right handed coiled coil structure ~ 95 Å long [117]. The validity of this in-registered³¹ structure was however disputed by Steigmler, using evidences from cross-linking experiments and double electron-electron resonance / electron paramagnetic resonance techniques [118]. More recent structures of the b-dimers included a parallel offset right-handed coiled coil structure [119] and a left-handed coiled coil structure [120]. Besides the dimerisation domain, structures of the tether domain and δ binding domain are also not resolved yet.

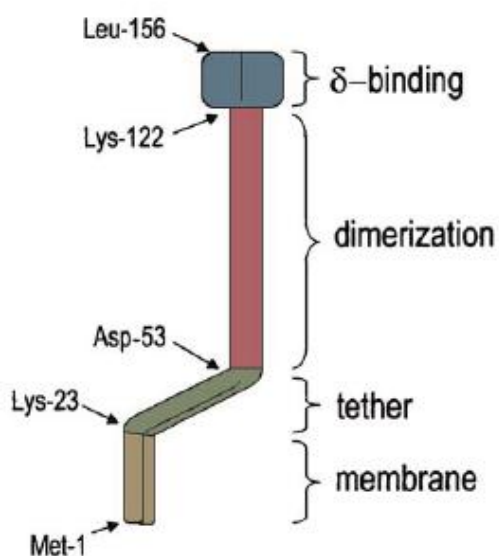


Figure 2-4. The four domains of “b” subunit of *E. coli* F-ATPase. Diagram is obtained from [121]

³¹ In-registered implies that every equivalent amino acid pair in the b-dimer is aligned with each other.

The function of the b-subunit is thought to be primarily structural. It forms part of the peripheral stalk, which connects the hexameric head piece ($\alpha_3\beta_3$) to the a-subunit in the membrane, thus forming a structure consisting of $\alpha_3\beta_3\delta b_2a$. This protein assembly is believed to behave like a stator unit with respect to the rotating $\gamma\epsilon c_{10}$ ensemble. Sambongi [122] showed that the c-subunits of intact EF_1F_0 ATPase did indeed rotate with respect to immobilised $\alpha_3\beta_3\delta b_2a$ subunits. In another report, F-ATPase mutants with cross-linked subunits of $\gamma\epsilon c_{10}$ were tested for their ability to synthesise and hydrolyse ATP [123]. The cross-linking was found to have little effect on the functions of the F-ATPases, further proving that the $\gamma\epsilon c_{10}$ move as a single unit.

It was also postulated that the peripheral stalk might serve as an elastic spring, capable of transiently storing the energy for ATP synthesis / hydrolysis [121, 124, 125]. This may be necessary because there is a mismatch in symmetry between the number of protons translocated (ten for *E. coli*) and ATP turnover (three), per complete rotation. One way to smooth out this mismatch is to transiently store energy via elastic elements in the protein. Such an energy storage model in F-ATPase had been considered before [125]. However, for this to be feasible, the interactions between the various subunits must be strong enough to withstand the elastic stress within the peripheral stalk. One can determine this by considering the dissociation constant (K_d) between subunits, which is in turn related to the free energy of binding³². The K_d between F_1 and δ subunit was estimated to be ~ 1.4 nM [126]. It was found that the binding strength could potentially be stronger if the b-subunits were present [127].

³² Standard free energy of binding = $kT \ln(K_d)$, where k is Boltzmann constant and T is absolute temperature. The actual free energy of the bond is however dependent on the concentrations of the binding entities.

The weakest link of this postulation lied actually in the $b - \delta$ interaction [128]. A K_d of ~ 100 nM was obtained for interaction between b -subunit and F_1 , in the presence of Mg^{2+} [129]. This K_d was increased to $1.36 \mu M$ when Mg^{2+} was removed using EDTA³³ [129]. However, these results were obtained using a truncated version of the b -subunit and in the absence of the F_o and might therefore not represent the true binding constant. When the effect of the whole F_o was considered, Krebstakie found that the dissociation constant reduced to ~ 2.7 nM [130]. The standard free energy of binding for this interaction was 48 kJ/mol³⁴. In comparison, the upper limit of the transient elastic energy, estimated as a constant torque of 40 pNnm over 120° , was 50.5 kJ/mol [124]. This was approximately equalled to the free energy for ATP hydrolysis under physiological conditions [131]. If the rotation of the F_1 is broken down into steps, which was shown to occur [132, 133], the transient elastic energy stored is likely to be smaller because of elastic relaxation during dwell times. Furthermore, it was also shown that the main stalk on the F_1 subunit is flexible and may store most of the elastic energy [134]. This can further relieve the peripheral stalk from the elastic strain. The difference between the elastic energy pulling the subunits apart ($\Delta G_{elastic}$) and the standard free energy of binding between the subunits (ΔG°) determines the proportion of intact peripheral stalks versus the disconnected constituents.

$$\Delta G_{elastic} - \Delta G^\circ = kT \ln \frac{[AB]}{[A][B]}$$

Where k is Boltzmann constant, T is absolute temperature. A , B are the constituents subunits and AB is the bound complex (intact peripheral stalk).

³³ Ethylene-diamine-tetra-acetate

³⁴ The actual free energy of binding is difficult ascertain. This is because the energy contributions due to concentrations of the subunits are not known. The use of standard free energy serves mainly as a gross comparison.

From this relationship, it is possible that the peripheral stalk is capable of storing part of the energy needed for the production of ATP while keeping itself intact most of the time, if the amount of elastic energy stored in the peripheral stalk is a small fraction of the standard free energy of binding.

Finally, the b-subunit may also interact with the other subunits to bring about certain conformational changes to the F-ATPase. For example, Kersten reported that the binding of b-subunits in free EF₁ resulted in an increase in the population of β -subunits adopting an “open” conformation (i.e. β_E conformation as discussed earlier) [135].

2.2.2 The c-subunit

The c-subunit monomer is a short membrane protein with a hairpin structure (see Figure 2-5). It comprises two transmembrane helices, joined together via a polar connecting loop [136]. The connecting loop is exposed to the F₁ (cytoplasmic) part of the membrane and contains conserved residues (Arg 41, Gln 42 and Pro 43 in *E. coli*) that interact with both the γ -subunit [88] and the ϵ -EF₁ subunit [90]. Another conserved residue is the Asp-61 (in *E. coli*), found near the middle of the C-terminal helix. Substitution of this residue with glycine or asparagine abolished proton translocation [137]. Reaction of the Asp-61 with DCCD (dicyclohexylcarbodiimide) also resulted in the inhibition of proton pumping by F-ATPase [137]. Furthermore, a modification of four residues around Asp-61 enabled the H⁺ translocating *E. coli* F_o to bind Li⁺ as well [138]. These evidences led to the suggestion that Asp-61 is an important residue responsible for proton translocation in the F-ATPase [137]. In the

case of Na⁺ translocating F-ATPase, multiple residues were found to be responsible for the binding of Na⁺, including the Asp-61 equivalent residue [139, 140].

Individual c-subunits oligomerise, *in vivo*, to form a ring structure. The number of c-subunits in this ring varies between organisms. Jiang et. al reported a preferred number of ten c-subunits in *E. coli*, although nine-subunit rings were also present under his prescribed experimental conditions [113]. Thermophilic bacteria were also found to have ten subunits in the c-ring. Furthermore, it was noted that this number was necessary for the proper function of the F_o as proton channels. Those c-rings containing slightly more or less c-subunits were found to be significantly less permeable to protons [141]. Other organisms with differing numbers of c-rings include the sodium conducting *Ilyobacter tartaricus* and *Propionigenium modestum* which contain eleven subunits [142, 143], a V-ATPase from *T. Thermophilus* [144] with twelve subunits, an A-ATPase (*Methanopyrus kandleri*) and alkaliphilic bacteria (*Bacillus pseudofirmus*) which contain thirteen subunits [145, 146], spinach chloroplast F-ATPase with fourteen [147] and a fifteen-subunit ring in *Spirulina platensis* [15].

High resolution crystal structures of the c-ring of sodium translocating F-ATPase (*Ilyobacter tartaricus*) [139] and proton translocating F-ATPase (*Spirulina platensis*, *Bacillus pseudofirmus*, spinach chloroplast) [15, 146, 148] were obtained only recently. I have chosen the H⁺ *Spirulina platensis* F-ATPase as a reference structure [15]. Notwithstanding this, one can still anticipate, by assuming homology, that the c-rings of other organisms would share similar features. The c-ring of the *Spirulina platensis* has an hourglass shape, with a height of ~ 65 Å. The diameter of this

hourglass is broadest ($\sim 65 \text{ \AA}$) at the top and bottom, and narrowest point ($\sim 54 \text{ \AA}$) at the centre. The inner diameter of the ring is $\sim 26 \text{ \AA}$ at the narrowest and was thought to be filled with lipids [149]. The orientation of each monomer c-subunit is such that the N-terminal helix forms the inner region of the c-ring while the C-terminal helix, which also contains the proton binding Glu-62 (equivalent of Asp 61 in *E. coli*), forms the outer ring. Both the N and C-terminal helices show pronounced inward bends at residue Pro-25 and Glu-62 respectively. These bends point towards the centre of the ring and give rise to the hourglass shape. The extent and direction of the bends, near the ion coordination site, were found to affect the relative distance between the amino acids and hence influence the affinity of the site for ions of different sizes. This was thought to be one of the reasons why the H^+ ATPase has superior affinity towards H^+ over Na^+ . The crystal structure also revealed the proton binding configuration of the Glu-62. In that structure, Glu-62 was in its protonated form and maintained hydrogen bonds with the surrounding residues to give a stable conformation. This 'closed' conformation discouraged the dissociation of the proton from the carboxyl group of Glu-62. It is also worth noting that no water molecule was detected in the proton coordination site of the structure, thereby suggesting that protons, rather than hydronium ions (H_3O^+), were translocated across F_0 . This was in contrast with the Na^+ c-ring where a water molecule was found to contribute to the coordination of Na^+ [150]. The role of H_2O appears settled until a recent structure of the H^+ ATPase of *Bacillus pseudofirmus* was reported to have a water molecule near the proton coordination site [146]. It remains to be seen how these structures will be reconciled.

The main role of the c-ring thus appears to be for the translocation of H^+ (or Na^+) across the membrane. It was found to rotate together with the γ -subunit during both

synthesis and hydrolysis modes [122, 123]. This coupled configuration allows conversion of electrical energy to mechanical energy and finally to chemical energy (and *vice versa*). Detail of the rotation mechanism is given in the section 2.4. Figure 2-5 shows a model structure of the c-ring of *Spirulina Platensis* that is adapted from [15].

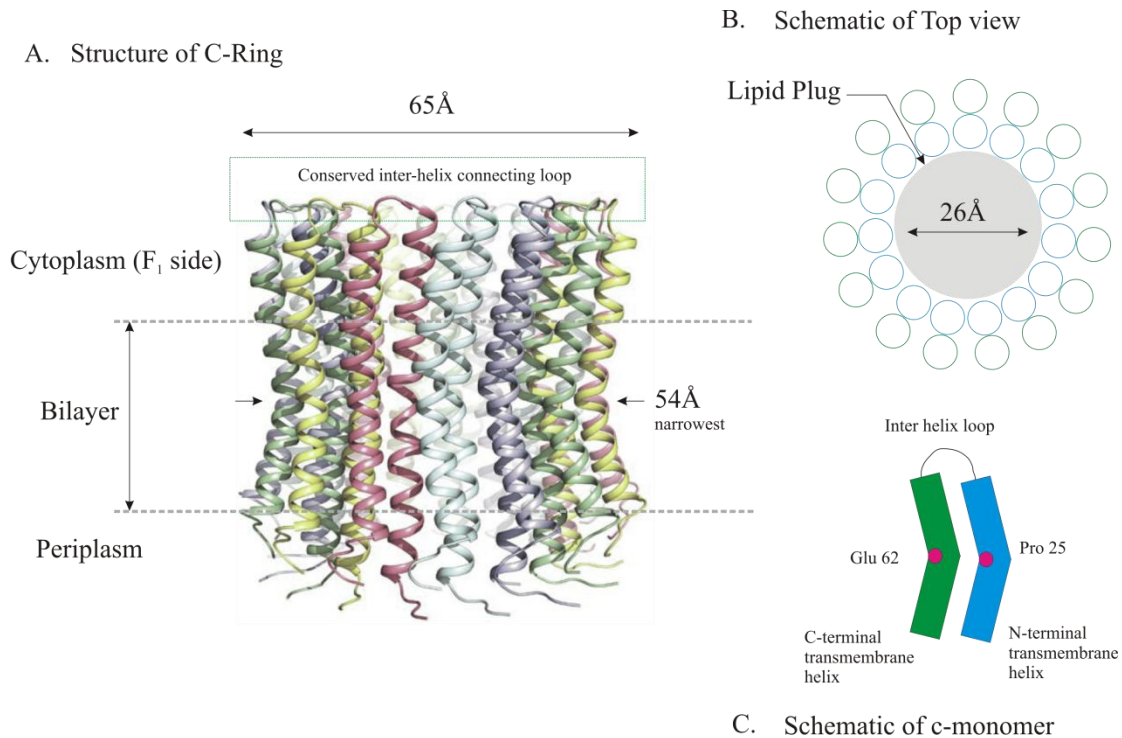


Figure 2-5. A) Structure of the c-ring with respect to the bilayer. Each individual c-subunit is represented by a unique colour. The hourglass shape is clearly evident. Diagram is obtained from [15]. B) Schematic of the c-ring from top view. The centre of the ring was thought to be filled with lipids. C) Side view of a c-monomer. Bends at Glu 62 (equivalent of Asp61 in *E. coli*) and Pro25 form the hourglass shape. The N-terminal helix (blue) resides at the interior of the c-ring while the C-terminal helix (green) lies at the outer periphery of the ring.

2.2.3 The a-subunit

The a-subunit is probably the least understood of all the subunits in the F-ATPase. Its high resolution structure is currently still not known. What is known, however, is the topological structure of the subunit. These are predicted structures obtained from indirect biochemical and mutagenesis experiments. From cross-linking and mutagenesis experiments, the proximity between residues was estimated [151, 152]. Moreover, by labelling the inter-helix loops with markers, one can predict the number of loops between helices and whether they reside on the periplasmic or cytoplasmic side of the membrane [153-156]. This data has provided a working model of the a-subunit. The currently accepted model contains five trans-membrane helices, linked together by inter-helix loops. The N-terminus of the a-subunit was thought to reside at the periplasmic domain while the C-terminus locate at the cytoplasmic domain [153-155]. For easy reference, these five trans-membrane helices are denoted as TMH1 to TMH5. See Figure 2-6.

Using electron cryo-microscopy, Rubinstein [157] studied the morphology of intact MF-ATPase and suggested that the a-subunit lay immediately beside the c-ring. This was supported by crosslinking experiments, where cysteine modified c-subunits and a-subunits were found to react with each other via their newly introduced thiol groups [158]. Moreover, the crosslinked residues were close to both c-Asp61 and a-Arg210 [158]. As these two residues were known to be critical for proton translocation [137, 159-162], it indicated that the proton translocation process is likely to occur at the a/c subunit interface. Besides interacting with the c-subunit, the a-subunit is also able to form a stable complex with the b-subunits, which could be purified without any need for crosslinking [163]. This shows that, besides lying next to the c-subunit, the a-

subunit is also in close proximity with the b-dimer. Interestingly, it was found that the a-subunit is not mandatory for the insertion of b and c-subunits [159]. It therefore has a small contribution in terms of maintaining the structural integrity of the F-ATPase, but is crucial in mediating proton translocation across the membrane [111].

E. coli mutants with deleted a-subunits were unable to grow in succinate buffer (i.e. unable to oxidise succinate to produce ATP [159]). As mentioned earlier, one of the most important residues that mediate this process is the a-Arg210 (in *E. coli*). Mutation of this conserved residue into various other amino acids (Lys, Gln, Val, Ile) prevented the functional proton translocation in F-ATPase [159-162]. As already discussed earlier, c-Asp61 is responsible for the binding and release of protons. The caveat to this is that c-Asp61 is located inside the bilayer, which is highly hydrophobic. There must therefore be a means for the protons to migrate into the c-subunits and interact with c-Asp61. It was suggested that the role of the a-subunit is to provide such an aqueous access for the c-Asp61 [164]. Using cysteine mutations on the a-subunits and chemicals³⁵ that react with thiol groups, Angevine et. al. was able to map the part of the a-subunit that had an aqueous environment [164-166]. After juxtaposing these parts with the predicted structure of the a-subunit [151], Angevine suggested that TMH1, TMH2 and TMH3 can form a half channel that connects to the periplasm, while TMH4 and TMH5, form the second part of the half channel that connects to the cytoplasm. Steed [167] did similar experiments, but modified the c-subunits, instead of the a-subunits. He was able to show that aqueous access to the c-subunit was strongly enabled by the presence of the a-subunit and that only one c-subunit in the c-ring (presumably the one that was exposed to the exterior of the

³⁵ Ag⁺, NEM (N-Ethyl maleimide) and methane thiosulfonate derivatives. These chemicals are known to preferentially react with the ionised thiolated form of cysteine – thus a good indication of accessibility to aqueous environment.

vesicle via a-subunit) was found to have its cysteine modified by NEM used. This further supports the hypothesis that the a-subunit enables proton translocation by providing an aqueous pathway across the membrane. Besides forming the aqueous pathway, the a-subunit was also thought to help regulate ion translocation across the membrane, via the Arg210. This residue is able to prevent “short-circuiting” of the proton path [168] and assist in the protonation and deprotonation of c-Asp61 [114]. This is discussed further in the next section.

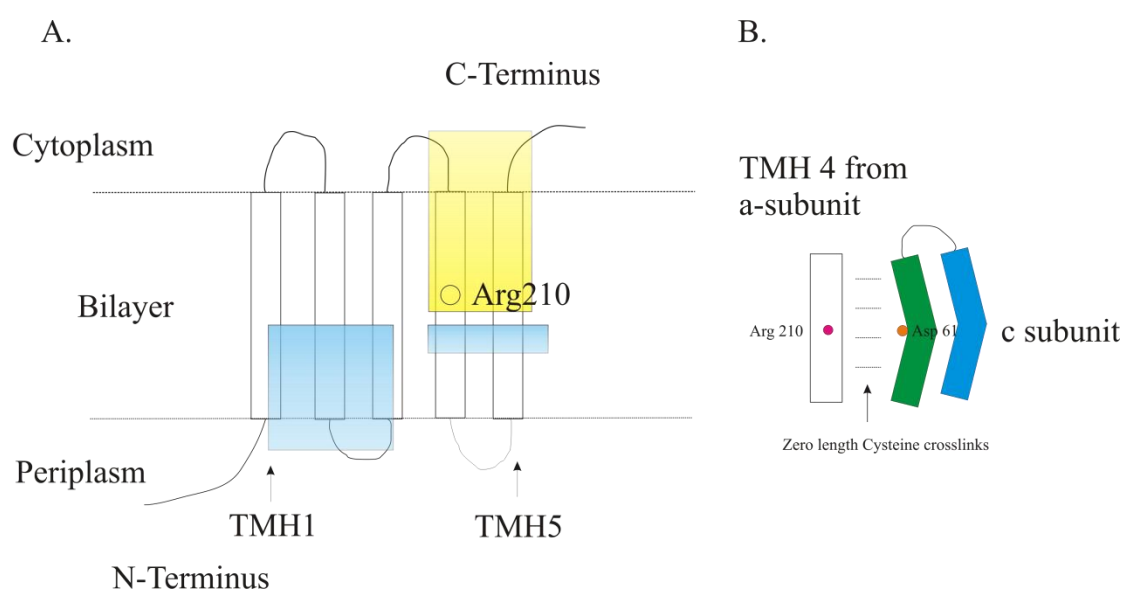


Figure 2-6. A) A schematic of an a-subunit showing a predicted five trans-membrane helix structure. Exact packing of the TMHs is unclear. Area shaded in yellow contains residues thought to be responsible for the half channel at the cytoplasmic end. Area shaded in blue is the second half channel at the periplasmic end. This is based on the data in [164]. B) Shows a schematic of the crosslinking experiment between the residues on TMH4 of the a-subunit and C-terminal helix of the c-subunit. The interface between the two subunits also contains the residues responsible for proton translocation (i.e. c-Asp61 and a-Arg210). This diagram is adapted from [158]

2.3 Summary of the Structure of F-ATPase

In this section, the structures and functions of the eight subunits that constitute the *E. coli* F-ATPase are presented. These eight subunits correspond to the simplest F-ATPase found in nature. More complicated F-ATPases can be found in eukaryotes.

With knowledge of the structure of various subunits and their relative location, a model of F-ATPase has been predicted. A cartoon of this model is given in Figure 2-7.

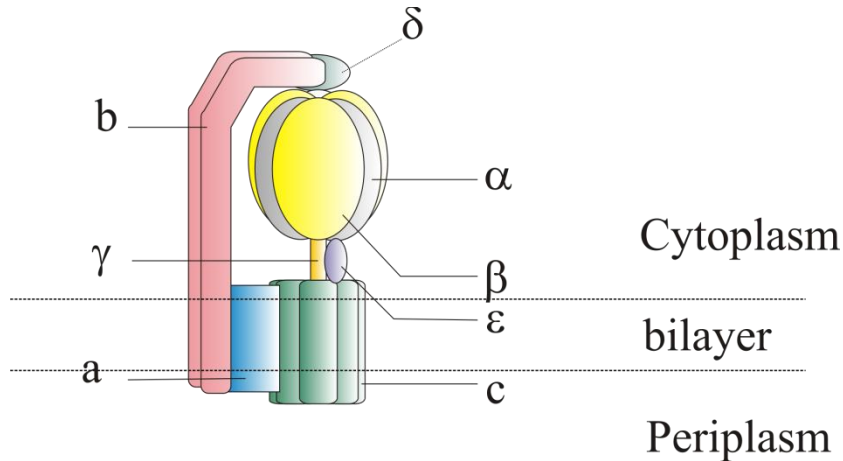


Figure 2-7. Current model of the *E. coli* F-ATPase

It has been shown that F-ATPase can be divided into two portions – the F_1 ATPase and F_0 ATPase. The former forms the water soluble part of the F-ATPase and is made up of five different subunits ($\alpha_3\beta_3\delta\epsilon\gamma$), while the latter contains three membrane embedded subunits (ab_2c). The α and β -subunits are arranged in an alternating sequence to form a six-segment headpiece. Located at the interfaces of the α and β -subunits are the nucleotide binding sites. There are thus six sites available for ATP binding when the subunits are arranged in a circular manner. However, only three of these sites, containing mainly residues from the β -subunits, are able to catalyse the hydrolysis or synthesis of ATP. Crystal structures have revealed that the three β -subunits are not of the same conformation. Rather, each one has a different affinity for nucleotides and represents a different phase during the ATP turnover cycle. These dissimilar characteristics of genetically identical β -subunits were thought to be due

them seeing different parts of the asymmetrical central stalk ($\gamma + \epsilon$ -subunits) during the different phases of the rotation.

The γ -subunit is a protein with a coiled coil structure that penetrates into the headpiece and a main stalk that binds with the c-ring and ϵ -subunit. It interacts with the hexameric headpiece by forming transient hydrogen bonds and obstructs the rotation of β_E , resulting in stabilisation of intermediate states during rotation and distortion of the β_E . The γ -subunit, ϵ -subunit and c-ring have been shown to rotate as a single body, with respect to the stator assembly comprising $\alpha_3\beta_3\delta ab_2$.

As the membrane embedded c-ring rotates with the γ -subunit, it can transport ions across the membrane. It does this by binding ions from one side of the membrane and releasing them into the other. The number of ions transported per revolution is the same as the number of c-subunits in the c-ring. The ion binding site in the c-subunit is located near the middle of the membrane. It therefore requires aqueous channels across the membrane to close the ion circuit. These channels were thought to be provided by the a-subunit. One of the F_o models predicts two half channels from the a-subunit, one connecting to the periplasm and the other to the cytoplasm.

The remaining subunits serve mainly structural purposes. The ϵ -subunit (*E. coli*) is necessary to hold the F_1 onto the c-ring, although it has also been shown to inhibit the hydrolysis activity of the enzyme. The δ and b-subunits form the peripheral stalk, whose functions are to connect the stator assembly together and also likely to act as an elastic spring for transient storage of energy during ATP synthesis.

With the structure and function of the subunits now understood, I will move on to look at the mechanisms in which the F-ATPase uses to synthesise and hydrolyse ATP.

2.4 Current Understanding of F-ATPase – Mechanism of F₁ and F_o ATPase

2.4.1 Binding Change Mechanism – F₁ rotation

In the previous section, I have mentioned briefly, the binding change mechanism proposed by Boyer [51]. This is the first model which postulates that ATP turnover is directly due to the cooperative interaction between the catalytic sites of F₁. The gist of the three-site model [54] is as follows: There are three catalytic sites in the F-ATPase. Each of these sites takes turn to adopt conformations of different affinity for nucleotide (ATP / ADP). The tightest site was found to have a K_d value of $\sim 10^{-10}$ M (*E. coli*) / 10^{-12} M (mitochondria) [87, 169] while the weakest site has K_d ~ 150 μ M [169]. At a low ATP to F₁ ratio, ATP binds to the catalytic site with the highest nucleotide affinity and is hydrolysed to form ADP and phosphate ions. However, the overall enzymatic rate is low because the hydrolysed products remain tightly bound [170]. This situation changes if excess ATP is present to bind to a second catalytic site. The presence of this ATP causes a simultaneous loosening of the first binding site and tightening of the second binding site [54], thus allowing the hydrolysed products to escape. This results in a dramatic increase in catalytic activity by $\sim 10^6$ fold [169]. The hydrolysis rate can further be increased by the presence of a nucleotide in the third catalytic site [169]. The sequential changing of affinity in each

of the three binding sites, in tandem with the state of bound nucleotide, forms the crux of the binding change mechanism. See Figure 2-8.

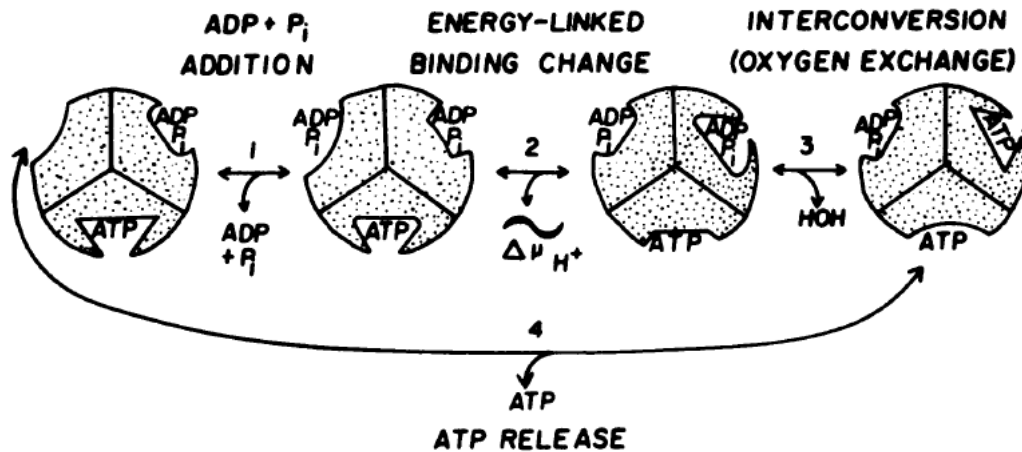


Figure 2-8. A schematic of the binding change mechanism proposed by Boyer et. al. Synthesis direction is from left to right while the hydrolysis is from right to left. Tight binding site is denoted by triangular binding sites. Diagram is obtained from [83]

The binding change mechanism was formulated in the 1970s and 80s. It is amazing how intricate mechanisms of single molecules could be inferred by observing average property changes using ensemble level experiments. With the advent of single molecule techniques, scientists have been able to make further inroads into the understanding of F-ATPase. They can now introduce changes in the environment or mutations to proteins, and observe directly the result of these changes, one molecule at a time. Using this approach, the chemo-mechanical coupling between ATP hydrolysis and rotation of the γ -subunit has been intricately mapped out. In this section, the mechanisms of both F₁ and F₀ ATPase are discussed

2.4.2 Chemo-Mechanical Coupling of F₁ rotation

The first direct observation of single molecule F₁ ATPase was made by Noji in 1997 [27]. It provided the much awaited evidence that proved, unequivocally, the rotary characteristics of F-ATPase. When this result was first presented in the American Biophysical Society Meeting more than a decade ago, spontaneous applause was reported to have erupted from the audience. Not only has this experiment shown what the binding change mechanism has predicted, it also provided scientists with a powerful technique to probe deeper into the mechanisms of the enzyme. The idea for the experiment is elegant and straight forward: Using mutant F₁ ($\alpha_3\beta_3\gamma$) from thermophilic bacteria, Noji immobilised the $\alpha_3\beta_3$ on a coverslip and label the rotating γ -subunit with a fluorescent filament. He observed a counter-clockwise rotation of the filament at a maximum speed of ~ 4 Hz. These rotations also appeared to have pauses spaced at 120° apart, corresponding to the turnover of one ATP. Every complete rotation therefore involved a turnover (hydrolysis / synthesis) of three ATPs, as predicted by the binding change model and crystal structures.

Yasuda [133] further resolved the 120° angle into sub-steps of 90° and 30° . In between these step changes were two dwell times. The first dwell time happened after the γ subunit had moved 30° (from -30° to $0^\circ \rightarrow 0^\circ$ was arbitrarily defined as the orientation of γ -subunit after it had made the first 30° step change). This dwell was dependent on the concentration of ATP in the buffer and attributed to the time taken for ATP to bind F₁. Binding of ATP in turn, triggered the 90° step change. The second dwell time was the time lapse between the end of the 90° step and start of the next 30° step. The latter was thought to be activated by the release of hydrolysed products

[132, 133, 171]. These stepping angles were later refined from $90^\circ/30^\circ$ to $80^\circ/40^\circ$ by Shimabukuro [171] and Nishizaka [132]. For consistency, 80° will now be used to represent the first sub-step and 40° to represent the second sub-step. The dwell after the 40° step is called the ATP binding dwell and the dwell after the 80° step, the catalytic dwell. Figure 2-9 shows the graphical representation of these angles in an ideal stepping trace.

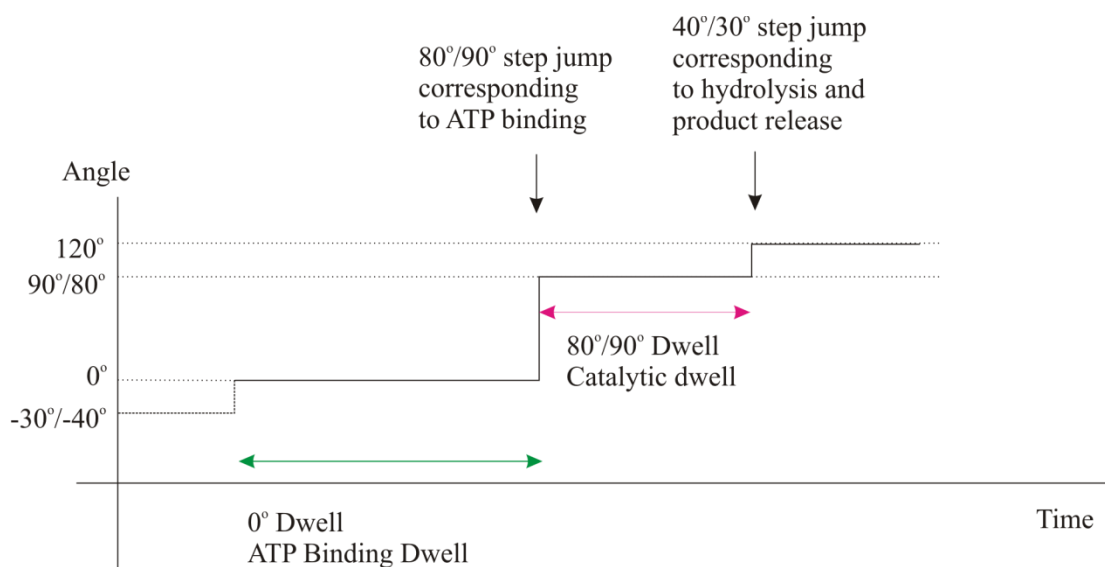


Figure 2-9. Idealised time trace of the stepping angle made by a rotating γ -subunit. The y-axis represents the angle of rotation and the x-axis the time. 0° is defined to be the orientation of γ after the end of the $30^\circ/40^\circ$ substep. The waiting time between the end of the $30^\circ/40^\circ$ substep and start of the $90^\circ/80^\circ$ substep is ATP dependent and hence called the ATP binding dwell. The dwell after the $90^\circ/80^\circ$ substep and before the $30^\circ/40^\circ$ substep is dependent on the catalytic activity at the nucleotide binding site. It is called the catalytic dwell.

Furthermore, the catalytic dwell was found to consist of two reactions of about 1 ms each [133]. To investigate this further, Shimabukuro [171] specifically slowed down the activity at the catalytic site by using F_1 mutants that could not effectively cleave ATP or an ATP analogue that does not get hydrolysed easily. He reported that while the catalytic dwell time increased significantly, the ATP binding dwell remained largely unchanged. This indicated that the cleaving of the phosphate bond happened during the catalytic dwell. Furthermore, Adachi [172] showed that the catalytic dwell

is also strongly dependent on the phosphate concentration in the buffer and that frequent back steps were seen if the phosphate concentration was increased significantly. He thus proposed that the release of phosphate also happens during the catalytic dwell and is responsible for the 40° rotation of the γ subunit. The two reactions that happen during the catalytic dwell are therefore thought to be the hydrolysis of ATP and release of phosphate product. To complicate matters, it has been mentioned recently that a third process may be present at the catalytic site [173, 174].

In addition to the type of reactions taking place during the dwells, scientists are also interested to know when and where the hydrolysed products are released. Using slow hydrolysing fluorescent ATP as markers, Nishizaka [132] demonstrated that bound ATP is not hydrolysed until the γ -subunit rotates 200° and ADP is not released at least until 40° later. The latter finding was further supported by recent experimental evidence from Shimo-Kon using tryptophan fluorescence quenching [174]. As for the release of phosphate, it is still not known whether it is released immediately after hydrolysis or 120° later [22, 174]. Taken altogether, the chemo-mechanical coupling scheme of F_1 ATPase is proposed to be as follows:

- ATP binds to empty catalytic site (1). Moves the γ -subunit by 80° . Figure 2-10 - I
- This process is accompanied by the simultaneous ADP release at site (2). Figure 2-10 - II
- Hydrolysis of ATP at site (3) occurs. Figure 2-10 - III

- Phosphate at site (2) or site (3) is released (Scheme A or B of Figure 2-10), causing a further rotation of 40° in the γ -subunit. It is currently not certain which phosphate is released from the enzyme. Figure 2-10 - IV
- Site 2 is now ready to bind a new ATP and the cycle repeats

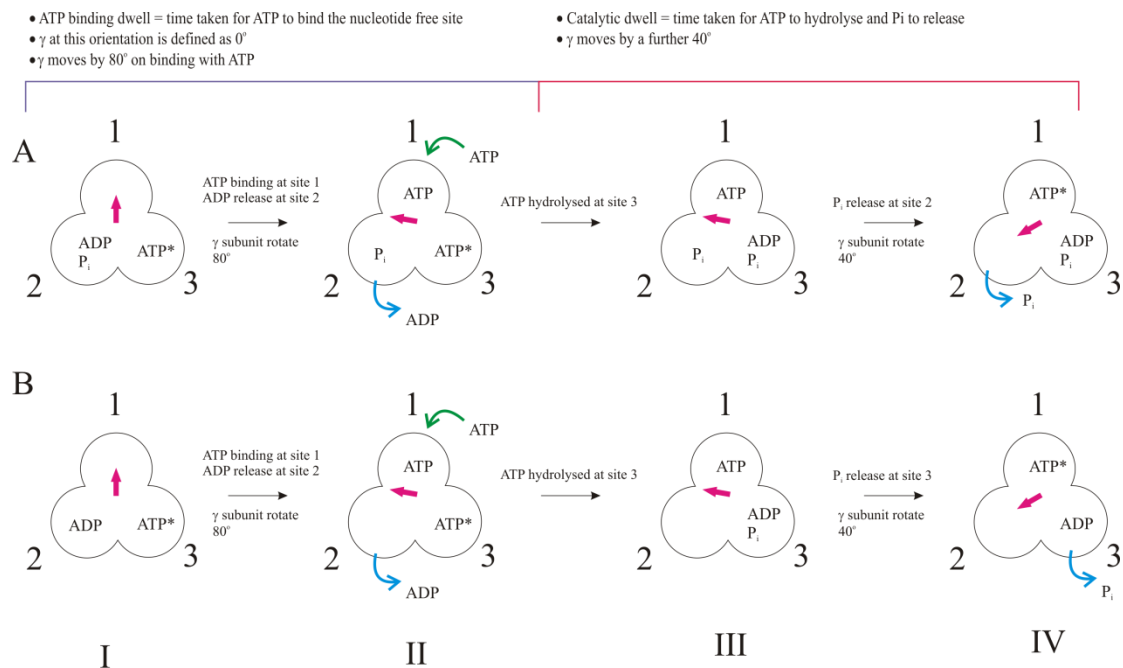


Figure 2-10. Schematic showing the coupling between chemical cycle and the mechanical cycle. “*” represents strong binding of ATP by the catalytic site. In scheme A, the phosphate ion is released one phase later than scheme B. The catalytic sites are labelled 1, 2 and 3. The different states of the enzyme are labelled state I – IV.

2.4.3 Theoretical Model of Torque Generation in F_1

A theoretical model of how torque is generated in F_1 is put forth, in details, by Oster [175, 176] and Kinosita [131]. This model takes into account the crystal structure, as well as data from single molecule experiments. Qualitatively, it can be summarised as follows:

As ATP binds to a free catalytic site in F_1 , a sequence of weak hydrogen bonds is swiftly formed between the nucleotide and the β -subunit. This binding is akin to a

zippering effect, resulting in a closing up of the binding pocket and bending of the β -subunit towards the γ -subunit, near the cavity entrance of the hexameric head piece. The free energy of binding is consumed to do two different types of work. Part of the energy is used to push the asymmetrical γ -subunit, resulting in a rotary motion of 80° . This provides the first power stroke of rotation. The other part of the binding energy is stored as elastic energy, ready to be used when the phosphate product is released. Thereupon, the second power stroke is executed and γ -subunit moved by another 40° . This model is further supported by recent findings that part of the torque for rotation is generated at the base of the hexameric headpiece [84, 85]. Due to the gradual annealing of the hydrogen bonds during binding, a relatively constant torque can be generated, which is consistent with experimental data [131, 133]. Furthermore, as the free energy is tightly coupled directly to mechanical transition and elastic energy storage, the motor can attain a very high efficiency. It has been pointed out that the thermodynamic efficiency of the motor is close to 100% [131]. Notably, this efficiency is not the Stokes efficiency reported previously [177], but the true efficiency of the motor. The main difference between the two is that while the former represents how tightly coupled the energy transduction is, the latter (Stoke's efficiency) describes how consistent the driving force is applied by the rotor (See references for explanation) [178, 179]. Incidentally both the efficiencies are close to 100% for F_1 .

The role of the actual cleavage of the phosphate bond in ATP has so far not been mentioned in the general scheme of things. It was found that the hydrolysis step is energetically neutral [169], i.e. there is no free energy change when the phosphate bond is cleaved. So what role then, does this process play in the rotation of the

enzyme? It was thought that the hydrolysis facilitates the release of products, so that the site can be reset to accept a new ATP molecule [175].

2.4.4 Inhibited state of the F_1

Before moving on to F_o , I will like to discuss about an inhibited state, which F_1 can lapse into, but is not represented in the schematic above (Figure 2-10). This state is characterised by prolonged inactivity of the enzyme and known to be induced by the presence of ADP [180, 181]. It is, by no surprise, known as the ADP inhibited state. Hirono-Hara tried to observe single molecule rotation of TF_1 and noted the angle made by the γ -subunit, when the enzymes lapsed into long pauses [180]. He found that these stalling angles coincide with the catalytic dwell angles of the enzyme and concluded that the ADP inhibited state happens at the catalytic dwell conformation [180]. Furthermore, it was earlier proposed that the first reported crystal structure of F_1 [21] corresponded to that of the ADP inhibited state as well. This postulation was later vindicated by Okuno [182], who proved that the crystal structure indeed represented the catalytic dwell state and that an ADP resided at the site where active catalysis was suppose to occur. It was likely that the ADP inhibited the F_1 by presenting itself at the active catalytic site. The F-ATPase, in anticipating an ATP, could not proceed further with the hydrolysis and became stalled.

2.5 Mechanism of F_o Rotation

The mechanism of the F_o motor is less certain because the structures of the subunits have either just been obtained (for the c-subunits) or are not yet available (for a-subunits & part of b-subunit). There are currently two models explaining how the F_o

motor can translocate ions when it rotates inside the membrane [111, 183-187]. The first model is used primarily to describe the mechanism of the Na^+ driven motor while the second model is used for the H^+ driven motor. These models differ mainly in the way ions are exchanged with the cytoplasm and the presence (or absence) of a horizontal channel in the a/c interface³⁶. Consequently, their free energy profiles at different stages of rotation are also different. In this section, I will first present the general concepts of ion translocation that are shared by the two models. This will then be followed by a more detailed discussion, highlighting the major differences and their implications.

Before going through the two main models, it is probably instructive to first recapitulate on what has been discussed about the structure of F_o . It is known that the simplest F_o consists of three subunits \rightarrow “a”, “b” and “c”. Most of these subunits are embedded inside the membrane. The subunit that connects to the rotating γ stalk is the c-subunit. It exists as an oligomer, forms a ring-like structure and can rotate together with the γ stalk. Each subunit on the c-ring contains one or more amino acid residues that bind to the target cation meant for translocation. In *E. coli* F_o , this residue is the Asp-61 [137], while in *P-modestum*, three residues (Glu-65, Gln-32 and Ser-66) were thought to be crucial for the binding of Na^+ [186]. Located on the exterior of the c-ring is another trans-membrane protein called the a-subunit. This subunit contains a positively charged arginine residue, which is also absolutely necessary for ion translocation [162]. The movement of ions across the membrane is mediated by the a/c interface. In the current understanding of F_o , the c-ring is thought to rotate with

³⁶ Interface between the a-subunit and c-subunit

respect to the a and b-subunits. Energy from this rotation comes either from the hydrolysis of ATP by F_1 , or an ion flux across F_0 .

The common features of F_0 rotation is summarised in Figure 2-11 and explained as follows: A cation (Na^+ or H^+) bound c-subunit enters the a/c interface from the left, where it interacts with the arginine residue on the a-subunit. At this position, the c-subunit is exposed to the cytoplasmic part of the membrane, via a half channel that connects the ion binding site to the cytoplasm. In conditions favourable for synthesis, there is a net ion motive force from the periplasm to the cytoplasm. i.e. the concentration of cation at the cytoplasm is lower, and/or the electrical potential less positive, than the periplasm. These conditions, aided by the positive charged arginine, favour the dislodging of the cargo cation to the cytoplasmic domain. After losing its cation, the empty c-subunit becomes negatively charged and is readily pulled by the positively charged arginine residue on the a-subunit. This movement causes the c-ring to rotate in the synthesis direction and brings the empty c-subunit in contact with another half channel that connects to the periplasmic domain. With a higher concentration of cations in the periplasm, the c-subunit readily rebinds a new cation. The occupied c-subunit can then leave the a/c interface and enter the membrane. This scheme thus sees a net transfer of charges from the periplasm to the cytoplasm, and couples it with the rotation of the c-ring.

One of the main differences between the Na^+ conducting F_0 model and H^+ model is the ability of the c-subunits of the former to freely exchange Na^+ with the cytoplasm, even when they are not in the a/c interface [188-190]. It was suggested that the half channel linking the cation binding site of the c-subunit to the cytoplasm, is formed by

the c-ring itself and not at the a/c interface. The implication of this is that bound Na^+ on the c-subunit can freely exchange with those in the cytoplasm once it leaves the a/c interface. Unlike the H^+ model, there is no need for the c-ring to rotate a full round before the ion can be released. However, a recent crystal structure of the Na^+ c-ring [139] could not support the presence of such aqueous half channels. This was quickly reconciled by the suggestion that temporary half channels, between the ion binding sites of the c-subunits and cytoplasm, might be formed by “dynamic fluctuations” in the c-ring [139]. Such fluctuations could allow ion exchanges but need not manifest as obvious channel-like structures. Nonetheless, in the latest model of the Na^+ F_o [111], the authors had appeared more ambivalent about the idea of such cytoplasmic channels outside the a/c interface. Another unique aspect of the Na^+ model is the existence of a horizontal channel, at the a/c interface, linking the two half channels together. This horizontal channel was postulated to convert the vertical electro-potential across the membrane to a horizontal potential difference between the half channels. The horizontal potential difference helps the arginine to align favourably during synthesis (or hydrolysis) [111] and drives the rotation of the c-ring in the direction of positive potential [186].

Figure 2-11a shows a schematic of the Na^+ conducting F_o , with the accompanying free energy diagram at the bottom. Two main features are identified in this model [186]. The first is a power stroke mechanism caused by charge interactions between the positive arginine, negative c-subunit and the horizontal potential difference. This pushes the empty c-subunit in the synthesis direction (state 3→4). Once it has moved past the arginine, the empty c-subunit remains trapped in an energy minimum (state 4) until it is able to bind a new Na^+ from the periplasm. Thereafter, it will be free to

escape into the membrane on the right. This ratchet mechanism forms the second aspect of the rotation, which is essential to prevent back stepping of the c-ring.

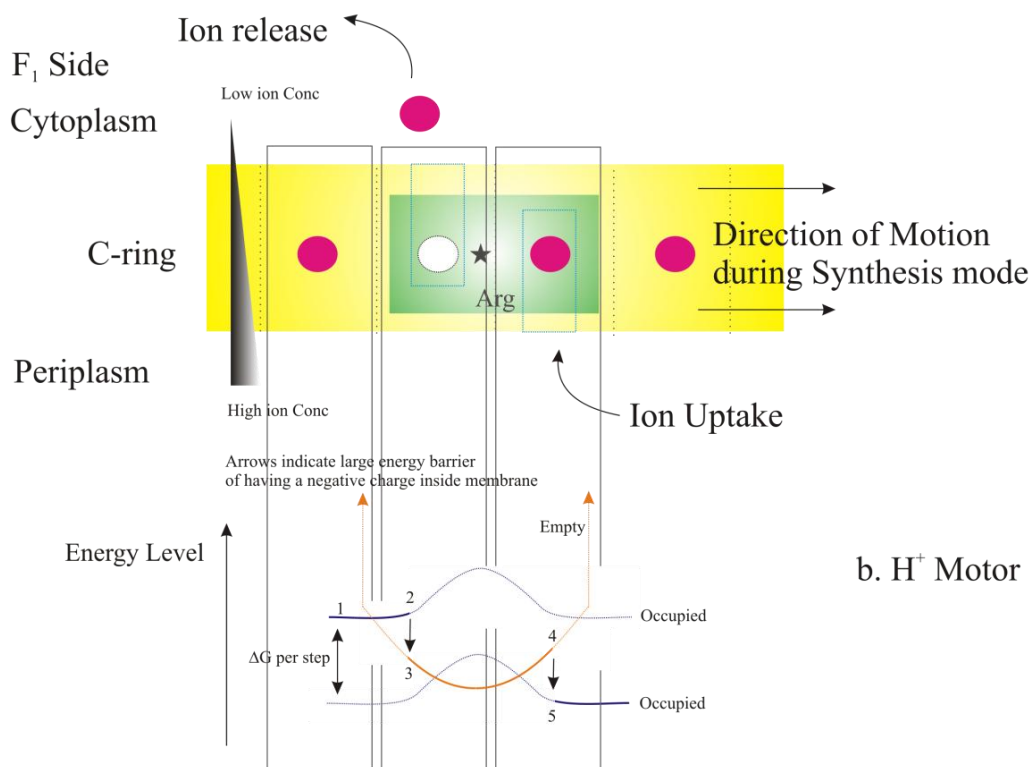
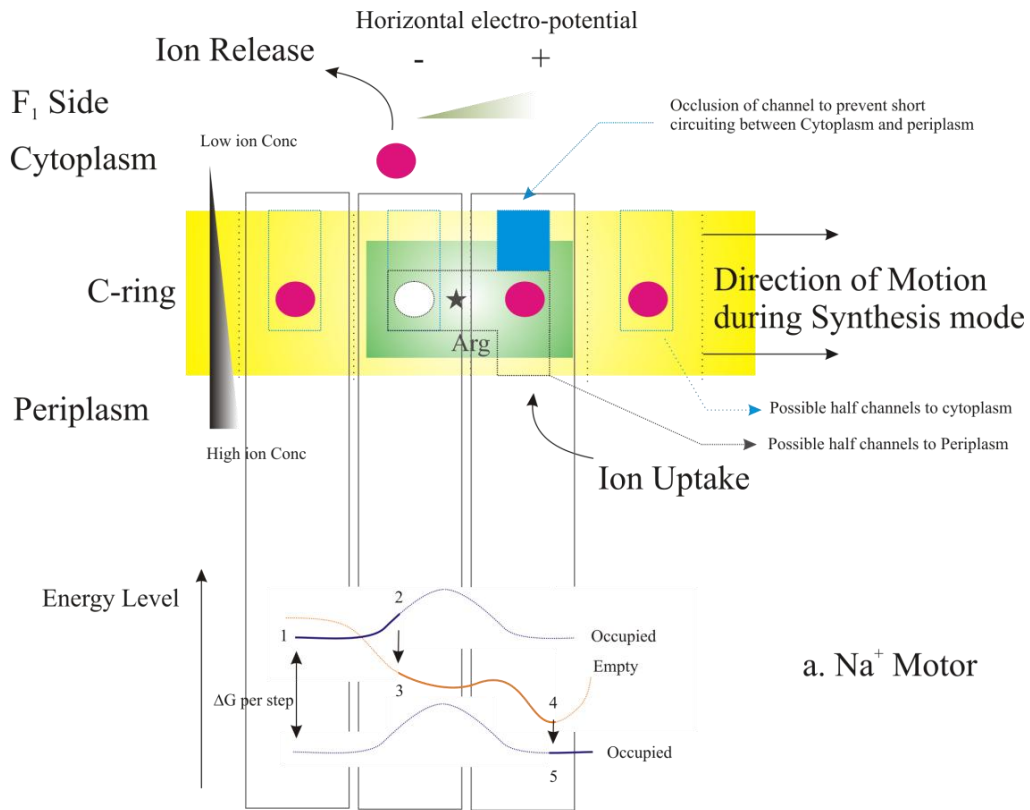


Figure 2-11. Schematics of the ion translocation in F_0 . The respective energy profile is below each schematic. The blue line represents the energy profile of a cation occupied c-subunit while the orange line represents that of an unoccupied subunit. The bold traces refer to the path taken during rotation. Schematic a. shows the salient features of the Na^+ driven motor. The half channel connecting to the cytoplasm is intrinsic to the c-ring. Furthermore, there is a horizontal electro potential difference across the a/c interface. This potential provides a power stroke for the movement of the c-ring. When an occupied c-subunit enters the a/c interface from the left, the presence of the positive arginine causes the c-subunit to lose its cargo (2→3). The now negatively charged c-subunit continues to move to the right, pulled by the horizontal potential as well as the Arg residue (3→4). Once in contact with the periplasm, the c-subunit is stabilised by the aqueous environment and remains there until it re-gains a Na^+ (4→5). Thereafter, the c-subunit can leave the interface to the right. Schematic b) shows the mechanism of the H^+ F_0 . Both the half channels are in the a/c interface. Furthermore, a horizontal electro potential is also missing (at least in the original version). The motor works on a thermal ratchet model. An occupied c-subunit moves in from the left and into the a/c interface. The low concentration of ion favours the c-subunit to lose its cargo (2→3). Thereafter, it slips into a potential well, stabilised by the electrostatic interactions with the arginine residue. This is a stable state but can be perturbed via thermal energy from the surroundings (3↔4). The perturbation can move the c-subunit to both the left and right. However, there is a strong preference to escape to the right. This is because there is a higher chance that charged c-subunit will meet a proton if it escapes to the right (periplasmic half channel) than to the left (cytoplasmic half channel). After gaining a proton (4→5), it can continue to move into the membrane, hence moving the ring forward in the right direction. The explanation given above is for movement in the synthesis direction. The schematics are adapted from [111]. Energy profiles for a) are adapted from [111] while those of b) are inferred from the mechanism described in [183].

The proton driven motor was suggested to work on a slightly different premise [183, 184]. Unlike the Na^+ motor, there is no access of the H^+ binding site by the cytoplasm outside the a/c interface. This means that those c-subunits that are surrounded by the hydrophobic lipid environment (i.e. outside the a/c interface) must be uncharged. If not, a large free energy will be incurred to maintain the negative charge in the hydrophobic environment. Consequently, only uncharged (i.e. protonated) c-subunits can enter or exit the a/c interface. The aqueous access to cytoplasm and periplasm is provided by two half channels on the a-subunit. Presence of these half channels was recently experimentally corroborated by the work done in the Fillingame lab [164-166].

In the proton driven model, the motor is powered mainly by a thermal ratchet mechanism, biased by the unequal proton motive force across the membrane and the influence of the arginine residue at the a-subunit [183]. It was however mentioned,

that a pure thermal ratchet model is insufficient to provide the necessary torque for ATP synthesis and the presence of a horizontal channel similar to the Na^+ driven motor was suggested [191]. Figure 2-11b shows a schematic of the model for the H^+ driven motor.

It remains to be seen how these models can eventually be reconciled. It may be true that despite their homology, the Na^+ conducting F_o functions differently from its H^+ counterpart. Alternatively, a new unifying model combining the features of both models may be formulated in the future. The key to this part of the puzzle lies probably in the structure of the a-subunit. Knowing the structure of the a-subunit with respect to the c-ring will provide convincing evidence of the mechanism of ion translocation. One of the important questions to be answered is whether the a-subunit provides a single or two half channels. And if the former is true, how then can the ion be released into the cytoplasm outside the a/c interface, despite a lack of structural evidence in the c-ring. Furthermore, the structure of the a-subunit will reveal the contribution of the arginine residue on the ion translocation process and whether a horizontal channel is actually present in the a/c interface.

Further on the function of F_o , it is probably worth mentioning about the ion motive force that is powering its rotation. The energy that drives the F_o motor can be divided into two components. The first part comes from the electrical potential difference across the membrane, while the second is a chemical potential gradient. Equation 2-1 shows the breakdown of the net proton motive force into the two contributing components.

$$PMF_{p \rightarrow c} = \Delta V_m + \frac{kT}{e} \ln \frac{[H^+]_{periplasm}}{[H^+]_{cytoplasm}} = \Delta V_m - \frac{2.3kT}{e} \Delta pH_{p \rightarrow c} \quad \text{Equation 2-1}$$

Where $PMF_{p \rightarrow c}$ is the proton motive force from periplasm to cytoplasm, ΔV_m is the electrical potential, k is the Boltzmann constant, T is the absolute temperature, e is the electron charge, $[H^+]$ is the concentration of the proton and $\Delta pH_{p \rightarrow c}$ is the pH difference between the periplasm and cytoplasm.

Dimroth showed that, contrary to common belief, these two components of the driving force are actually not equivalent in F_1F_0 ATPase [192]. An electrical potential difference is absolutely necessary for the synthesis of ATP. This was demonstrated to be true in *P. modestum* [193], *E. coli* [194] and chloroplasts [195]. Feniouk however suggested that this dependence is due to the interaction between F_1 with F_0 and not the intrinsic characteristics of F_0 itself. Isolated F_0 appear to treat these two terms as equal and does not require a mandatory voltage to rotate [187]. Further inconsistency is created when a V-ATPase from *T. thermophilus* was recently found to synthesise ATP via only a pH gradient [144]. One of the motivations of this project is thus to answer the question of whether the two components of PMF are thermodynamically equivalent.

2.6 Summary of Mechanism of F-ATPase

In this section, the possible mechanisms describing the rotation of both F_1 and F_0 ATPase are separately discussed. The basic tenet of F_1 rotation is the “binding change mechanism”. This model states that the activity of any one catalytic site on F_1 is

dependent on the states of the others. To achieve high enzymatic rates, the binding sites have to function in a choreographed sequence of events: When ATP binds to an empty catalytic site, the β -subunit experiences a conformational change, which pushes the asymmetrical γ -subunit and causes it to rotate by 80° . This is followed by the hydrolysis of an ATP and a release of phosphate ion in the adjacent catalytic site/s. The latter provides the remaining energy for the γ -subunit to move by another 40° . ATP bound to the enzyme will not be hydrolysed until it has moved 200° , while the ADP product is not released until 240° after binding. There are also two dwell times in between the angular changes. The first is dependent on the binding of ATP and is called the ATP binding dwell. The second is dependent on two back-to-back reactions: 1) The rate at which the enzyme cleaves the phosphate bond on the ATP; 2) The rate of phosphate release from the catalytic site. This combined dwell time is called the catalytic dwell. Finally F_1 can lapse into an inhibited state, whereupon it will stop rotating for an extended period of time. The structure of this state has been solved and found to have the same dwelling angle as the catalytic dwell state.

The mechanism of F_o rotation is less certain. Two models are generally accepted at this point to describe the Na^+ translocating F_o and H^+ translocating F_o . The common feature of these two models is the strong coupling between ion flow and rotation. i.e. directional rotation of the c-ring requires a close coordination of ion movement from the cytoplasm to the periplasm or *vice-versa*. Also featured strongly is the contribution of the arginine residue in facilitating the movement of protons. In the Na^+ model, the periplasmic half channel is provided by the a-subunit while the cytoplasmic half channel is intrinsic to the c-ring. There is also a horizontal channel, linking both the half channels, which converts the vertical potential difference across

the membrane into a horizontal potential difference across the channels. The rotation of this model is powered by a combination of thermal ratchet and power stroke mechanism. The H^+ model is slightly less complicated, with both half channels provided by the a-subunit. As such, there will be no exchange of H^+ between the c-subunit and cytoplasm outside the a/c interface. In the current model, there is also no horizontal drop in potential at the a/c interface to provide the partial power stroke [184], although a modified model was suggested [191]. Rotation of the c-subunit is therefore mainly described by a thermal ratchet mechanism. Finally, it has been found that the synthesis of ATP requires a compulsory electrical potential difference across the membrane, but this may not be true for isolated F_o rotation. A summary of the two models is given in the caption of Figure 2-11.

2.7 Current Understanding of F-ATPase – Combined Rotation of F-ATPase

The simplest ensemble needed to observe rotation in F_1 is $\alpha_3\beta_3\gamma$. However coupled rotation of F_1F_o requires all the eight subunits to be intact and functional. This inevitably decreases the chances of getting functional enzymes because some of them may become denatured or dissociated, especially if they are kept for a prolonged period at room temperature. Furthermore, the F_o portion of the protein is hydrophobic and needs to embed itself inside a lipid bilayer to function properly. This requirement has imposed an additional dimension of difficulty in the characterization of coupled F_1F_o rotation. On one hand, one can obtain stable and robust bilayers using lipid vesicles. Such vesicles are however isolated internally and have a limited internal volume. This causes ions to build up easily inside the vesicles, leading to eventual stalling of the motor. On the other hand, non-isolated bilayers (e.g. planar suspended

bilayers) are painfully unstable by themselves, let alone after reconstituted with proteins. Moreover, conventional planar bilayers are formed vertically using the method of Montal and Mueller [196]. Such a configuration is incompatible with high resolution microscopy techniques. Coupling this with a fragile target protein like F_1F_0 , the endeavour to study the rotation of the F-ATPase appears bleak. These reasons may explain why, despite advances in single molecule work, the observation of combined rotation of F_1F_0 ATPase is still only exclusive to a few research groups.

Some of these difficulties have been overcome by using novel and carefully designed experiments. One of the first direct rotation experiments of intact F_1F_0 rotation is that by Sambongi using detergent stabilised EF_1F_0 [122]. In that experiment, the α -subunits was attached to the cover slip and rotation observed via an actin filament probe attached to the c-subunit (see Figure 2-12a). However, the findings were disputed by Tsunoda [197], who raised the deleterious effect of detergent on the coupling of F_1 with F_0 . This prompted Nishio to expand on the study by demonstrating rotation of the β -subunit and a-subunit with respect to an immobilised c-ring embedded in a detergent free membrane fragment [198] (Figure 2-12b/c). These experiments prove that the α -subunit, β -subunit and a-subunit are part of the same moving body with respect to the c-ring. In a later experiment [199], it was found that rotational characteristics of lipid stabilised TF_1F_0 is similar to isolated F_1 , in terms of the V_{\max} (maximum enzymatic activity), dwell times and sub-steps angles. This suggests that the friction imposed by F_0 in a non-energised membrane is insignificant.

In the experiments mentioned thus far, F_1F_0 ATPase has been stabilised using either membrane fragments or detergent. This means that no potential difference is imposed

across the a/c interface. It might be possible that the characteristics of rotation will differ if there is an ion motive force driving the rotation. Single molecule observation of F_1F_0 rotation under an energised membrane is therefore the next “*Holy Grail*” for the experimentalists in the F-ATPase fraternity. Among the more notable work in this area is that by Kaim using polarisation measurement [200] (Figure 2-12d) and Börsch [201] / Diez [202] / Zimmermann [203] using FRET³⁷. In the latter, two fluorophores, which form a FRET pair, were used to label the rotor (γ -subunit / ϵ subunit) and stator (b-subunit) respectively. The labelled F-ATPase was then reconstituted into vesicles and the FRET states recorded under a fluorescence confocal microscope. When ATP was added to the buffer, the FRET state began to switch in a sequential manner, changing from low \rightarrow medium \rightarrow high \rightarrow low. This was thought to be due to the rotation of the γ -subunit, which in turn caused a change in the distances between the γ -subunit and b-subunit and therefore the FRET efficiency. Conversely, when an ion motive force was provided across the membrane, the sequence of the change in FRET state became reversed, indicating rotation in the opposite direction (Figure 2-12e). Despite the ten repeating units of the c-ring powering the rotation during synthesis mode, only three stable FRET states could be detected. There was however an obvious broadening of each FRET level, which might indicate possible presence of substeps between the three states. Indeed, ten substeps rotation in *E. coli* F_1F_0 ATPase during synthesis was recently reported by Düser using a similar FRET based technique [204].

The methods mentioned above involved using a measurable phenomenon to determine rotation (i.e. change in polarisation or FRET level). Direct observation of

³⁷ Fluorescence Resonance Energy Transfer

rotation, in ways similar to that pioneered by Noji, has still not been reported. A close attempt was made by Zhang [205] (Figure 2-12f). In a nut shell, it involved trapping an F_1F_0 -reconstituted-vesicle on the surface and attaching a filament on the β -subunits. The rotation of the filament was powered by an ion motive force induced by co-reconstituted bacteriorhodopsin. In that experiment, the δ -subunit was depleted from F_1 , leaving only a and b-subunits as the “stator”. This “stator” was also not immobilised like the previous experiments. This meant that the rate of rotation measured was not the absolute speed of the rotor as “stator” might still move in relation of the rotor, albeit more slowly due to a higher viscous drag in the membrane. Moreover, F_1F_0 ensemble could also move freely along the surface of the vesicles, thus making rotation measurements more difficult. Figure 2-12 summarises the various methods of F_1F_0 rotation experiments discussed thus far.

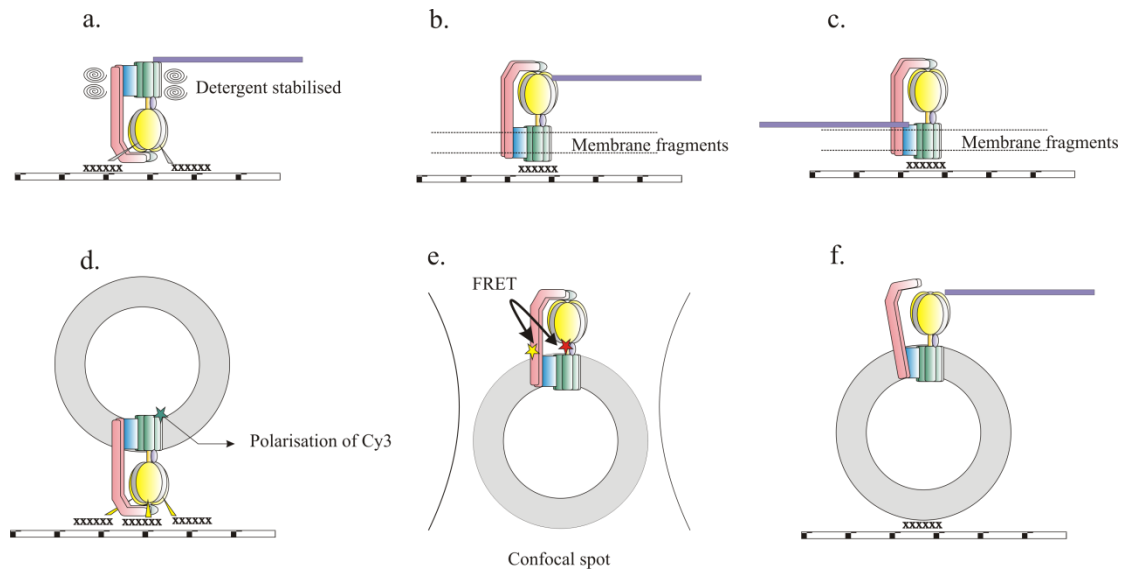


Figure 2-12. Summary of the single molecule F_1F_0 rotation experiments. Purple rod represents the actin filament and stars represent fluorophores. Attachment points to coverslips are designated by “xxx”. a) Rotation of c-subunit in *E. coli* F_1F_0 stabilised by detergent. α -subunits were immobilised onto coverslip [122]. b) and c) represent rotation of the β and α -subunits in *E. coli* F_1F_0 , stabilised by membrane fragments [198]. The c-subunits were immobilised onto coverslip. In the first three examples, the energy from rotation came from hydrolysis of ATP. d) shows the schematic for detecting rotation of F_1F_0 ATPase via a change in polarisation of the fluorophore attached on one of the c-subunits. The F-ATPase used was a chimera of *P-modestum* and *E. coli*. [200]. e) shows a schematic for detecting rotation via a change in FRET state in *E. coli* F_1F_0 . The vesicles were allowed to diffuse freely into the confocal volume [201] [202] [203]. f) shows a schematic for observing direct rotation of TF_1F_0 (less δ -subunit) via a fluorescent actin filament. The vesicle was immobilised on the coverslip [205]. In the last three examples, rotation was powered by an induced ion motive force.

3

Preparation of F-ATPase

3.1 Introduction

The first stage of this DPhil work began in the biochemistry department where F_1F_0 ATP Synthase from *Escherichia coli* (*E. coli*) was purified. Although the final aim of the thesis is to study single molecule rotation of F_1F_0 ATPase, a large part of the work is in fact about the preparation of the enzyme. It is therefore instructive to dedicate one chapter of the thesis especially for this purpose. The current chapter covers purification and reconstitution of F_1F_0 ATPase into vesicles. Tests characterising the activity of the enzyme and vesicle–F-ATPase stoichiometry will also be presented. It is important to ensure a good protein quality before the more challenging single molecule experiments can be attempted.

By the end of this chapter, I hope to have provided enough evidence to show that the purified F-ATPases contained all the necessary subunits; were successfully reconstituted into vesicles; and exhibited good enzymatic and proton translocation activities. These would form the premises for the next chapter, which describes the characteristics of the purified F-ATPase on a planar bilayer setup.

It is not easy to purify this enzyme, let alone by an engineer dabbling with biology and slightly disoriented with the myriad assays used in the biochemistry department. This is because F_1F_0 ATP synthase (*E. coli*) is relatively big in size (~530kDa) and comprises eight different subunits, all of which can possibly be detached or denatured, yet have to be intact for proper coupled rotation. Furthermore, the subunits exhibit different hydrophilicity / hydrophobicity. While some subunits are readily soluble in water, others are hydrophobic in nature. The additional step of using detergent to extract the hydrophobic subunits from the membrane is therefore necessary. However, different detergents had been found to have different effects on the efficiency of purification [206] and reconstitution [207].

From my experience, the yield of F_1F_0 ATPase is generally poorer than F_1 in terms of purity, activity and quantity. A bad purification attempt is usually characterised by low enzymatic activity and missing subunits. To ensure proper functionality of F-ATPase after purification, it is necessary to carry out a suite of experiments to evaluate the quality of the purified F-ATPases. Specifically, these experiments should assess the enzyme in terms of its concentration, hydrolysis activity and purity (as well as presence of all subunits). Results for these tests are presented in this chapter.

This chapter is organised according to the work flow used for sample preparation. A brief list of the materials and equipment used in the experiments is first given. This is followed by descriptions of the assay used and the corresponding results. The chapter ends with a summary of what has been achieved, in terms of purification and reconstitution into vesicles. For brevity, only an overview of the procedures is described. Exact protocols for the tests are documented in Appendix 1.

3.2 Materials and Instruments

3.2.1 Chemicals

DNase-I was obtained from Perbio Science (UK). Nickel chromatography columns for the purification are from GE Healthcare (UK). SM2 Biobeads and a protein concentration test kit were obtained from Biorad Laboratories Ltd (UK). Fluorescent streptavidin and dextran were obtained from Invitrogen (UK). Agarose was obtained from Sigma Aldrich and Lonza Biologics (UK). Phospholipids used for vesicles reconstitution were from Avanti Polar lipids (US). A mixture of natural lipids and synthetic lipids were used (See appendix 1 – A1-3). All other chemicals used for the purification were obtained from Sigma Aldrich (UK). Detailed description of the chemicals and buffers used can be found in Appendix 1.

3.2.2 Equipment

Standard equipment used for purification include centrifuges (Beckman Coulter Avanti J-26XP) and ultracentrifuges (Optima L-XP / Optima TLX), for sample separation and washing; French press (Sim Amanco, SLM Instruments) for lysing of bacteria; spectrophotometer (Shimadzu UV-Vis mini-1240 / Varian Cary 50 UV-Vis) for absorbance measurement. An L-format spectro-fluorometer (Photon Technology International) was used for bulk fluorescence measurement to determine the activity of reconstituted F_1F_0 ATP synthase. Dynamic light scattering system (Viscotek 802DLS - Malvern Instruments Ltd) was used to measure the size of vesicles formed.

3.2.3 Bacteria

F₁F₀ ATPase was expressed from an *E. coli* strain - DK8 ΔUncB-C, *ilv::Tn10*. In this strain, the genes that code the wild type F₁F₀ ATPase (Unc B to Unc C) were removed. In replacement of the lost genes, a plasmid containing genes for the F₁F₀ mutant was incorporated into the bacteria. This plasmid also encoded an ampicillin resistant gene so that the bacteria could be selectively cultured in an ampicillin medium. In the first mutant, a 10-histidine chain was added to the N-terminus of the α-subunits and a single amino acid mutation was made to change the N-terminal glutamic acid of the c-subunit to cysteine. In the other mutant, a 106 amino acid long biotin binding domain was added at the N terminus between Met-1 and Ala-2 of the β-subunit. This allowed *in-vivo* incorporation of biotin on the β-subunit when the bacteria were cultured in a biotin rich medium. Furthermore, a 6-histidine tag was inserted at the N-terminus of the c-subunit after Met-1 [198]. Both of these strains were published in literature and shown to rotate under detergent or lipid stabilised condition [122, 198]. Generally, these mutations were introduced to act as conjugation tags which bind the F-ATPases to various substrates. The histidine tags were used as anchors for the F-ATPases to adhere to nitrilotriacetic acid (NTA) coated substrate, while the biotin tags were conjugated to suitable streptavidinated probes so that the movement of the F-ATPases could be tracked. Figure 3-1 shows the schematics of the mutations. Modified subunits are coloured for clarity. All the experiments described hereinafter are conducted using the latter mutant (Figure 3-1b right), unless otherwise stated.

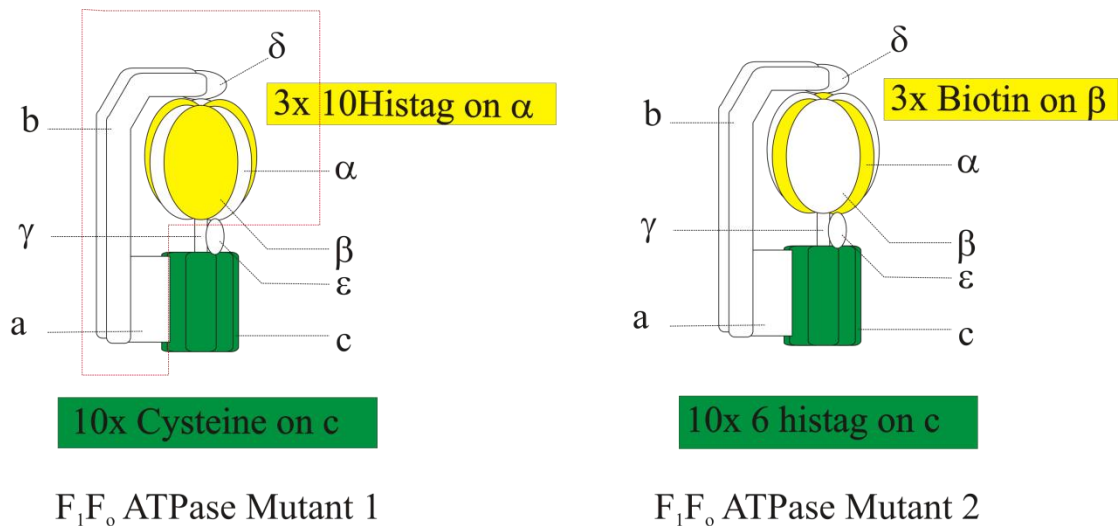


Figure 3-1. Schematics of the mutant used in the experiments with respect to the various subunits that constitute the F-ATPase. The section enclosed by the magenta box indicates the ensemble about which the rest of the enzyme rotates. Mutated subunits are coloured yellow and green.

3.3 Methods & Results

3.3.1 F-ATPase Purification

The protocol used for F-ATPase purification was obtained directly from Professor M. Futai³⁸. An original version can be found in the thesis by Dr Pilizota³⁹ [208]. The protocol currently in use is a fine-tuned version, with new inputs from existing literature [206, 209, 210] and an evolved work flow motivated by the desire to finish the day at reasonable times. Notably, the use of protease inhibitors 6-aminohexanoic acid and p-amino-benzamidine were included in the purification protocols [211, 212] to help stabilise the F-ATPase. Furthermore, an alternative method of purification using a nickel chromatography column was introduced [213]. In the original method, a glycerol column was used to separate the ATPase by density. The new method uses

³⁸ Professor Futai is a collaborator in this research. He has kindly provided the strains and plasmid for the expression of F-ATPase, as well as the protocols for purifying it. Professor Futai is currently based in Iwate Medical University, Japan

³⁹ Dr Pilizota was a grad student in Berry's Group. She is currently a post-doc in the Shaevitz group at Princeton University, US.

a chromatography column and separates the F-ATPases via their affinity to nickelated resins. I have presented the results from these two different methods and compared them in terms of their yield, activity and purity. The main F₁F_o ATPase mutant used in the purification was expressed in *Escherichia coli* bacteria. For brevity, this section provides only an overview of the steps taken in the purification. Readers seeking more information can refer to Appendix 1 (A1-1). Purification usually takes about 3 days to complete.

Procedure for Purification

Bacteria were first pre-cultured in small quantity using rich Luria-Bertani (LB) medium⁴⁰ until the optical density (OD) at 600 nm was approximately 1 – 1.5. They were then transferred to a nutrient poor medium, comprising glycerol as the sole carbon source, and cultured until the OD reached 1 to 1.5. The bacteria were harvested and washed by spinning them in a centrifuge. To produce inverted vesicles and better separate the outer and inner membrane, a French press was used to lyse the bacteria [214, 215]. Large particulates, as well as unlysed bacteria, were removed by centrifugation after French pressing. Heavier membrane fragments containing the F-ATPase were then separated from other water soluble proteins by pelleting them using ultracentrifugation.

The next step involved extracting the F-ATPase from the membrane fragments. To do this, the membrane was stirred in detergent (C₁₂E₈) and then ultracentrifuged to remove undissolved membrane fragments. A yellowish brown supernatant was

⁴⁰ Appendix 1 contains a full listing of the buffers, their constituents and the protocols for experiments

collected and passed through an appropriate purifying column to further separate the F_1F_0 ATPase from other dissolved membrane proteins. Two different methods of separation were chosen and compared. The first required ultracentrifuging the F-ATPase-detergent mix in a tube containing five discrete layers of glycerol at different concentrations (from 30 % w/v to 10 % w/v). This method separates the F-ATPases by their density (See Box 3-1). In the second method, the F-ATPase – detergent mixture was passed through a gravity driven chromatography column filled with nickelated resin. F_1F_0 ATPases were captured via the histidine tags expressed on their c-subunits. The enzymes were then eluted using buffer containing a high concentration of imidazole and dialysed to exchange the buffers. Figure 3-2 shows the schematic of the purification process.

Box 3-1. Separation of molecules via centrifugation is dependent on size and density of F-ATPases

By force balance, the difference between weight and lift of the molecule must be balanced by the viscous drag. Hence

$$mg - F_{lift} = \text{Stokes' drag}$$

F_{lift} is due to the displaced water volume. By assuming that the volume occupied by the F-ATPase is approximately spherical,

$$(\rho_{molecule} - \rho_{buffer}) \frac{4}{3} \pi a^3 (\omega^2 r) = 6\pi a \eta v$$

Where ρ refers to density in kg/m^3

a is the hydrodynamic radius of the molecule in meters

ω is the angular velocity of the rotor in rad/s

r is the average radius of the centrifuge rotor in meters

η is the dynamic viscosity of the medium in $\text{Pa}\cdot\text{s}$

v is the sedimentation velocity of the molecule in m/s

Hence

$$v = \frac{2a^2(\omega^2 r)(\rho_{molecule} - \rho_{buffer})}{9\eta} \quad \text{Equation 3-1}$$

The speed at which the F-ATPases move across the glycerol column is thus dependent on their size and density. If the density of the F-ATPase = density of the buffer, then it will remain stationary.

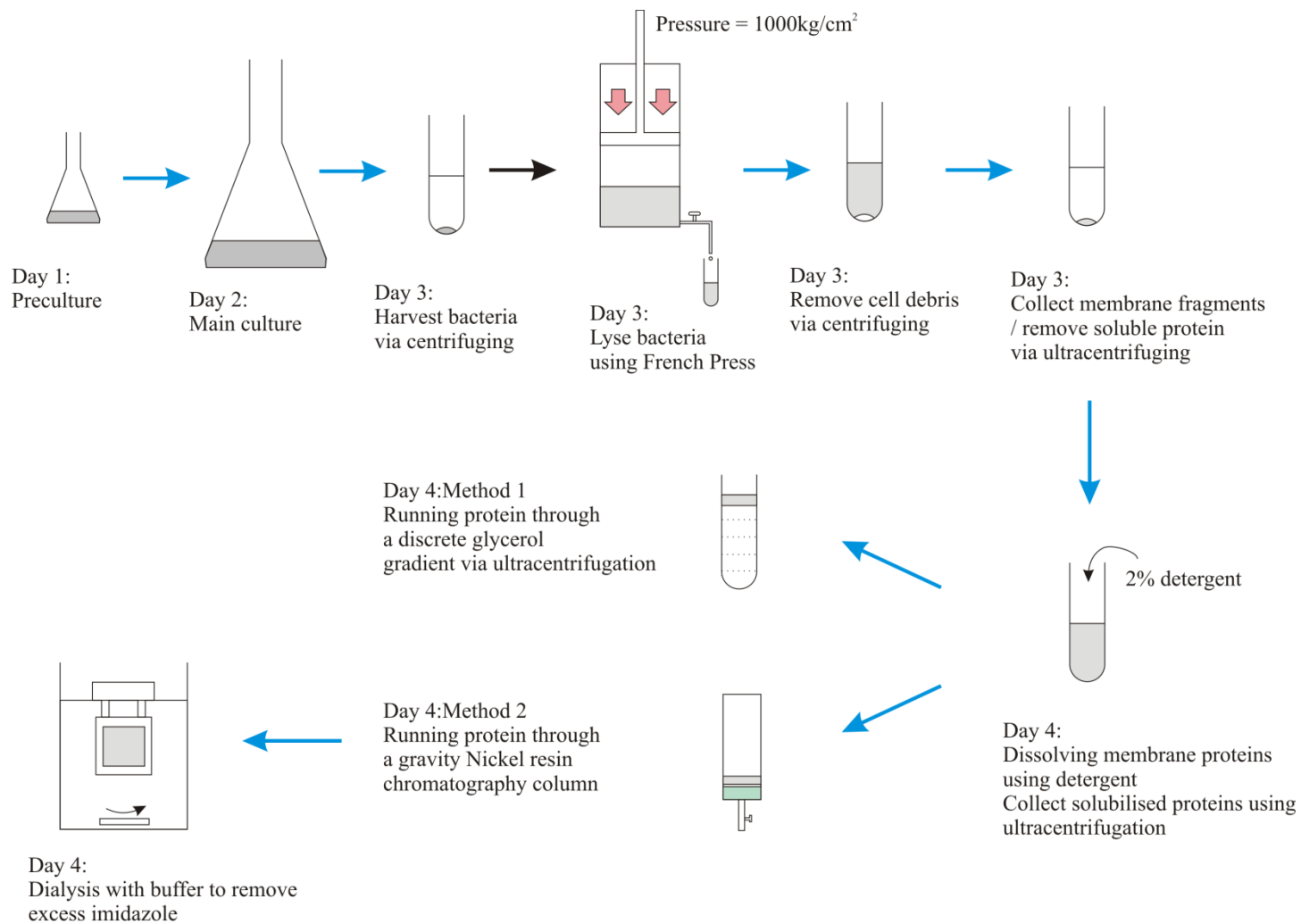


Figure 3-2. Schematics of the purification protocols.

Once purified, the activity, purity and concentration of the F-ATPase were evaluated using various assays. The basic activity assay measured the bulk enzymatic efficiency of F₁F₀ ATPase in hydrolysing adenosine-tri-phosphate (ATP). This was done using ammonium molybdate [216], which formed a complex with the free phosphate ions that were released by ATP hydrolysis. Under a reducing agent (Fe²⁺), the complex exhibited a strong light absorbance at a wavelength of 850nm. The amount of phosphate produced by ATP hydrolysis was determined by measuring absorbance at this wavelength and comparing it with a calibration curve obtained from known concentration of free phosphate. To determine the concentration of the F-ATPase, a commercial protein concentration test, based on the Lowry method, was used. Finally, to measure the purity of the F-ATPase, SDS PAGE⁴¹ was used.

Results of purification

Table 3-1 summarises and compares the quality of the F-ATPase obtained using the nickel gravity column and glycerol density column. The yields of F-ATPase were found to be comparable for both methods of purification. However, when their activities were measured, it was found that the F-ATPase obtained from the nickel column was almost twice as active as that from the glycerol column. The activity measured was based on the average amount of ATP hydrolysed per minute by F₁F₀ ATPase in a detergent stabilised environment. This was surprising considering that the protocol for the nickel column required a further 24 h of dialysis to remove excess imidazole. One would expect further degradation of the F-ATPase during dialysis, due to dissociation and denaturation of subunits. A possible explanation for this

⁴¹ SDS polyacrylamide gel electrophoresis – This is a standard biochemical assay that uses SDS to denature proteins and separates them by their size.

discrepancy in F-ATPase activity might be that lipids added during the nickel column elution could possibly have stabilised the subunits and prevented the further denaturation of the enzyme. It was reported that membrane bound F₁ ATPase from *B. megaterium* was able to retain most of its hydrolysis activity when flash frozen and then thawed. On the contrary, solubilised F₁ of the same protein suffered a drop in activity when it underwent the same treatment [217].

One may ask whether it is possible to add lipids to the F-ATPase / detergent mix before running it in the glycerol column. This is thought to be difficult because doing so will vary the size and density of the F-ATPase-lipid-detergent micelles over a wide range for the detergent concentration used ~ 2%. On the occasion when this was tested, the F-ATPase band obtained was broad and spanned across a large length of the glycerol column. Alternatively, adding lipids after glycerol column purification, but before flash freezing, may improve the stability of the F-ATPase. This can easily be incorporated into the purification process.

The activity of the F-ATPase in terms of its ability to translocate protons across a bilayer was also measured. Briefly, a fluorescent dye was used to measure the acidification of the vesicles as protons were translocated into the vesicle during ATP hydrolysis. The rate of reduction in fluorescence was used as an indicator for the activity of F-ATPase. Procedure for the test is discussed in the next section. It was found that the rate of fluorescence quenching by F-ATPases purified using the nickel column was also about twice that of the glycerol column. This result was consistent with the hydrolysis activity described earlier.

On the purity of the sample, although it was possible to identify all the subunits on the SDS PAGE, the additional protein bands along the lanes suggested that there were still some unidentifiable impurities in the sample. This was not a problem since these proteins neither interfered with the activity of the ATPase nor produced a strong background under both fluorescence and dark-field microscopy. It could also be seen from the gel that the β -subunit band of the F_1F_0 ATPase was higher than the F_1 ATPase. This was because the F_1F_0 ATPase mutant contained an additional biotin binding domain (~106 amino acids). From the SDS PAGE, there was no apparent difference between the two methods of purification.

Table 3-1 A comparison of the F-ATPase obtained using two different methods of purification. The same amount of starting material is used for both the methods.

	Ni Column	Glycerol Column	Assay used
Yield - Mass purified per 39 mg protein in Lysate	0.47 mg (conc = 0.34 mg/ml)	0.48 mg (conc = 0.92 mg/ml)	Lowry protein concentration assay
Activity – Hydrolysis of ATP per mg of F-ATPase per minute	7.3 $\mu\text{mol mg}^{-1}\text{min}^{-1}$ Or 67 ATP/s	3.4 $\mu\text{mol mg}^{-1}\text{min}^{-1}$ Or 31 ATP/s	Phosphate detection using ammonium molybdenum with Fe^{2+} as reducing agent
Activity – Initial rate of Proton translocation across membrane – As measured by change in fluorescent intensity per second (Semi Quantitative)	0.0029 units of fluorescence quenching /s	0.0014 units of fluorescence quenching /s	Fluorescence quenching of ACMA dye for F-ATPase on vesicles
Purity	Larger amount of high MW proteins retained (Qualitative)		SDS Page

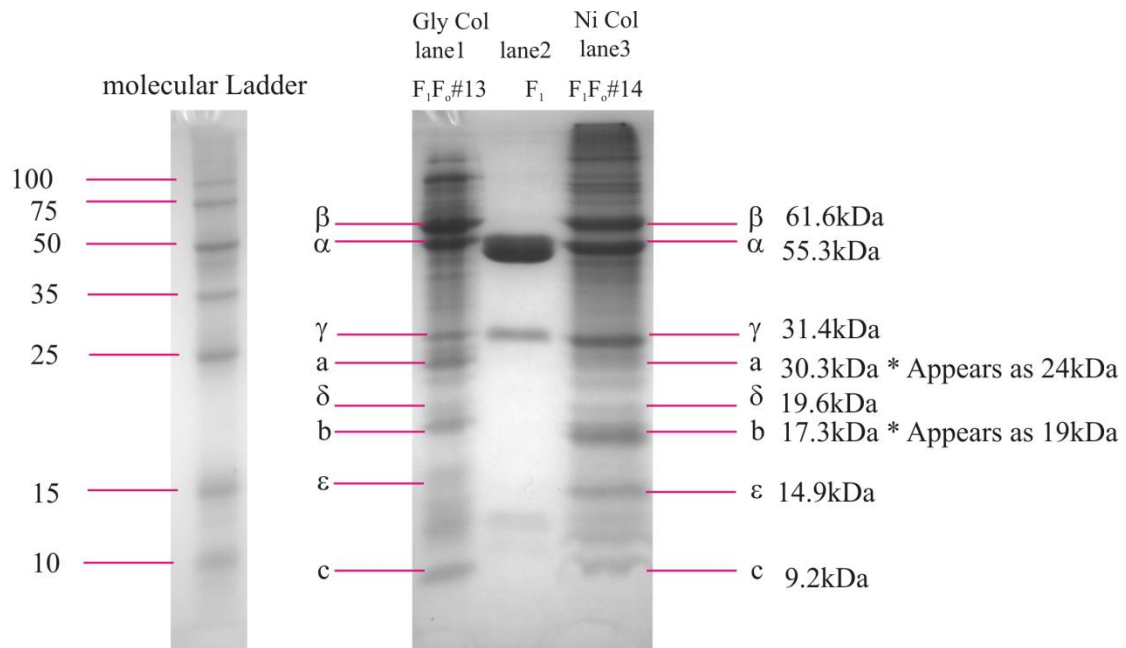


Figure 3-3. SDS PAGE of F-ATPases obtained from two different purification techniques. The reference molecular ladder is shown on the extreme left. Lane 1 shows the proteins from the glycerol column while lane 3 shows that from the Ni column. Lane 2 is a second reference lane containing only the β , α and γ -subunits from F₁ ATPase (purified by me). Note that a and b-subunits appear shorter and longer (respectively) than their actual size. This has previously been reported in [218] and may be due to the inability of SDS to fully denature some of the hydrophobic sections of the a-subunit, as well as the native elongated structure of the 'b' subunits.

3.3.2 Reconstitution of F₁F₀ ATP Synthase into Vesicles and Testing its Activity

Before testing the coupled activity of the F-ATPase, it was necessary to first reconstitute them into vesicles. The detailed protocols for forming vesicles and reconstituting them with F-ATPases can be found in Appendix 1 (A1-3). A comprehensive review was authored by Rigaud et. al [207]. The protocols used here were mainly adapted from this review, as well as other relevant literature [207, 209, 213, 219].

Procedure for Vesicle Formation

The reconstitution protocol were broken down into two main steps. In the first step, vesicles were pre-formed in the absence of F-ATPases. Briefly, lipid mix⁴² in chloroform was dried under nitrogen and then re-suspended in MES buffer⁴³. To ensure thorough hydration of the lipids, the suspension was vortexed continuously for about 1 min. It was further sonicated at 4 °C in a bath sonicator for 10 min to break down undissolved cakes of phospholipids. Sonication was also found to have the advantage of making the vesicles less permeable to ions [220]. However, it could reduce the average size of the vesicles in the sample. To increase the size of the vesicles after sonication, the lipid suspension was flash frozen in liquid nitrogen and allowed to thaw under room temperature. This freeze thaw cycle was repeated two more times. Effects of cyclic freeze thaw include increasing the average size / encapsulated volume of the vesicles [220, 221] and promoting the formation of unilamellar vesicles [222]. The suspension was finally forced through a 0.2 µm track-etched polycarbonate membrane, which effectively homogenised the size of the particles and further increased the proportion of unilamellar vesicles in the suspension [223]. Vesicles were then set aside in ice, ready for reconstitution. F₁F₀ ATPases were added only at this stage because the harsh conditions of vesicle preparation (sonication and freeze thawing) might potentially denature the fragile protein. Natural lipids are susceptible to oxidation and hydrolysis because of the prevalence of unsaturated bonds. As such, they were usually prepared fresh everyday and unused

⁴² See Appendix 1 (A1-3) for the constituents of the natural lipid mix.

⁴³ MES buffer comprises 20mM MES-Tricine pH ~ 7 (adjusted with NaOH), 80mM NaCl, 2mM MgCl₂, 10% w/w glycerol.

lipids discarded at the end of the day. Figure 3-4 shows the schematics of the vesicle preparation process.

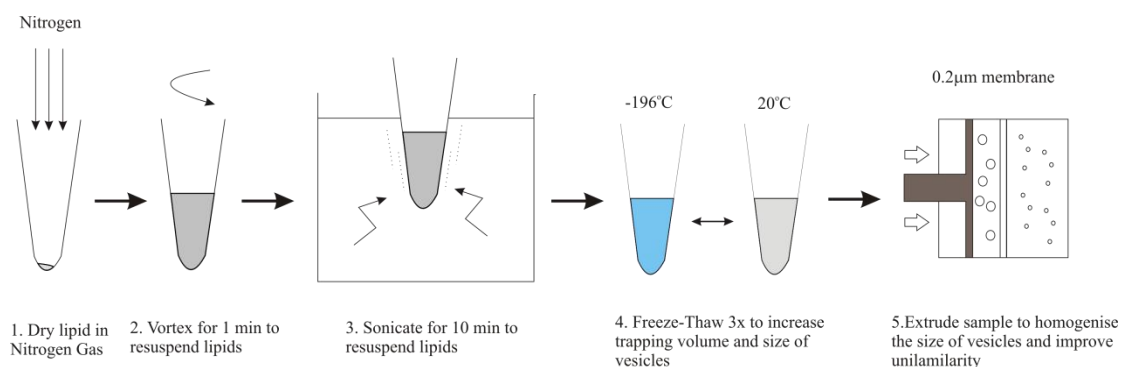


Figure 3-4. Schematics of the vesicle preparation process

Procedure for F-ATPase Reconstitution⁴⁴

The second step of the reconstitution involved incorporating F_1F_0 ATPase onto the pre-formed vesicles. To do this, $10\ \mu\text{L}$ of purified F-ATPases at $0.3\ \text{mg/ml}$ in MES buffer (see dialysis buffer from purification protocol in Appendix 1) was first thawed and added slowly into $10\ \mu\text{L}$ of pre-formed vesicles at $16\ \text{mg/ml}$. $1.74\ \mu\text{L}$ of 10% Triton X-100 (Molecular Weight ~ 647) was then added to the mixture slowly, with constant mixing and stirring using the pipette tip. It was important to mix the detergent evenly in order to prevent localised high concentration of detergent. The typical enzyme to lipid ratio used was about 1:50 by mass. This gave approximately 12 F-ATPases per vesicle, if all the enzymes were reconstituted (See Box 3-2)

⁴⁴ See Appendix 1 (A1-3) for protocols

Box 3-2. Calculation for the number of F-ATPase per vesicle based on a vesicle diameter of 200 nm.

Approx area of 1 lipid = 0.6 nm^2 [224]

Total surface area (inner and outer) of a 200 nm diameter vesicle = $4\pi(100)^2 \times 2 = 251 \times 10^3 \text{ nm}^2$

No. of molecules per vesicle = $251 \times 10^3 / 0.6 = 420 \times 10^3$ molecules = 7×10^{-19} mol

No. of moles of lipid used (10 μL of 16 mg/ml) = $\frac{10 \times 16 \times 10^{-6}}{787.5} = 2 \times 10^{-7}$ mol (M_r Lipid ~ 787.5)

No. of vesicles = $2 \times 10^{-7} / 7 \times 10^{-19} = 3 \times 10^{11}$ vesicles = 5×10^{-13} mol of vesicles

No. of mol of F-ATPase (10 μL of 0.3 mg/ml) = 6×10^{-12} mol (M_r F-ATPase ~ 500 KDa)

Ratio F-ATPase to vesicle = $6 \times 10^{-12} / 5 \times 10^{-13} = 12$

A final detergent concentration of $\sim 0.8 \%$ v/v was obtained, as suggested by Fischer et. al. [209]. This concentration of detergent corresponded to a detergent-to-lipid molar ratio of ~ 1.2 , which was consistent with the optimal concentration recommended by Pitard et. al., for reconstituting F_1F_0 ATPase of *Thermophilic bacillus PS3* [219], and Richard et. al. for chloroplast F_1F_0 ATPase [225]. At this ratio, the lipid to detergent concentration corresponded to about 30 % complete solubilisation⁴⁵ of the pre-formed vesicles into lipid-detergent micelles [207].

The lipid-detergent-F-ATPase mix was left to incubate on ice for 1 hour. Three batches of detergent-absorbing SM2 biobeads were added consecutively over 4 hours, while keeping the sample at 4°C and under constant stirring. The rate of detergent extraction was deliberately kept low so that complete detergent removal occurred only after 4 hours of incubation. Slow detergent removal was important to ensure homogeneity of the size and unilamilarity of proteoliposomes⁴⁶ formed [226]. Care should also be taken not to add too much biobeads in total as they could remove lipids

⁴⁵ Solubilisation refers to the complete breaking down of the lipid vesicles to micelles

⁴⁶ Proteoliposomes are protein reconstituted lipid vesicles

at the same time. Detergent extraction using biobeads was preferred over dialysis or chromatography because of its ease of use and effectiveness in removing detergent with low critical micelle concentration (e.g. Triton X and C₁₂E₈) [207]. Figure 3-5 summarises the procedures for this step of reconstitution.

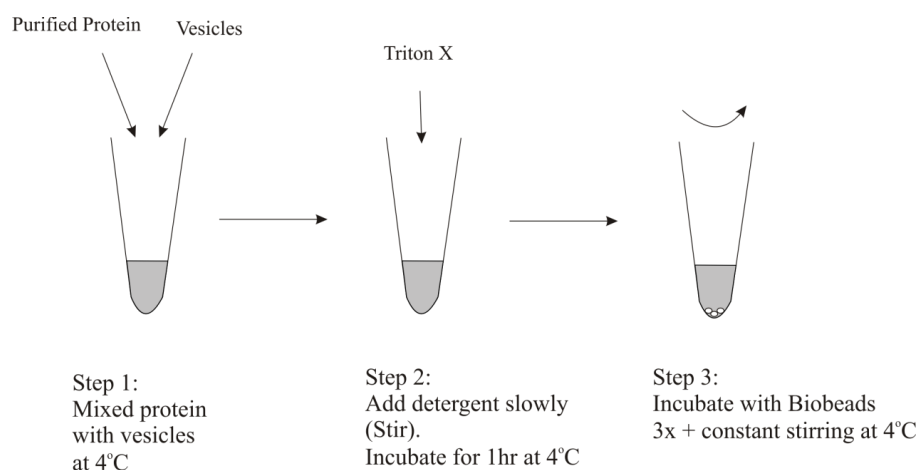


Figure 3-5. Schematic for the reconstitution of F-ATPases onto pre-formed vesicles

Procedure for Measuring the Size of Vesicles

Characterization of the size of the vesicles / proteoliposomes during each stage of the preparation was carried out, using a method called Dynamic Light Scattering (DLS). This is a non invasive technique for measuring sub-micron sized particles. It makes use of the idea that particles scatter light and that the intensity of the scattered light fluctuates as the particles undergo Brownian motion. Under a coherent excitation laser source, scattered light from particles interferes constructively and destructively, depending on their relative positions, and produces regions of low and high intensities. Since the interference pattern is dependent on the positions of randomly moving particles and a particle cannot change its position instantaneously, it means

that at very small time scales, there will be little change to the scattered intensity measured – thus a high autocorrelation⁴⁷ of the detected intensity. At large time scales, the particles would have diffused far enough to give very little intensity autocorrelation. In fact, the trend is that the smaller the particle, the faster it will diffuse and hence the shorter the time it takes before intensities become uncorrelated. By looking at the intensity autocorrelation, one can thus obtain a characteristic time of diffusion and use it to calculate the average size of the particles. An elementary guide to DLS can be obtained from [227]. Box 3-3 gives the salient mathematics behind the DLS technique. For a more rigorous treatment of the calculation, readers can refer to [228].

Box 3-3. Basic equations in Dynamic Light Scattering Technique

The correlation function for the fluctuations in scattered intensity $G(\tau)$, is defined by	
$G(\tau) = \frac{1}{n} \sum_{i=1}^n I(t_i)I(t_i + \tau)$	Equation 3-2
Where $I(t)$ is the intensity measured at time t , and τ is the time scale of the autocorrelation function.	
For homogeneous ⁴⁸ sample of constant size, it can be shown that the autocorrelation curve fits a single exponential decay function given by:	
$G(\tau) = A(1 + B \exp^{-2\Gamma\tau})$	Equation 3-3
Where A , B and Γ are the fitted parameters and	
$\Gamma = D[(4\pi n / \lambda_0) \text{Sin}(\theta / 2)]^2$	Equation 3-4
Where D is the translational diffusional coefficient, λ_0 is the wavelength of the laser illuminator, n is the refractive index of the dispersant and θ is the scattered angle.	
From Γ , it is possible to calculate the radius of the dispersant using the Stokes – Einstein Equation:	
$R = \frac{kT}{6D\pi\eta}$	Equation 3-5
Where k is the Boltzmann's Constant, T is the temperature in Kelvin, η is the viscosity of the medium.	

⁴⁷ See Box 3-3 for the definition of autocorrelation.

⁴⁸ For heterogeneous samples, the exponential fit expressed in Equation 3-3 is expressed as a sum of exponentials.

A commercial DLS system (Viscotek 802 DLS) was used to measure the size of the vesicles at different stages of the preparation. Samples were diluted 1 to 20 times with MOPS⁴⁹ buffer and placed directly into a 15 μ L cuvette. The intensity of the laser was adjusted to about 5 % to 10 % of the maximum intensity. The concentration of the samples was diluted further if the scattered intensity was too high. The concentration of glycerol used in the buffer was also ascertained. This was because glycerol would change the viscosity of the buffer and hence the calculation of the particle size. The software automatically calculated the distribution of vesicle sizes, based on the strengths of scattered intensities.

Results for F-ATPase Reconstitution and Size Measurement

Figure 3-6 shows the size of the vesicles measured using DLS at different stages of vesicle formation. The plots show the size of vesicles and the relative intensities of light scattered by those vesicles. In the Rayleigh scattering regime, the scattered intensity is proportional to the sixth power of the radius of the dispersant [229]. A small amount of large vesicles will therefore scatter more light than a large amount of small vesicles. This suggests that although smaller vesicles show a lower scattered intensity, their quantities are actually much larger than the bigger vesicles. The second point to take note is that while DLS is able to differentiate particles of different sizes, it has problems getting an accurate distribution of the sizes, especially for samples with sizes spanning across several orders of magnitude. This is because fitting the data to a sum of exponentials is an ill posed problem where a small amount of noise will significantly alter the solution of the curve fit. A best fit may therefore not necessarily give the true distribution of sizes. As such, I have interpreted the

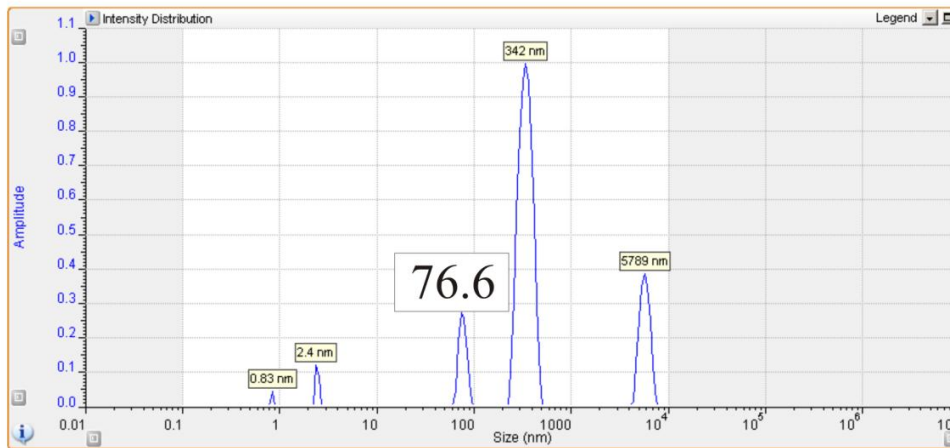
⁴⁹ MOPS buffer comprises 20mM MOPS pH ~ 7 (adjusted with NaOH), 80mM NaCl, 2mM MgCl₂, 10% w/w glycerol.

results from DLS using only the average size in each population cluster⁵⁰, weighted by their scattered intensity (See Figure 3-6). Furthermore, for plots with more than one population cluster, only the cluster which has the largest amount would be considered.

The change in size of vesicles during various steps of preparation was consistent with the expected outcome. When the lipid was first hydrated (before sonication), there was a wide distribution of vesicle sizes, spanning over several orders of magnitude. A decrease in size of the vesicles was observed after sonication, although this process did not fully break down all the large vesicles in the buffer. The freeze-thawing cycles increased the size of the vesicles slightly, consistent with those reported in [220, 221]. The size of vesicles was swiftly and effectively homogenised by extrusion. Unexpectedly, the average radius of the vesicles after treatment with F-ATPase and detergent was reduced to ~ 39nm. This was half the size of the original vesicles used for the reconstitution (radius~84.1 nm). Some of the proteoliposomes must therefore have been formed from fully solubilised lipid micelles. For such proteoliposomes, one should expect roughly equal chances of having F-ATPase reconstituted in an orientation where its F₁ portion is pointing into the interior of the vesicle, as well as the inverse of that. For the rotation study, it is necessary that the F₁ is pointing out because the enzymatic portion contains the biotin site for binding with the streptavidin gold nano-particles, which is in turn used to track rotation. As a indicative number, for bacteriorhodopsin under similar reconstitution conditions, about 80% to 85% of the protein was found to insert with the hydrophilic end pointing out of the vesicles [207].

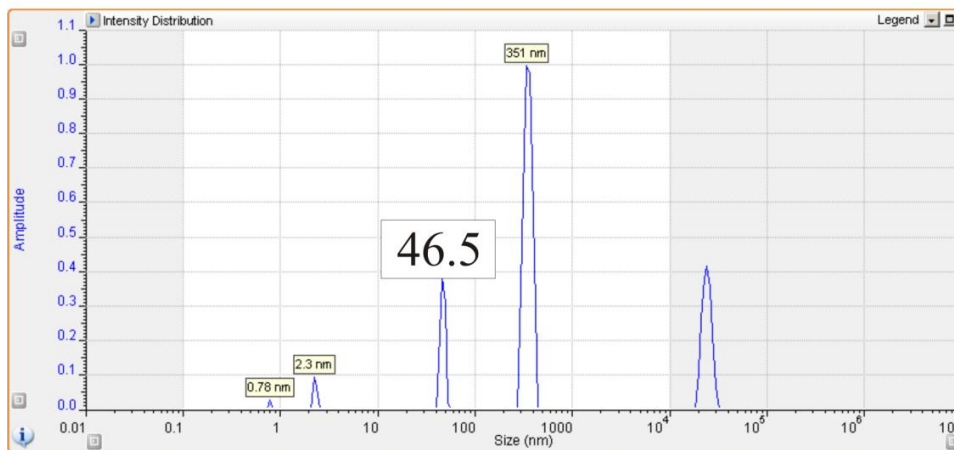
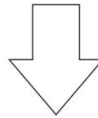
⁵⁰ A population cluster is a group of vesicles that is recognised by the DLS software as belonging to the same distribution (as delineated by their size). In Figure 3-7, the population clusters are represented by peaks on the graphs.

1. Before Sonication



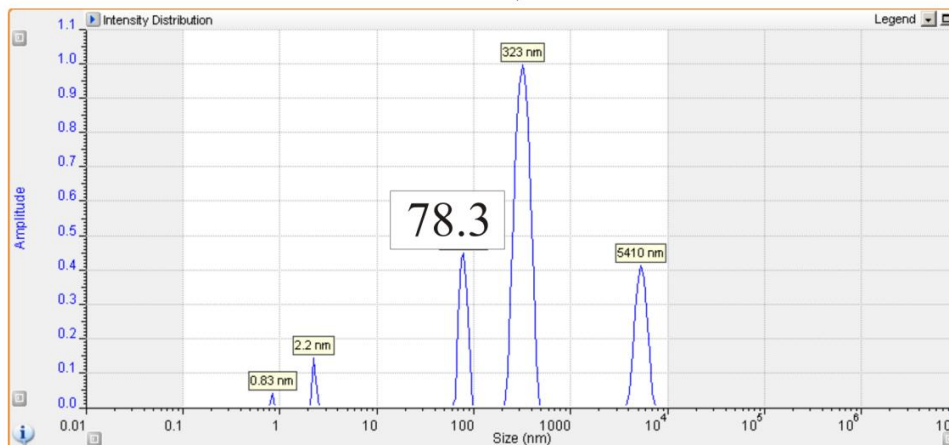
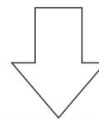
2. After Sonication

Effect: Increase the number of small vesicles and decrease their mean size



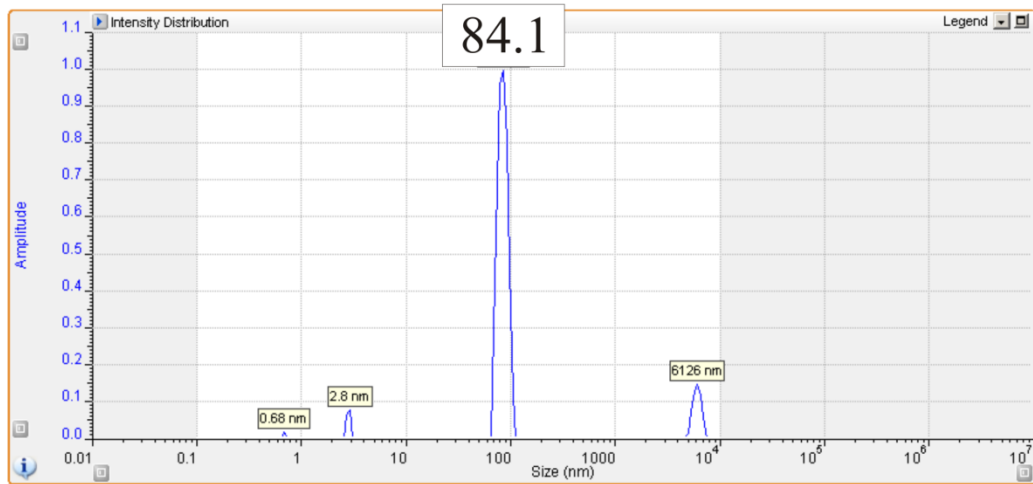
3. Freeze Thawing

Effect: Increase the number of small vesicles and increase their mean size



4. Extrusion

Effect: Remove large vesicles and decrease the variance of vesicle size



5. Detergent Treatment

Effect: Decrease the mean size and increase the spread of vesicle size

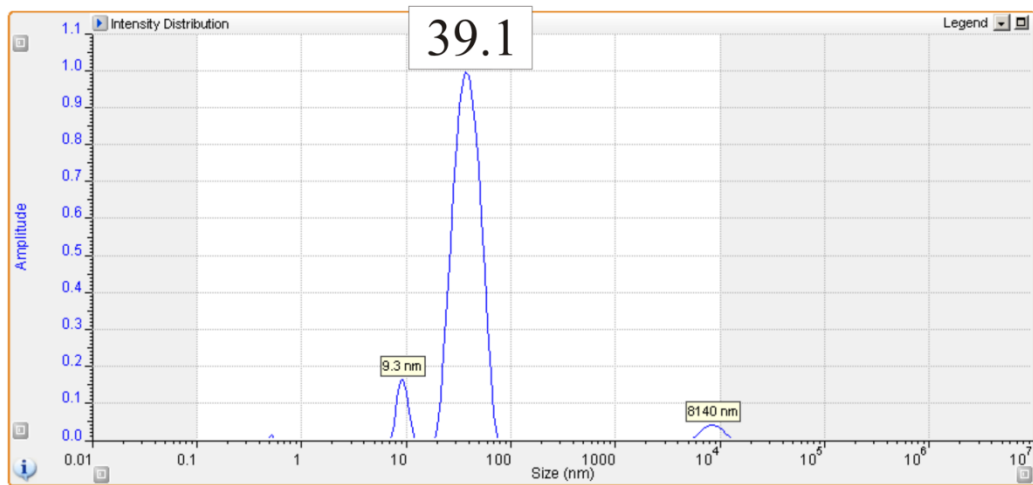


Figure 3-6. Changes in size of vesicles at different stages of vesicle preparation. The number on top of the peaks shows the average radius of the dispersant in nano-meters

Procedure for Testing the Coupled Activity of Reconstituted F-ATPases

Measuring the activity by hydrolysis of ATP is not sufficient as it does not confirm whether F_1 ATPase is coupled to F_0 . To measure the coupled activity, a more elaborate assay has to be used. In this section, the method used to measure the coupled activity is explained. The concept of the assay is as follows: F-ATPases are first reconstituted into pre-formed vesicles. When ATP is added to the vesicle suspension, the F_1 domain hydrolyses ATP and rotates as normal. If F_1 is coupled to F_0 , this rotation also drives the c-subunits and causes the transportation of protons into vesicles. This acidifies the interior of the vesicles which can in turn be measured by a pH sensitive fluorescent dye.

Figure 3-7 shows a schematic of the process.

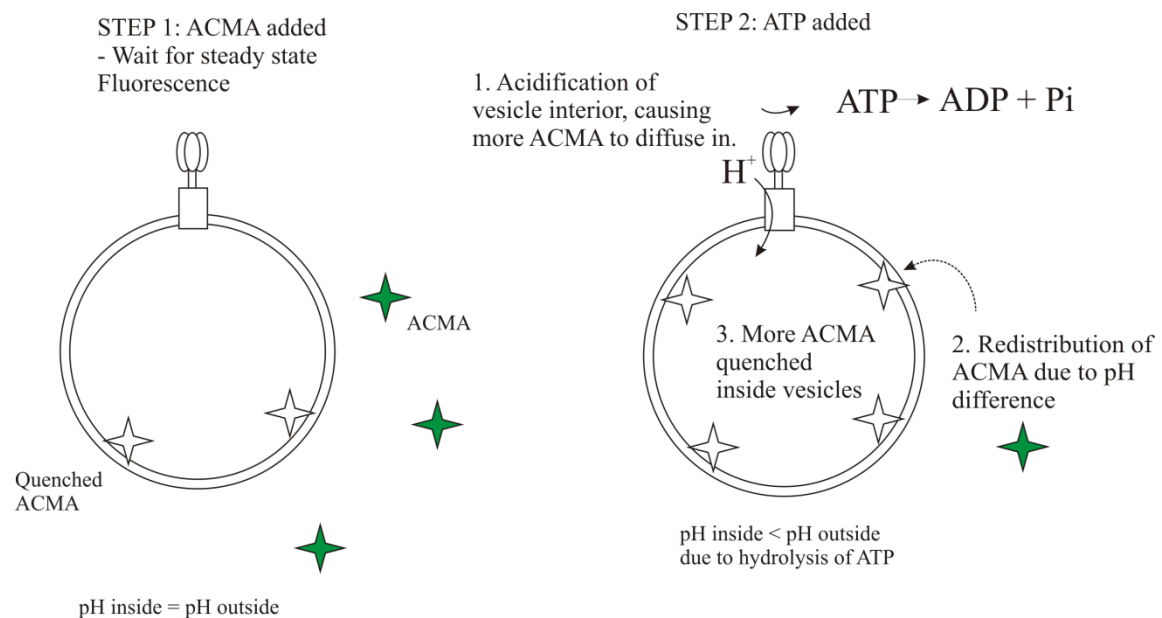


Figure 3-7 Schematic of the mechanism of ACMA quenching assay that was used to test the coupled activity of F_1F_0 ATPase

F-ATPase proteoliposomes were mixed with MES buffer and allowed to equilibrate. 9-Amino-6-chloro-2-methoxyacridine (ACMA) was then added to the suspension and mixed thoroughly by slow pipetting. ACMA is a fluorescent dye that has been frequently used to study the acidification of vesicles due to proton translocation by F_1F_0 ATPase [213, 230, 231]. Fluorescent emission of the dye was first measured using a standard fluorometer at intervals of 55 s until the signal stabilised. F_1F_0 ATPases were then activated by adding saturating concentration of ATP (~ 4 mM) and the fluorescent intensity recorded again, but at intervals of 20 s instead. For vesicles with successfully reconstituted F-ATPases, protons were translocated into the vesicles and their internal pH therefore reduced. This caused a net migration of deprotonated ACMA into the vesicles, which became quenched due to interactions with lipids. A gradual drop of fluorescence in the proteoliposome suspension would therefore be observed.

The main advantage of using ACMA is that it can be added straight into the samples and tested immediately. Unlike most pH sensitive dyes, there is no need to incorporate the dyes into vesicles or remove extra-vesicular dyes from the buffer. ACMA, by itself, is membrane permeable and exhibits a significant change in fluorescence, when a small Δ pH is formed across vesicular membranes. Changes in fluorescence can be easily detected using a spectrofluorometer.

However, the exact mechanism of ACMA quenching is still not completely understood. It was postulated that the dye works by interacting with the negatively charged phospholipids and becoming quenched during the process. This interaction is in turn accentuated by a low pH environment inside the vesicle [232-234]. From the

study of 9-aminoacridine⁵¹, it was found that the extent of fluorescence quenching is also sensitive to several other factors, including the concentration and types of salts present in the buffer, the charge and amount of lipids used and the presence of negatively charged molecules or proteins [232]. As such, any calibration curve relating the quenched intensity to change in pH is unique only to the specific conditions used in the experiment. Furthermore, when the pH gradient across the vesicles is allowed to equilibrate, Grzesiek et. al. [232] reported that the quenched fluorescence recovered at least 10 times faster than the recovery of pH. It appeared that there is no tight coupling between fluorescence recovery of the dye and the recovery of pH inside the vesicles.

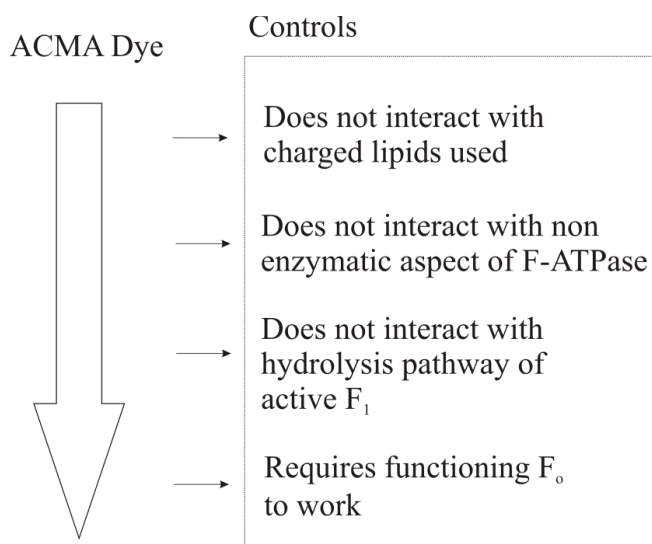
Given the reasons above, the quenching results of ACMA were used only as a relative measurement for the activity of the F-ATPase. This assay is useful to determine if a batch of F-ATPase is generally active or not. However, if comparison of the relative activities is needed, then care must be taken to assess the samples under similar experimental conditions. Due to the reasons above, this assay was not used to calculate the absolute pH change within the vesicles.

Results for Testing the Coupled Activity of Reconstituted F-ATPases

To show that the decrease in fluorescent intensity was due to the acidification of the vesicles, several controls were prepared to rule out possible interactions between the dyes and non enzymatic aspects of the system. Figure 3-8 shows the schematics for the various controls. To show that the fluorescence quenching was not due to

⁵¹ 9-Aminoacridine is an analogue of ACMA. It lacks a chlorine and methoxy group, but otherwise shares similar characteristics

interactions between the negatively charged lipids and the dye, a control using plain lipid vesicles + ACMA was tested. To show that the fluorescence quenching was not due to non enzymatic interaction between the F-ATPases and ACMA, a control consisting of F-ATPases first denatured by heat + ACMA was prepared. To show that the fluorescence quenching was not due to decoupled hydrolysis of F_1 ATPase, F_1 ATPase was used instead of F_1F_0 ATPase. Finally to show that proton translocation mechanism by F_1F_0 ATPase was necessary for observing quenching, Di-cyclohexylcarbodiimide (DCCD) was added to inhibit proton transport. DCCD works by reacting with the carboxyl group of the Asp61 (aspartic Acid) in the c-subunit F_1F_0 ATPase, thereby preventing the Asp61 from binding to free protons (see [235] and reference therein). To do this, 100 μ M of (DCCD) was pre-incubated with the proteoliposomes before testing with ACMA.

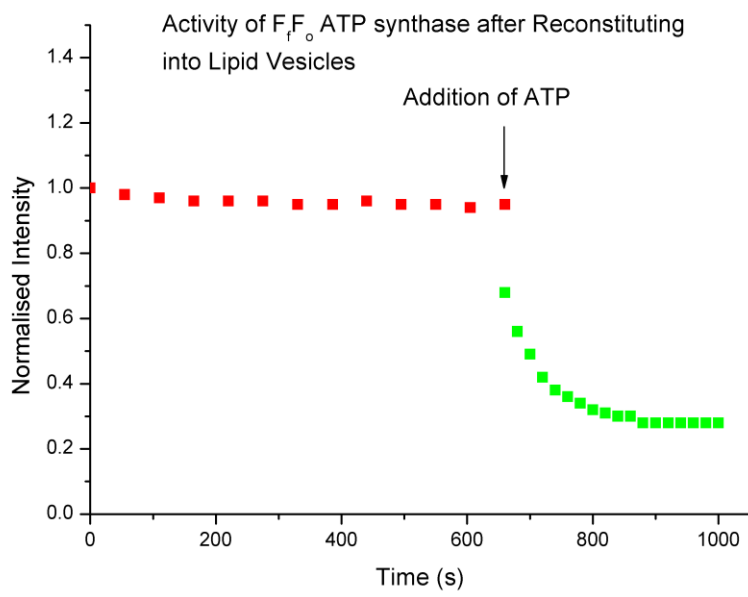


Observed Results: Gradual decrease in fluorescence when ATP is added

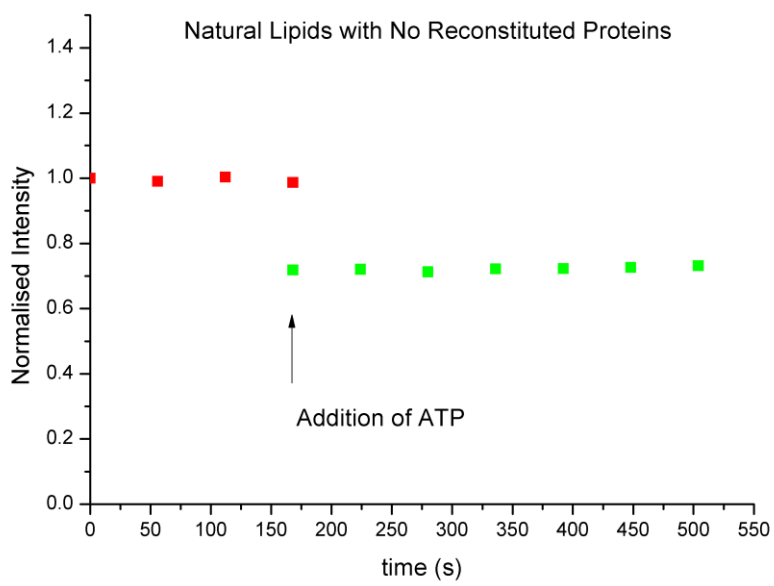
Figure 3-8. Four different controls of increasing specificity were prepared to show that the decrease in fluorescence signal (or increase in quenching) over time was due to acidification of the vesicles' interior by the activity of coupled F_1F_0 ATPase.

All the controls gave negative results. Figure 3-9 shows the summary of the quenching experiments. Figure 3-9a shows the results when functional F-ATPase was used. It can clearly be seen that hydrolysis of ATP by F_1F_0 ATPase was accompanied by a gradual decay in fluorescence. It was also noticed that there was an instantaneous drop in fluorescence immediately after ATP was added. This happened in both the sample and controls and could be attributed to the interaction between ACMA and the ATP, as noted in [230]. Figure 3-9b and Figure 3-9c prove that the gradual decrease in fluorescence observed in Figure 3-9a was not due to non enzymatic interactions between the dye and the lipid or F-ATPase respectively. Figure 3-9d also shows no gradual reduction in fluorescence, proving that fluorescence was not affected by the hydrolysis activity of F_1 ATPase (without F_0 domain). Finally, Figure 3-9e shows no gradual quenching when the pathway for proton translocation was disrupted. This further reinforced the assertion that the gradual decrease in fluorescence was due to the coupled action of F_1F_0 ATPase, activated by ATP.

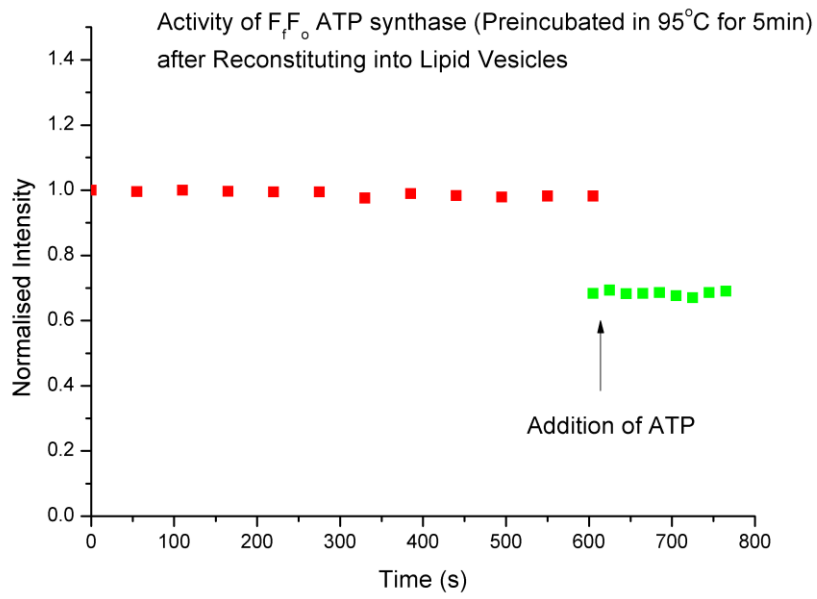
The activity of F_1F_0 ATPase under different lipid systems was investigated next. Both synthetic and natural lipids were used for the tests. While natural lipids from egg (egg phosphatidyl-choline and phosphatidic acid) and *E. coli* (polar lipids) showed good activity, synthetic lipids gave only a small amount of fluorescent quenching. Figure 3-10a and Figure 3-10b show the quenching curves for F_1F_0 ATPase reconstituted with diphytanoyl-phosphatidyl-choline (DPhPC)/egg PA (20:1 molar ratio) and 1-palmitoyl-2-oleoyl-*sn*-glycero-3-phosphocholine/ phosphoethanol -amine / egg PA (POPC / PE / PA in 10:5:1 molar ratio) respectively. The low activity could be due to poor insertion of the F-ATPases onto these synthetic lipid vesicles. With this finding, natural lipids were used in all further reconstitutions of F-ATPase.



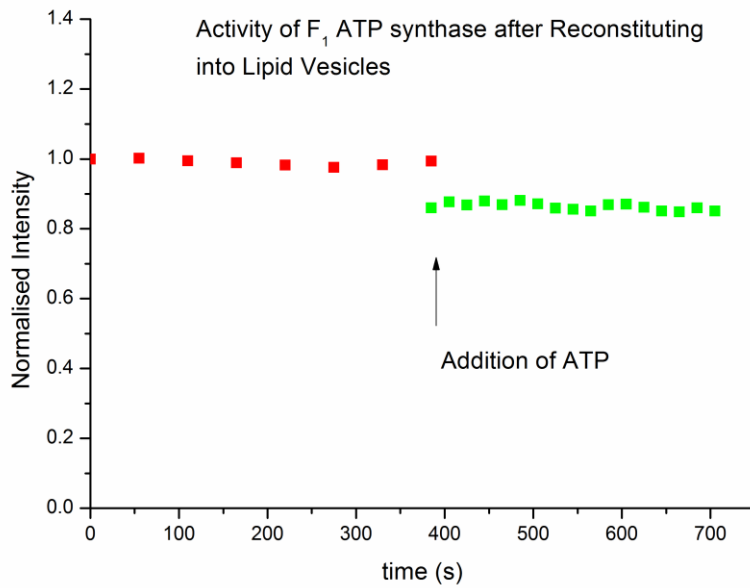
a.



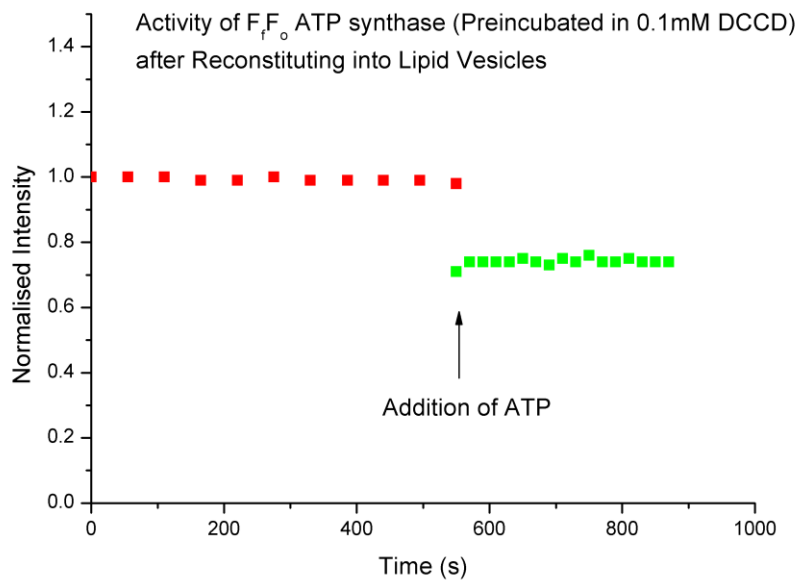
b.



c.

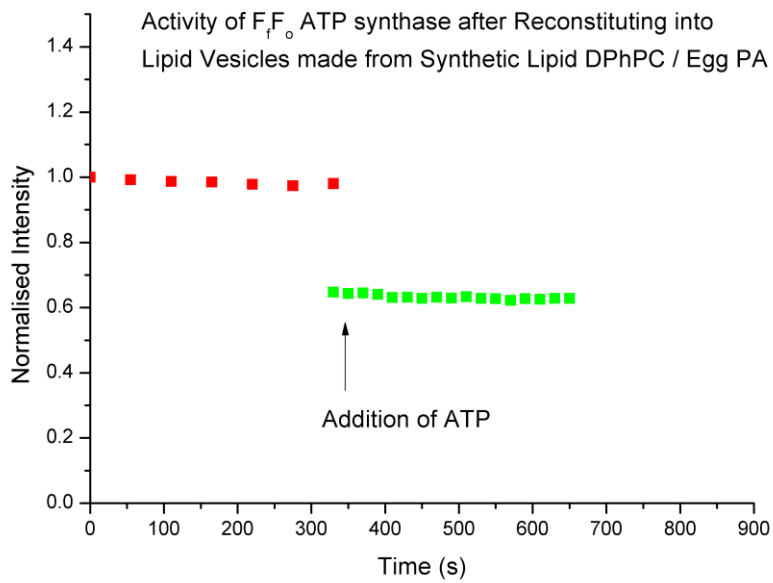


d.

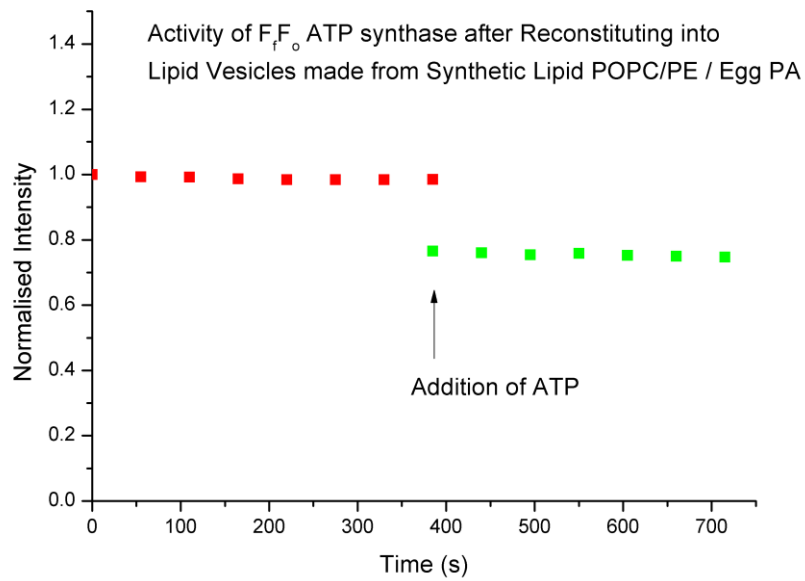


e.

Figure 3-9. Verifying the coupled activity of F_1F_0 ATPase using ACMA. Graph a) shows the time dependent decrease of the fluorescence when ATP was added. This reduction in fluorescence was due to gradual decrease of pH inside the vesicles as protons were translocated into the vesicles via hydrolysis of ATP. In this sample F_1F_0 ATPase was reconstituted into a lipid mix comprising predominantly of natural lipids. Graph b) and c) show no gradual reduction in fluorescence when F_1F_0 ATPase was removed or heat denatured F_1F_0 ATPase was used. Graph d) also shows no time dependent decrease in fluorescence when only F_1 ATPase was used in the experiment. Finally, graph e) also shows no gradual fluorescent reduction when the proton translocation pathway was disrupted by DCCD. All these controls indicated that the time dependent quenching of ACMA was due directly to the pumping of protons into the vesicles by F_1F_0 ATPase during ATP hydrolysis.



a.



b.

Figure 3-10. Graphs showing the activity of F_1F_0 ATPase when reconstituted into artificial lipids. a) shows the activity in DPhPC / egg PA while b) shows activity in a mix of POPC / POPE / egg PA. The inclusion of PA provided a small fraction of negatively charged lipids to the vesicles, similar to the natural lipid system. Time dependent fluorescent quenching in both cases were low.

3.3.3 Estimating the number of F-ATPases per Vesicle

Ideally, one would like to have a single outward facing F_1F_o ATPase per vesicle. This condition is necessary to prevent more than 1 F-ATPase sticking to a gold nanoparticle during the incubation of proteoliposomes with GNPs (see Figure 3-11). The incubation is a necessary step prior to reconstitution onto planar bilayer. It was shown earlier that by controlling the F_1F_o ATPase to lipid ratio, one could calculate the number of F-ATPases per vesicle. However, practically, this number is subject to various uncertainties, including:

- The actual size of vesicles after incubation with detergent
- The actual concentration of lipids and F-ATPase.
- The ratio of inward facing F-ATPase to outward facing F-ATPase after reconstitution. This is important because only those enzymes with F_1 pointing outwards are useful for rotational studies. F-ATPases reconstituted with inward facing F_1 , cannot be labelled with gold nano-particle and are thus unable to have their rotation tracked.

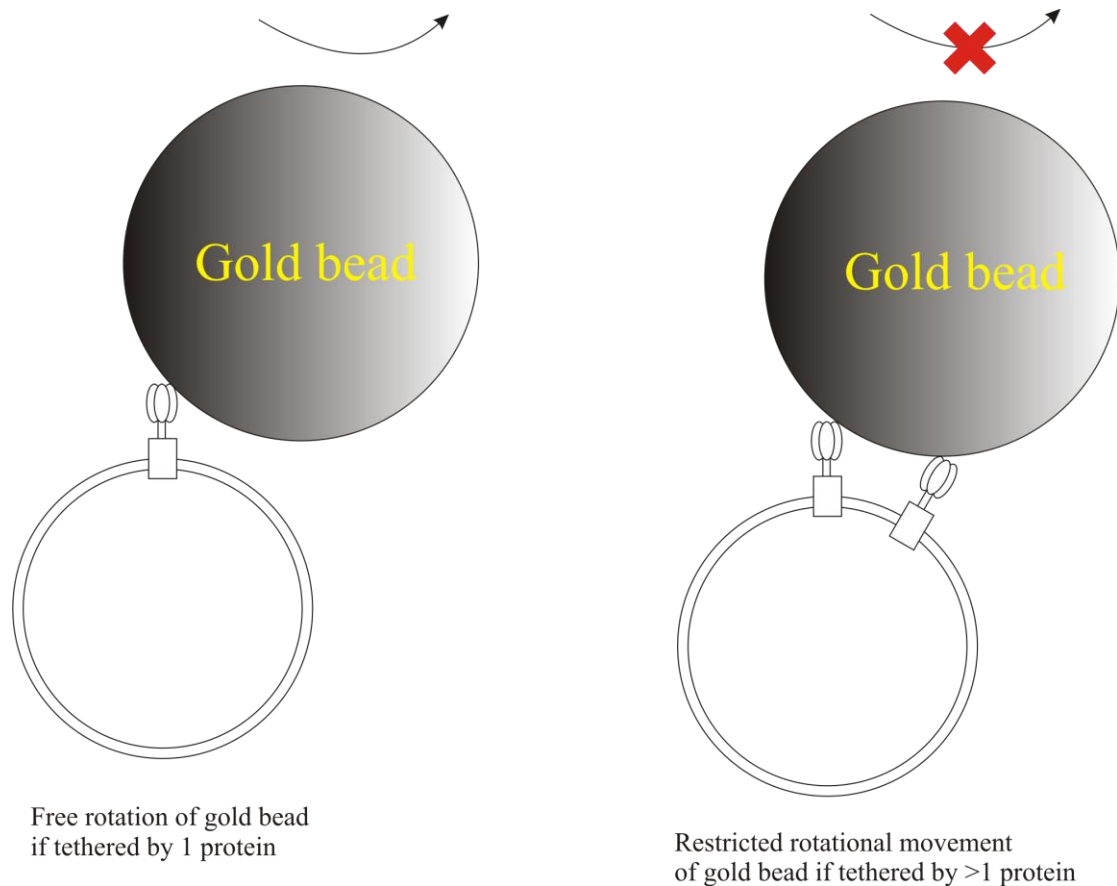


Figure 3-11. To detect free rotation of the gold beads, F_1F_0 ATPase must be tethered to just one F-ATPase. Gold beads that are tethered to more than one F-ATPase will have its rotational degree of freedom severely limited. The optimal number of outward facing F-ATPase per vesicle for rotation study must therefore be 1. It is also noted that this limitation exists only when the gold beads are incubated together with proteoliposomes before the formation of bilayer. If F-ATPases are first delivered into the bilayer prior to the addition of gold beads, then having a stoichiometry of one protein per vesicle is not strictly necessary. This is because the F-ATPases can diffuse away from each other while in the planar bilayer, resulting in sufficiently spaced F-ATPase.

An experiment was devised to estimate the average number of F-ATPase per vesicle. This method combined the results from two different fluorescence based techniques: alternating laser excitation (ALEX) [236, 237] and fluorescence correlation spectroscopy (FCS) [238, 239]. Detailed descriptions of the two systems are not included in this thesis. Readers seeking more information can consult the references given. The descriptions below provide a brief concept of how the two techniques work.

Using Alternating Laser Excitation⁵² (ALEX)

In ALEX, two excitation lasers (at wavelength of 532 nm and 635 nm) are fired alternately, each for a short duration of 50 μ s. Two avalanche photo diodes (APD) are placed downstream in the emission path to capture the emitted photons from the fluorescent samples. One of the APDs is designed to collect the emission due to green fluorophores (green APD), while the other from the red fluorophores (red APD). In addition, the timings of the APDs readout are synchronised with that of the excitation laser so that four different types of signals can be collected:

- Photon counts by the green APD when the 532 nm laser is on - I_{Dex}^{Dem} ⁵³. This represents the presence of green fluorophores.
- Photon counts by the red APD when the 635 nm laser is on - I_{Aex}^{Aem} . This represents the presence of red fluorophores.
- Photon counts by the red APD when the 532 nm laser is on - I_{Dex}^{Aem} . This represents the presence of FRET⁵⁴.
- Photon counts by the green APD when the 635 nm laser is on - I_{Aex}^{Dem} . This channel is spurious and therefore not considered normally.

In the following application, only I_{Dex}^{Dem} and I_{Aex}^{Aem} are considered. For simplicity, I_{Dex}^{Dem}

is called the green signal and I_{Aex}^{Aem} called the red signal.

⁵² ALEX microscope used for this experiment belongs to the Kapanidis group

⁵³ As part of the standard nomenclature, D represents donor, A represents acceptor; em represents emission, while ex represents excitation.

⁵⁴ Fluorescence Resonance Energy Transfer. This is a process in which energy is non-radiatively transferred from one fluorophore to another via induced dipole interaction.

The sample tested was a suspension containing F_1F_0 ATPase reconstituted vesicles, but with Alexa-647⁵⁵-dextran trapped inside the vesicles and Alexa-532⁵⁶-streptavidin added on the outside. If F_1F_0 ATPases were successfully reconstituted, the vesicles should bind the fluorescent streptavidin via the biotin tag on F_1 . Figure 3-12a shows a schematic of the sample. With this configuration of dyes, one could interpret a spike increase in red signal as an indicator for the presence of vesicles in the detection volume. Simultaneously, the intensity of the green signal could be measured and attributed to the fluorescent streptavidin molecules attached on the vesicle. This green intensity was used to estimate the number of streptavidin molecules on the vesicle, with the help of a calibration curve obtained from FCS data of soluble free streptavidin molecules.

It was however noted that for this method to work properly, the concentration of the vesicles must be kept low enough so that only one vesicle was in the detection volume during each spike in red signal. Furthermore, the size of vesicle must also be small compared to the detection volume, so that the background green intensity was not affected by the presence of the vesicle⁵⁷ and that both the green and red fluorophores could be assumed to be co-localised. The exact protocols for the sample preparation are given in Appendix 1 (A1-4).

⁵⁵ This fluorescent molecule is excitable by 635nm laser

⁵⁶ This fluorescent molecule is excitable by 532nm laser

⁵⁷ The finite volume of the vesicle replaces part of the buffer in the confocal volume. Non specific green fluorescence of the vesicle might be different from the buffer, thus resulting in a different intensity of background fluorescence, if the vesicle was large relative to the confocal volume.

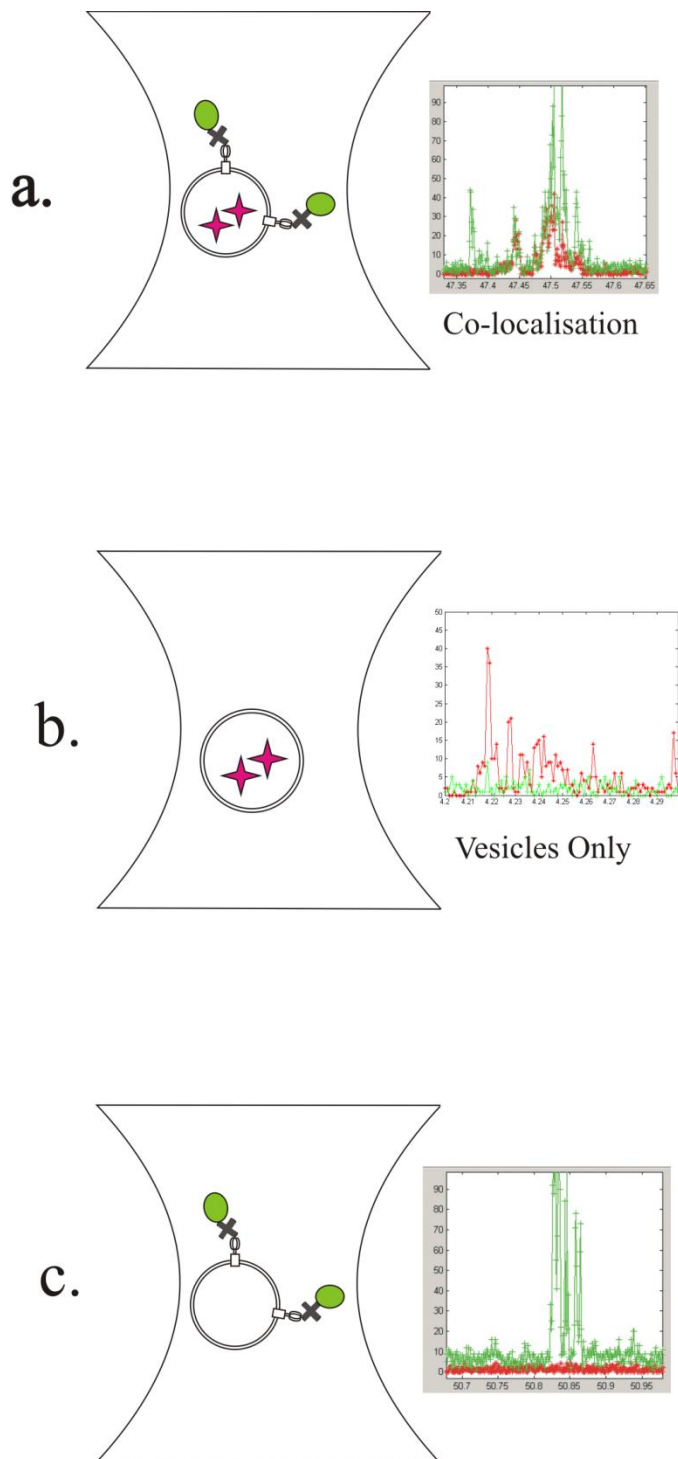


Figure 3-12. Schematics of the sample tested. a) Alexa 647-dextran was trapped inside the vesicles while Alexa 532-streptavidin was attached to the vesicles exterior via the F_1F_0 ATPase. When a vesicle passed through the detection volume, both the red emission and green emission were increased. b) and c) show the scenarios where either the red or green fluorophores were detected. These cases arose when fluorophores were photobleached or entity possessing only one kind of fluorophore was in the confocal volume.

FCS can be understood qualitatively by considering the following: In general, molecules move across a small detection volume with a characteristic time scale. At times much shorter than this time scale, all fluorophores that are originally in the detection volume will still be close to their original position. The measured fluorescent intensity is thus highly correlated. At timescales that are much longer than the characteristic time scale, all the original fluorescent molecules would have diffused away and replaced by new ones. There is therefore little correlation with respect to the previous signal. By looking at the autocorrelation curve, one is therefore able to estimate the characteristic timescale of diffusion for the fluorophores.

Furthermore, the higher the number of fluorophores in the detection volume, the smaller will be the change in autocorrelation value. From Equation 3-6, the autocorrelation is defined as the product of the intensities separated by a time lapse τ , normalised by the square of the overall mean intensity. For complete correlation ($\tau = 0$, which is also equivalent to the y-intercept in the autocorrelation function), the numerator of Equation 3-6 will scale with N (number of fluorophores in the detection volume), while the denominator scales with N^2 (see Appendix 2). This means that in a detection volume of high fluorophores density (where N is big), the y intercept of the autocorrelation function will be close to unity. Conversely, in a volume where there are hardly any fluorophores (where N will be small), the y-intercept will be large. As seen in Box 3-4, the average number of fluorophores (N) in the detection volume is in fact inversely proportional to $g(0) - g(\infty)$.

To obtain the calibration curve, a mixture of free red and green dyes with known concentration was used. Autocorrelation data of the sample was fitted to Equation 3-7 to obtain the average number (N) of red and green fluorophores in the detection volume. Using the same test sample and equivalent laser intensity, the microscopy mode was switched to ALEX so that the corresponding intensities of the green and red emissions could be obtained. By plotting the fluorophore number obtained from FCS against the intensities recorded with ALEX, and repeating for samples of different concentrations, a calibration curve relating the number of fluorescent molecules inside the detection volume to the average intensity was obtained. Figure 3-13 shows a schematic of the work flow.

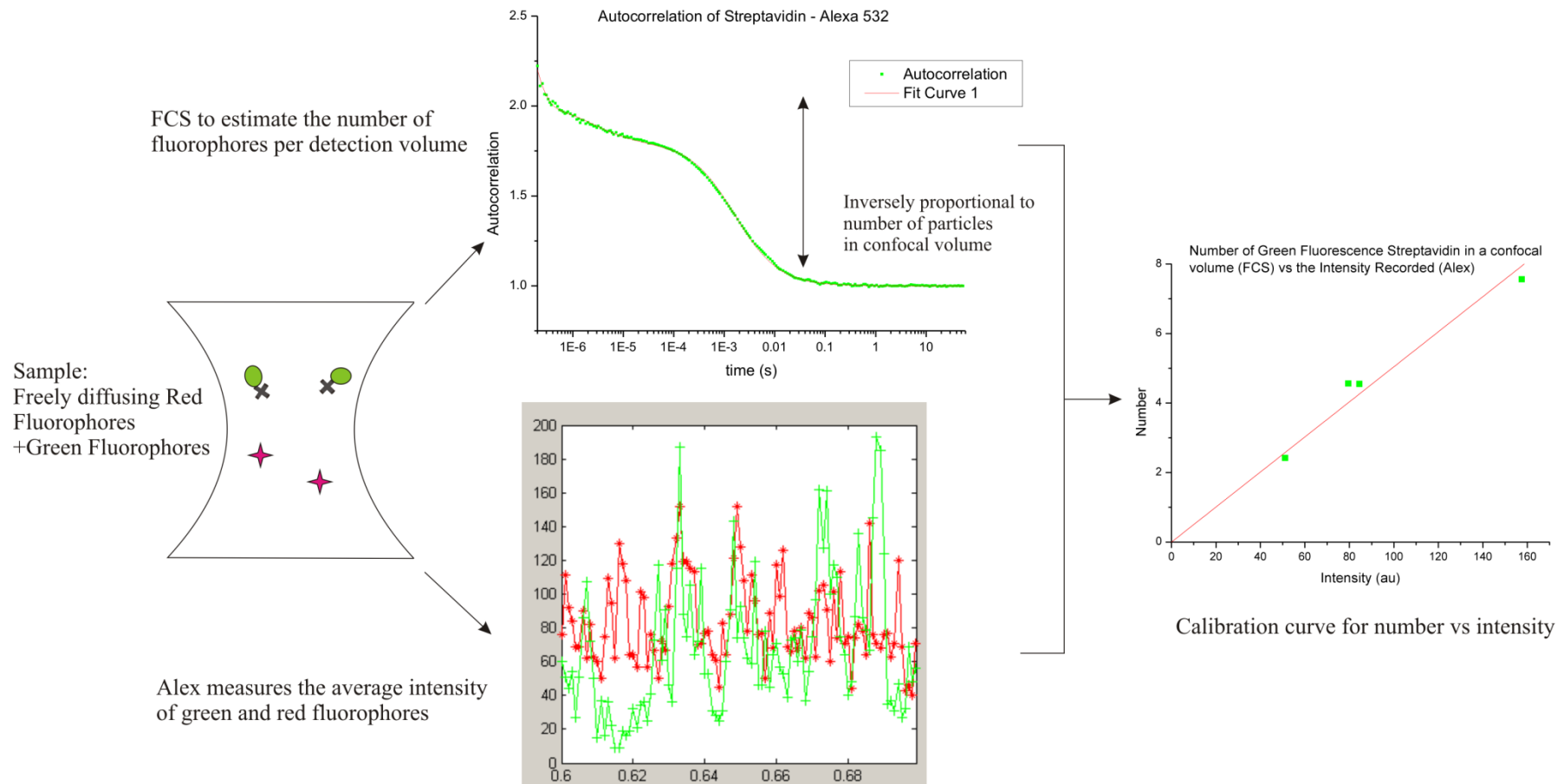


Figure 3-13. Illustration on how the relationship between number of fluorophores and their corresponding intensities was obtained. From a mix sample of free Alexa 647 dextran and Alexa 532 streptavidin, I was able to use FCS to obtain the number of fluorophores in the detection volume and the corresponding emission intensity from ALEX. The former was then plotted against the latter to obtain the calibration curve.

Results1: Verification of the Method using Controlled Samples

Before using the method to estimate the number of molecules per vesicle, it was first tested against controls with known characteristics. The controls contained vesicles with a known number of trapped streptavidin-Alexa 532 and streptavidin-Alexa 647 molecules. These controls were prepared by incubating the vesicles in different concentrations of red and green fluorophores – three different concentrations of fluorophores were used to form the vesicles. The average number of fluorophores inside the vesicles was calculated based on the fluorophore concentration and the average size of the vesicles. Detailed protocol for obtaining vesicles with trapped streptavidin molecules can be found in Appendix 1-4. By measuring the intensities of the green and red fluorophores every time a vesicle was detected, I obtained the average green and red intensities associated with a vesicle and therefore the number of fluorophores that corresponded to these intensities.

There were two approaches to define the presence of vesicles. The first approach was mentioned earlier, where a vesicle was defined by the intensity increase in the red signal. Green intensities were recorded whenever a “red vesicle” was detected. The average number of these green intensities corresponded to a specific number of green fluorophores. To avoid incorrect assignment of freely diffusing red fluorophores, only red intensities that were three standard deviations greater than the background intensities were used. Furthermore, only signals that persisted in the detection volume for greater than 4 ms were considered. This value was four times greater than the diffusional time constant for free streptavidin (~ 1 ms) as measured by FCS. There would however still be cases where aggregates of red fluorophores or non-specific

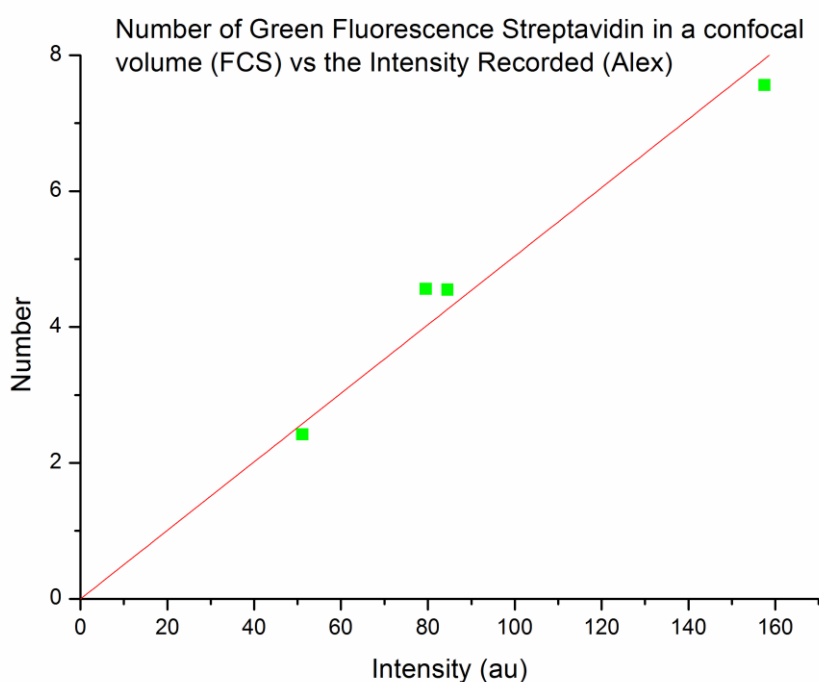
fluorescent entities were wrongly considered as vesicles. Moreover, vesicles with photobleached green fluorophores might also be present. For these cases, the green signal would be close to the background. Consequently, the average green signal obtained using this method tended to be lower, thus giving an underestimation of the actual number of green fluorescent streptavidin molecules on the vesicle.

The second approach to detect vesicles was to consider a simultaneous presence of green and red burst. (i.e. defining a vesicle by the criteria that both the green and red signals were three times greater than the standard deviation of their respective average intensities). This made the selection criteria of vesicles more stringent. However, it also tended to bias the recorded intensity towards a higher value since only signals with high intensities were selected (e.g. bigger vesicles or clump of vesicles might preferentially be selected using this approach). This method of analysis therefore resulted in an overestimation of the number of streptavidin molecules on the vesicles.

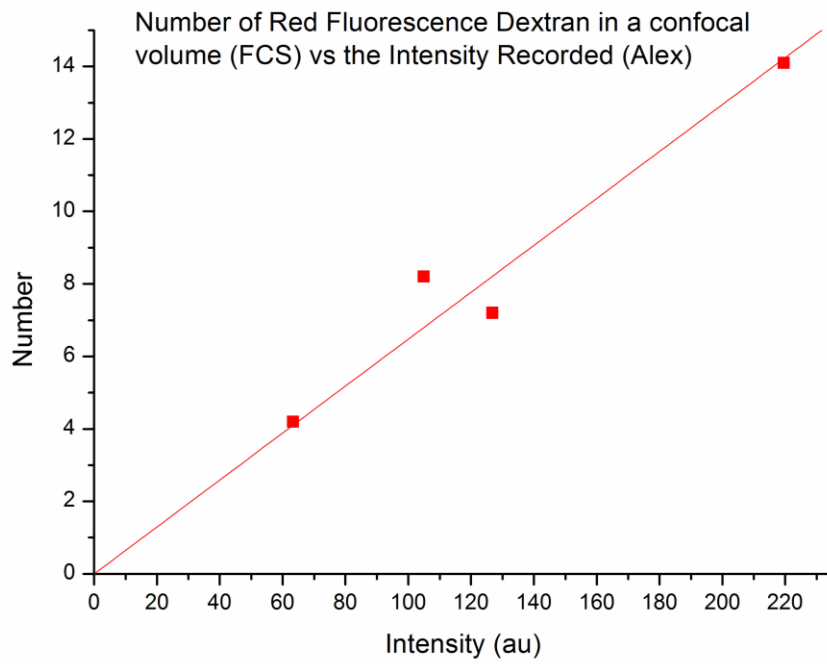
Figure 3-14 shows the results of the control experiment. The calibration curve relating the number of green fluorophores to the average green intensity is given in Figure 3-14a. Figure 3-14b shows the equivalent calibration curve in the red fluorophore. Both graphs give a general linear relationship between the amount of fluorophore and the average intensity measured. This was consistent with the expectation that intensity of fluorophores is proportional to their number in the detection volume.

The calibration curve was then used to predict the number of green and red fluorophores inside the vesicles to confirm that the method was reliable. When the green intensity was used to predict the number of green fluorophores, presence of

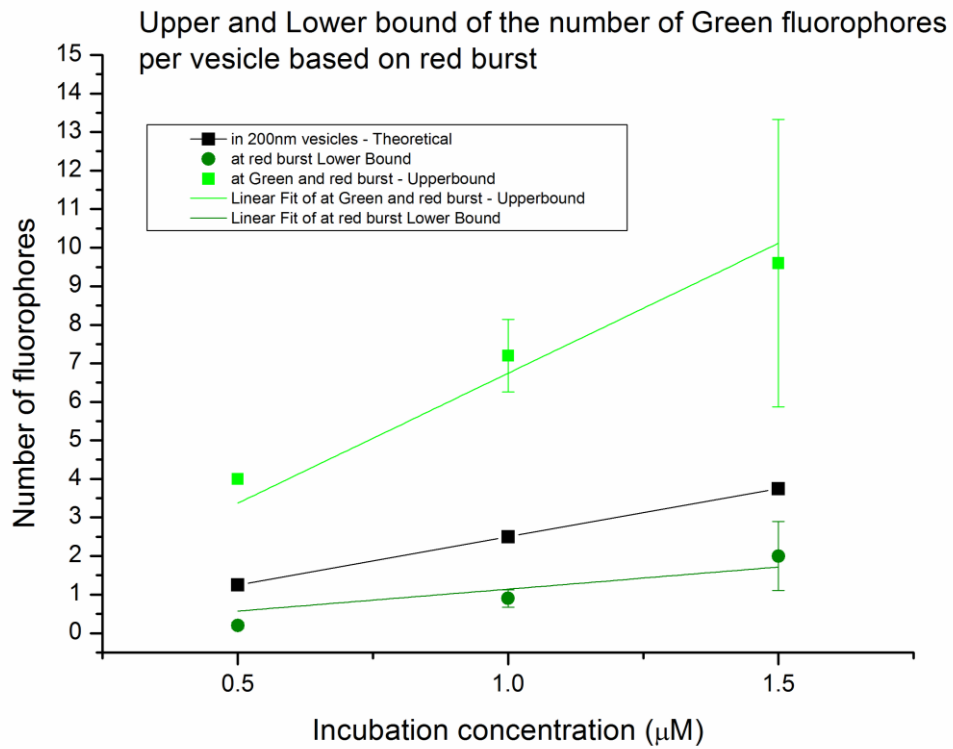
vesicles were either defined by red intensity spike or simultaneous red and green intensity spikes. The former gave a lower estimation of the fluorophore number while the latter gave the upper limit. Results are shown in Figure 3-14c. Conversely, when the red intensity was used to predict the number of red fluorophores, similar upper and lower estimates could be obtained. Results are given in Figure 3-14d. In both graphs, the y-axis represents the number of fluorophores inside the vesicle while the x-axis represents the concentrations of fluorophores used during the formation of vesicles. The black lines on both graphs indicate the theoretical number of fluorophores inside the vesicles, as calculated from the known fluorophore concentrations. The two coloured lines that are drawn above and below the black line represent the upper and lower estimate of the number of fluorophores in the vesicles.



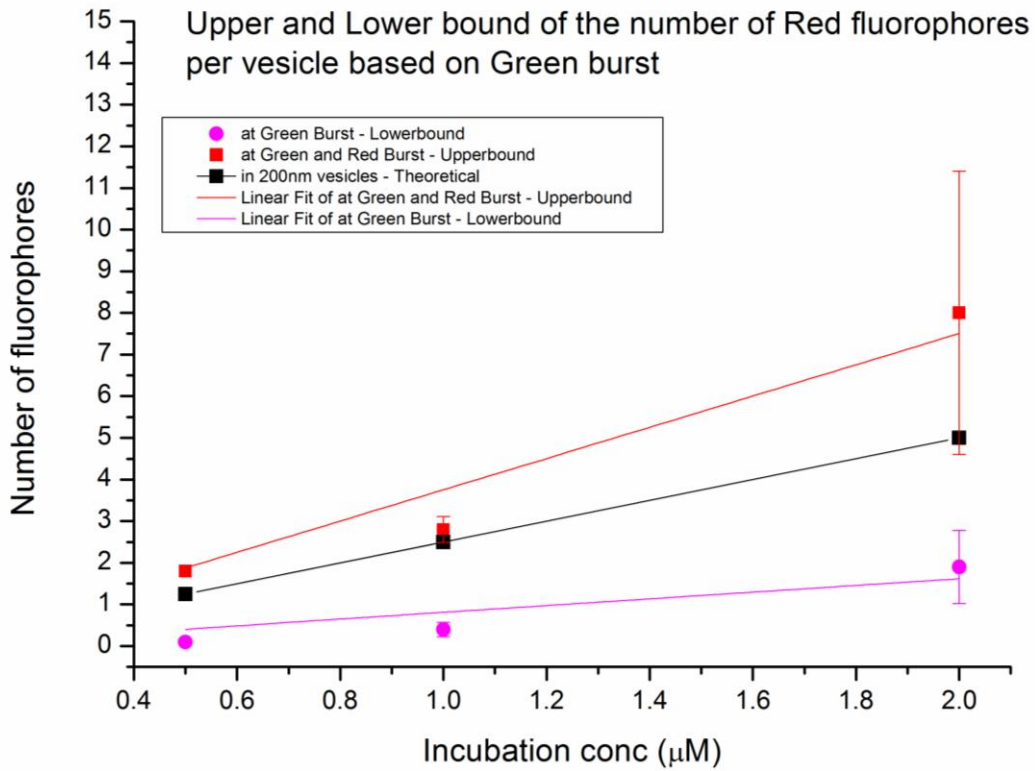
a.



b.



c.



d.

Figure 3-14 Results for the control experiments where the number of fluorophores per vesicle were known. Graph a) shows the curve relating the number of green fluorophores to the average green intensity, while graph b) shows the equivalence in the red channel. Graph c) shows plot relating the number of green fluorophores to the initial concentration of green fluorophores used to form the vesicles. The light green graph shows the upper bound of the estimate, obtained by defining a vesicle as having both burst on red and green intensity. The dark green lower bound was obtained by defining a vesicle as having burst only in the red intensity. Graph d). shows similar results where the number of red fluorophores were estimated. The error bars represented the standard errors.

It can be seen from Figure 3-14c and Figure 3-14d that the theoretical numbers of fluorophores (black lines) are bound by the lower and upper estimates obtained from the experiments. All the plots give an upward trend with respect to increasing fluorophore concentrations. Although it was not possible to obtain the exact number of fluorophores inside the vesicle, an estimation of the minimum and maximum number of fluorophores was possible. This control provided the confidence that the method used was reasonable and able to give a good approximation of the average number of fluorophores associated with the vesicles.

A final control was done to show that the co-localisation of red and green fluorophores was not due to freely diffusing fluorophores interacting with each other. In this control, the fluorophores were added only after the vesicles were formed. These fluorophores were thus not trapped inside the vesicles. The average green intensity measured during a red intensity burst (“red vesicle” detection event) was almost the same as the background green intensity. This suggested that there was no co-localisation of the green and red fluorophores. The same results were obtained when the average red intensity was measured during detection of a “green vesicle”. This control further supported the postulation that co-localisation of red and green bursts was the result of trapped fluorophores inside vesicles.

As mentioned earlier, the actual sample contained vesicles with Alexa647-dextran trapped inside and biotin modified F_1F_0 ATPase reconstituted onto the vesicles (Figure 3-12a). Alexa 532-streptavidin was added after the proteoliposomes were formed. After ½ hour incubation, excess fluorophores were removed via ultracentrifugation. The number of fluorescent streptavidin molecules per vesicle was measured and

found to have an upper bound of ~ 13.7 and lower bound of ~ 5.8 . If one assumed that all the free biotins were bound to streptavidin (there are three biotin per F_1F_0 ATPase), then one would expect an upper bound of 4.6 and lower bound of 1.9 F_1F_0 ATPase per vesicle. The theoretical number of F-ATPase per vesicles (80 nm in diameter) was calculated to be ~ 6 . This theoretical calculation was based on 100% efficiency in F-ATPase reconstitution (10 μ L of F-ATPase at 0.92 mg/ml) and that all F-ATPases were inserted with the right orientation. The average number of correct facing F-ATPases determined experimentally was about 3.25 (average(4.6, 1.9)) F-ATPases per vesicle. This was about half of the theoretical value. Basing on this value, the working concentration for stock F_1F_0 ATPase was reduced three times in order to get about one F-ATPase molecule per vesicle (i.e. 0.3 mg/ml).

3.4 Conclusion and Summary

In this chapter, the protocols for purifying the F_1F_0 ATPase from *E. coli* and reconstituting them into vesicles are shown. Conditions for reconstitution were also adjusted to get approximately one F-ATPase per vesicle. This is necessary so that any probe attached to the F-ATPase will retain its rotational degree of freedom. The procedure of delivering F_1F_0 ATPase onto planar bilayers using these proteoliposomes will be shown in the next chapter.

It was found that the ATPases purified with nickel columns were twice as active as those from glycerol columns. This could be due to the stabilising effect of the lipids added to the former. Otherwise, there was no significant difference between the two techniques in terms of the yield and purity. It was also shown that F_1F_0 ATPases could

be reconstituted back into lipid vesicles and that they retained the ability to translocate protons across vesicular bilayers during hydrolysis of ATP. However, not all lipids were suitable for the reconstitution. While natural lipids from egg PC / egg PA and *E. coli* Polar lipids were suitable, synthetic lipids like 1,2-diphytanoyl PC (DPhPC) and 1-palmitoyl-2-oleoyl PC / PE (POPC) gave very little activity. Reconstitution for all subsequent experiments was thus done with a predominantly natural lipid mix.

Using DLS, it was found that the diameter of vesicles was about half the size before reconstitution. This reduction was probably due to the solubilisation of the lipid vesicles by detergent and re-formation of vesicles as the detergent was slowly removed from the buffer. From the size of the vesicle, one could estimate the theoretical number of outward facing F-ATPases per vesicle. However, as this number was subject to uncertainty such as the concentration of intact F-ATPases and the orientation in which they were inserted into the vesicles, the actual number of correctly oriented⁵⁸ F₁F_o ATPase per vesicle was experimentally obtained instead. This number was found to be between 4.6 F-ATPases and 1.9 F-ATPases per vesicle when 0.9 mg/ml of F-ATPase was used. From this estimate, it was decided that the optimal concentration of F-ATPase used for incubation should be ~ 0.3 mg/ml. This was the enzyme concentration which, when added to an equal volume of lipid vesicles (16 mg/ml and extruded with 200 nm membrane), corresponded to an experimentally determined ratio of one correctly oriented F-ATPase per vesicle.

⁵⁸ The right orientation is defined as one where the F₁ domain of the protein is at the exterior of the vesicle

4

Preparing Planar Bilayer and Incorporating F-ATPase

4.1 Introduction

After purifying the F-ATPase and ascertaining its functionality, the next stage was to create an environment to hold the enzyme in place. This environment should contain two unique regions – an aqueous region to contain the hydrophilic part of the F-ATPase and a hydrophobic region to house the F_o subunits. The hydrophobic region must also be sufficiently thin to allow aqueous access of the c and a-subunits on both sides. A planar phospholipid bilayer (as oppose to vesicular bilayers) was chosen as the preferred system to stabilise the enzyme. The main advantage of using planar bilayer is that it can be accessed electrically from both sides of the membrane. Moreover, planar bilayers typically have a bigger surface area, which allow them to hold a larger number of enzymes. The large volume reservoirs on both sides of the membrane can also act as chemical/ion sources or sinks for reactions occurring at the enzymatic sites. However, the main drawback of planar bilayers is that they are far less robust than their vesicular counterpart.

One popular way of forming planar bilayer is by the method of Montal and Mueller [196]. This method has traditionally been the workhorse for many electrophysiological experiments. Two monolayers are first formed by spreading phospholipids on top of two reservoirs of buffer, separated by a partition. Bilayers are then created by the “zippering” of the two monolayers, as the heights of the reservoirs are raised and the monolayers meet at a small aperture located in the partition. This method produces a freely suspended vertical bilayer that is of relatively large size and stable for few hours⁵⁹ [196]. However, its vertical configuration makes it not amenable to high resolution microscopy. To address this, methods that form horizontal planar bilayers were devised [240-244]. A general characteristic of these methods is the use of a small aperture, where the planar bilayer are formed. To create the bilayer, a small amount of lipid is first painted on the aperture. Conditions favourable to the formation of the bilayer are then applied, either by drying [241], pressure [242], natural thinning and spreading of lipid-solvent [244] or solvent extraction [243]. Like the Montal-Mueller method, such techniques allow full control of the buffers and electrical potential at both sides of the membrane. In addition, the aperture can be brought very close to the microscope objective to achieve high magnification of the bilayer. They are however still plagued by the perennial problems of instability and inconsistency in bilayer formation.

More recently, a new method of forming bilayers was invented, which involved a clever paradigm shift from the conventional techniques. Instead of having lipids in an aqueous environment, the inverse condition of introducing buffer in an oil environment was used. In this technique, a relatively large aqueous droplet is

⁵⁹ Although experience with such system seems to suggest a bilayer of more delicate nature.

immersed in an oil-lipid mix. The immiscibility between the two liquid media (oil and water) prevents dispersion of the aqueous droplet and maintains its integrity in the hydrophobic environment. Furthermore, the lipids that are dissolved in the oil environment form a surface of self-assembled monolayer (or possibly multiple layers of lipid stacks) around the aqueous droplet. When two of these surfaces are brought together, a bilayer can be formed. The use of such a method has been reported by Funakoshi [245], Heron [246] and Holden [247]. A good review of the technique and its potential applications can be found in [248]. While this technique has the advantage of producing ultra-stable bilayers (> 2 weeks) [249], they are however pseudo-isolated. This means that it is difficult to introduce or remove content into or out of the droplet, once it is inside the oil. It is even more difficult if the bilayer is already formed. Electrically accessing a droplet has however, been shown to be relatively easy using an agarose coated Ag/AgCl electrode [246, 250].

4.2 About this Chapter

This chapter contains the details of how a planar bilayer can be formed and reconstituted with F-ATPase. The method adopted is the droplet-on-hydrogel-bilayers (DHB) developed by Heron [246]. It is a variant of the oil based method mentioned earlier. Bilayers formed using this method have been shown to be ultra stable [249]. Furthermore, rather than having two reservoirs of buffer, one side of the bilayer is supported by an agarose based hydrogel instead. The presence of the hydrogel beneath the bilayer is essential for the tethering of the c-ring so that the rest of the motor can rotate with respect to it. This will be expanded upon in Chapter 5. The other obvious reason for using the system is that the inventors of the technique are

just two streets from the physics department and are ever willing to lend a helping hand to pestering graduate students like me!

In this chapter, the general concepts of bilayer formation are first discussed. This is followed by a description of how the setup was characterised and the procedures for inserting F-ATPase into the bilayer. Proof of successful F-ATPase incorporation was demonstrated by detecting fluorescent labelled F-ATPase using total internal reflection fluorescence microscope (TIRFM) and studying the lateral diffusion of the enzyme on the membrane.

To unequivocally show that ATPase in the bilayer was intact and functional, one would have to devise a means of assessing its functionality. A possible way of doing this is to measure the proton current due to the rotation of F-ATPases. This is however challenging because unlike conventional ion channels, the F-ATPases on the bilayer allow only a small amount of protons across at a time. This is because rotation of the c-ring is strongly coupled with enzymatic reactions at F_1 , which are rate-limiting. For the DHB method, one may get about a few thousand enzymes on the bilayer⁶⁰. Assuming that each F-ATPase rotates with a speed of ~ 11 Hz [201], the total amount of current will still be in the order of 0.1 pA. This current may potentially be lower because not all F-ATPases will rotate at the same time. With such small current, it is difficult to differentiate the actual signal from background noise. An alternative way of measuring activity is to observe direct movement of the enzyme. This was attempted and the results are discussed in Chapter 6.

⁶⁰ This number is estimated from the density of fluorescent spots on a bilayer that has been reconstituted with fluorescent streptavidin labelled F-ATPase. See also section 4.4.3 for more details.

4.3 Material

All chemicals used in this section were obtained from Sigma Aldrich (UK) unless otherwise stated. Lipids used were obtained from Avanti Polar Lipids. Alexa-532 streptavidin and Alexa-647 dextran were obtained from Invitrogen, and agarose was obtained from Sigma and Lonza biologics. Fluorescent beads were purchased from Molecular Probes - Fluospheres carboxylate-modified microspheres, 0.2 μm , orange fluorescent (540/560) 2% solid – Cat number: F8809. In the experiments, MOPS buffer comprised 20 mM MOPS pH \sim 7.2 (adjusted with NaOH), 80 mM NaCl, 2 mM MgCl_2 , 10% glycerol. Agarose (Lonzo biologics) coated on the coverslip was prepared at a concentration of 1.5% w/v using double distilled water. Hydrating agarose (Sigma) was prepared at 2% w/v using MOPS buffer. Descriptions of the methodology given herein are mainly qualitative. Readers interested in the exact protocols can find them in Appendix 1 (A1-5).

To create the housing for the bilayer, a poly-methy-metha-acrylate (PMMA) device was made using computed numerically controlled (CNC) machining. This device was produced by the Wallace group in the Chemistry department, University of Oxford. Figure 4-1 shows a schematic of such a device. There are twelve wells in each device, in which bilayers can be formed. These wells were designed to contain the hexadecane / lipid mix. Two through holes, labelled I and III on Figure 4-1, were used to incorporate the hydrating agarose. Molten agarose (2% Agarose) was introduced into the device via inlet I and escapes via outlet III. The hole labelled II was used to contain an Ag / AgCl electrode. The device also contains shallow channels at the bottom, which were meant to lead the molten agarose from inlet I, past

the wells and finally exiting through outlet III. The next section provides a detailed explanation of how the bilayer can be formed.

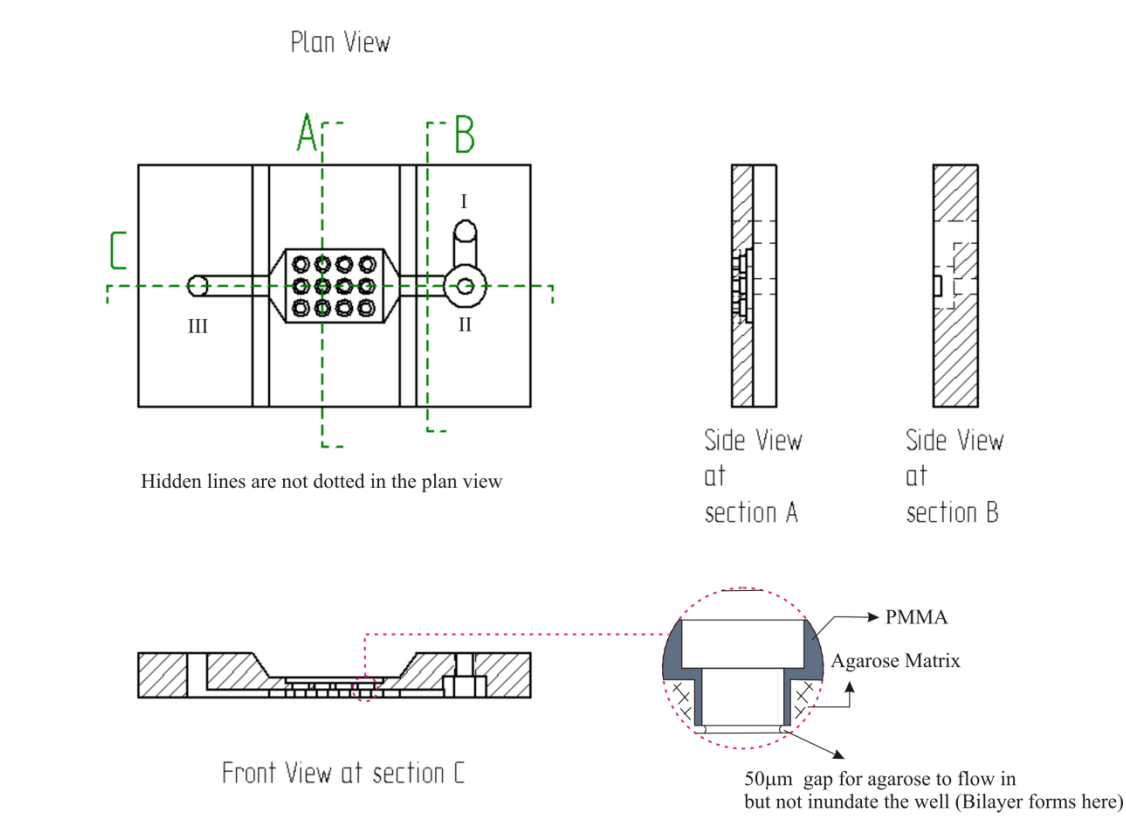


Figure 4-1. Overall schematic of the device use for the creation of the DHB.

4.4 Methods & Results

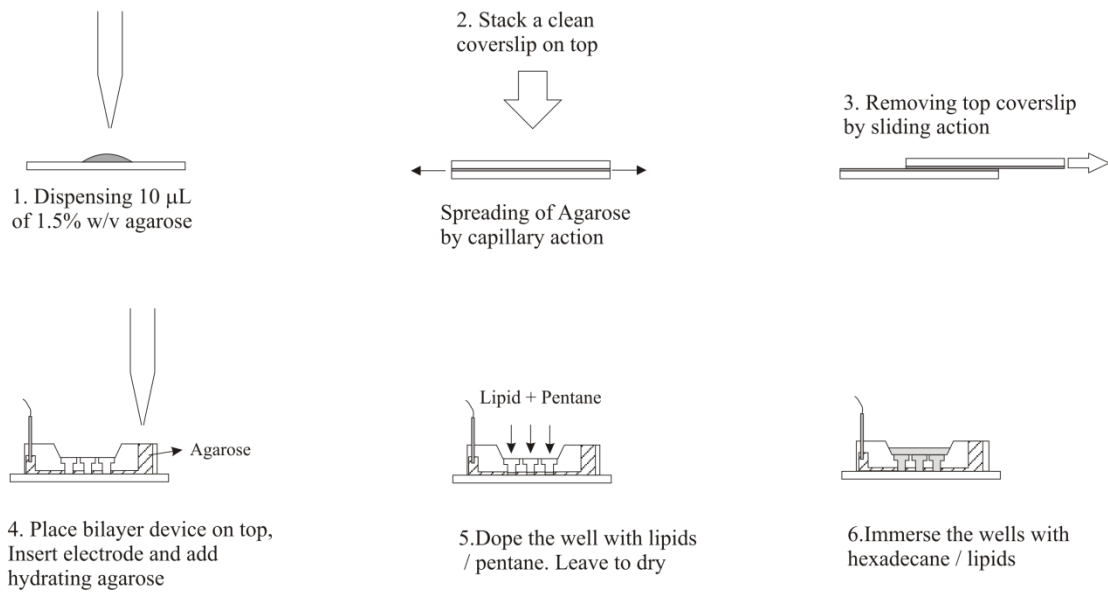
4.4.1 Preparing Droplet On Hydrogel Bilayers

The bilayer was formed between two hydrophilic surfaces, each containing layer/s of lipid molecules. The first surface was around the aqueous droplet introduced into the well and the second was on a very thin layer of agarose coated on the surface of the coverslip (See Figure 4-2b). Agarose was used as a substrate because it satisfied three essential conditions:

1. It is hydrophilic. This allows at least a monolayer of lipids to form spontaneously and with the hydrophilic end pointing towards the substrate.
2. In its hydrated state, agarose forms a 3D porous matrix filled with buffer. This enables movement of ions across itself. An electromotive force can thus be applied across the bilayer without too much drop in electrical potential across the substrate.
3. It is modifiable with functional groups. The hydroxyl groups within polysaccharides can be modified to accept either nitrilo-tri-acetic acid (NTA) or biotin functional groups, both of which can be used to immobilise proteins.

To ensure that the agarose was well coated on the coverslip, the latter was first cleaned using an oxygen based plasma etcher (Biorad - Plasma Barrel Etcher PT 7100). Once cleaned, 10 μ L of molten agarose at 1.5% w/v and heated to 90 °C was added onto the coverslip, this was followed immediately by placing another coverslip on top. Capillary action would spread the agarose evenly across the coverslip surface. The top coverslip was then removed using a swift sliding action and the bottom coverslip left to dry in room temperature for approximately 10 minutes (See also Figure 4-2a). The thin layer of agarose on the coverslip will now be referred to as the substrate agarose.

a.



b.

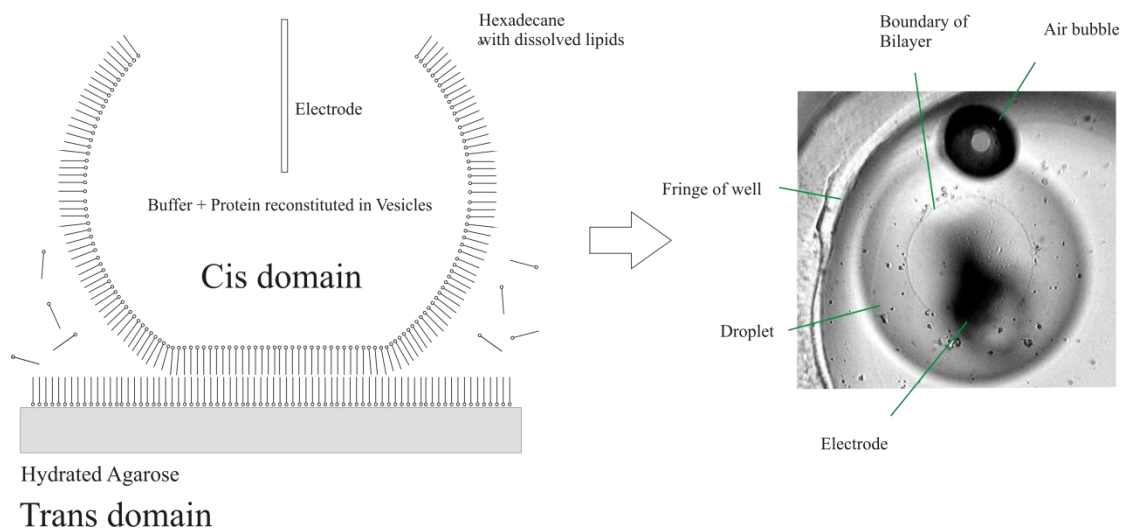


Figure 4-2. Schematic showing how a bilayer device can be created. a) shows the steps taken to build the bilayer device. b) shows a schematic of a droplet on the agarose and a picture of a typical bilayer.

After the substrate agarose had completely dried out, the PMMA device was placed on the coverslip, positioned roughly at the centre. Molten agarose heated to 95°C (2% agarose w/v in MOPS buffer⁶¹ – now referred as hydrating agarose) was flowed slowly into inlet I using a manual pipette. This was a delicate process because it was important to get enough hydrating agarose to surround the wells but not too much to cover the entire substrate agarose inside the well with hydrating agarose. Otherwise, the agarose thickness beneath the well would become too large and uneven for total internal reflection fluorescence microscopy to work. The functions of the hydrating agarose were multi-fold. It served to hold the device onto the coverslip and form a seal that prevented the hexadecane (to be added later) from escaping. Moreover, it also rehydrated the substrate agarose coated on the coverslip and equilibrated it with buffer and salt. The substrate agarose, on the contrary, had only the sole function of forming a support for the bilayer to rest on. If an electro-potential difference was to be applied, an electrode could be inserted into inlet II (see Figure 4-1) prior to adding the hydrating agarose.

Once the hydrating agarose had solidified, a small amount of lipids (~ 0.3 µL of 1 mg/ml), pre-dissolved in pentane, was added to each well. This pre-coated the wells with lipids and allowed the bilayer to form more easily. Excess hydrating agarose at the entrance of inlet I and III was also removed and the inlets sealed with tape to prevent further evaporation. Once the pentane from the doping process had fully evaporated, lipids in hexadecane (at 5mg/ml) were added to cover the wells. The device was then left to stand for thirty minutes before use. Figure 4-2a gives a pictorial illustration of the process described.

⁶¹ Refer to Appendix 1 (A1-5) for constituent and exact protocols

When the device was ready, a small droplet ($\sim 0.2 \mu\text{L}$) of buffer containing preformed proteoliposomes was added into one of the wells using a pipette. This droplet was previously left to brew in a separate reservoir of hexadecane and lipids for three minutes. The brewing process allowed a monolayer to form around the aqueous buffer. When inside the well, the aqueous droplet sank to the bottom and came in contact with another monolayer formed on the hydrated substrate agarose. Excess hexadecane and lipids were expelled from the interface between the droplet and the agarose, resulting in the formation of a lipid bilayer. A typical bilayer was about few hundred micrometers in diameter, as measured with a low magnification objective. After the bilayer was formed, it was allowed to rest for ~ 5 min before measurements are taken. If an electrical potential was needed, a thin electrode could be inserted into the droplet. This process was facilitated greatly by doping the tip of the electrode with trace amount of agarose. Figure 4-2b shows the schematic and actual image of the droplet on the agarose, with the bilayer forming at the interface.

4.4.2 Estimating the Thickness and Hydration of Substrate Agarose

The average pore size and level of hydration of the substrate agarose are useful information because these factors directly affect the extent of interaction between the membrane-bound F-ATPase and the substrate agarose, as well as the amount of charged ions the substrate agarose can accommodate. To obtain an approximation of the pore size and hydration level, the amount and thickness of the substrate agarose on the coverslip were measured. In this section, the methods to do these are described.

Method 1 – Measuring the weight of agarose retained on the coverslip

To determine the level of hydration in the substrate agarose, one must first determine the amount of agarose retained on the coverslip. The basic principle of doing this is to coat the coverslips with agarose and measure their weight directly. However, as the amount of agarose used was minute, the cumulative weights of several coverslips were recorded. The amount of agarose retained on the surface of the coverslip was estimated by simply measuring the weight of the coverslip before and after the agarose was applied. Figure 4-3 illustrates the procedure used. The steps involved were similar to the DHB preparation:

- Step 1a. 10 μL of 1.5% (w/v) molten agarose was dispensed on a coverslip and its weight measured. This step allowed one to calculate the actual amount of agarose on the coverslip. It was necessary to do this because some of the agarose was observed to remain in the pipette tip after pipetting. i.e. not all agarose was dispensed. These coverslips were discarded once the weight was recorded
- Step 1b / 2. To measure the amount of agarose retained on the bottom of the coverslip, about 10 μL of 1.5% (w/v) molten agarose was applied on a fresh coverslip and spread across by placing a new coverslip on top.
- Step 3. The top coverslip was then removed in a quick sliding action.
- Step 4b. The top coverslip was discarded and two of the bottom coverslips were then stacked together to prevent drying of the agarose.
- Step 4a. Evaporation due to the short time during which the agarose was exposed to air, was accounted for by doing a control where both the top and bottom coverslips were retained, but exposed to air for the same amount of time as the test

samples. The weight loss in this control, compared to step 1a, would therefore be due solely to evaporation.

- Step 5. The pairs of coverslips were weighed and the difference between the new weight and original dry weight (weight prior to adding agarose) was the amount of agarose on the surface of the coverslip.
- Given that the initial concentration of the agarose was known (1.5% w/v), the actual weight of dry agarose per coverslip could be estimated.
- To reduce the standard error of the estimate, the experiments were performed over 3 pairs of coverslips with 4 sets of repetitions.

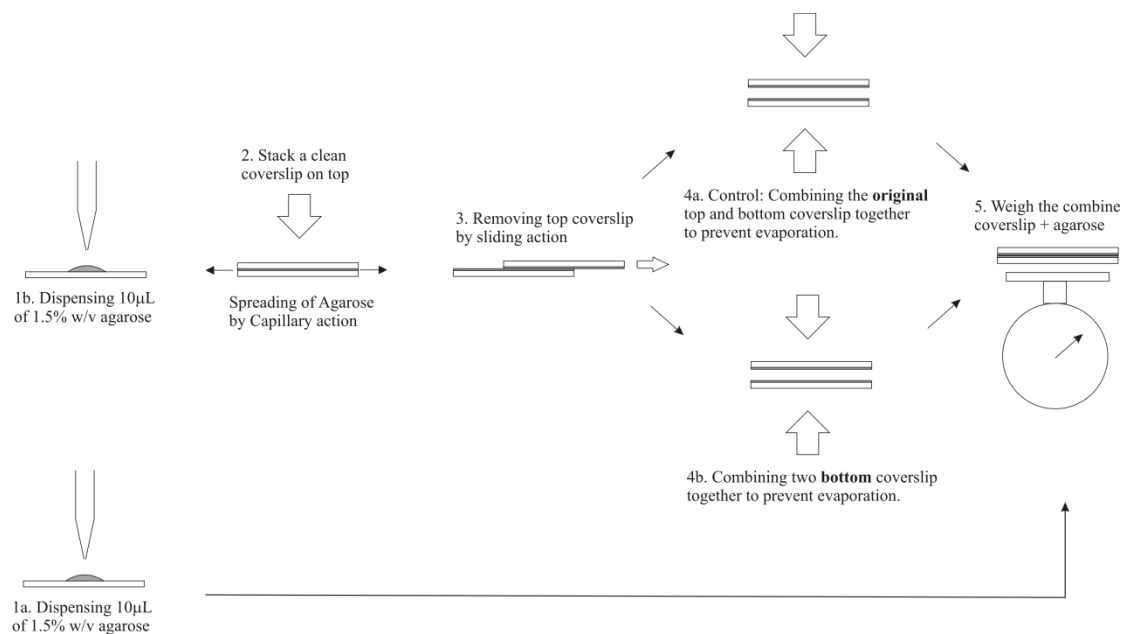


Figure 4-3. Schematic of the method used to measure the amount of agarose on coverslip.

Results 1 – Measuring the weight of agarose on the surface

- 10 µL of dispensed agarose was found to have a mean mass of $8.4 \text{ mg} \pm 0.6 \text{ mg}$ (n=13) instead of the expected 10 mg (corresponding to 10 µL). The difference in weight could be due to retention of a small quantity of viscous agarose on the

walls of the pipette tip. Each pair of coverslips should therefore ideally contain 8.4 ± 0.6 mg of wet agarose, instead of 10 mg.

- From the control, the combined weight loss due to evaporation for 3 pairs of coverslips was calculated to be = 6.5 mg.
- The weight of agarose on 3 pairs of bottom coverslips, after accounting for evaporation = combined weight of agarose for 3 pairs of coverslip (measured = 27 mg) + weight loss due to evaporation for 3 pairs of coverslips (6.5 mg) = 33.5 mg
- Weight of hydrated agarose in every pair of bottom coverslip must now be = $33.5/3 = 11.2$ mg.

This weight was slightly more than the ideal case of 8.4 mg. The larger amount of agarose retained on the bottom coverslip could be due to the bottom coverslip being in contact with the table top, which acted as a heat sink for the warmer molten agarose. There was thus an asymmetry in temperature distribution between the bottom coverslip and top coverslip, which might have caused the cooler bottom coverslip to solidify first and hence retain more agarose. Gravity might also have played a part in the asymmetrical distribution of agarose. Table 1 summarises the results obtained

Table 4-1. Summary of results for direct measurement of weight of agarose on coverslip

	Weight of agarose in 3 pair of coverslips with both top and bottom retained (Control)	Weight of agarose Sample with 3 pairs of bottom coverslips retained
1 st measurement	21.0 mg	30.4 mg
2 nd measurement	18.3 mg	27.8 mg
3 rd measurement	18.3 mg	22.7 mg
4 th measurement	17.3 mg	27.3 mg
Mean weight	18.7 ± 1.6 mg	27.0 ± 3.2 mg

Weight loss in agarose due to evaporation in 3 pairs of coverslip ⁶²	6.5 ± 3.4 mg
Weight of agarose in 3 pairs of bottom coverslips (before evaporation)	$27.0 + 6.5 = 33.5 \pm 6.6$ mg
Weight of agarose retained on each bottom coverslip	$33.5 / 6 = 5.6 \pm 1.1$ mg
Weight of dry agarose on each bottom coverslip (at 1.5% w/v)	$0.015 \times 5.6 = 0.084 \pm 0.017$ mg

Method 2- Measuring thickness of the rehydrated agarose

After determining the mass of agarose on the coverslip, the next step was to measure the height of the agarose after it was hydrated by the hydrating agarose. The basic principle for measuring the height of agarose is straightforward: Two sets of markers were placed on the bottom and the top of the agarose and the vertical distance between them measured. Fluorescent beads were used as markers and their distances apart were calculated by the change in the ‘sharpness’ of the image, as the focus of the microscope was moved up incrementally by a piezo stage. Figure 4-4 gives a pictorial illustration of the method used.

Fluorescent beads of size 0.2 μm were diluted 1:500 times in double distilled water, spin-coated onto an oxygen plasma etched coverslip and allowed to dry. 10 μL of molten agarose was then applied on the coverslip and spread across evenly as given in the previous section. After drying, the agarose was re-hydrated using the PMMA device and covered with hexadecane/lipid. To form a layer of fluorescent beads on top of the agarose, 0.2 μL of buffer containing a 1000 times dilution of fluorescent beads (in MOPS buffer) was dropped into each well. The droplet was deliberately burst to produce a thin layer of buffer on the agarose, instead of forming a bilayer. Under

⁶² Correction for evaporation was estimated by difference between the theoretical amount dispensed (8.4 mg x3) and the actual weight measured (18.7 mg).

these conditions, fluorescent beads would spread across the well and rest on top of the agarose. The negatively charged carboxyl beads were observed to adhere to the agarose. Using bright field imaging, two populations of beads were observed. The first was a bottom layer of beads that were directly on the coverslip. These beads appeared immobilised. Moving up the focus, one could see another population of beads that was tethered but wobbling slightly. These were assumed to be beads resting directly on top of the agarose.

To determine the vertical distance separating the fluorescent beads, they were imaged using a collimated laser source in epifluorescent mode. Fluorescence based microscopy was used, instead of ordinary bright field microscopy, because it gave a better signal to noise ratio. The focus was first lowered in the z direction, so that the lowest bead was above the focal plane. It was then moved up in steps of 20 nm using a piezo stage, and with an image of the beads taken at each step. This process was automated to prevent human error during height adjustment. As the bead moved into focus, its image became sharper and the width of the fluorescent point spread function (PSF) was reduced. The width of the PSF reached a minimum point when the bead was fully in focus but started to increase again as the focus continued to shift upwards. By fitting a two-dimensional gaussian to the PSFs and plotting the width of the upper and lower beads against displacement by the piezo stage, the relative vertical positions of the beads could be determined. To ensure that the lower bead was truly resting on the bottom of the agarose, and not partially suspended in the agarose, the lowest bead in the field of view was selected. Beads on the top of the agarose were characterised by a slightly wobbly movements and only those close to the bottom beads were chosen.

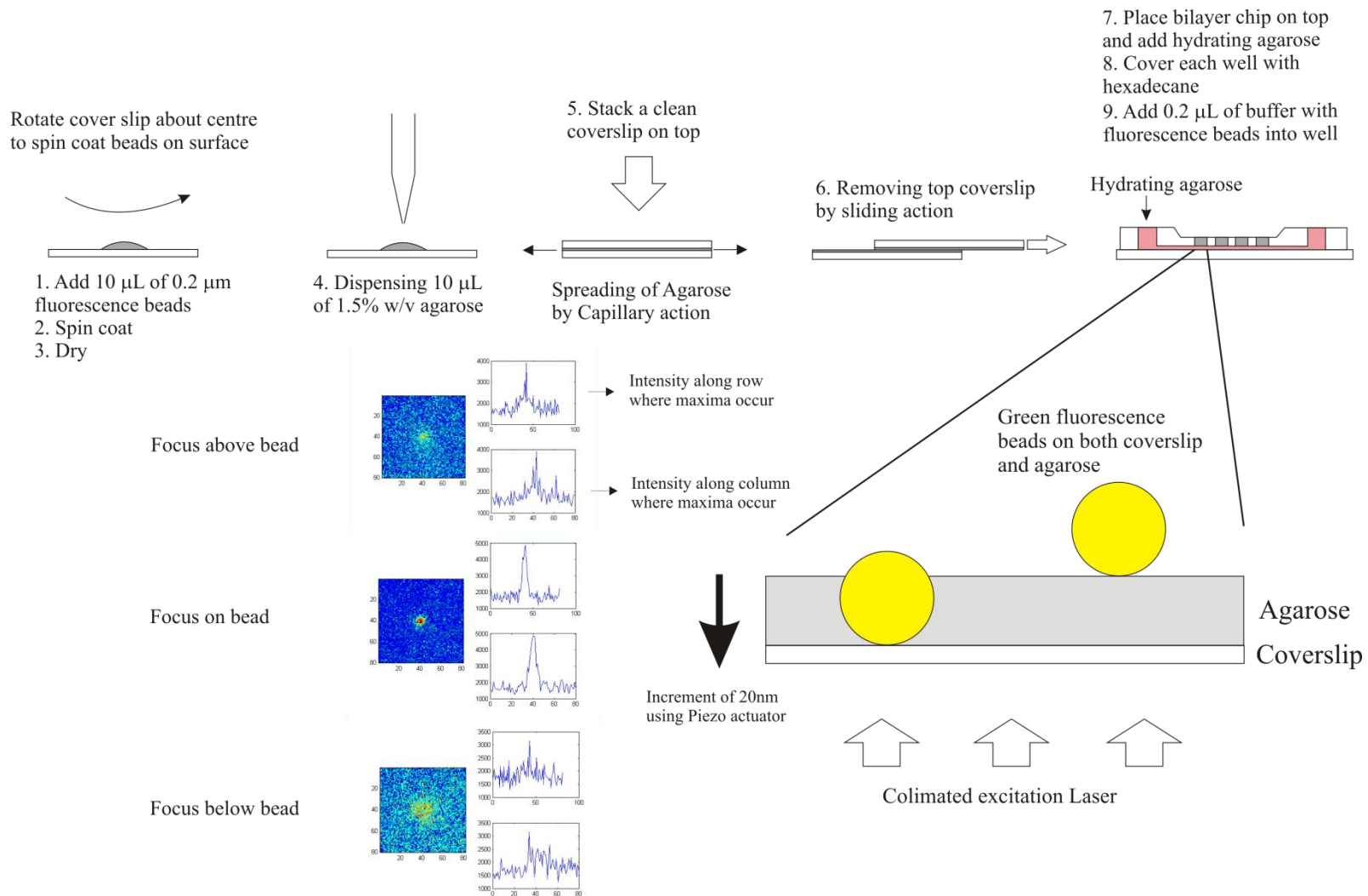


Figure 4-4. Schematic of protocols for measuring the thickness of agarose

Results 2 - Measurement of the thickness of the rehydrated agarose

A simple 2D Gaussian was used to fit the point spread function of the fluorescent beads – See Equation 4-1. Of the five parameters that were used in the Gaussian function, one of them (A_4) described its width, which is strongly dependent on the height of the bead. This parameter was used to plot against the z-displacement made by the piezo stage. See Figure 4-5.

$$PSF = A_1 \exp \frac{-((x-A_2)^2+(y-A_3)^2)}{A_4^2} + A_5 \quad \text{Equation 4-1}$$

Where

A_1 is the amplitude of the 2D Gaussian

A_2 and A_3 are the x and y coordinates of the centre of the Gaussian

A_4 is the standard deviation of the Gaussian

A_5 is the intensity of the background.

To determine the vertical distance between the bottom and top bead, the data points from the plots of A_4 versus z were fitted to two 4th order polynomials. In addition, the polynomial fits were constrained to share the same shape and differed only in their relative positions on the axes (i.e. the curves were translated in the axes). This constraint assumed that the beads were identical and therefore their widths should also vary in similar ways. When this was done, the distance between the curves in the x-axis represented the actual vertical displacement separating the two beads. The average thickness obtained for five sets of beads was $240 \text{ nm} \pm 93 \text{ nm}$ ($n=5$). This was thicker than the suitable distance for TIRFM mode ($\sim 136 \text{ nm}$ – this is the distance at which the intensity of a 532nm laser is reduced by 63% with respect to the intensity at the surface of the coverslip). To explain why TIRFM could still be successfully used with the substrate agarose, it was noted that the amount of agarose

used for TIRFM experiments was typically $\sim 8 \mu\text{L}$ instead of $10 \mu\text{L}$. (From my experience, when the latter was used, TIRF images might sometimes be difficult to obtain. The norm of the lab is therefore to use a lesser amount of agarose whenever TIRFM is required). Furthermore, while there was a small amount of buffer ($0.2 \mu\text{L}$) directly hydrating the agarose in the experiments conducted above, no direct hydration was provided for the actual bilayer setup used in conjunction with TIRFM. In the latter case, the buffer and agarose were separated by a thin bilayer. One would therefore expect the agarose used in the TIRFM to be less hydrated and therefore thinner. The value obtained here hence gave an upper limit for the actual agarose thickness. It should also be mentioned that the preferred method of measuring the agarose (i.e. with an intact droplet and planar bilayer) was not possible here because the top beads did not stick onto the bilayer like they did on agarose. This made it impossible to place a prominent marker on the bilayer.

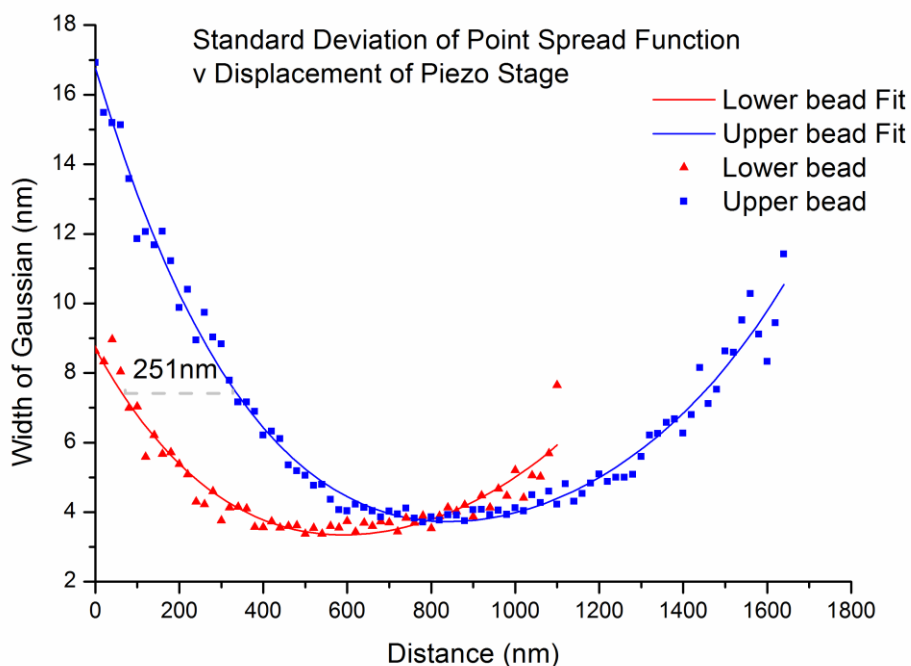


Figure 4-5. Changes in the width of the point spread function with respect to the distance moved by the piezo stage. The red data points represent the bead resting on the coverslip while the blue data points represent beads on the agarose.

Calculating the % by mass of the substrate agarose

It has been established thus far that:

- The amount of dry substrate agarose on each coverslip was 0.084 ± 0.017 mg
- The thickness of the rehydrated agarose was $\sim 240 \pm 93$ nm on a 22 mm x 40 mm coverslip.
- Based on the measured thickness, the total volume of the agarose on coverslip after rehydration was therefore $= 22 \times 40 \times 240 \times 10^{-6} \text{ mm}^3 = 0.21 \text{ mm}^3$.

The weight of agarose as a ratio to the total volume of the rehydrated substrate agarose could be calculated as $0.084 \text{ mg} / 0.21 \times 10^{-3} \text{ mL} = 0.4 \text{ g/ml}$ or 40 % w/v. This was high compared to the original agarose concentration (1.5% w/v) used to form the substrate agarose. An estimation of the pore size was made using the empirical power law relating the size of pores (a) to the mass percentage of agarose (C), [251] [252].

$$a = kC^\eta$$

For low and moderate concentration of agarose (<5% w/v), $\eta \sim -0.59$ and $k \sim 550$ (Pernodet et. al. [251] [252]). Using these parameters, a pore size estimation of about 60 nm was obtained. It must however be stated that this estimation was merely an extrapolation of the curve and would at best be a first approximation of the actual agarose sample. Nonetheless, it could be established that the agarose, though hydrated, was still fairly dense and that the size of the pore might be small enough to locally confine the movement of diffusing proteins on the bilayer. In fact, as reported in the next section, F-ATPases on the bilayer were found to diffuse freely initially, but

typically became immobilised after some time, possibly confined by the small agarose pores or entangled by agarose strands.

4.4.3 F₁F₀ ATPase in Bilayers

Delivering F-ATPases onto Bilayers

Once the bilayer was formed, the next task was to deliver F-ATPase into it. Two methods of delivering F-ATPase into the bilayer were tested. The first method involved using F-ATPase directly (i.e. they were not reconstituted into vesicles first). Excess detergent left in those samples after purification (~0.05 % C₁₂E₈) was removed by short incubation with SM2 bio-beads and diluting with buffer. If too little detergent was removed from the F-ATPase, the droplet became very unstable and tended to break easily. However, if too much detergent was removed, F-ATPases became unstable and began to aggregate. These protein aggregates could be seen on the Total Internal Reflection Fluorescence (TIRF) images as bright fluorescent spots that were much brighter than those obtained using vesicle fusion (to be described later). Due to these difficulties, the direct reconstitution method was not pursued further and an alternative method was adopted instead. This method required the F-ATPase to be first reconstituted into vesicles and excess detergent removed. The proteoliposomes were then diluted in MOPS buffer and brewed in hexadecane / lipids. This mechanism however assumed that the vesicles were able to fuse spontaneously with the planar lipid bilayer. To facilitate the fusion process, 15 mM of CaCl₂ was added into the buffer. The presence of divalent cations helped shield the electrostatic repulsion between the negatively charged lipids and promote fusion [253, 254]. Furthermore, a small osmotic gradient could be induced by either changing the

concentration of the glycerol or NaCl in the droplet (see later part of this section for more details) [255, 256]. Finally, the presence of phosphatidyl-ethanolamine (PE) in the lipid mix was also conducive for vesicle fusion to take place [254].

Lipid Constituent of Bilayer

It has been found in the previous chapter that synthetic lipids gave proteoliposomes with low proton translocating activity. On the assumption that the same applied to planar bilayers, it would be necessary for one to use natural lipids instead of synthetic ones. Originally, DHB planar bilayers were formed using a synthetic lipid – diphytanoyl phosphatidyl-choline (DPhPC), as the lipid of choice. This is because DPhPC has a shape factor⁶³ ~ 1 , which favours the formation of planar bilayers [257]. DPhPC also has fully saturated bonds in its aliphatic chains, making it more resistant to oxidation. In contrast, natural lipids usually contain a myriad of different lipids with different lengths of hydrocarbons and extents of unsaturated bonds. Furthermore, some natural lipids (e.g. *E. coli* extract) also contain a mix of phosphatidyl-glycerol (PG) and phosphatidyl-ethanolamine (PE)⁶⁴. While PG also favours bilayer formation [257], PE has a shape factor >1 and tends to form inverted micellar structures instead. This inevitably lowers the stability of the planar lipid bilayer. Different formulae of lipid mix were tested. On one hand, egg PC + egg PA (phosphatidic acid) + cholesterol in hexadecane were found to be too viscous and could not form any bilayers. On the other hand, *E. coli* polar lipids readily formed bilayers but were unstable, probably due to their high PE content. After a series of trials, a final formula

⁶³ Shape factor (S) is defined as the ratio between the volume occupied by the lipid molecule (V) to the product of the area of the hydrophilic head group (A) and the length of the lipid (l_c). i.e. $S=V/A_0l_c$. If a lipid has a large hydrophilic head group, $S<1$ and this favours the formation of micelles. If the hydrophilic head group is small, $S>1$ and this favours the formation of inverted micellar structures.

⁶⁴ Source taken from website of Avanti Polar Lipids. www.avantilipids.com

consisting of *E. coli* polar lipids, egg PC, DPhPC, egg PA and cholesterol was used. Cholesterol and egg PA were added because they were found to increase the activity of F-ATPase [219]. Moreover, it has been reported that cholesterol is able to increase orderliness of the aliphatic chains and the stiffness of the bilayers, but does not compromise the lateral diffusivity of the lipids [258]. These properties may help to improve the stability of the bilayer. The exact formula of the various lipids used is as follows:

Lipid Mix

Final conc	Lipid / Chemicals	Amount needed	MW
7.7 mg/mL	E-Coli Polar Lipids @25 mg/mL	225 μ L	~800
0.85 mg/mL	Diphythanoyl PC @ 10 mg/mL	62.5 μ L	846
2.2 mM	Cholesterol @ 10 mM (in chloroform)	160 μ L	387
7.8 mg/mL	Egg PC @ 25 mg/mL	228 μ L	760
0.78 mg/mL	Egg PA @ 10 mg/mL	57 μ L	697

Imaging F_1F_0 ATPase on bilayer using Total Internal Reflection Fluorescence

Microscopy

A home-made⁶⁵ total internal reflection fluorescence microscope (TIRFM) was used to detect the presence of F-ATPases resting on the lipid bilayer. This technique was used because the laser illumination of the TIRFM (otherwise known as evanescent waves) could only penetrate a few hundred nano-meters into the sample. Fluorophores above the membrane were therefore not be excited as much, resulting in a marked increase in the signal to background ratio in the image. Figure 4-6 shows a schematic of the TIRFM. The principle of TIRFM is as follows: a laser beam is focused on the back focal plane of the objective. If the focal spot is placed at the optical axis (centre) of the objective, a collimated beam parallel to the optical axis is obtained to illuminate

⁶⁵ This microscope is built by the Wallace group in the chemistry department, University of Oxford

the sample. Such a method of illumination is also known as epifluorescent illumination. To obtain evanescent illumination, the focal spot of the laser is displaced from the centre of the back focal plane. This changes the incident angle of the collimated light on the specimen. If the angle is greater than or equal to the critical angle, total internal reflection occurs and an evanescent wave is obtained. Fluorescence emission from the sample is then collected by the objective, passed through the dichroic mirror at the bottom of the objective and finally imaged on an intensified CCD camera.

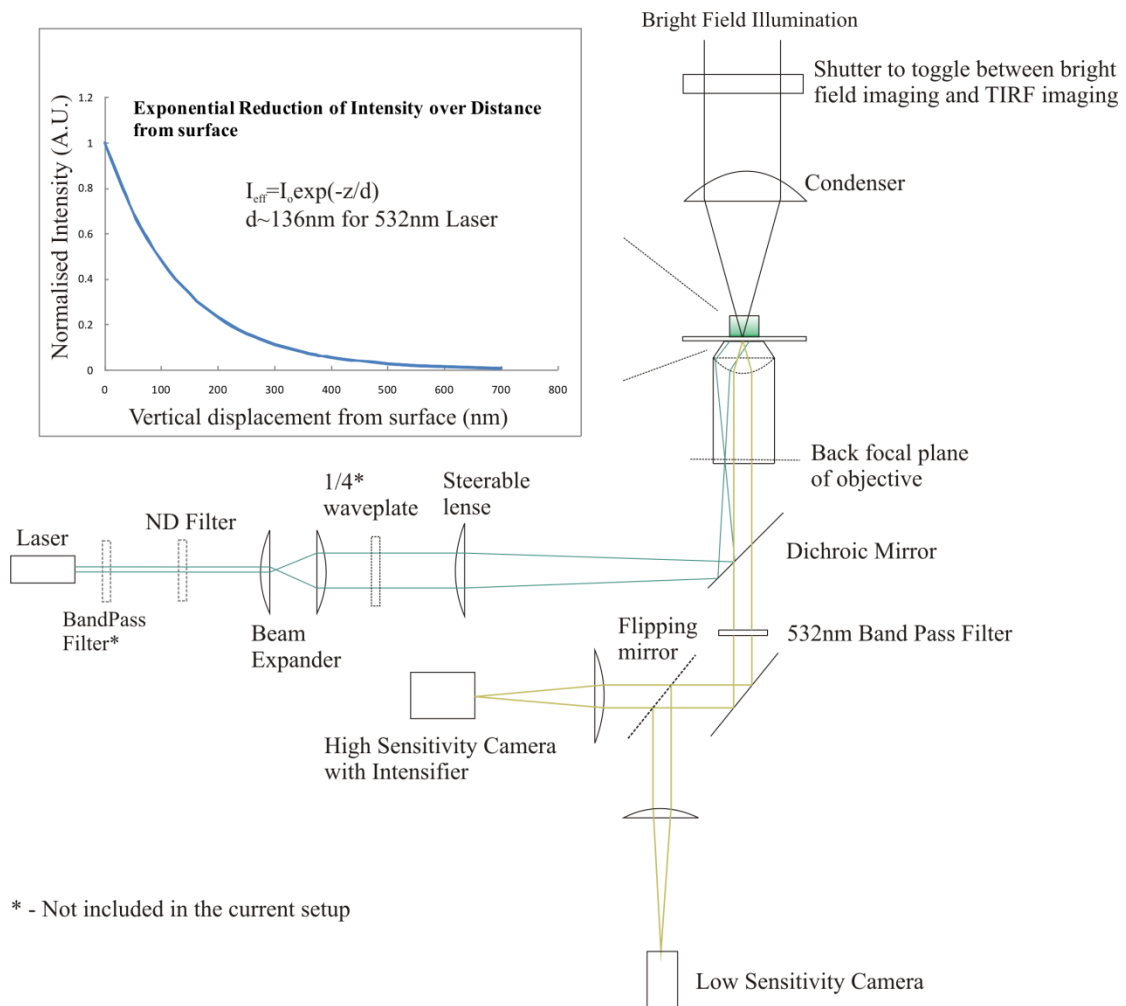


Figure 4-6. A schematic of a typical total internal reflection fluorescence microscope (TIRFM) coupled with bright field illumination

In order to image the F-ATPase using TIRFM, it was necessary to label it with an appropriate fluorophore. Recalling that one of the mutant F-ATPases already had a biotin group at the β -subunits (see section 2.2), it was straight forward to make use of this to conjugate a fluorescent streptavidin molecule onto the F-ATPase. Pre-formed proteoliposomes were mixed with Alexa-532-streptavidin (final concentration = 1 nM) and brewed in hexadecane / lipid mix for 3 minutes. The droplet was then inserted into the wells and observed, first under low magnification using bright field illumination, and then with TIRFM when the bilayer was formed. Fluorescent spots were readily observed on the bilayer (See Figure 4-7 – sample). The following were used as controls for the experiment:

- Control 1: No fluorescent streptavidin added. This was meant to show that the fluorescence detected was not due to non specific contaminants in the buffer or lipids.
- Control 2: No F-ATPase added. This was meant to show that fluorescent streptavidin molecules did not bind non-specifically to the bilayer.
- Control 3: F-ATPase with no biotin modification was added. This was meant to show that streptavidin molecules did not bind non-specifically to other parts of F_1F_0 ATPase.

Results of the TIRFM are presented in Figure 4-7. Comparing the sample with control 1, it was clear that the fluorescent spots observed had to come from fluorescent streptavidin molecules. Furthermore, since only the presence of biotinylated F_1F_0 ATPase resulted in fluorescent streptavidin molecules sticking on the bilayer (control 2 and 3), it was inferred that the F-ATPases were causing streptavidin molecules to

adhere to the bilayer via specific biotin-streptavidin interaction. Following from this, it was deduced that the F-ATPase must also be present on the surface of the bilayer.

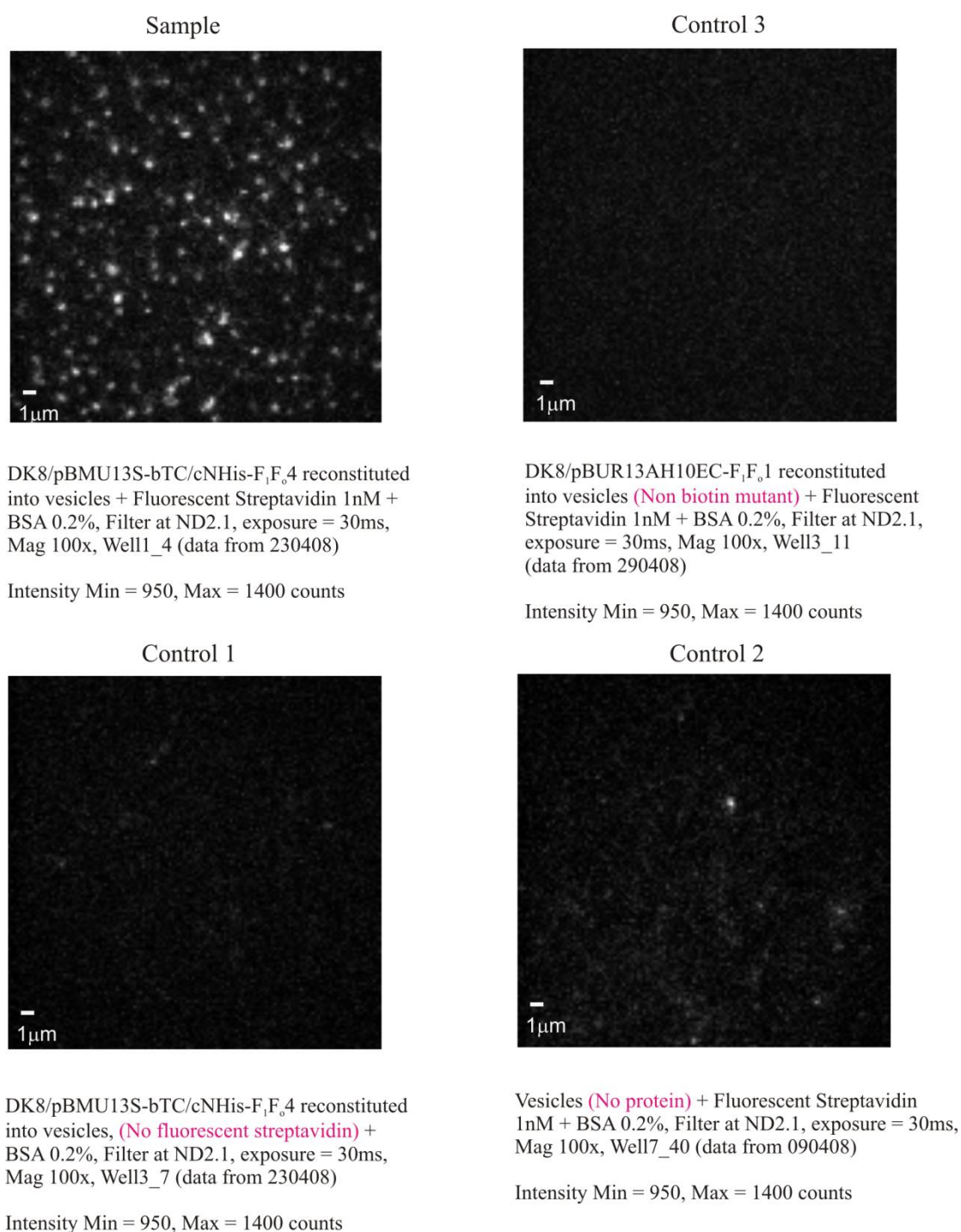


Figure 4-7. Images showing the results of the TIRFM. Conditions under which the images were obtained are given in the caption below. These results indicated that the fluorescent spots observed were directly due to fluorescent streptavidin molecules and that streptavidin molecules would not adhere to the bilayer unless biotinylated F₁F_o ATPases were used. All buffers contained 15 mM CaCl₂ to promote vesicle fusion. DK8/pBMUS13-bTC/cNHis-F₁F_o4 represents the mutant with biotin modification on the β-subunits. DK8/pBUR13AH10EC-F₁F_o1 represents the mutant without the biotin modification.

Interpreting Fluorescence on Bilayers

Figure 4-8 presents three possible configurations which F-ATPase could adopt in the experiments described previously.

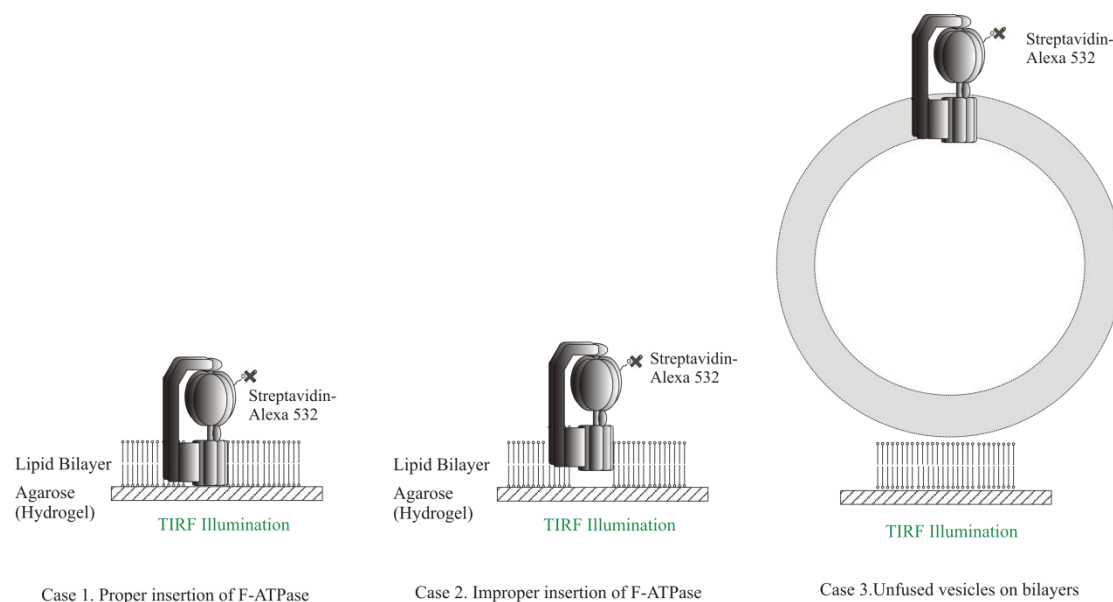
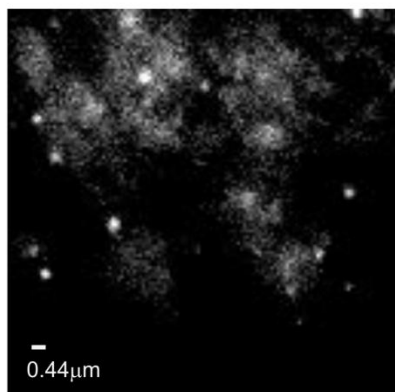


Figure 4-8. Possible configuration of F-ATPase on planar bilayer.

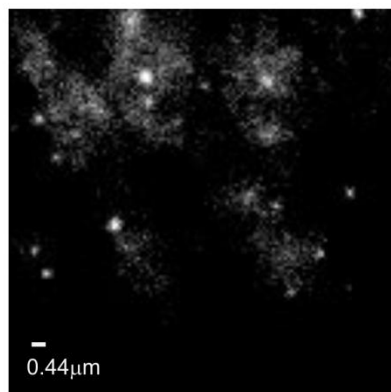
Case 1 is the ideal situation which one hopes to achieve. Case 2 represents incomplete insertion of F-ATPase or insertion of denatured F-ATPases. Finally, case 3 represents the scenario where the proteoliposomes remain on the planar bilayer, but without fusing with it. For the third case, it may still be possible for the fluorophore to be illuminated by the evanescent wave despite being further away from the bilayer surface. This is because the diameter of the vesicles is only ~ 80 nm (See chapter 3 for measurements), making it still sufficiently close to the bilayer to be illuminated. In order to eliminate the possibility of case 3 occurring, two controls were done. The first involved using fluorescent lipids to form the proteoliposomes, while the second was performed with proteoliposomes containing non-biotinylated F-ATPase, but with streptavidin-Alexa-532 trapped within the vesicles (See Appendix 1 for protocol). Both these controls allowed one to ascertain if vesicles did indeed rest on the bilayer

and if so, compare their behaviour with the actual F-ATPase sample. Figure 4-9 summarises the results.

a.

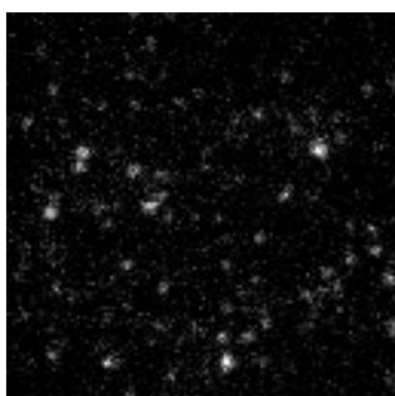


DK8/pBMU13S-bTC/cNHis-F₁F₀,4 reconstituted into fluorescent lipid vesicles + Non Fluorescent Streptavidin 1 nM + BSA 0.2%, Filter at ND3.1, exposure = 30 ms, Mag 225x, Well2_13 (data from 300408)
Time = 0.36s
Intensity Min = 2500, Max = 3600 counts

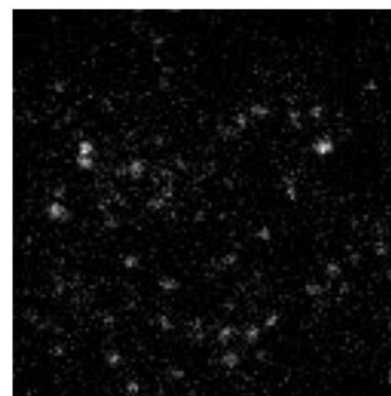


DK8/pBMU13S-bTC/cNHis-F₁F₀,4 reconstituted into fluorescent lipid vesicles + Non Fluorescent Streptavidin 1 nM + BSA 0.2%, Filter at ND3.1, exposure = 30 ms, Mag 225x, Well2_13 (data from 300408)
Time = 14.8s
Intensity Min = 2500, Max = 3600 counts

b.



DK8/pBUR13AH10EC-F₁F₀,1 reconstituted into vesicles + fluorescent streptavidin inside vesicles ~ 1 per vesicles (based on incubation conc of 6.7 μM and vesicle diameter of 80 nm) + BSA 0.2%, Filter at ND2.6, exposure = 30 ms, Mag 225x, Well4_3 (data from 080508)
Time = 0.3 s
Intensity Min = 980, Max = 1150 counts



DK8/pBUR13AH10EC-F₁F₀,1 reconstituted into vesicles + fluorescent streptavidin inside vesicles ~ 1 per vesicles (based on incubation conc of 6.7 μM and vesicle diameter of 80 nm) + BSA 0.2%, Filter at ND2.6, exposure = 30ms, Mag 225x, Well4_3 (data from 080508)
Time = 14.7 s
Intensity Min = 980, Max = 1150 counts

Figure 4-9. The images on the left represent the beginning of the video while those on the right are the same field of view after ~ 15 s. The conditions of the experiments are given in the caption below each picture. a) shows the control where the proteoliposomes were formed with fluorescent lipid while b) shows the control where the vesicles had trapped fluorescent streptavidin inside. In both controls, most fluorescent spots remained immobilised and no sustained lateral diffusing fluorescent spots were observed. 15mM CaCl₂ were added into the buffers of a) and b).

What was clear from these controls was that most of the fluorescent spots resting on the bilayers remained immobilised over the duration of the recording (~ 15 s). There were no fluorescent spots showing sustained two-dimensional lateral diffusion on the bilayer. If these fluorescent spots represent vesicles, this means that they can indeed rest on the surface without fusing and that most of these vesicles also remain immobilised. In contrast, two distinct populations of fluorescent spots were observed for the sample with streptavidin labelled F-ATPase on bilayers. The first population was immobilised on the bilayer while the second was able to diffuse within the bilayer for a sustained period of time (time > 5 s) (See next section for details). This population was unique and might represent case 1 or case 2 as shown in Figure 4-8. To differentiate case 1 from case 2, a functional assay is necessary. This is discussed in more details in Chapter 6.

To encourage the fusion of vesicles, the osmotic pressure across the bilayer was manipulated. By removing glycerol from the buffer inside the droplet, a positive osmotic pressure from the *cis* domain (inside the droplet) to the *trans* domain (substrate agarose) of the bilayer (see Figure 4-2 for illustration) was induced. Such a condition discouraged vesicle fusion (Figure 4-10b) because vesicles resting on the bilayers tended to ‘shrink’ by losing water to the *trans* domain of the bilayer. To promote fusion of vesicles, there must be a driving force to induce osmotic swelling instead [255]. This can be achieved by increasing the osmoticant (glycerol) concentration in the *cis* domain. Figure 4-10 shows a schematic explaining the conditions that encourages or discourages swelling.

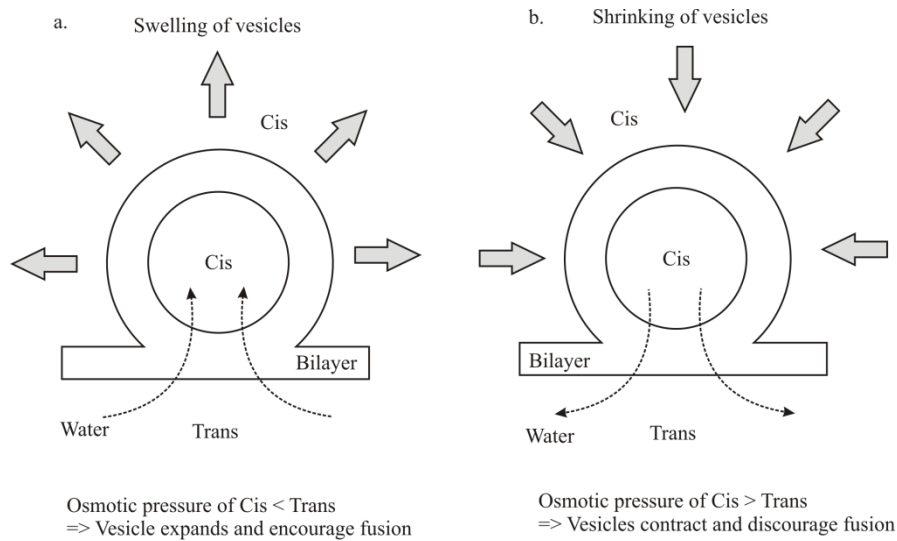
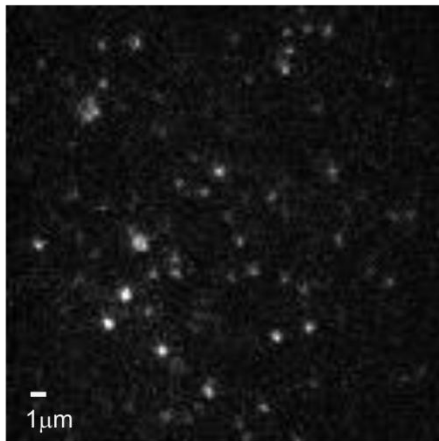


Figure 4-10. Schematic showing conditions favouring and disfavouring fusion of vesicles. Fusion is discouraged if there is a net outflow of water from the *cis* to the *trans* of the membrane due to a positive osmotic pressure (case b). The converse is true if there is a net osmotic pressure into the droplet (case a). Chemicals used to induce osmotic pressure include glycerol and NaCl. It is assumed here that the osmotic pressure inside the vesicle is equal to the osmotic pressure inside the droplet. This is because the vesicles are normally made with the same buffer used in the droplet.

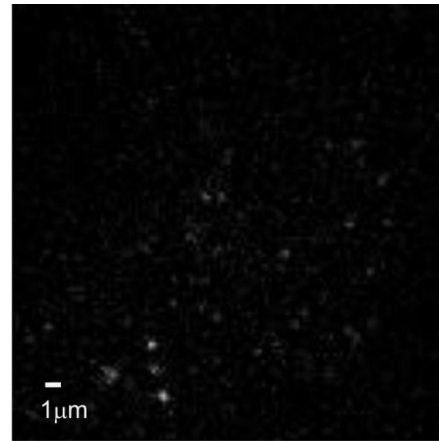
Figure 4-11 compares the TIRF images between normal condition and the condition that discourages vesicle fusion. It was clear that there were far less fluorescent spots in the latter. On the assumption that adherence of vesicles on bilayers was not affected by osmotic pressure, the reduction in the number of fluorescent spots could be explained by fewer F-ATPase on bilayers due to reduced fusion events. This experiment further supported the conclusion that at least some F-ATPases had been successfully delivered to the bilayer via vesicle fusion. When the reverse osmotic condition was tested (i.e. conditions that promote fusion), the bilayer became unstable and were easily broken. This might be due to swelling of the droplet by the influx of water. As such, in all the experiments shown, the buffer conditions in the *cis* and *trans* region were made identical, although milder conditions promoting vesicle fusion might be tried in the future.



DK8/pBMU13S-bTC/cNHis-F1Fo3 reconstituted into vesicles + Fluorescent Streptavidin 1 nM + BSA 0.2%, Filter at ND2.1, exposure = 30 ms, Mag 100x, Well5_30 (data from 090408)

(10% glycerol in both the droplet and agarose)

Intensity Min = 950, Max = 1400 counts



DK8/pBMU13S-bTC/cNHis-F1Fo3 reconstituted into vesicles + Fluorescent Streptavidin 1 nM + BSA 0.2%, Filter at ND2.1, exposure = 30 ms, Mag 100x, Well8_49 (data from 090408)

(No Glycerol => positive osmotic pressure from droplet to agarose. Not conducive to fusion)

Intensity Min = 950, Max = 1400 counts

Figure 4-11. Comparison of the TIRFM images of proteoliposome sample formed under normal conditions (left image), and a condition that discourages vesicle fusion (right). By reducing the concentration of glycerol inside the droplet, osmotic pressure from the *cis* to the *trans* side of the bilayer was increased. This resulted in less fusion activity by the vesicles. The amount of vesicles resting on the bilayer should not be affected by this condition. There was a marked reduction of fluorescent spots on the bilayer with poor fusion conditions. This indicated that at least some of the fluorescent spots on the bilayer of the normal sample (left image) were not vesicles, and likely to be F-ATPase molecules on bilayer.

4.4.4 Studying diffusion of F-ATPase on Bilayers

This section looks at the diffusional characteristics of those fluorescent spots with sustained (time > 5s) lateral diffusion. Fluorescent spots were traced using a simple imaging processing code written in MATLAB. The spots of interest were selected manually and their movement followed by tracking the centroid of the spot over time. The displacements made by the particle after successive fixed time intervals (Δt) were squared and then averaged. This gave the mean square displacement in time Δt (MSD (Δt)). The procedure was then repeated for various Δt and the values were plotted against the corresponding Δt (See Box 4-1 and Figure 4-12b). If the particle was diffusing freely in a 2D plane, this plot could ideally be linearly fitted. Furthermore,

the fitting was weighted against the inverse variance of the MSD (Δt) value (See Appendix 2 for how the weighting was done). From Equation 4-4, it can be seen that the larger the Δt , the bigger will be the variance and therefore the smaller the influence of that MSD point on the line fit. Twenty five diffusing spots were analysed this way and a histogram of the diffusion constant was plotted.

Box 4-1. Calculations of the Diffusion constant – D

Mean Square Displacement at characteristic time $n\Delta t$ was obtained from the video using the following formula [259]:

$$= \text{MSD}(n\Delta t) = \frac{1}{N-n} \sum_{i=1}^{N-n} (\mathbf{x}_{i+n} - \mathbf{x}_i)^2 + (\mathbf{y}_{i+n} - \mathbf{y}_i)^2 \quad \text{Equation 4-2}$$

Where

Δt is the time between each frame

N is the total number of frames

n is the number of time intervals Δt

x_i and y_i are the x and y coordinates of the particle at the i -th frame

For free 2-D diffusion [260],

$$\mathbf{D} = \frac{\text{MSD}(\Delta t)}{4(\Delta t)} \quad \text{Equation 4-3}$$

Where D is the diffusional constant, Δt is the time of diffusion

Since $\text{MSD} / \Delta t$ is the gradient of the line fit,

$D = \text{Gradient of Line} / 4$

Finally since the MSD obtained were not statistically independent, the variance of each MSD point was no longer proportional to $\frac{1}{N-n}$

Qian [259] calculated the actual variance⁶⁶ to be

$$\text{variance} [\text{MSD}(n\Delta t)] = (4\mathbf{D}n\Delta t)^2 (2n^2 + 1) / 3n(N - n) \quad \text{Equation 4-4}$$

The average diffusion constant for twenty five such fluorescent spots was $0.37 \mu\text{m}^2/\text{s}$.

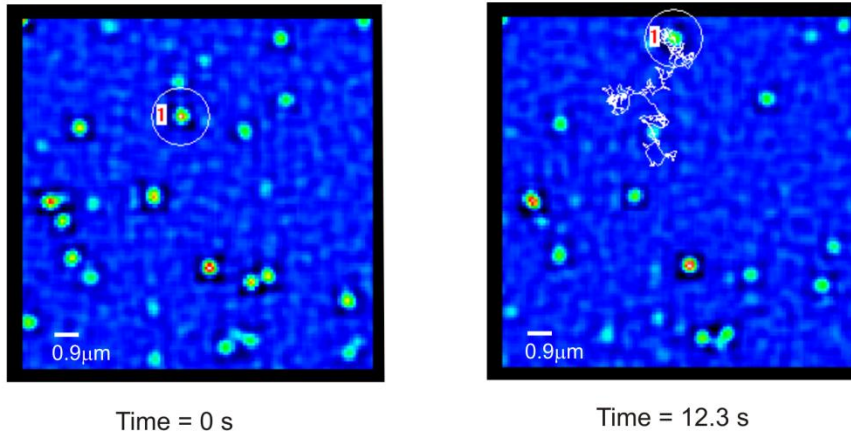
To put this value in perspective, the diffusion constant of rat liver F_1F_0 ATPase, on purified inner mitochondria membrane measured using fluorescence recovery after

⁶⁶ Note that the denominator in the reference paper is $N-n-1$. This is due to the slight difference in the definition of N used here.

photobleaching (FRAP), was found to be $0.084 \mu\text{m}^2/\text{s}$ [261]. This value was lower than the current reported value, probably because of the high F-ATPase to lipid ratio of the intact inner membrane used by the authors. In contrast, the diffusion constant obtained for the sarcoplasmic reticulum ATPase⁶⁷ (SR-ATPase), reconstituted into native lipid extract at a lipid / F-ATPase molar ratio of 5000, was between $1.8 \mu\text{m}^2/\text{s}$ and $0.99 \mu\text{m}^2/\text{s}$ [262]. This was faster than the measured value, probably because the diffusion of F-ATPase in the current setup was slowed down by the interaction with the substrate agarose beneath the bilayer. Nonetheless, the value of the diffusion constant was close to published values of membrane proteins of similar size / type (SR-ATPase / mitochondrial F-ATPase), albeit at slightly different membrane conditions. This further corroborated the postulation that F-ATPase had been successfully reconstituted into the planar lipid bilayer. It is also worth noting that most of the diffusing fluorescent spots became immobilised after an extended period of time, suggesting the influence of the substrate agarose on the mobility of the F-ATPase.

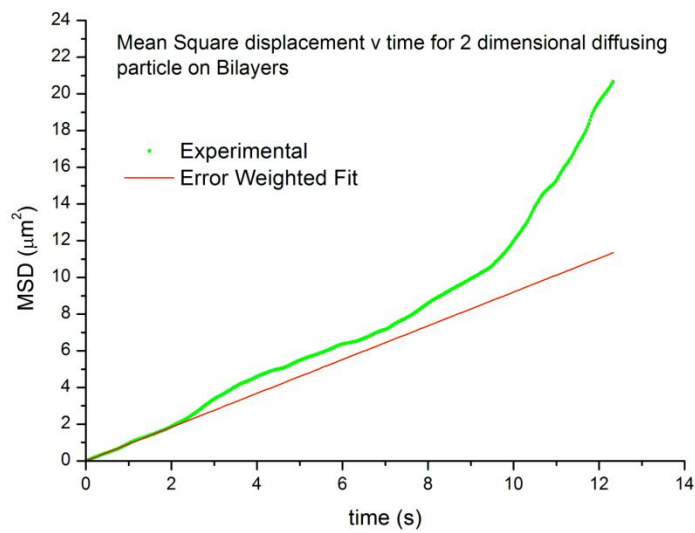
⁶⁷ Note that monomeric SR-ATPase has a diameter $\sim 7\text{nm}$ and F-ATPase has a diameter $\sim 6.5\text{nm}$ (C-ring)

a.



Sample: DK8/pBMU13S-betaTC/cNHIS-F1Fo3 vesicles + 1nM strep BSA 0.2% ND2.1 exp30ms Mag 225x_well5_32 (090408)

b.



c.

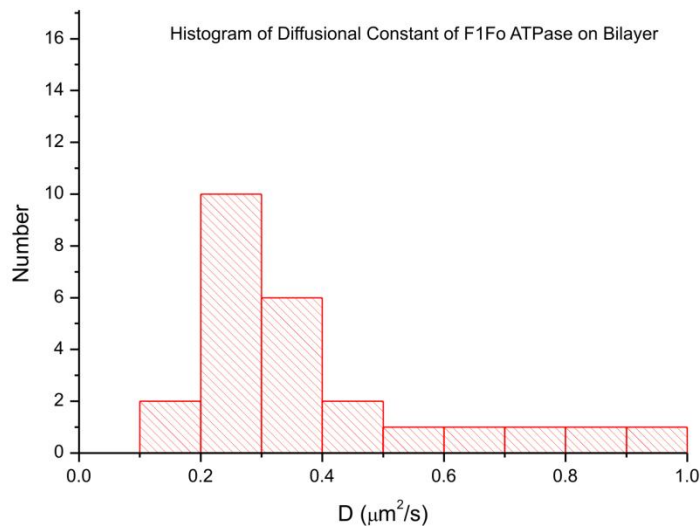


Figure 4-12. a) Shows the path taken by a selected fluorescent spot over duration of 12s. Description of the sample is given below the images. b) Shows the MSD of the spot plotted against time. The analysis was repeated for 24 other spots and the histogram of the diffusion constants was plotted in c).

4.5 Summary of Chapter

In this chapter, the use of the “droplet on hydrogel bilayers (DHB)” method to reconstitute F-ATPase into planar bilayers is explained. This system was chosen because of its relative stability and the ease of applying an electrical potential across the bilayer. The setup was first characterised by measuring the thickness of the agarose substrate that was used to support the bilayer. It was found that the hydrated substrate agarose was, on average, about 240 nm thick and had a mass to volume ratio of $\sim 40\%$ w/v. To deliver F-ATPase into the bilayer, the enzyme was first reconstituted into vesicles, and then induced to fuse with the planar bilayer. Furthermore, a new formula of lipids was used to form the bilayer so that the F-ATPase could remain active after reconstitution.

TIRFM was used to detect the fluorescently labelled F-ATPase on planar bilayers. Two populations of fluorescent spots were detected. One was immobilised on the bilayer while the other was actively diffusing. It was demonstrated that some of the immobilised fluorescent spots might be vesicles resting on bilayer. The diffusing spots were most likely to be F-ATPase reconstituted onto planar bilayer, after fusion of the carrier vesicles. This conclusion is supported by the following evidence:

- Sustained free diffusing fluorescent spots were not detected when the vesicles (and not the F-ATPases) were visualised using TIRFM.
- There was a reduction in the number of fluorescent spots when condition favouring fusion was removed. Some of fluorescent spots seen on the positive

sample should therefore be the result of vesicle fusion events (i.e. F-ATPase on planar bilayers).

- The average diffusion constant of the diffusing fluorescent spots was comparable to the reported values for proteins of similar size.

In the next chapter, functionalisation of gold nano-particles (GNP) with streptavidin is explained. This was needed so that the biotinylated F-ATPase could be labelled for high resolution detection using laser dark-field microscopy. Furthermore, the modification of agarose with nitrilotriacetic (NTA) groups is also described. This functionalised agarose was able to immobilise the c-ring of the F-ATPase, leaving the GNP labelled F_1 to rotate at full speed.

5

Functionalising Agarose and Gold Nano-Particles

5.1 Introduction

In this chapter, two more aspects of the setup that are important for observing the rotation of F-ATPase is discussed. The first is the modification of the substrate agarose with a suitable functional group so that part of the F-ATPase can be immobilised. This step is necessary to allow one to measure the full rotating speed of the $\alpha_3\beta_3\delta ab_2$ ensemble with respect to the immobilised $\gamma\epsilon c_{10}$. As one of the mutants already contained a hexa-histidine mutation at the c-subunit, a nitrilotriacetic acid (NTA) functional group⁶⁸ was used to modify the agarose. This concept was similar to the rotation experiments conducted for F₁ ATPase [27]. It is shown in this chapter that the agarose modification was successful and the substrate, on which the NTA was conjugated to, was not likely to affect the binding strength of the NTA.

To observe rotation, gold nano-particles (GNPs) were chosen to label the F-ATPases. This was done via a biotin–streptavidin interaction. GNPs were first modified with streptavidin and then incubated with the F-ATPase mutant that contained *in-vivo* expressed biotins on the β subunits. This concept was similar to the method employed

⁶⁸ NTA and histag form a non covalent conjugating pair

for high resolution rotation studies of F_1 [133]. It is shown in this chapter that the GNP modification was successful and an estimation of the number of streptavidin molecules per GNP was made.

5.2 Material

All chemicals used in the modification were obtained from Sigma Aldrich (UK) unless otherwise stated. Maleimido-C3-NTA was obtained from NBS Biologicals. Histag-YFP was a kind gift from Dr George Wadhams and Dr Mostyn Brown. GNPs were obtained from BB International and prepared by Dr Bradley Steel. Histag-GFP and DNA modified with tris-NTA were obtained from Dr Christoph Erben and Dr Russell Goodman. DSP (dithiobis-[succinimidylpropionate]) was obtained from Perbio Science UK. Measurements of the emission spectra for GFP titration were done using a standard spectrofluorometer (Photon Technology International, L-Format).

5.3 Method & Results

5.3.1 Modification of Agarose with NitriloTriAcetic Acid

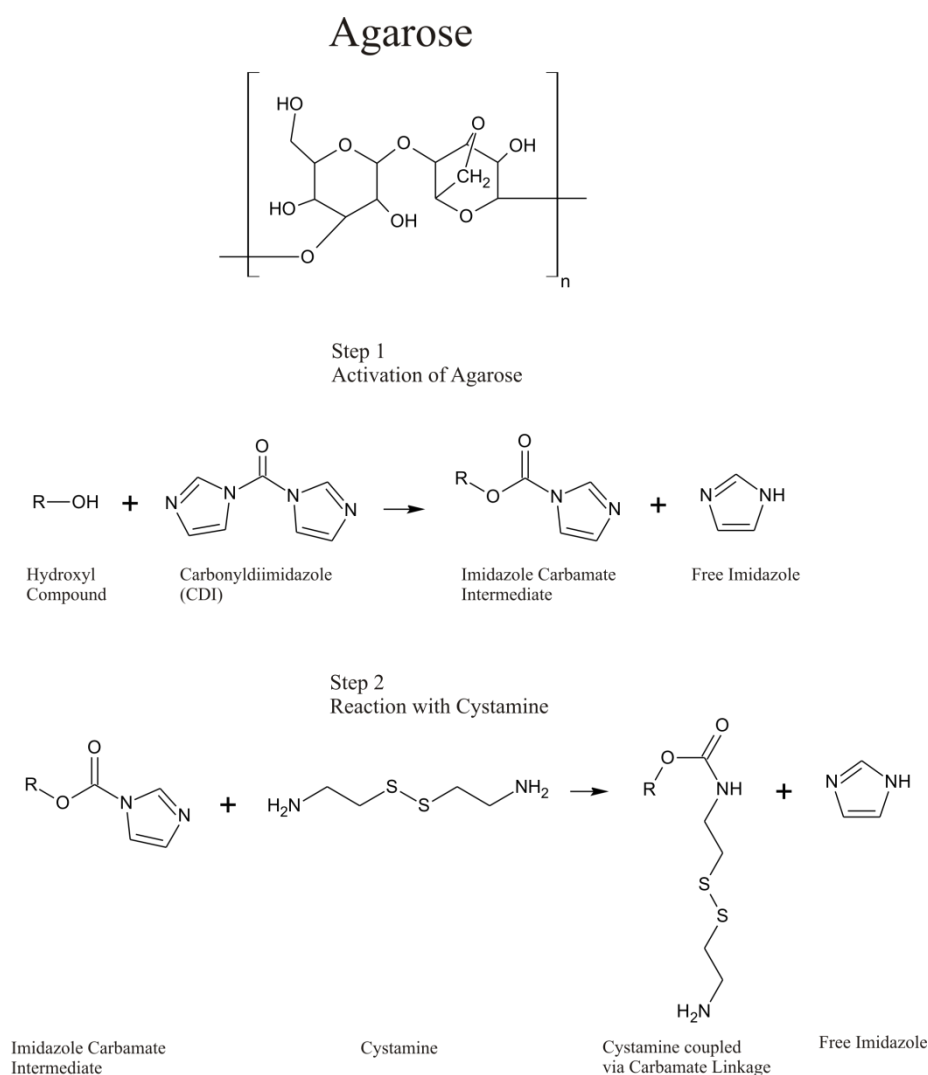
Agarose is a heterotypic polysaccharide containing repeating units of D-galactose and 3,6-anhydro-L-galactopyranose (See Figure 5-1) The carbon backbone is substituted, to a varying extent, with neutral (e.g. hydroxyl) or charged groups (e.g. sulphates) [263]. Nitrilotriacetic acid (NTA) can be attached onto agarose polysaccharides via

the conversion of these functional groups into reactive intermediates, and then conjugating them with NTA containing molecules.

The protocol for the modification of agarose was adapted from [264] [265] (See Appendix 1, A1-6). Briefly, carbonyldiimidazole (CDI) was added to modify the relatively inert hydroxyl groups of the agarose into an active imidazole carbamate intermediate (Figure 5-1: Step 1). The carbamate intermediate could react with an amine group, which would cause the release of an imidazole and the formation of a one carbon spacer carbamate linkage (Figure 5-1: Step 2). It was however not possible to mix amino-butyl nitrilotriacetic acid (an amino terminated NTA) directly with the imidazole carbamate agarose because excess CDI left in the mixture could react with the carboxyl functional group of the NTA and denature the NTA.

To circumvent this problem, cystamine was introduced as an intermediate conjugation step. The disulfide bond in the cystamine is stable and does not react with CDI [266]. Upon the addition of cystamine, the CDI activated agarose slowly solidified due to the cross linking of the agarose strands by the double ended amine of the cystamine (Figure 5-1: Step 2). After reaction for 12 hrs, excess CDI and cystamine were removed by dialysis in double distilled water (DDW) for 24 h, with three changes of DDW. Tris (2-carboxyethyl) phosphine (TCEP) was then added to reduce the disulfide bond (Figure 5-1: Step 3). The mixture was dialysed again for 48 hrs in a slightly acidic solution of hydrochloric acid. This step removed both the oxidised TCEP, as well as cysteamine molecules generated from the reduction of singly bound cystamine. The agarose was then spun in the centrifuge to remove excess water. Finally TCEP was added again and mixed thoroughly for 1 hr before adding

maleimido-C3-NTA to complete the agarose modification (Figure 5-1: Step 4). The mixture was then dialysed for 48 hrs in DDW and dried. Upon rehydration with DDW and melting⁶⁹, the agarose re-solidified slowly into a yellowish translucent gel. Gelation⁷⁰ was affected by the presence of NTA groups because they were thought to affect the formation of the double helix branched matrix that gives the agarose its unique gel property [263, 267].



⁶⁹ Some of the modified agarose formed clumps and could not be dissolved despite heating for an extended period of time. This might be due to the oxidation of unmodified thiol groups in the agarose, forming crosslinked disulphide bonds,

⁷⁰ The modified agarose was no longer able to form a gel, after a few cycles of repeated heating and cooling

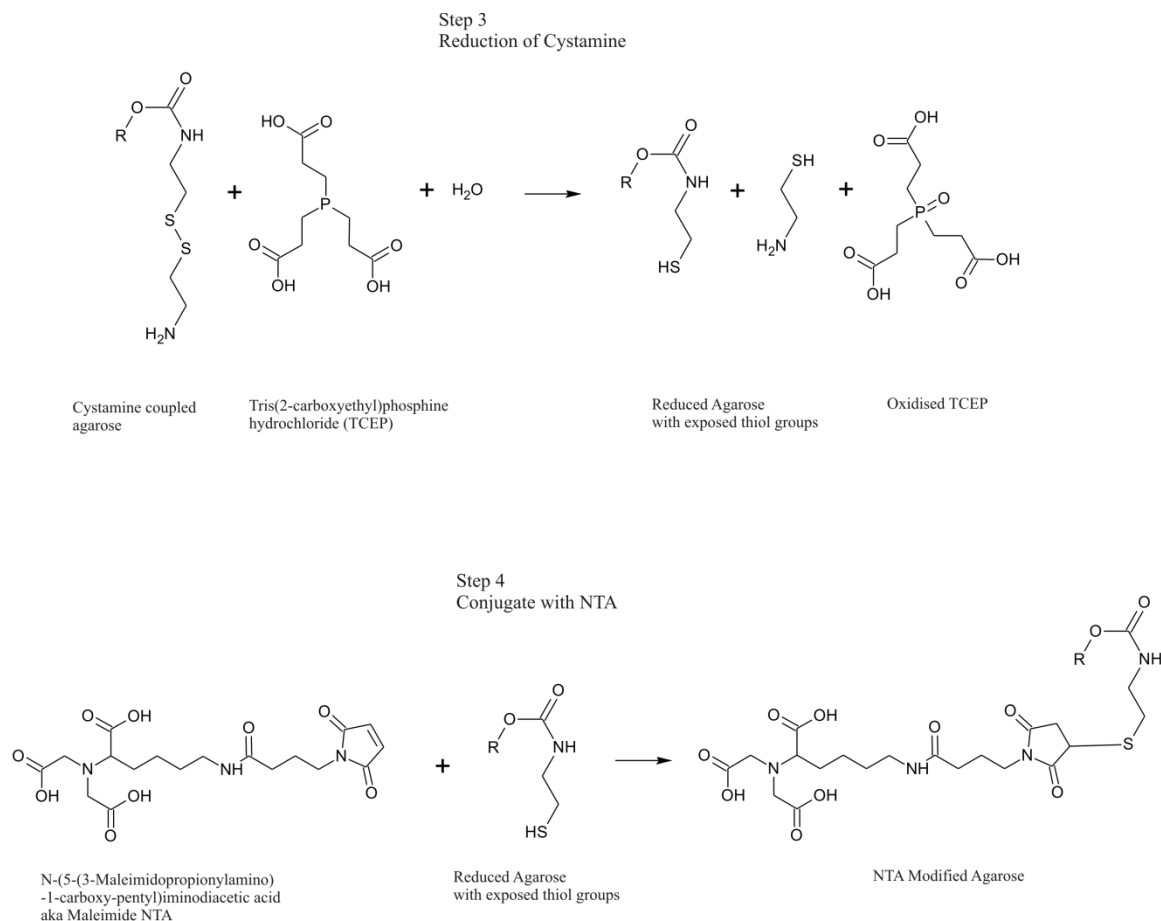


Figure 5-1. Chemical schematics for modifying hydroxyl groups in agarose using CDI (Protocol was modified from [265] and [264])

5.3.2 Characterisation of the Interaction between Histag YFP and NTA Agarose

The NTA modified agarose was melted and coated on a 22 x 22 mm coverslip. The coverslip was then used to create a two-channel tunnel slide as shown in Figure 5-2. Nickel chloride was flowed into the top channel labelled ‘Sample’ while magnesium chloride was flowed into the bottom channel labelled ‘Control’. Both cations can be chelated by the NTA, but only Ni-NTA has a strong affinity for histag due to the availability of two coordination sites for the histidine molecules [268]. After incubating both tunnels with histag-YFP and washing them thoroughly, the tunnel

slide was imaged under epifluorescence mode and the average intensity of the field of view calculated. Figure 5-3 shows the histogram of the results obtained.

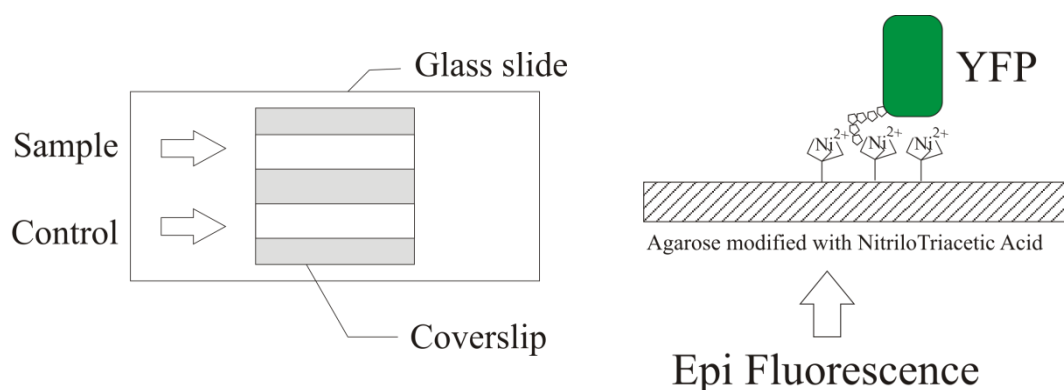


Figure 5-2. The schematic on the left shows the tunnel slide used for testing the affinity of histag YFP on NTA modified agarose. Schematic on the right is a cartoon of a YFP molecule immobilised by NTAs on the agarose.

Three different concentrations of agarose were tested. For the first test, 100% of the NTA agarose was used to coat the coverslip (See Figure 5-3a). At a low laser power of 0.41 mW, the average intensity of the sample was about five times higher than the control. A two tailed Wilcoxon rank sum test at $p\text{-value} = 0.05$ showed a significant statistical difference between the two. When the NTA agarose was diluted in normal agarose by 100 times and tested again. A smaller difference in average fluorescence (~ 500 counts) was seen between the sample with nickel and the control with magnesium (See Figure 5-3b). This difference was still statistically significant as measured by the two tailed Wilcoxon rank sum test. However, the power of the excitation laser had to be increased to 1.4 mW. Finally, when the NTA agarose was diluted by 1000 times (and power increased to 4.2 mW), the difference between the control and the sample became statistically insignificant (See Figure 5-3c). Nonetheless, it was possible to see individual fluorescent spots that might correspond to YFP molecules immobilised on the agarose surface (Figure 5-3d). There appeared to be more spots on the Ni^{2+} treated sample than the control. It was deduced from

these tests that the modified agarose had a high affinity for histag-YFP only when the right cation was chelated by the NTA. The control ruled out any non specific binding between the agarose and YFP. Interaction between the agarose and YFP must be due to the specific NTA-histag interaction.

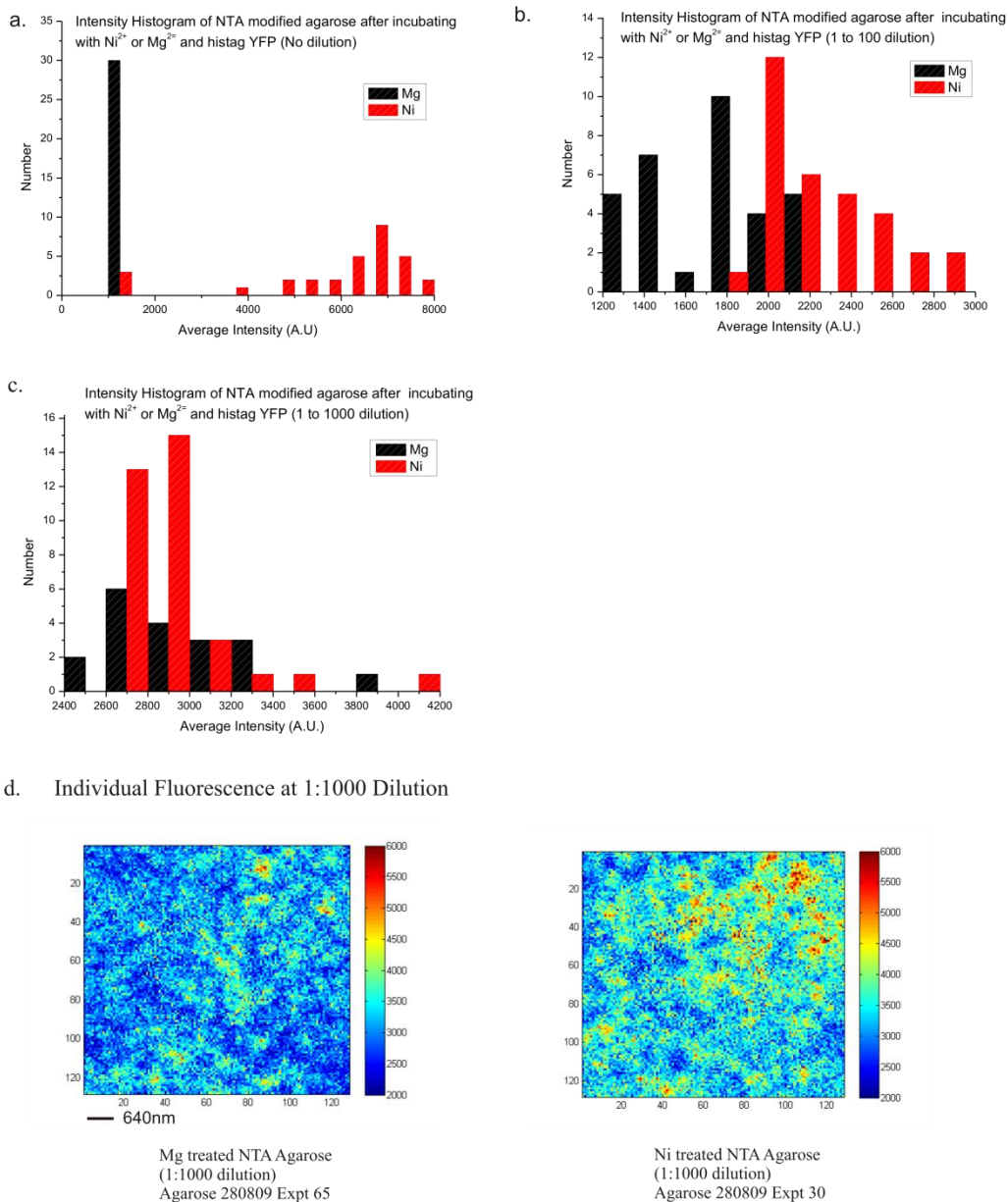


Figure 5-3. Histogram of the average fluorescent counts on a field of view spanning an area of $6.4 \mu\text{m} \times 6.4 \mu\text{m}$. The histogram in red is for areas exposed to Ni^{2+} while the histogram in black shows the counts for areas exposed to Mg^{2+} instead. The fluorescence was due to histag YFP sticking on the agarose. Two tailed Wilcoxon rank sum test at p value = 0.05 was used to ascertain if the two populations were the same. a) represents 100% of the modified agarose while b) and c) represent agarose diluted 100 times and 1000 times with normal agarose. d) shows the fluorescence image of samples at 1000 times agarose dilution. Individual spots of fluorescence could be distinguished, with more spots obtained in the samples incubated with nickel. It was clear that the agarose incubated with Ni^{2+} ions was able to better immobilise YFP.

5.3.3 Finding the Dissociation Constant (K_d) of NTA – Histag bond using DNA substrate

Ni-NTA surfaces have been used with much success, to immobilise F_1 for rotation studies. The net holding force of multiple histag – NTA interactions was shown to be sufficient to bear the roughly constant torque of $\sim 40 - 44$ pNnm generated from ATP hydrolysis [131]. For studying F_1 rotation, the NTAs used were mainly immobilised on glass surfaces. However, in my application, the NTAs were conjugated to an agarose substrate. It is interesting to see if different substrates, on which the NTAs are conjugated to, can affect their interaction with histagged molecules. To do this, the dissociation constants (K_d) between NTA (on a DNA substrate) and hexa-histidine YFP were measured. The results were compared with the published values of similar interactions, but using NTAs that were not conjugated to a polymer substrate.

Lata has characterised the dissociation constants (K_d) of mono, bis and tris NTA with histidine tagged proteins⁷¹ [269]. The best dissociation constant was obtained with a tris-NTA structure. Tris-NTA is a construct of three NTA bound in close proximity. It's exceptionally high affinity to histidine is due to the ideal valency of the chelated nickels for the free electron pairs from the hexa-histidine molecules. Each nickel-NTA is able to accept two pairs of electrons from two adjacent histidine molecules within the histidine tag. For a hexa-histidine chain, the ideal number of NTA needed to fully bind the histag is therefore three.

Lata's value was measured using freely diffusing tris-NTA molecules. For the K_d values measured in this thesis, a DNA oligomer (27 units long) was used. This

⁷¹ Human type I interferon receptor subunit- ifnar2-EC and maltose binding protein are used.

originated as a side project with Dr Goodman⁷² for making protein binding DNA structures [270]. The results were nonetheless relevant to the current work of immobilising F-ATPase to agarose, as both involved linking histag proteins to a substrate. The K_d values obtained for the interactions between hexa-histag-GFP and tris / bis-NTA modified DNA were close to that reported by Lata, despite the presence of a long polymer substrate.

Overview of Experiment

To measure the dissociation constant between a hexa-histidine chain and tris- Ni^{2+} NTA, hexa-histag GFP was titrated with a fluorophore (Cy3) bound DNA that had been pre-modified with tris- Ni^{2+} NTA (hereinafter denoted as Ni^{2+} :NTA-DNA). When GFP binds to Ni^{2+} :NTA-DNA, it becomes partially quenched, possibly due to charge interactions between Ni^{2+} and the excited GFP [269]. Furthermore, GFP and Cy3 also form a FRET pair when in close proximity, which results in the emission of Cy3 (558-564nm) if GFP is excited. By assuming that the changes in intensities were proportional to the concentrations of the NTA-Histag complex, it was possible to calculate the concentrations of the respective species in the solution during different points in the titration (i.e. the concentration of free Ni^{2+} :NTA-DNA, free GFP and Ni^{2+} :NTA-DNA-GFP complex – see Appendix 2 for calculations). The dissociation values (K_d) of the tris and bis Ni^{2+} :NTA-DNA could thus be deduced. Intensity changes at different wavelengths were measured by a standard spectrofluorometer. Figure 5-4 illustrates a schematic of the interactions between the two fluorescent species and the change in emission spectrum when tris Ni^{2+} :NTA-DNA was added to a solution of GFP.

⁷² Dr Goodman was a post doc from Turberfield's group.

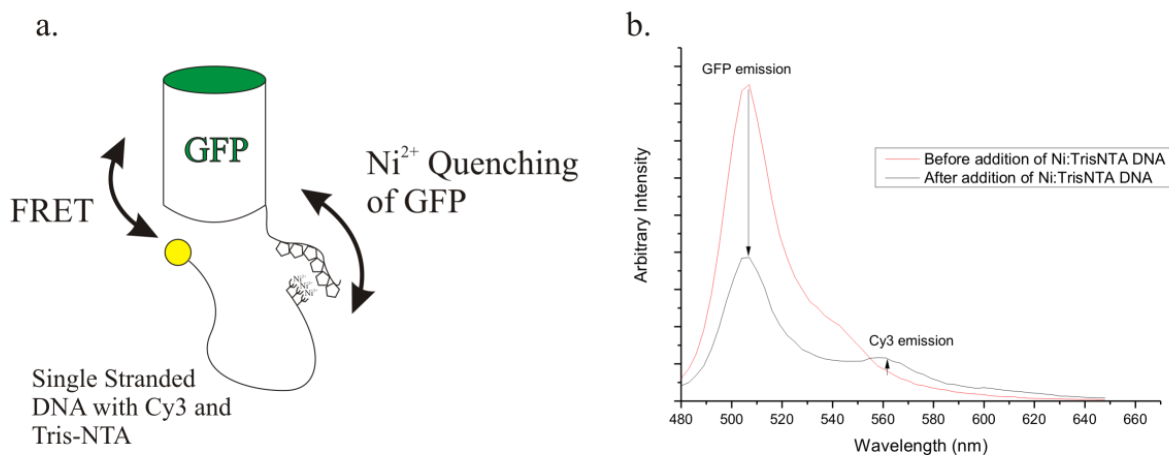


Figure 5-4. Schematic showing the overall concept of measuring the K_d of the tris/bis Ni^{2+} :NTA-DNA histag interaction. When the tris or bis Ni^{2+} :NTA-DNA strand was bound to the GFP via its histag, emission of GFP was decreased due to FRET and quenching by Ni^{2+} ions, while emission of Cy3 was increased due to FRET. These changes could be evidently seen in the emission spectrum before and after Ni^{2+} :NTA-DNA was added, as shown in b). The red curve represents the emission curve before tris Ni^{2+} :NTA-DNA is added while the black represents the emission curve after tris Ni^{2+} :NTA-DNA addition.

Results of K_d Characterisation

Figure 5-5 shows the changes in intensity at the emission wavelength of the GFP (504 nm) and Cy3 (558 nm – 564 nm), when tris Ni^{2+} NTA DNA was titrated. Using a two parameter curve fit, a dissociation constant of $\sim 5.5^{+0.0033}_{-0.0011}$ nM (number of measurements = 10) was obtained. The K_d value for bis Ni^{2+} NTA DNA was $0.12^{+0.03}_{-0.03}$ μ M. The asymmetrical error bounds were due to the consideration of systematic error during the fitting process. In comparison, Lata's K_d values using two different approaches were 20 nM / 2.1 nM for free tris-NTA-fluorescein molecule and 0.27 μ M / 0.068 μ M for bis-NTA-fluorescein.

The K_d values obtained from the measurements above (i.e. using DNA as the substrate for NTA) were comparable to that reported by Lata [269]. It appeared that the DNA substrate had had a small influence on the NTA-Histag interaction. If NTAs

on the agarose substrate behave in a similar manner, the interaction between the NTA conjugated agarose and histagged F-ATPase should remain strong despite the presence of the agarose substrate.

There must also be adequate NTAs on the agarose support to hold the F-ATPase in place during rotation. At least two anchor points are needed to immobilise the c-ring so that rotation can be observed. Returning to Figure 5-1, it was noted that there are four hydroxyl groups in close proximity in each repeating unit of agarose. These hydroxyl groups can potentially be converted into a tris (or quad) NTA motif. Furthermore, the F-ATPase mutants used in the experiments contained ten hexahistidine chains per c-ring. One would expect to have more than 1 histag / NTA interaction per F-ATPase. It might also be possible that some of these interactions involved histag binding with bis or tris NTA motifs.

Finally, to unequivocally test the suitability of the NTA agarose for rotation study, F-ATPase on de-energised membranes were immobilised on NTA-agarose treated coverslips and rotation induced by adding ATP. When this was done, rotation was indeed observed. Results for this experiment are described in the chapter 6. All these arguments suggest that the NTA agarose can be a suitable substrate for the immobilisation of the F-ATPase for rotation studies.

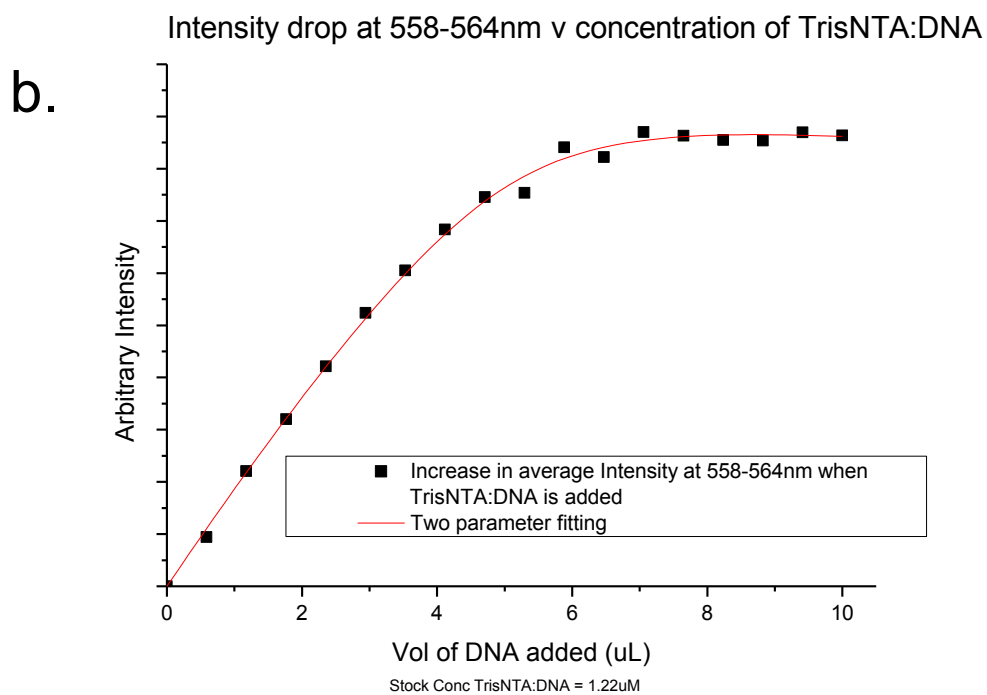
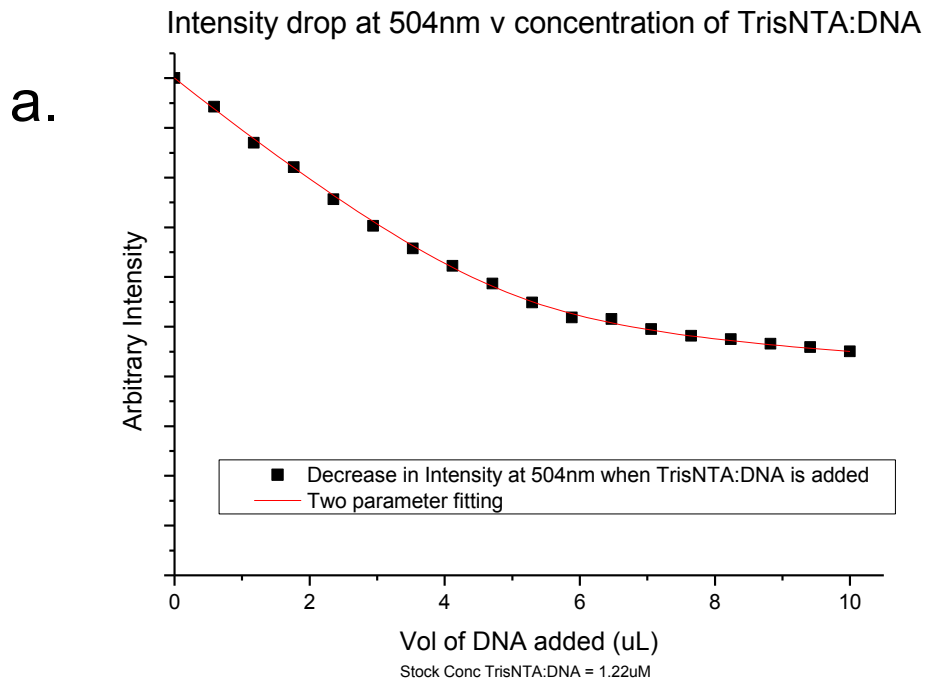


Figure 5-5. a) shows the intensity drop at wavelength = 504 nm with respect to the amount of tris Ni^{2+} NTA DNA added. This drop was due to the formation of GFP-tris Ni^{2+} : NTA-DNA complex. b) shows the increase in intensity at wavelength = 558 to 564 nm (average is taken) with respect to the amount of tris Ni^{2+} NTA DNA. This increase was due to FRET between GFP and Cy3.

5.3.4 Modifying Gold Nano-particles (GNPs) with Streptavidin

As reported in chapter three, the mutant F-ATPases used in the rotation experiments contained a short insert near the N-terminus of the β -subunit. This was a transcarboxylase domain [271], which allowed *in-vivo* attachment of biotins to the β -subunits. There were three biotins per F-ATPase, which could be used to visualize rotation by conjugating any one of them to a suitable streptavidin modified probe. Gold nano-particles (GNP) were thought to be a good choice for such probes as they are relatively small in size, strongly scatter light and can readily be modified with functional groups.

The use of GNP to look at the rotation of F-ATPase is not new. It has been used successfully to study low load rotation of *E. coli* and thermophilic bacterial F_1 [133, 272]. In this study, streptavidin coated GNPs were used to label immobilized F-ATPases on planar lipid bilayers. However, before doing so, it was necessary to decorate the GNPs with streptavidin molecules and determine whether the modification had been successful.

The protocol for labeling the GNPs is given in Appendix 1 (A1-9). This protocol was adapted from Furuike et. al. [273]. GNPs used for the experiments were prepared by Dr Bradley Steel⁷³. Briefly, GNPs of appropriate size were taken from stock and mixed with streptavidin, dithiobis-[succinimidylpropionate] (DSP) and tris (2-carboxyethyl) phosphine (TCEP). DSP contains NHS-ester groups that react with the amino groups of streptavidin molecules. It also contains a disulphide bond that can

⁷³ Dr Steel is a post-doc in Berry's Group

bind to the surface of GNP, through a thiol – gold dative interaction. The suspension was allowed to react in a single pot, under room temperature and constant mixing for 2 hours, before storing at 4°C.

5.3.5 Characterising the Number of Streptavidin per GNP

Overview of Experiment

To ensure that the GNPs had been successfully modified with streptavidin molecules, a simple photobleaching experiment was conducted. Modified GNPs were first washed with 10 mM HEPES buffer to remove excess reagents, and then incubated with fluorescently labeled biotin (biotin- Atto 565 (Sigma)). Excess biotins were removed by centrifugation and the GNPs were flowed into a tunnel slide, similar to the one shown in Figure 5-2. Some of the GNPs would stick to the plasma cleaned coverslips. Stuck GNPs were first selected using a normal bright field microscope. Once a bead was positioned at the centre of the field of view, the microscope was then switched to epifluorescence mode. The power of the excitation laser at wavelength = 532 nm was set to $\sim 3 / 0.3$ mW to induce swift photobleaching of the biotin fluorophores on the surface of the GNP. Fluorescence emissions of the nano-particle were recorded using an intensified camera at 1 second intervals (exposure = 0.1 s) over a duration of 300 s. Figure 5-6 shows a schematic of the experiment.

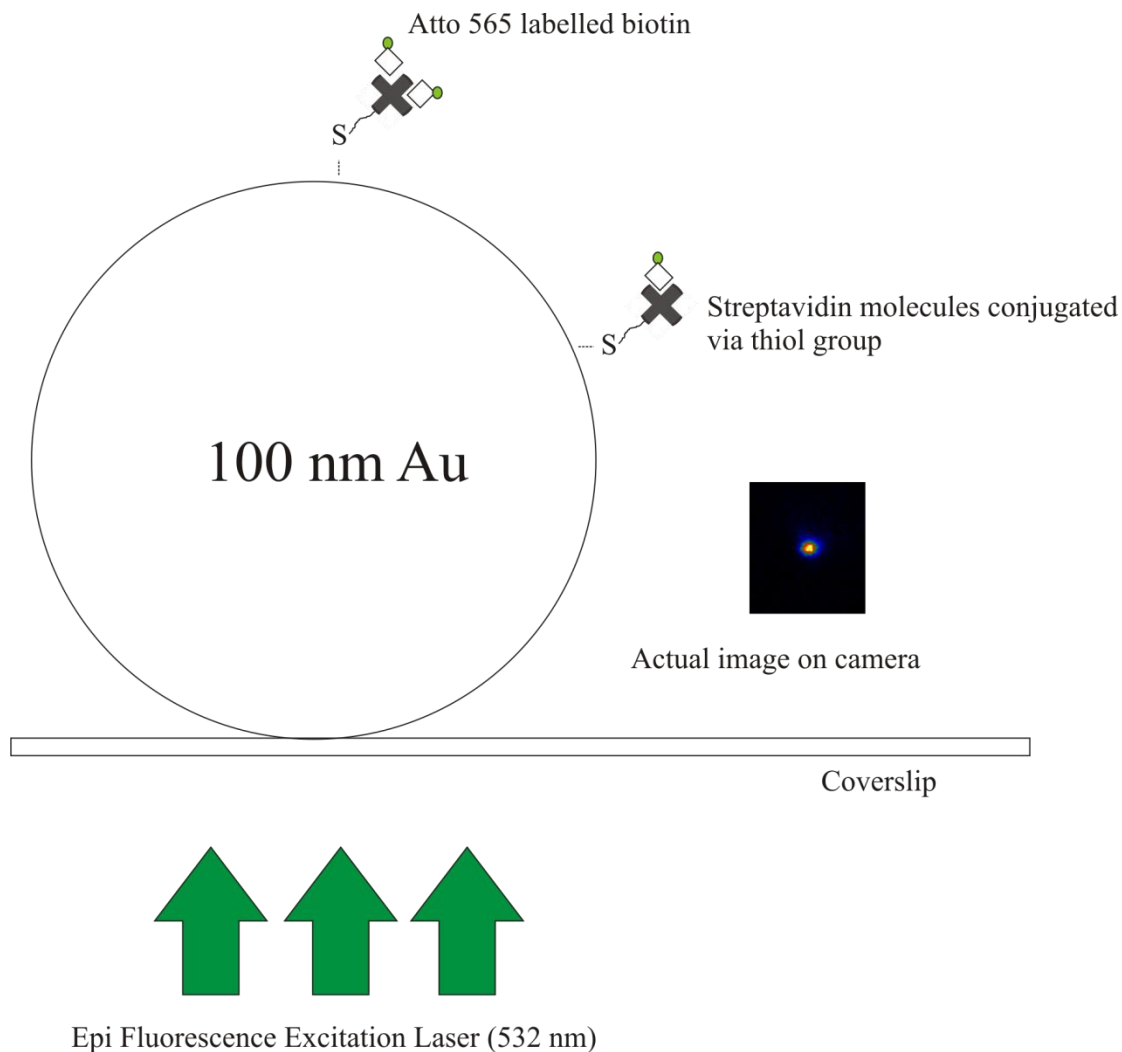


Figure 5-6. A schematic for the photobleaching of fluorescent biotins on the surface of GNP. This experiment was conducted to ascertain the number of functioning streptavidin molecules conjugated onto the surface of the GNP.

Results of GNP – Streptavidin Counting

The method used for analysing the photobleaching signal was adapted from Leake et. al. [274]. Briefly, a window of size 10 pixel x 10 pixel was first drawn around the fluorescent image to define the area of analysis (see Figure 5-7). The image was then fitted with a simple 2D Gaussian (Equation 5-2) to give the positions (x_0 , y_0), width (σ), amplitude (A) and background (BG) of the fluorescent point spread function (See

equation 5-2). The position (x_0, y_0) of the Gaussian was used to dynamically adjust the centre of the window in the next frame. After subtracting the fluorescent counts of each pixel in the prescribed window by the background (BG), the intensity counts of the pixels were averaged. This process was repeated for the subsequent frames to give a plot of average intensity v time.

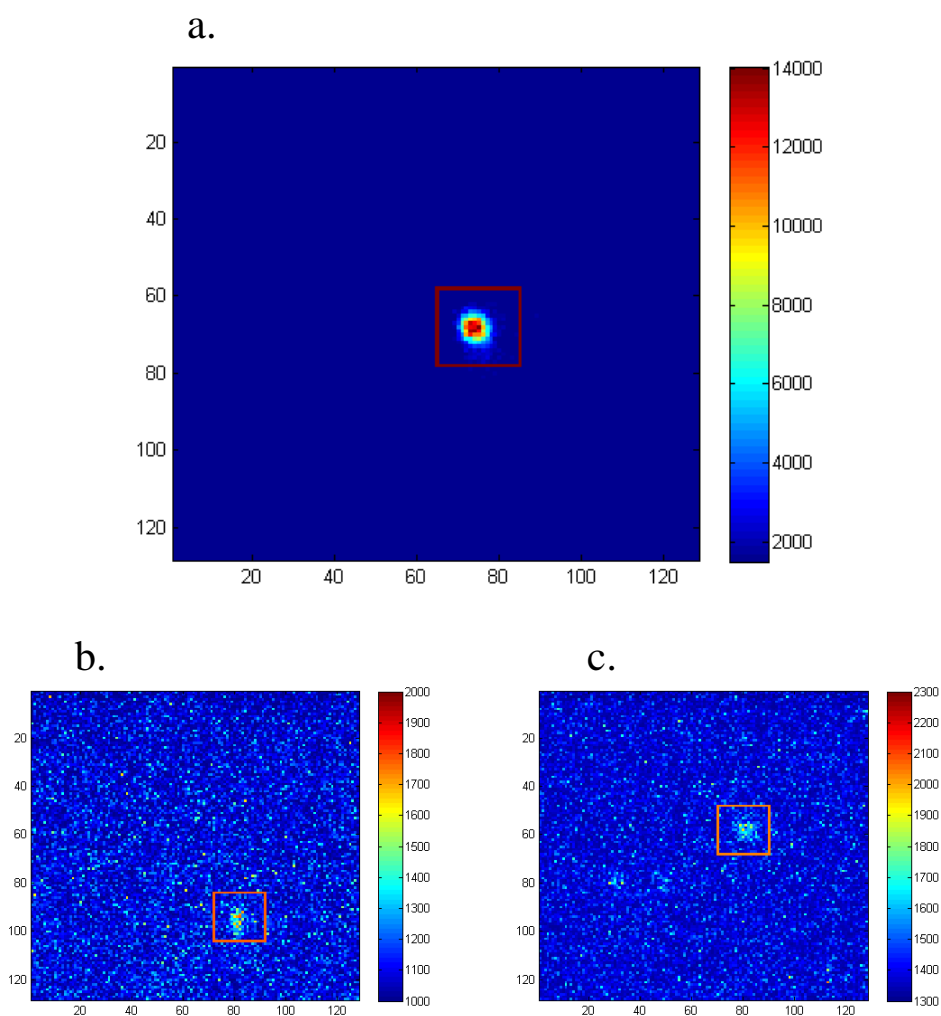


Figure 5-7. Fluorescent images of the streptavidin GNP and controls. a) shows the sample where streptavidin GNPs were incubated with fluorescent biotin-Atto 565 for 6 hours. b) shows the image of a similar streptavidin GNP, but preincubated first with non-fluorescent biotin before fluorescent biotin was added. Significantly less fluorescence was detected. This control showed that interaction between the streptavidin GNP and biotin-Atto565 could be blocked using a non-fluorescent biotin blocker. The blocking was likely to be due to the saturation of biotin binding sites of the streptavidin on the GNP. c) shows another control with non-streptavidin GNP only. This control demonstrated that the GNP, by itself, does exhibit a small level of fluorescence. All images correspond to an obvious GNP when viewed under bright field illumination. Also worth noting is that b) and c) were obtained under 10 times more illuminating power than a).

$$y = Ae^{-\frac{(x-x_0)^2+(y-y_0)^2}{\sigma^2}} + BG \quad \text{Equation 5-1}$$

Where A , x_0 , y_0 , σ and BG are fitted parameters representing amplitude, location, spread of the Gaussian and the background intensity.

The intensity plot was filtered with a non linear, edge preserving Chung-Kennedy filter [275] to remove high frequency noise. The output was essentially a smoothed step-wise photobleaching curve of the fluorophores on the GNP. Each of these steps corresponded to the intensity contribution of one fluorophore. By taking the ratio of the initial GNP intensity to the fluorescent count per step, I was able to estimate the number of fluorophores on the GNP. Figure 5-8 shows the result of the intensity v time plot.

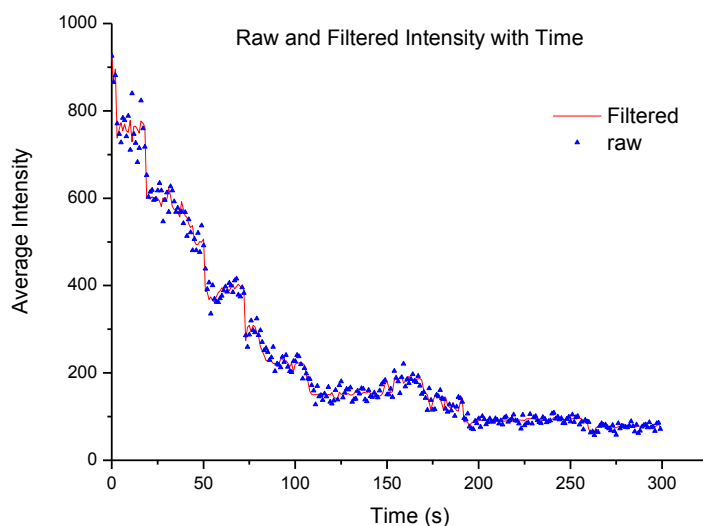


Figure 5-8. Changes in average signal over time. Triangles represent the average intensities within the prescribed window, after subtracting the background. The red line represents the signal after passing the raw data through an edge preserving Chung-Kennedy filter.

To find the intensity drop per step, each filtered data point was paired up with every other data point of the same data set. The difference between each pair was then calculated. When these differences were plotted on a histogram, a pairwise difference

distribution function (PDDF) was obtained (See Figure 5-10). Mathematically, the PDDF is defined by:

Pairwise difference = $I_i - I_j$, where i and j are the frame number and $i < j$

Finally, the value of each photobleaching step was obtained by applying a Fourier transform on the PDDF and selecting the frequency that gave the highest power. The inverse of this frequency (i.e. period of oscillation) was the intensity of each step in the original stepwise bleaching curve.

To explain the rationale for these procedures, it is instructive to imagine how the data will behave for an ideal stepwise function. An ideal stepping function with unitary stepping height and a small amount of white noise embedded was first simulated (See Figure 5-9). After using the Chung-Kennedy filter, the differences between each data point with all others were calculated and plotted as a histogram (i.e. PDDF). As the data points were distributed around the steps (Figure 5-9a/b), the PDDF tended to appear as localised peaks, with the distance between adjacent peaks representing the size of the step (Figure 5-9c). Another way to look at the PDDF is to imagine it as comprising many sinusoidal functions. The dominating sinusoidal function must have the same peak occurrences as that in the PDDF. Or in another words, the period of that dominant function corresponds to the distance between adjacent peaks. Therefore, by converting the PDDF to the frequency domain (i.e. subjecting it to a Fourier transform), and looking at the frequency with the highest contribution, one will be able to obtain the step size of the stepping function. Figure 5-9d shows the power spectrum of the simulated PDDF, but with the x-axis inverted to show the period

instead of frequency. The reciprocal of the dominating frequency gives the dominating period, which is the step size of the stepping function. In the case of the simulated data, the result of the step size was indeed ~ 1 .

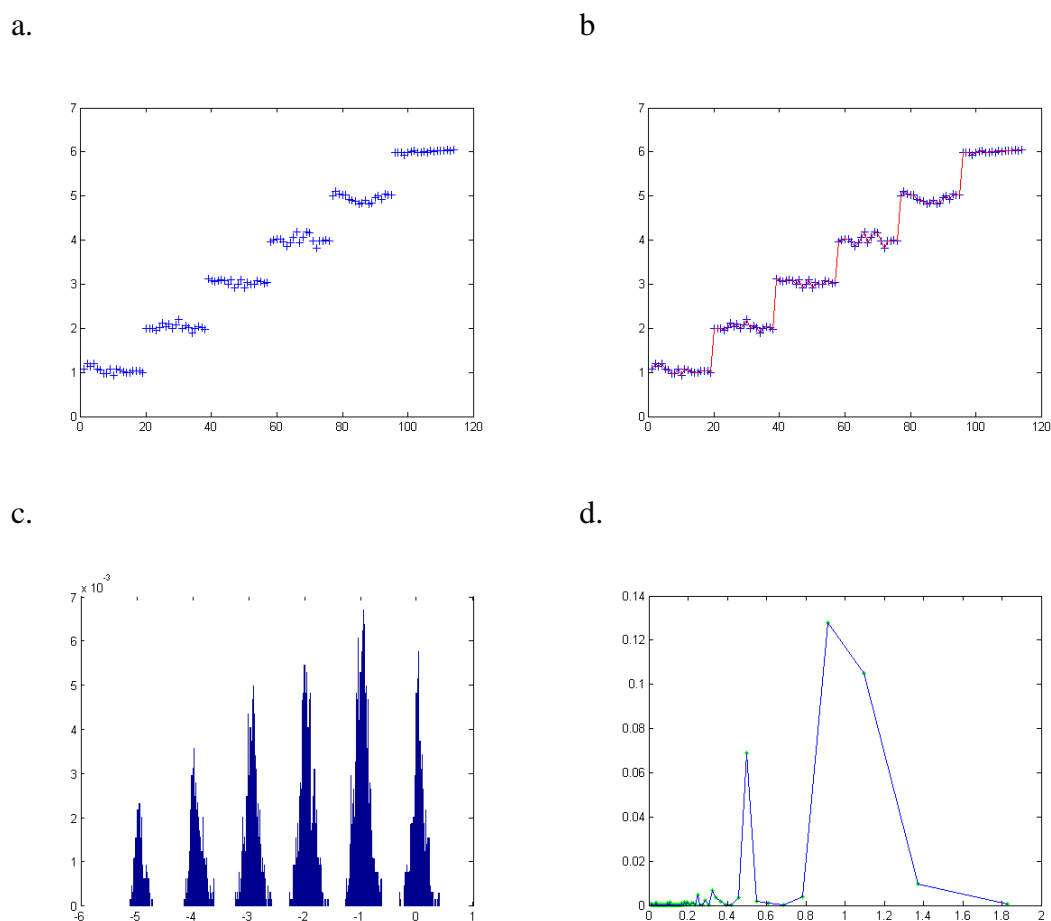


Figure 5-9. Simulation results of an ideal step-wise signal. The raw data used was a step function embedded with a small amount of white noise. The magnitude between each step was one. a) represents a plot of the raw data. b) shows the signal after the raw data was passed through a Chung Kennedy filter. c) shows the PDDF of the filtered signal. There was an obvious periodic pattern in the PDDF, with the peaks repeating at a regular interval of one unit. d) shows the visualisation of the PDDF in the frequency domain, but with the x-axis inverted to represent the inverse of frequency (i.e. period). The x-axis inverted power spectrum revealed the dominant period in the PDDF. This dominant period was also the size of the step in a).

For the actual test samples, when a fluorophore became photobleached, a steep drop in the average intensity of the fluorescent signal could be observed. Assuming that the contribution of each fluorophore was similar under the same excitation intensity, one could expect the PDDF to show a regular repetition of peaks similar to that seen in

Figure 5-9c. Figure 5-10 shows the actual PDDF for the photobleaching curve shown in Figure 5-8. The distance between adjacent peaks represented the step size of the photobleaching curve. Figure 5-11 shows the power spectrum of the PDDF, but with the x-axis inverted to show the period of oscillation instead. The peak period was the size of the photobleaching step.

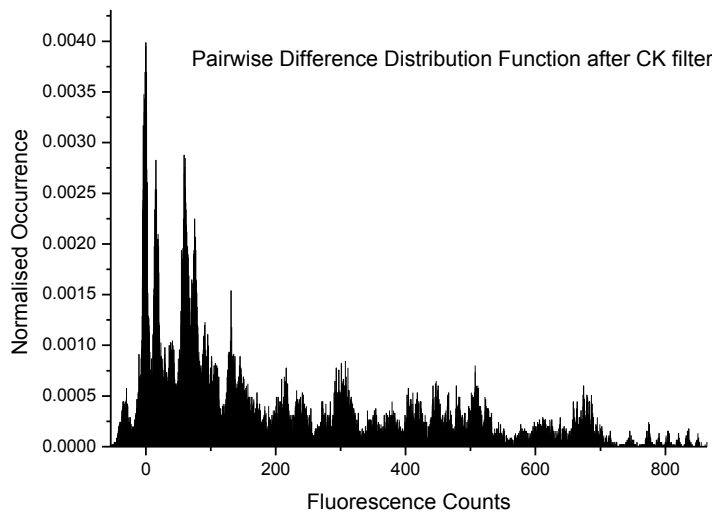


Figure 5-10. Histogram of the pairwise difference of the intensity plot over a data set of 300 video frames.

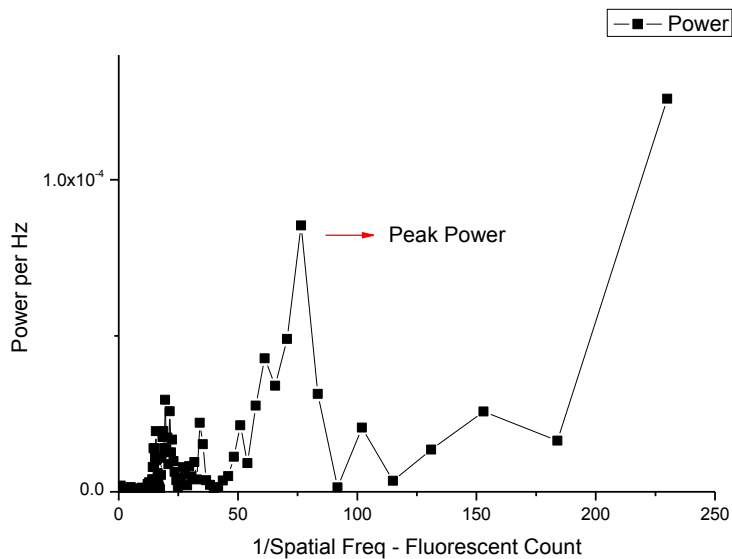


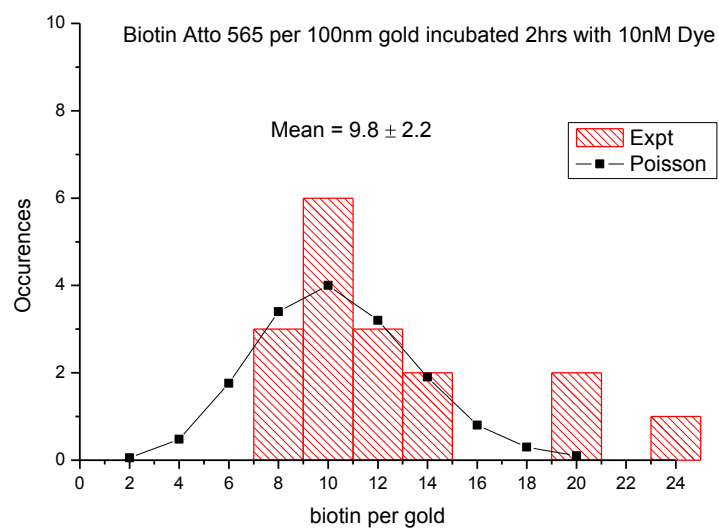
Figure 5-11. Plot showing the power spectrum of the PDDF. For better illustration, the power was plotted against the reciprocal of frequency rather than the frequency itself. This was because the reciprocal of the peak frequency corresponded directly to the intensity contribution of a single fluorophore.

The total number of fluorophores on the gold nanoparticles is simply given by the quotient of the initial intensity over the value of the step size. These calculations were repeated for nineteen different GNPs. Figure 5-12a shows the histogram of the number of biotin fluorophores per GNP. An average of 9.8 biotin dyes was obtained. The appearance of a minor peak at the right of the histogram might have corresponded to pairs of nano-particles, instead of singles. To ensure that this number was close to saturation, the same experiment was done but with 3x longer incubation and 10x higher concentration of biotin Atto 565. Figure 5-12b shows the histogram obtained. The average number of biotin molecules on the surface was increased by less than two fold to 16.1. If the GNPs were far from saturation, then one would expect a marked increase in the number of biotin fluorophores counted. It was therefore concluded that the number of biotin fluorophore per GNP was close to 16. Given that each streptavidin molecule can theoretically bind to 4 biotin fluorophores, the number of streptavidin molecules per GNP might be as little as four. This was much less than the theoretical number of streptavidins if a dense monolayer of streptavidin molecules was formed around the GNP. With an average area of 5 nm x 5 nm per streptavidin molecule [276], one would expect about 1256 streptavidin per 100 nm GNP if completely saturated. The discrepancy in number was attributed to the following reasons:

- Some of the streptavidin molecules might have been denatured during the conjugation process and cannot bind biotin.
- Not all available sites of the streptavidin molecules were exposed for binding with biotin.

- Some of the streptavidin molecules might have been removed from the surface when the GNPs were washed to remove excess biotin.
- Some of the biotin might have been bleached by the start of the experiment.
- There was competitive binding from other thiol molecules (e.g. DSP) present in the gold suspension, thereby blocking the conjugation of streptavidin to GNPs.

a.



b.

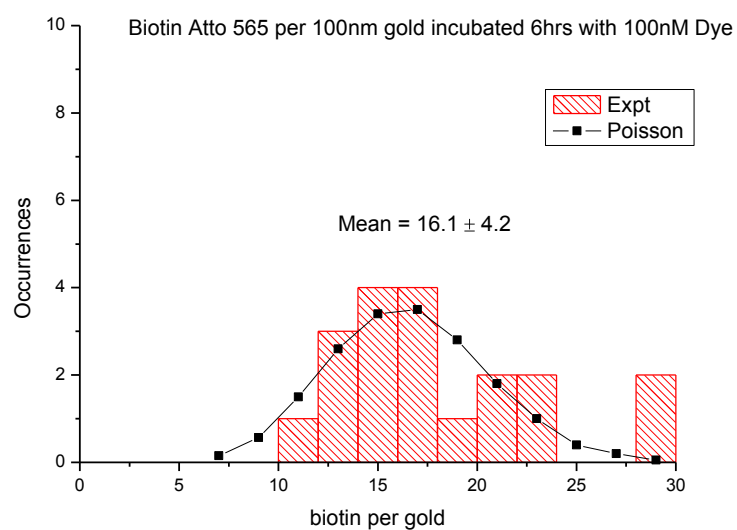


Figure 5-12. a) Histogram of the number of biotin per GNP (n=19) after 2 hrs incubation in 10 nM biotin Atto565. The black lines indicate the ideal Poisson distribution with the same mean. b). Histogram of the number of biotin per GNP (n=20) after 6 hrs incubation in 100 nM biotin Atto565.

5.4 Summary of Chapter

This chapter explains the two additional steps that were needed to be done before rotation studies of F-ATPase could be carried out. The first was the modification of the substrate agarose so that it could immobilize F-ATPases that had inserted into the bilayer. This was done using a NTA – Histag interaction. A novel protocol for agarose modification is reported. Using histag YFPs as probes for immobilization, the modification was shown to be successful. YFPs were attached to the NTA modified agarose only when the right cation was used to activate the NTA. Furthermore, the fluorescent signals of YFP decreased with the dilution of NTA agarose by normal agarose. At 1:1000 times dilution, individual fluorescent spots could be seen, which might correspond to individual YFP molecules. Using a NTA-modified DNA oligomer, the NTA-Histag interaction was shown to be not adversely affected by the presence of a substrate. To ensure adherence, there must be at least two histag – NTA interactions. In comparison, the c-ring contained ten hexa-histags and there were four modifiable hydroxyl groups per repeating unit of agarose. It was therefore likely that at least two of the ten histags could find the corresponding NTAs on the modified substrate agarose.

The second procedure discussed in this chapter was the modification of gold nanoparticles (GNP) with streptavidin molecules. A protocol for the modification is given. In addition, the number of functional streptavidin molecules per GNP was determined using a simple photobleaching experiment. It was found that there might be as little as 4 functioning streptavidin molecules attached to each GNP.

6

Rotation Studies of *E. coli* F-ATPase in an Energisable Lipid Bilayer

6.1 Introduction

The preparatory work that was done thus far was meant to create the right conditions for one to observe the rotation of single molecule F-ATPase on bilayers. To this end, the enzyme was purified and incorporated into the bilayer; agarose was modified to enable immobilisation of F-ATPase; and gold nano-particles (GNP) were conjugated with streptavidin molecules to track the movement of the biotinylated enzyme. With all these conditions implemented, the next step was to observe the motion of the F-ATPase. In this chapter, protocols and results of the rotation assay are presented and discussed.

Before doing that, a short description of the laser dark-field microscope (LDM) is given (laser dark-field is the microscopy technique used to visualise GNPs on bilayers). This is followed by an overview of the protocol for the rotation assay and the results obtained. Although unidirectional rotation was not detected in the immobilised GNPs, some of the GNPs were found to be preferentially located around three specific angles of their circular trajectory. This is discussed in details later.

Work on this project is still ongoing and improvements to the current setup are already in the pipeline. It is hoped that with these improvements, one may finally be able to observe the rotation of F-ATPase at high resolution for an extended period, powered by either ATP hydrolysis or proton motive force.

6.2 Material and Instrument

Pyruvate kinase was obtained from Roche UK. Phospholipids were obtained from Avanti Polar Lipids. All other chemicals were from Sigma Aldrich (UK). The high speed camera was obtained from Photron (FastCam 1024 PCI). The dark-field microscope was homemade, first by Dr Yoshiyuki Sowa⁷⁴ (manuscript submitted and under review), and later modified by Dr Bradley Steel⁷⁵ and Miss Ashley Nord. The programme for analysing the rotation data was written in MATLAB by Dr Bradley Steel.

6.2.1 Laser Dark-field Microscope

Figure 6-1 shows a schematic of the LDM setup. The microscope was originally designed to capture images of F₁ and bacteria flagellar motor rotation, with high temporal (max = 10 μ s) and spatial resolution (shot noise ~ 0.6 nm). It was later found to be compatible with the planar bilayer device. The working concept of the setup is to collect light that is back-scattered by the specimen, while removing the reflected laser by means of a small mirror. Images of the specimen therefore appear bright

⁷⁴ Dr Sowa was a visiting research fellow in Berry's group.

⁷⁵ Dr Steel is a post doc and Ms Nord is a graduate student from Berry's group.

against a dark background – hence the term laser dark-field. A qualitative description of the optical design is as follows: Polarised laser illumination first passes through a rotatable half wave plate (HWP) so that the polarisation angle of the laser beam can be controlled. The beam is then split into two paths by a polarising beam splitter (PBS), with the intensity in each path depending on the polarisation angle of the incident beam. The HWP thus acts as an analogue dial that controls the beam intensities in both paths. Each of these optical paths is focussed by a lens of prescribed focal length, so that different extent of beam expansion can be obtained. For F_1F_0 work, a large and evenly illuminated field of view is needed. The path with a bigger beam expanding ratio was hence chosen. The other path is usually used for flagellar motor work and blocked with a manual shutter during the F-ATPase experiments. The expanded beam then passes through a quarter wave plate (QWP) where its polarisation is changed from linear to circular. It is focussed onto the back focal plane of the objective, with the help of a lens and a 1 mm diameter rod mirror (RM) placed at the bottom of the objective. Collimated illumination emanates from the objective and onto the sample. Part of this beam is reflected back into the objective. However, since it follows the same path as the original illuminating beam, it is reflected away by the same rod mirror. On the contrary, scattered light from the specimen is projected in all directions and captured by the objective and collimated across the entire area of the back focal plane (dotted lines in Figure 6-1). Although a small amount of scattered light is blocked by the small mirror and its holder, the majority (~92%) passes unobstructed and is focussed onto an ultra high speed CMOS camera (Photron). Alternatively, the image can be visualised on a quadrant photo diode (QPD) or a CCD camera, using two flipping mirrors (FM).

Besides having high resolution, the other advantage of this setup is the availability of working space at the top of the sample. This allows the bilayer device and electrodes to be used without much restriction. However, in order to incorporate the electrode, one needs to modify the stage to accommodate an additional micromanipulator. Unfortunately, this improvement was not implemented when the experiments were conducted. As such, for all the experiments described herein, only ATP was used to induce the rotation in F-ATPase. Future work has been planned to include electrodes into the system.

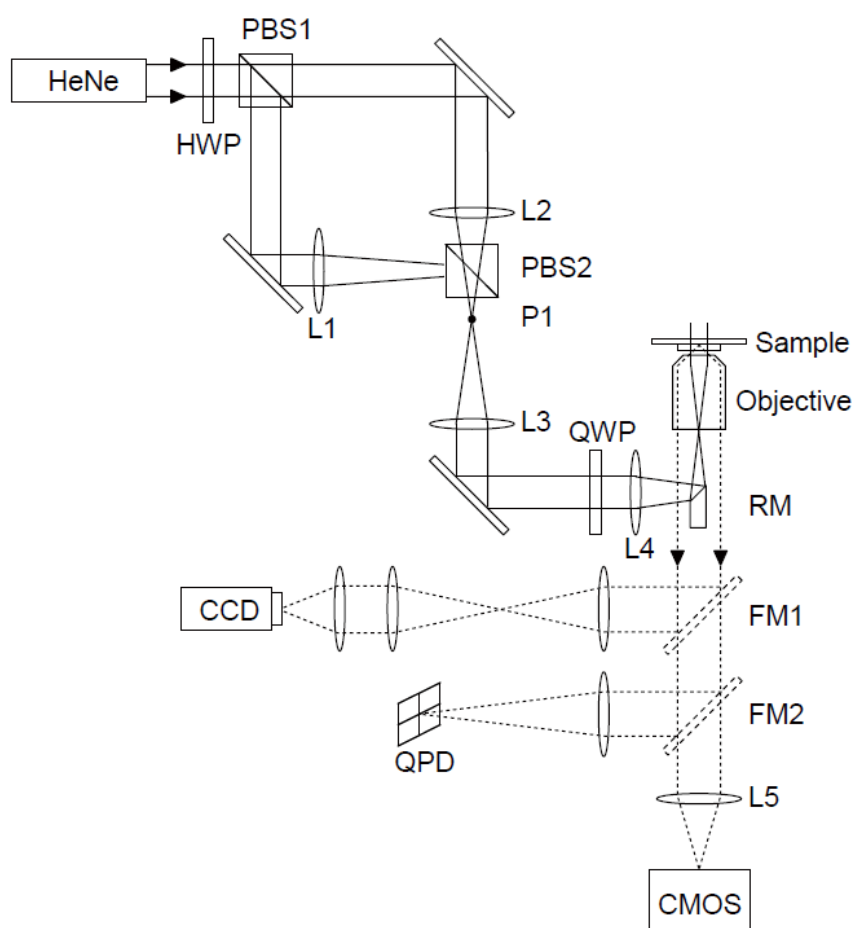


Figure 6-1. A schematic of the laser dark-field microscope. The diagram was extracted from the manuscript of Dr Sowa, Dr Steel and Dr Berry. Abbreviations: HWP – half wave plate, L – lens, PBS – polarising beam splitter, QWP – quarter wave plate, RM – rod mirror, FM – flipping mirror, QPD – quadrant photodiode, CCD – charged couple device camera, CMOS – complementary metal oxide semiconductor camera.

6.3 Methods & Results

6.3.1 Preparation of Samples

Vesicles were prepared and reconstituted with freshly defrosted F-ATPase, according to the protocols in Appendix 1 (A1-3). The lipids and F-ATPase were mixed in a fixed ratio so that the number of F-ATPases per vesicle was about 1. Proteoliposomes were freshly made before the experiments and unused samples were discarded at the end of the day. After the proteoliposomes were prepared, they were incubated with pre-washed streptavidin modified GNPs for ~ 10 mins.

Separately, the bilayer device was prepared using protocols given in Appendix 1 (A1-5). The substrate agarose used was a mix of NTA modified agarose and normal agarose in the ratio of 1:10. After the device was prepared, it was allowed to rest for thirty minutes. To form the bilayer, MOPS buffer and an ATP regeneration system, comprising ATP, phospho(enol) pyruvate (PEP) and pyruvate kinase (PK), were added to the GNP-proteoliposome suspension. The mixture was then brewed in hexadecane and natural lipids for three minutes before being transferred into the bilayer device. A bilayer formed spontaneously within a few minutes in the well. Formation of the bilayer was first observed using bright field illumination. Once the bilayer was fully formed, the microscopy mode was changed to laser dark-field. Bright spots corresponding to GNPs were observed on the bilayer. A video rate of 1000 frames per second was used to record the images and the power of illumination was set to ~ 100 μ W.

6.3.2 Images from Laser DarkField Microscopy

Two controls were done in the laser dark-field experiments. The first control contained proteoliposomes with no GNPs while the second contained GNPs, but with no proteoliposomes. The purpose of these controls is similar to those seen in chapter 4 using fluorescent streptavidin. They served to clarify whether the observed bright spots were indeed due to the GNP and if so, was the sticking of GNP conditional on the presence of the F-ATPases.

In the first control, GNPs were absent from the droplet used to form the bilayer. The bilayer thus formed was clean and had a low background when seen under dark-field illumination (Figure 6-2a). Nonetheless, some low intensity spots were occasionally spotted on the surface of the bilayer. These spots were sparse and might correspond to proteoliposomes or contaminating particles (small dust particles etc) resting on the bilayer. Compared with the positive control (Figure 6-2c), they were not significant, in both numbers and intensity. This control indicates that the agarose and bilayer surface do not significantly affect the background and that the buffer is generally free from impurities that possess large scattering cross sections.

In the second control, proteoliposomes were absent and GNPs were added. This time, bright spots were occasionally seen diffusing in and out of focus (Figure 6-2b). The image shows a faint interference pattern made by a GNP that was not in focus. The background of the bilayer remained low and no bright spots were seen immobilised on the bilayer. The characteristic diffusing height of GNPs ($\phi = 100$ nm) was estimated to be ~ 43 μm (See Box 5-1). This distance is large relative to the depth of

view⁷⁶ of the objective used (~ 0.5 μm). Diffusing GNP should, on average, remain a fair distance away from the focus and only come near it occasionally. This was indeed seen in the current control. Furthermore, this control also suggests that the bilayer has a low affinity for streptavidin modified GNP. i.e. the GNP does not stick readily onto the bilayer in the absence of F-ATPase.

Box 6-1. Calculation of the characteristic diffusing height of a 100 nm GNP

The characteristic diffusing height is the average equilibrium height at which the GNP will remain.

Potential energy required in maintaining this height is simply $(\rho_g - \rho_w)Vgh$, where ρ_g and ρ_w are the density of the gold and water, V is the volume of the particle, g is the gravitational acceleration and h is the characteristic height.

This energy is supplied by the thermal energy approximated by kT , where k is the Boltzmann constant and T is the temperature. Equating the two:

$$(\rho_g - \rho_w)Vgh \approx kT$$

Since $\rho_g = 19300\text{kg/m}^3$, $\rho_w = 1000\text{kg/m}^3$ and radius of GNP (r) = 50nm, we get

$$h \approx \frac{kT}{(\rho_g - \rho_w)Vg} = \frac{kT}{\pi r^3 (\rho_g - \rho_w) g \frac{4}{3}} = 4.3 \times 10^{-5} \text{ m}$$

Finally, in the buffer containing both the proteoliposomes and GNP, a number of bright spots immobilised on the bilayer was detected (Figure 6-2c). These spots also tended to be brighter than those in the first control. From control 1, it was concluded that the constituents in the bilayer and buffer could not have caused the appearance of such bright spots. These spots were therefore likely to be due to GNPs. From control 2, it was concluded that GNPs, by themselves, do not adhere to bilayers. The proteoliposomes must therefore have caused the GNPs to stick onto the bilayer. Since it was established in chapter 4 that some of the F-ATPase were delivered onto the bilayer via vesicle fusion, it was therefore possible that GNPs on the bilayer might

⁷⁶ Depth of view is the maximum vertical distance between which an object will be in focus. The depth of view of the objective used was obtained from Nikon: <http://www.microscopyu.com/tutorials/java/depthoffield>

have been immobilised by F-ATPases that were inserted into the bilayers and held down by the substrate agarose.

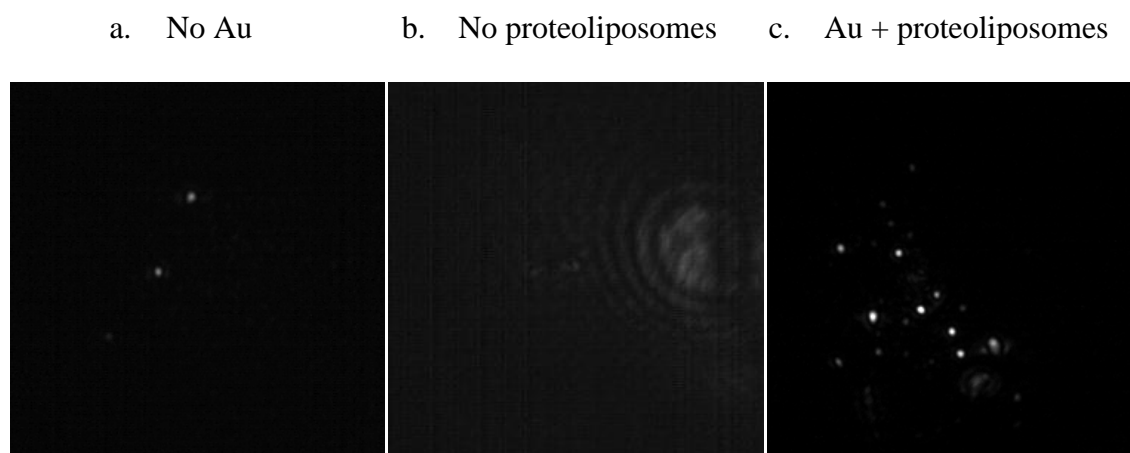


Figure 6-2. Dark-field images of controls and working samples. a) shows the control where no GNPs were added. The bilayer was generally clean and free from bright spots. Occasionally, spots with moderate intensities were observed. They were sparse in number and attributed to proteoliposomes or impurities resting on bilayers. This control suggests that the surface of the bilayer is generally clean and does not scatter significant amount of light. b) shows the second control where proteoliposomes were removed and GNPs added instead. Bright spots were seen coming in and out of focus. These were probably diffusing GNPs that occasionally come close to the surface. No gold beads were observed on the surface of the bilayer. c) shows a typical image when both the proteoliposomes and GNPs were added together. Bright spots were observed and most remained immobilised. These spots were likely to correspond to GNPs on the surface of the bilayer. Frame rate = 1000 fps and laser power ~ 112 μ W.

6.3.3 Analysing Movement of Immobilised GNPs

In order to ascertain the functionality of F-ATPase, ATP was incorporated into the droplet. A relatively high concentration of ATP was used to compensate for hydrolysis reaction taking place while the droplet was being prepared and observed. If a final concentration of 5 mM ATP is added in the buffer, and assuming an activity of $7.3 \mu\text{mol mg}^{-1}\text{min}^{-1}$ (See Chapter 3), it will take ~ 45 mins for the ATP to be fully hydrolysed (See Box 6-2 for calculation). With an ATP regeneration mix added into the buffer, the working duration can potentially be extended by two times (5 mM PEP will at most regenerate 5 mM ATP from free ADP). The short brewing time of three

minutes in hexadecane and observation time of about thirty minutes is therefore acceptable for one to detect rotation of active F-ATPase.

Box 6-2. Calculation for the amount of time the ATP can last before becoming fully expended

Concentration of F-ATPase used for forming proteoliposomes = 0.3 mg/ml

Protocol: 10 μL of F-ATPases were mixed with 10 μL of lipids to form 20 μL of proteoliposomes.

→ Amount of F-ATPase in 20 μL of proteoliposomes = $0.3 \times 0.01 = 0.003 \text{ mg}$

→ Amount of F-ATPase in 10 μL of proteoliposomes = 0.0015 mg

Protocol: 10 μL of proteoliposomes was mixed with 10 μL of GNP, after which 2 μL of the GNP-proteoliposome suspension was incubated with 8 μL of buffer + ATP (final conc = 5 mM) to form 10 μL of final buffer mix.

→ Amount of F-ATPase in 10 μL of final buffer mix = $0.0015 / 10 = 1.5 \times 10^{-4} \text{ mg}$

→ Amount of ATP in final buffer mix = $5 \text{ mM} \times 10 \mu\text{L} = 5 \times 10^{-8} \text{ mol}$

Assuming a constant activity of ATPase (from Chapter 3) = $7.3 \mu\text{mol mg}^{-1} \text{min}^{-1}$

→ Activity of F-ATPase in final buffer mix = $7.3 \mu\text{mol mg}^{-1} \text{min}^{-1} \times 1.5 \times 10^{-4} \text{ mg} = 11 \times 10^{-10} \text{ mol min}^{-1}$

→ Time taken to consume $5 \times 10^{-8} \text{ mol ATP} = 5 \times 10^{-8} / 11 \times 10^{-10} = 45 \text{ mins}$

Regeneration solution consist of 5 mM phosphoenolpyruvic acid (PEP) and 50 $\mu\text{g/ml}$ pyruvate kinase

$\text{PEP} + \text{ADP} \leftrightarrow \text{Pyruvate} + \text{ATP}$ (catalysed by pyruvate kinase)

5 mM of PEP can potentially produce 5 mM ATP, base on the stoichiometry of reaction.

Movements of GNPs immobilised on the bilayer were recorded and analysed computationally. The analysis code was written in MATLAB by Dr Bradley Steel for studying F_1 ATPase rotation. Briefly, it is divided into several steps:

1. The point spread function of each GNP per image frame is selected by identifying clusters of high intensity pixels.
2. A Gaussian mask is then fitted over each of these spots in order to calculate the centres of the GNPs [277]. This approach allows a faster way of calculating the centre than a full Gaussian fit and is more accurate than simply finding the centre

of brightness (centroid). The procedure is repeated for all image frames, so that the coordinates of every GNP at different times can be obtained.

3. The frequencies of rotation are analysed by applying a Fourier transform on the coordinates i.e. $\mathcal{F}(x + iy)$, where (x,y) are coordinates of the GNPs, i is the complex number notation ($\sqrt{-1}$) and \mathcal{F} represents the Fourier transform. The result is a frequency power spectrum whose resolution is given by the reciprocal of the duration of measurement, and frequency range given by half the reciprocal of the time between each frame. At a frame rate of 1000 frames per second over a duration of 3.264 s, the frequency resolution is 0.3 Hz and over a frequency range of ± 500 Hz. This frequency power spectrum essentially describes the movement of the GNP in the frequency domain. For example, if a bead is rotating at a speed of 20 Hz, there will be a sharp peak that corresponds to 20 Hz on the power spectrum. Moreover, directionality of rotation is also defined by the power spectrum. The positive frequency in the power spectrum represents clockwise⁷⁷ direction of rotation while negative frequency represents counter clockwise. For a unidirectional clockwise rotating bead, a peak will therefore appear in the positive frequency of the power spectrum but not the negative frequency and *vice versa*.
4. In order to detect the direction of rotation of the GNP (either clockwise or anticlockwise), the power spectrum in the positive frequency (x-axis) is subtracted from that in the negative frequency (i.e. $p(f) - p(-f)$, where p is the function that defines the power spectrum). This modified power spectrum removes any unbiased rotating components, while retains the biased ones. A positive value in the modified power spectrum represents a bias clockwise rotation at the

⁷⁷ For the power spectrum of point (x,y) in Cartesian coordinates, a counter clockwise rotation corresponds to positive frequency. However, in our current configuration, the y axis was flipped 180° (pointing down). A positive frequency therefore corresponded to clockwise rotation instead.

corresponding frequency, while a negative peak represents counter clockwise motion. Furthermore, in order to quantify the extent of bias in directionality, the area under the curve of the modified power spectrum is expressed as a ratio of the entire area under the curve for the original power spectrum. This gives a variable now termed as CW bias. In general, the higher the CW bias, the stronger is the unidirectionality of rotation. A good rotating bead usually has a high CW bias value and a well defined “donut” trajectory. See Figure 6-3a.

5. Finally, the trajectory of the GNP is visualised in a scatter plot with an ellipse fitted to it. The angle of each point in the trajectory is defined with respect to the centre of the fitted ellipse and presented in an angle histogram. Both the scatter plot and histogram allow visual inspection of any steps that may occur during rotation.

To ensure that the F-ATPase, GNPs and agarose were working as expected, rotation of F-ATPase on de-energised membrane was first investigated. A tunnel slide with NTA agarose was prepared and then activated using 10 mM NiCl₂. This was followed by the sequential addition of detergent stabilised F-ATPase, GNPs and an ATP regeneration solution. Each constituent was washed with buffers containing lipids before the next one was added. This assay allows the gradual building up of “components” needed to observe rotation of the enzyme and is similar to the assay used by Ueno et. al. [199]. Appendix1 (A1-10) gives the detailed protocol used. When the samples were observed under the darkfield microscope and analysed using the approach mentioned above, rotating GNPs were detected. To show that these rotations were fully coupled (i.e. F₁ is attached to F₀), a control with DCCD incubated enzyme was tested. No rotation was observed for this control, suggesting that the rotation of

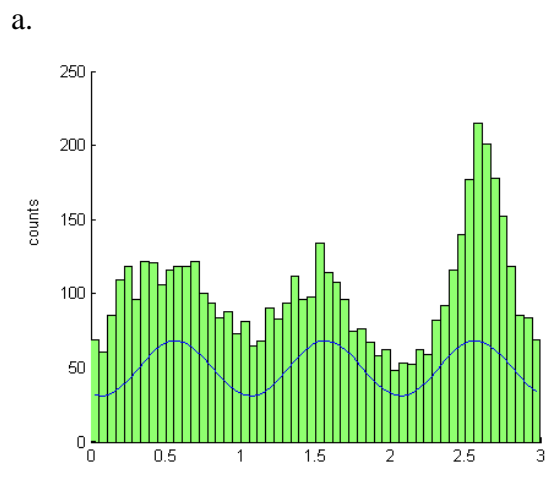
the β -subunit could be stopped by preventing the rotation of the c-ring. Figure 6-3a shows the typical characteristics of a rotating F-ATPase immobilised on the coverslip⁷⁸.

When the same enzyme was used in the DHB setup, no obvious unidirectional rotation was observed. However, about 0.1% of the trajectories showed a “donut” shape (Figure 6-3b, second column). Such a trajectory is a signature of tethered movements, pivoted about a fixed point. When the angles with respect to the centre of the ellipse were plotted on a histogram, some trajectories also showed three broad peaks spaced roughly 120° apart (Figure 6-3b, first column). Furthermore, for those GNPs that showed a nice donut shape, most of them also displayed the abovementioned three peaks in their angle histogram. Brownian motion is not able to explain the three fold periodicity. Such examples of threefold dwells of intact F-ATPase have also been seen in F-ATPase rotations during both synthesis and hydrolysis of ATP [201, 203, 278, 279].

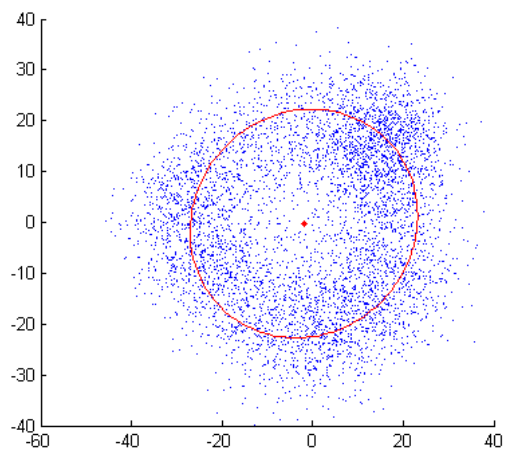
However, almost all the beads with threefold peaks exhibited only a small CW bias value i.e. there is no continuous rotation in a particular direction. There were a very small number of GNPs ($\sim 0.01\%$) that showed a high bias ($>20\%$), albeit rotating at a very low speed $< 10\text{Hz}$. Figure 6-3b shows the characteristics of one such GNP. This bead gave a high CW bias (40 %) but rotated at a speed of $\sim 1\text{-}2\text{ Hz}$.

⁷⁸ Note that this is an open membrane system, where the enzymes are stabilised by membrane patches formed by the lipid vesicles in the buffer.

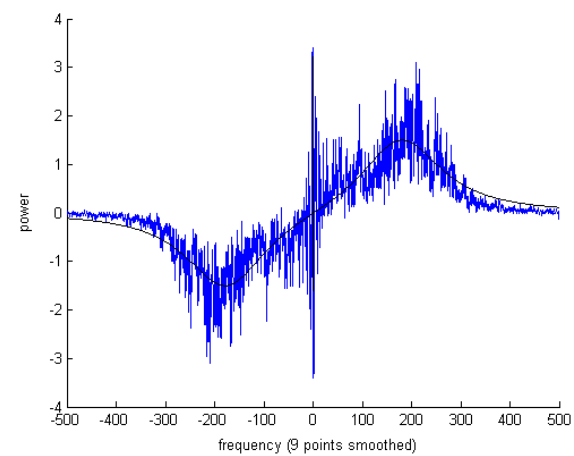
Angles Histogram



Trajectory



Modified Power Spectrum



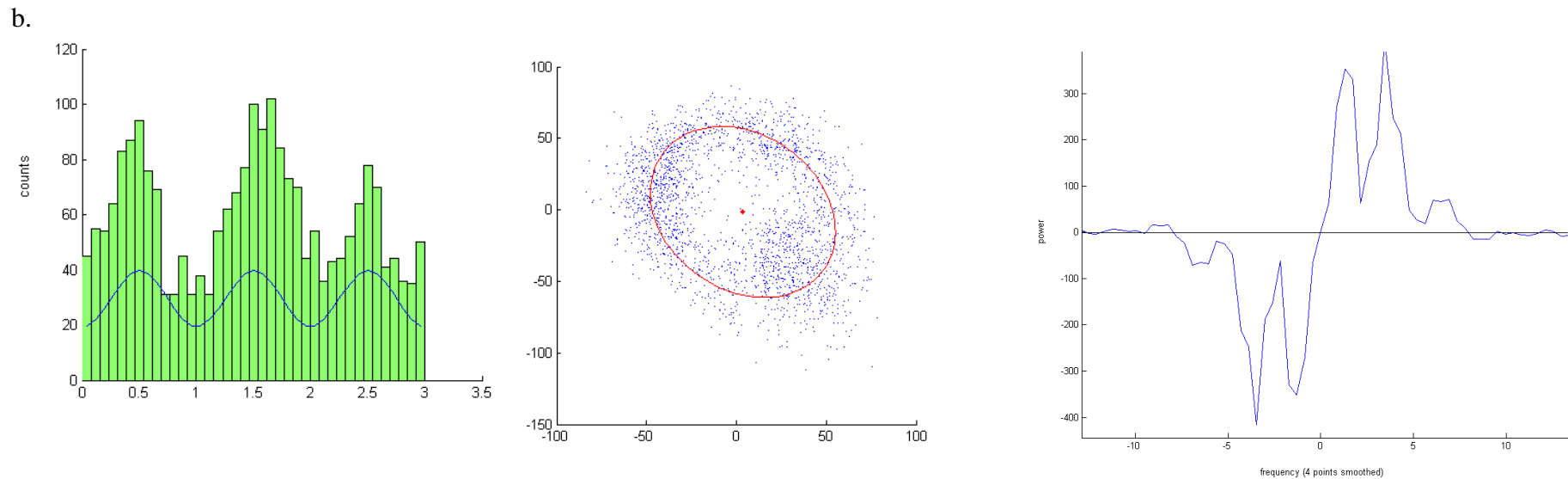


Figure 6-3. Characteristics of immobilised GNPs. The histogram in the first column shows the distribution of the angles with respect to the centre of trajectory. The x-axis is scaled in multiples of 120° (i.e. 1 unit = 120°). Three peaks can be seen in both examples. The blue curves are spaced at exactly 120° apart and positioned to fit the peaks of the histogram. The second column shows the trajectories of the GNPs. “Donut” shape trajectories were observed in some of the trajectories. They suggest a tethered movement about a point. The scales in both the x and y axes are in nano-metres. Finally, the last column represents the power spectrum after the values at the positive frequencies were subtracted by values at the negative frequencies (i.e. $p(f)-p(-f)$). a) shows the characteristics of rotation for F_1F_o ATPase immobilised on NTA agarose in a de-energised membrane. Detergent solubilised F-ATPase was first immobilised on the agarose surface before buffer, containing lipid vesicles, was flowed in to stabilise the enzyme. b) shows a GNP obtained on energised bilayers, formed using the DHB method. None of the GNPs were found to rotate at high speed, although bias dwells at three angles and “donut” trajectories were still observed.

6.4 Discussion

For the bilayer used in the experiments, the *cis* and *trans* domains of the membrane were electrically and chemically isolated from each other. It was shown earlier that the substrate agarose had relatively low water content (~ 40% w/v) and an average height of just 240 nm. There was therefore a possibility that protons could accumulate in the small volume of the substrate agarose and produce an opposing proton motive force (PMF) that impeded further hydrolysis of ATP. To assess the likelihood of this happening, the change in PMF due to protons translocated by F-ATPase was estimated. This PMF was divided into two components. The first was a pH change due to the increased concentration of H⁺ ions. To calculate this, the rate of proton addition by the F-ATPase was compared with the rate of proton removal due to diffusion across the substrate agarose. The net concentration of H⁺ ions was found by dividing the amount of the protons translocated across the bilayer, by the volume of the substrate agarose defined by the average diffused distance of hydronium ions (H₃O⁺). It was found that the pH would only be reduced by slightly more than 1 unit, from pH 7 to pH 6. This was true when the buffering effect of MOPS was not considered. However, if the presence of MOPS was taken into account, the pH change due to the contribution of protons would be reduced further. This was because the concentration of MOPS in the substrate agarose was about two order of magnitude higher than the amount of additional H⁺ contributed by the F-ATPase rotation (within the timescale of the experiment). Detailed calculations for the pH are found in Box 6.3.

The contribution of the proton charges on the overall electrical potential across the membrane was found by dividing the total amount of charges transported across the bilayer, by the capacitance of the bilayer. The total amount of protons across the bilayer was estimated by finding the number of F-ATPase on the bilayer and multiplying it by the activity of the enzyme, while the specific capacitance of the bilayer was obtained from literature [246]. It was found that for every minute of rotation, proton conduction could create an opposing voltage of ~ 32 mV. In comparison, the amount of voltage needed to oppose the hydrolysis of ATP was ~ 169 mV. The opposing voltage due to the capacitance of the bilayer was within an order of magnitude from the stalling voltage in just the first minute of experiment. There was hence a possibility that the condition in the bilayer had become unfavourable for ATP hydrolysis when the GNPs were observed. The proposition that an opposing PMF was generated and resisting the rotation of F_1F_0 ATPase thus appeared to be a reasonable one. This can explain why unidirectional rotation could not be observed in the experiments done so far.

Box 6-3. Calculations for the contribution of proton transport on the pH and electropotential of the agarose.

To study the contribution of H^+ on the pH of the agarose, the diffusion of hydronium ions was calculated

Two cases were considered. For the case where the F-ATPases were far from each other such that effect of neighbouring enzyme could be ignored:

- Diffusion of hydronium ion in buffer = $D = \frac{kT}{6\pi\eta a} = \frac{1.38 \times 10^{-23} (293)}{6\pi(1.3 \times 10^{-3})(1.5 \times 10^{-10})} = 1.1 \times 10^{-9} \text{ m}^2/\text{s}$

k is Boltzman constant,

T is temperature in K

η is viscosity of buffer ~ 1.3×10^{-3} Pa.s

a is the hydrodynamic radius⁷⁹ of the hydronium ion ~ 1.5×10^{-10} m [280]

⁷⁹ The size of unhydrated K^+ ion was used as an approximation. Reference shows that the size of unhydrated hydronium is between the size of Na^+ and K^+ . The hydration is not expected to have a large influence on the diameter of the hydronium ion.

- Since the thickness of agarose (~ 240 nm) was small compared with lateral dimension $\sqrt{Dt_0} \sim 3 \mu\text{m}$. (See below for value and definition of t_0), two-dimensional diffusion was assumed. Hence

$$\langle \Delta r^2 \rangle = 4D\Delta t$$

Where t is the time of diffusion in second and

$\langle \Delta r^2 \rangle$ is the mean square displacement of a single proton after time Δt .

- If one assumes a rate of rotation (ω) ~ 11Hz [201], and that each rotation strongly couples with the translocation of ten protons (Since there are ten c-subunit per c-ring). Then:

Number of protons coupled per second = $10\omega = 110$ protons/s

- To find the excess concentration of protons as seen by the F-ATPase, the number of protons translocated was divided by the volume covered by the protons due to diffusion. This can be expressed as

$$\Delta C = \sum_{T=t_0}^{T=t} \frac{\text{Protons transported over time } \Delta T}{\text{Volume occupied by protons due to diffusion after } T}, \Delta T \rightarrow 0$$

$$= \int_{t_0}^t \frac{10\omega dT}{A_v \langle \Delta r^2(T) \rangle h} = \int_{t_0}^t \frac{10\omega dT}{4A_v DTh} = \frac{10\omega}{4A_v Dh} \ln \frac{t}{t_0}$$

ΔC is the change in concentration of the environment, as seen by F_o in Molar

A_v is the Avogadro number

h is the thickness of the agarose in metres

t is the time elapse and t_0 is the time to translocate one proton through.

t_0 is chosen as the lower limit of integration because the proton that sees ΔC will only do so after t_0 . ($t_0 = 1/110\text{s}$)

ω is the rate of rotation in Hz

- However, some of the volume was due to dry agarose. It was noted that:

Density of dry agarose ~ 1.64 g/ml

Mass of dry agarose in 1 ml hydrated agarose = 0.4 g (from chapter 4)

Vol of dry agarose per 1 ml hydrated agarose = $0.4 / 1.64 = 0.24$ ml

Vol of water per 1 ml hydrated agarose = $1 - 0.24 = 0.76$ ml

- Hence $\Delta C = \frac{110}{4A_v Dh(0.76)} \ln \frac{t}{t_0} = \frac{110}{4(6.02 \times 10^{23})(1.1 \times 10^{-9})(240 \times 10^{-9})(0.76)} \ln \frac{t}{t_0} = 2.3 \times 10^{-7} \ln \frac{t}{t_0}$

The above approximation indicates that for a single ATP Synthase, the local increase in concentration due to proton flux is small. It took less than a second for the pH to reduce from pH 7 to pH 6 but a long time ($> 10^{16}$ seconds) to achieve pH 5. Contribution of H^+ to the pH is smaller if buffering effect of 20 mM of MOPS is considered. These calculations are applicable only if the influence of neighbouring ATPase is negligible.

For the second case where adjacent F-ATPase contributed to the overall change in pH:

- It is more difficult to consider the cumulative effect of multiple F-ATPase. If one assumes instant mixing and all H^+ stayed within the boundary of the bilayer, then the combined effect of multiple F-ATPase can be calculated by dividing the total amount of protons translocated across, by the volume of substrate agarose beneath the bilayer.

By counting the number of fluorescent spots in Figure 4-7, one can estimate the density of F_1F_o ATP synthase on bilayer. This was found to be $\sim 0.2 / \mu\text{m}^2$. Therefore

$$\Delta C_{\text{All}} = \frac{10\rho A\omega t}{(0.76)AhA_v} \times 10^{15} = \frac{10\rho\omega t}{(0.76)hA_v} \times 10^{15} = 2 \times 10^{-7} t \text{ M} \quad - \quad \text{Equation 6-1}$$

ΔC_{All} is the average H^+ concentration in mol/dm^3
 ρ is the density of ATPase in bilayer $\sim 0.2/\mu m^2$
 ω is the rate of angular rotation ~ 11 Hz
 t is the times elapsed since the addition of ATP
 A is the area of the bilayer
 h is the thickness of substrate agarose $\sim 240 \mu m$
 A_v is Avogadro's Number
 $\times 10^{15}$ is needed to convert from $mol/\mu m^3$ to mol/dm^3

$\Delta C_{All} = 0.36$ mM for time = 30 minutes

The change in concentration was small, within the experimental time scale, relative to the concentration of MOPS ~ 20 mM. pH therefore was thought to have only a small contribution to the overall opposing PMF.

To study the contribution of H^+ on the voltage across the membrane, the capacitance of the membrane was used

- Voltage across membrane = Q/C

Where C is the capacitance of the bilayer and Q is the charge stored.

- But $Q = 10e\rho A \omega t$

Where the definitions of the symbols are the same as equation 6-1 and e is the charge of the proton in Coulomb

- And $C = \epsilon A$

ϵ is the specific capacitance of the bilayer in F / cm^2

- Thus

$$V = \frac{10e\rho A \omega t}{\epsilon A} = \frac{10e\rho \omega t}{\epsilon}$$

- Assuming that

Specific capacitance of the bilayer $\sim 0.65 \times 10^{-6}$ F / cm^2 [246]

$$\rho \sim 0.2 / \mu m^2$$

$$e = 1.6 \times 10^{-19} \text{ C}$$

$$\omega \sim 11 \text{ Hz}$$

$$V = 0.54 \text{ mV for time} = 1 \text{ s}$$

$$V = 32 \text{ mV for time} = 1 \text{ min}$$

- Assuming further that the free energy per ATP molecule is ~ 90 pNm [131], each rotation that produces 3 ATP therefore requires 270 pN nm of energy or 2.7×10^{-19} J.

To prevent the hydrolysis of ATP, the opposing voltage (V_o) should give at least the same amount of energy for 1 round of rotation (ten protons translocated across). Hence

$$V_o \times 10e = 2.7 \times 10^{-19} \text{ J}$$

$$V_o = 2.7 \times 10^{-19} / (10 \times 1.6 \times 10^{-19}) = 169 \text{ mV}$$

The voltage contribution of the protons was thus not negligible.

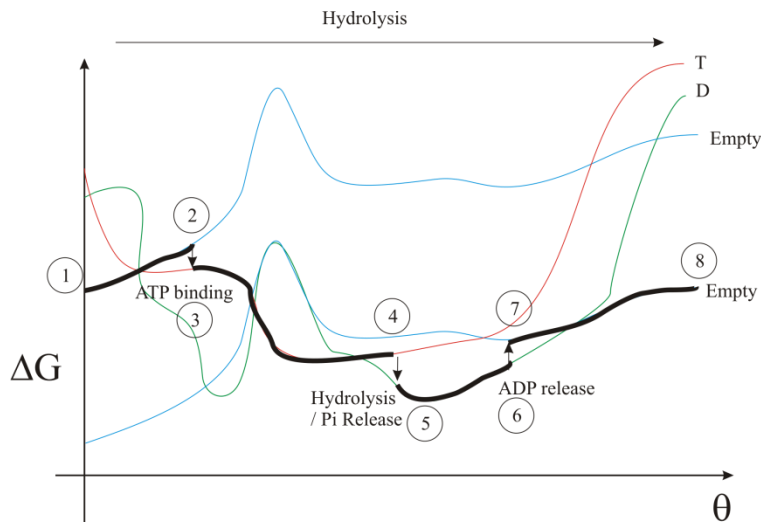
To account for the observation of the three dwell angles, the free energy diagram during rotation was considered. Figure 6-4a shows the free energy diagram adapted from Xing [281]. It gives the various energy profiles of the β -subunit at different states of occupancy and angular positions of the γ -subunit. The bold lines show the path taken by the β -subunit as the γ -subunit rotates. Briefly, an empty β -subunit is able to favourably bind ATP when the γ -subunit is rotated slightly forward (1 to 2). Upon ATP binding, hydrogen bonds are incrementally formed between the ATP and the β -subunit, which results in simultaneous rotation of the γ -subunit and steady lowering of free energy (step 3 to 4). At the catalytic dwell angle (step 4), the phosphate bond in the ATP is hydrolysed and the phosphate molecule released (step 4 to 5). Finally, ADP is freed from the β -subunit (Step 6 to 7), assisted by the binding of a second ATP at the adjacent empty β -subunit. Detailed mechanism of rotation can be found in Chapter 2. A more in depth description is also given in the caption below Figure 6-4.

The diagram in Figure 6-4 was originally created to study the synthesis of ATP [281]. It is now adapted for hydrolysis, with the assumption that the free energy profiles for ATP synthesis are the reverse of hydrolysis. In the original free energy diagram shown in Figure 6-4a, there was already a PMF incorporated into the energy profile. This PMF was modelled as a constant torque exerting in the synthesis direction (or opposing torque in the hydrolysis direction). The graph in Figure 6-4b shows the approximate free energy profile if the opposing PMF is increased (in purple) or reduced (in orange). If a larger opposing PMF is present, an increase in θ will require a larger energy input, hence a steeper increase in the free energy profile. Conversely, the opposite is true for a smaller opposing PMF. For all the three cases, it can be seen

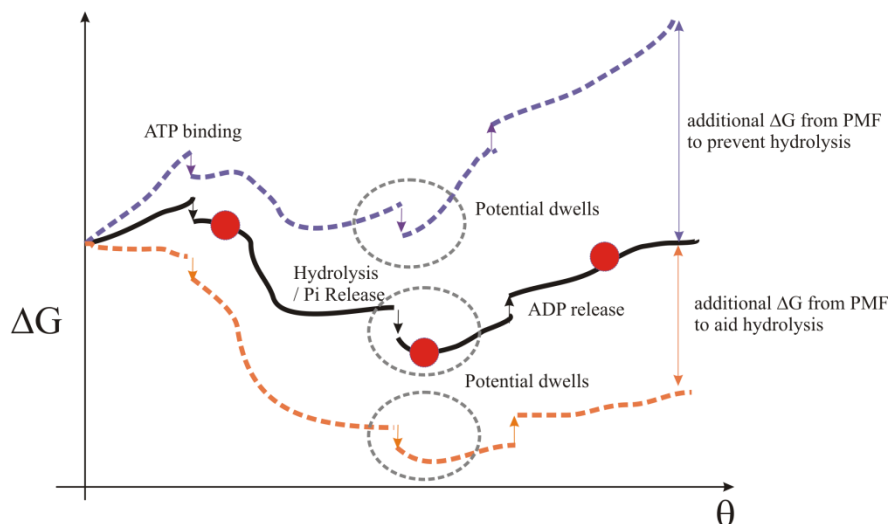
that an energy minimum exists just after the phosphate release. This state corresponds to the catalytic dwell of F_1 described in chapter 2. It is therefore possible to explain the observed 120° dwells by assuming that the β -subunits were trapped at this location. Occasionally, thermal energy would allow it to overcome the energy barrier in either direction. However, as it did so, it swiftly fell into another energy minimum at 120° away. Such a qualitative argument could explain why dwells were observed but not rotation.

The explanation for the observed data is premised on the presence of an opposing PMF that prevented the rotation of F-ATPase and trapped the β -subunit at angles corresponding to catalytic dwell angles. Clearly, this remains a hypothesis and requires corroborations from more experimental evidence. The next part of the work is thus to attempt to neutralise the opposing PMF and observe the movement of the F-ATPase tethered GNPs again. This can be achieved by applying an external PMF, using electrodes placed on both sides of the membrane. To do this on the dark-field microscope requires modifying the stage so that it can incorporate a micromanipulator to control the electrode. Furthermore a variable voltage control will also have to be integrated into the setup. Although this part of the work has been routinely done on the TIRFM in the Wallace group⁸⁰, it still requires some effort to incorporate the electrodes on the LDM.

⁸⁰ Dr Mark Wallace is a collaborator who has provided us with the bilayer device



a. Free energy diagram for hydrolysis against a opposing PMF that is just sufficient to allow synthesis



b. Free energy diagram for hydrolysis against a larger or smaller opposing PMF

Figure 6-4. a) shows a possible free energy diagram of the various states which the β -subunit can be in, based on [281]. The blue lines indicate the free energy change of an empty β -subunit at different angles of rotation. The red and green represent the corresponding ATP bound and ADP bound state. Bold lines show the path taken by the β -subunit as the ATPase hydrolyses ATP. Starting from the zeroth angle (1), ATP binding of an empty β (blue line) is triggered by an initial angular displacement (1) \rightarrow (2). Once bound (2) \rightarrow (3), the β -subunit transits from loose to tight, turning the γ -subunit at the same time (3) \rightarrow (4). There is a gradual drop in the overall free energy. The hydrolysis of ATP to ADP and phosphate is omitted here because the process does not incur any change in free energy [83]. Release of phosphate causes the free energy to further lower (4) \rightarrow (5). The release of ADP (5) \rightarrow (7) is aided partly by the binding of ATP at the empty β -subunit that is 120° ahead, thus freeing the β -subunit for the next binding cycle. This free energy model is modified from [281], which is used to describe ATP synthesis instead of hydrolysis. It was assumed that the process of ATP hydrolysis is approximately the reverse of ATP synthesis. b) shows the possible change in free energy profile when the PMF is increased (purple line) or decreased (orange). In all cases, an energy minimum is seen at the catalytic dwell position. This may explain the occurrence of three fold dwells observed in the experiments. The red dots in the figure indicate the relative positions of the three β -subunits spaced 120° apart.

6.5 Summary of chapter

In this chapter, the movement of GNP tagged F-ATPase on planar bilayer was tracked and analysed. For the experiments reported, rotation was induced by addition of ATP. A back scattering laser dark-field microscope was used to observe the motion of the GNPs adhered on the bilayer. Schematics and principles for the dark-field microscope were also given. Control experiments showed that free GNPs did not bind to the bilayer, unless proteoliposomes were present. Most of the GNPs found on the F-ATPase reconstituted bilayer were immobilised. When these GNPs were tracked, persistent rotation in a fixed direction was not observed. However, some of the GNPs (~ 0.1 %) showed three dwell angles spaced roughly 120° apart and had “donut” shaped trajectories.

It was thought that the rotation of F-ATPase might have been impeded by an opposing PMF built up between the bilayer. This PMF was unlikely to be due to a pH difference but probably caused by proton charges transferred across the membrane. The opposing PMF also changed the free energy profile during rotation. It was possible that prolonged dwells at specific angles were due to β -subunits trapped at a minimum point in the free energy profile. The three fold dwells observed also lent support to the postulation that the GNPs were successfully tethered to the bilayer via an immobilised F-ATPase molecule.

7

Summary, Future Work and Conclusion

7.1 Summary

In Chapter three, I have described how F_1F_0 ATPase was purified from *E. coli* and shown to be functional. Two methods of purification were used. It was found that the nickel column yielded F-ATPases with higher enzymatic activity. F-ATPase was reconstituted into vesicles such that there was approximately one F-ATPase per vesicle. This was supported by experimental evidence obtained using alternating laser excitation (ALEX) and fluorescence correlation spectroscopy (FCS). The condition for maintaining unitary stoichiometry is important to avoid having more than one F-ATPase attached to the gold nano-particle. If the latter occurs, the rotation of the F-ATPase will be affected. It was also found that not all lipids were suitable for reconstituting with *E. coli* F-ATPase. Those reconstituted with synthetic lipids exhibited less activity than those reconstituted with natural lipids. The main deliverable of chapter 3 is the protocol for reconstituting functional F-ATPase into vesicles and with a stoichiometry of one F-ATPase per vesicle.

After obtaining functioning proteoliposomes, the next challenge was to build a stable planar bilayer so that F-ATPases could be embedded into it. The droplet on hydrogel bilayer (DHB) was used. To characterise this system, the substrate agarose beneath

the bilayer was investigated. It was found that the thickness of this agarose was ~ 240 nm (upper limit). This corresponded to a mass percentage of ~ 40 % (w/v), which put the bilayer sufficiently far away from the glass substrate but near enough to allow imaging using total internal reflection fluorescent microscopy (TIRFM). F-ATPases were then reconstituted into the bilayer by vesicle fusion. It was shown using TIRFM that fluorescently labelled F-ATPases were adhering on the planar bilayer. Furthermore, some of these molecules showed sustained two-dimensional diffusion. The diffusional constant was about 3x slower than the values reported for a membrane protein of similar size (SR-ATPase). The main deliverable for chapter four is the protocol for preparing planar bilayers and reconstituting F-ATPase into it via vesicle fusion.

Chapter five describes the procedure for modifying both the substrate agarose and the gold nano-particles (GNPs). The substrate agarose was modified with nitrilotriacetic acid (NTA) so that it could immobilise the 6-histag c-ring of the F-ATPase mutant. With this arrangement, the $c_{10}\gamma\epsilon$ ensemble would act as a stator about which the rest of the F-ATPase could rotate. The increased affinity of the NTA modified agarose towards histag proteins were demonstrated using epi-fluorescent microscopy and histag YFPs as fluorescent probes. In the second part of the chapter, GNPs were modified with streptavidin molecules. Using a fluorescent bleaching assay, the number of streptavidin molecules per GNP was estimated to be 4. The main deliverables for chapter five are the protocols for modifying both the agarose and GNP with the appropriate functional groups.

Chapter six describes the results of the experiments that combined the various aspects described in the preceding chapters. The bilayer was setup using NTA modified substrate agarose and F-ATPases were labelled with streptavidin GNPs. Movements of GNPs were observed using a laser dark-field microscope. To my dismay, no unidirectional rotation was detected. There was however three fold dwells spaced at about 120° apart. It was hypothesized that an opposing electrical potential might have been created as protons were accumulated on the other side of the bilayer. This inhibited the hydrolysis of ATP (hence no rotation) and trapped the position of the β -subunits at an energy minimum point (hence the dwells). To test this, an external potential that negates the contribution of this opposing potential has to be applied.

7.2 Future Work

This is an ongoing project that will continue beyond the thesis. The immediate task is to explain why rotation was not observed with the current setup. To do this, the laser dark-field microscope has to be slightly modified to include electrodes at the *cis* and *trans* side of the bilayer. The electrode can then be linked to a voltage clamp so that the potential between the bilayer can be regulated. If this is successful in powering the rotation of F-ATPase, it will vindicate the postulation given in chapter 6. At the same time, a plethora of interesting experiments can also be performed. One may, for example, measure the rate of rotation and step size under different PMFs and chemical conditions.

To study the activity of F-ATPase under different buffer conditions, it may be necessary to add or remove chemicals into / out of the buffer. One of the main

limitations of the bilayer device is that the droplet is completely isolated. To change the content inside the droplet, a perfusable system has to be incorporated. This was attempted with limited success. The gist of the droplet perfusing procedure is as follows: content of the droplet was extracted or inserted via two glass pipettes with tip diameter of about 30 μm . The pipettes were inserted into the droplet using micromanipulators and flow rates within the pipettes were kept low and carefully balanced. This was done using small diameter tubing as resistors and hydrostatic pressure as pumps to move the buffer within the system. By balancing the flow of the inlet pipette and outlet pipette, I was able to successfully perfuse droplets using this technique (results not shown). However, the process of perfusing was very intricate and the success rate was low. This is the main reason why it has not been incorporated into the main setup yet. Part of the future work will therefore be making improvements to the existing perfusion system so that one can truly manipulate both the electrical and chemical potential of the bilayer.

7.3 Conclusion

This thesis describes the procedure for creating an experimental setup to observe the rotation of F_1F_0 ATPase on planar bilayer. The project, if successful, will help fill a telling gap in the study of the chemo-mechanical cycle of intact F_1F_0 ATPase. Up to now, it is still very difficult to directly observe the movement of the F-ATPase in its native bilayer environment. This is perhaps ironic considering that F-ATPase activity is one of the most ubiquitous processes in the body. Although the rotation of F_1 has been well characterised, scientists are still unsure about the mechanism of F_0 and coupled interactions between F_1 and F_0 . This is due to a lack of both structural and

kinetic data of intact F-ATPase. Structures of the c-subunit are only recently elucidated, while there is still no structure for the a-subunit. On the kinetic studies, although F_1F_0 rotation in an energisable membrane has been observed, there are still many technical issues concerning the resolution and controllability of the conditions for rotation. Indeed, behind the facade of this straightforward objective lie many technical challenges.

These challenges include the need to 1) create stable bilayers for sustained observation, 2) maintain the integrity and functionality of F-ATPases, 3) immobilise the F-ATPases on bilayers and 4) do high temporal and spatial resolution recordings of rotation. All of the work in this thesis is meant to resolve these issues. I am able to progress to a stage where F-ATPases are thought to be immobilised on a planar bilayer and their movement monitored via GNP probes. Unfortunately, rotation of ATP synthase was not observed. The solution to this may be as straightforward as adding an electrical potential across the membrane. Or perhaps it could be something more complicated that require elaborate fault finding. In any case, this work is an important milestone in our attempt to enable the observation of one of nature's most fundamental processes.

Reference

1. Capaldi, R.A. and R. Aggeler, *Mechanism of the F(1)F(0)-type ATP synthase, a biological rotary motor*. Trends Biochem Sci, 2002. **27**(3): p. 154-60.
2. Yoshida, M., E. Muneyuki, and T. Hisabori, *ATP synthase--a marvellous rotary engine of the cell*. Nat Rev Mol Cell Biol, 2001. **2**(9): p. 669-77.
3. Atkinson, D.E., *The energy charge of the adenylate pool as a regulatory parameter. Interaction with feedback modifiers*. Biochemistry, 1968. **7**(11): p. 4030-4.
4. Knowles, J.R., *Enzyme-catalyzed phosphoryl transfer reactions*. Annu Rev Biochem, 1980. **49**: p. 877-919.
5. Rolfe, D.F. and G.C. Brown, *Cellular energy utilization and molecular origin of standard metabolic rate in mammals*. Physiol Rev, 1997. **77**(3): p. 731-58.
6. Futai, M., Y. Wada, and J.H. Kaplan, eds. *Handbook of ATPases*. 2004, Wiley-VCH. 459.
7. Amory, A., F. Foury, and A. Goffeau, *The purified plasma membrane ATPase of the yeast Schizosaccharomyces pombe forms a phosphorylated intermediate*. J Biol Chem, 1980. **255**(19): p. 9353-7.
8. Toyoshima, C., et al., *Crystal structure of the calcium pump of sarcoplasmic reticulum at 2.6 Å resolution*. Nature, 2000. **405**(6787): p. 647-55.
9. Olesen, C., et al., *The structural basis of calcium transport by the calcium pump*. Nature, 2007. **450**(7172): p. 1036-42.
10. Beyenbach, K.W. and H. Wieczorek, *The V-type H⁺ ATPase: molecular structure and function, physiological roles and regulation*. J Exp Biol, 2006. **209**(Pt 4): p. 577-89.
11. Nishi, T. and M. Forgac, *The vacuolar (H⁺)-ATPases--nature's most versatile proton pumps*. Nat Rev Mol Cell Biol, 2002. **3**(2): p. 94-103.
12. Murata, T., et al., *Structure of the rotor of the V-Type Na⁺-ATPase from Enterococcus hirae*. Science, 2005. **308**(5722): p. 654-9.
13. Jefferies, K.C., D.J. Cipriano, and M. Forgac, *Function, structure and regulation of the vacuolar (H⁺)-ATPases*. Arch Biochem Biophys, 2008. **476**(1): p. 33-42.
14. Cross, R.L. and V. Muller, *The evolution of A-, F-, and V-type ATP synthases and ATPases: reversals in function and changes in the H⁺/ATP coupling ratio*. FEBS Lett, 2004. **576**(1-2): p. 1-4.
15. Pogoryelov, D., et al., *High-resolution structure of the rotor ring of a proton-dependent ATP synthase*. Nat Struct Mol Biol, 2009. **16**(10): p. 1068-73.
16. Saroussi, S. and N. Nelson, *The little we know on the structure and machinery of V-ATPase*. J Exp Biol, 2009. **212**(Pt 11): p. 1604-10.
17. Imamura, H., et al., *Evidence for rotation of V1-ATPase*. Proc Natl Acad Sci U S A, 2003. **100**(5): p. 2312-5.
18. Zhang, Z., et al., *Structure of the yeast vacuolar ATPase*. J Biol Chem, 2008. **283**(51): p. 35983-95.
19. Senior, A.E., *ATP synthesis by oxidative phosphorylation*. Physiol Rev, 1988. **68**(1): p. 177-231.
20. Brookman, J.J., et al., *Proton translocation in cytochrome-deficient mutants of Escherichia coli*. J Bacteriol, 1979. **137**(2): p. 705-10.

21. Abrahams, J.P., et al., *Structure at 2.8 Å resolution of F₁-ATPase from bovine heart mitochondria*. *Nature*, 1994. **370**(6491): p. 621-8.
22. Kabaleeswaran, V., et al., *Novel features of the rotary catalytic mechanism revealed in the structure of yeast F₁ ATPase*. *EMBO J*, 2006. **25**(22): p. 5433-42.
23. Kabaleeswaran, V., et al., *Asymmetric structure of the yeast F₁ ATPase in the absence of bound nucleotides*. *J Biol Chem*, 2009. **284**(16): p. 10546-51.
24. Hausrath, A.C., et al., *Structural features of the gamma subunit of the Escherichia coli F(1) ATPase revealed by a 4.4-Å resolution map obtained by x-ray crystallography*. *Proc Natl Acad Sci U S A*, 1999. **96**(24): p. 13697-702.
25. Rodgers, A.J. and M.C. Wilce, *Structure of the gamma-epsilon complex of ATP synthase*. *Nat Struct Biol*, 2000. **7**(11): p. 1051-4.
26. Groth, G. and E. Pohl, *The structure of the chloroplast F₁-ATPase at 3.2 Å resolution*. *J Biol Chem*, 2001. **276**(2): p. 1345-52.
27. Noji, H., et al., *Direct observation of the rotation of F₁-ATPase*. *Nature*, 1997. **386**(6622): p. 299-302.
28. Noji, H., et al., *Rotation of Escherichia coli F(1)-ATPase*. *Biochem Biophys Res Commun*, 1999. **260**(3): p. 597-9.
29. Omote, H., et al., *The gamma-subunit rotation and torque generation in F₁-ATPase from wild-type or uncoupled mutant Escherichia coli*. *Proc Natl Acad Sci U S A*, 1999. **96**(14): p. 7780-4.
30. Hisabori, T., A. Kondoh, and M. Yoshida, *The gamma subunit in chloroplast F(1)-ATPase can rotate in a unidirectional and counter-clockwise manner*. *FEBS Lett*, 1999. **463**(1-2): p. 35-8.
31. Iwabe, N., et al., *Evolutionary relationship of archaebacteria, eubacteria, and eukaryotes inferred from phylogenetic trees of duplicated genes*. *Proc Natl Acad Sci U S A*, 1989. **86**(23): p. 9355-9.
32. Muller, V., et al., *ATP synthases with novel rotor subunits: new insights into structure, function and evolution of ATPases*. *J Bioenerg Biomembr*, 2005. **37**(6): p. 455-60.
33. Lee, L.K., et al., *The structure of the peripheral stalk of Thermus thermophilus H⁺-ATPase/synthase*. *Nat Struct Mol Biol*, 2010. **17**(3): p. 373-8.
34. Wikipedia. *Antoine Lavoisier*. 2010 [cited 2010 May 21]; Available from: http://en.wikipedia.org/wiki/Antoine_Lavoisier.
35. *Otto Meyerhof and the Physiology Institute: the Birth of Modern Biochemistry*. 2010 [cited 2010 May 21]; Available from: http://nobelprize.org/nobel_prizes/medicine/articles/states/otto-meyerhof.html.
36. Kresge, N., R.D. Simoni, and R.L. Hill, *JBC Centennial - 1905-2005 - 100 years of biochemistry and molecular biology - Otto Fritz Meyerhof and the elucidation of the glycolytic pathway*. *Journal of Biological Chemistry*, 2005. **280**(4): p. -.
37. Wikipedia. *Glycolysis*. [cited 2010 May 20]; Available from: <http://en.wikipedia.org/wiki/Glycolysis>.
38. Langen, P. and F. Hucho, *Karl Lohmann and the discovery of ATP*. *Angewandte Chemie-International Edition*, 2008. **47**(10): p. 1824-1827.
39. Fiske, C.H. and Y. Subbarow, *Phosphorus Compounds of Muscle and Liver*. *Science*, 1929. **70**(1816): p. 381-382.
40. Lipmann, F., *Metabolic Generation and Utilization of Phosphate Bond Energy*. *Advances in Enzymology and Related Subjects*, 1941. **1**: p. 99-158.

41. Engelhardt, W.A., *Life and Science*. Annual Review of Biochemistry, 1982. **51**: p. 1-19.
42. Wikipedia. *Oxidative Phosphorylation*. 2010 [cited 2010 20 May]; Available from: http://en.wikipedia.org/wiki/Oxidative_phosphorylation.
43. Alberts, B., et al., *Molecular Biology of The Cell*. 2nd ed. 1989: Garland Publishing. 351.
44. Lipmann, F., *Coupling between Pyruvic Acid Dehydrogenation and Adenylic Acid Phosphorylation*. *Nature*, 1939. **143**: p. 259-308.
45. Krebs, H. *The citric acid cycle*. 1953 [cited 2010 June 04]; Available from: http://nobelprize.org/nobel_prizes/medicine/laureates/1953/krebs-lecture.pdf.
46. Krebs, H.A. and W.A. Johnson, *Metabolism of ketonic acids in animal tissues*. *Biochem J*, 1937. **31**(4): p. 645-60.
47. Friedkin, M. and A.L. Lehninger, *Esterification of inorganic phosphate coupled to electron transport between dihydrodiphosphopyridine nucleotide and oxygen*. *J Biol Chem*, 1949. **178**(2): p. 611-44.
48. Keilin, D., *On Cytochrome, a Respiratory Pigment, Common to Animals, Yeast, and High Plants*. *Proceedings of the Royal Society B, Biological Sciences*, 1925. **98**: p. 312 - 339.
49. Slater, E.C., *Keilin, cytochrome, and the respiratory chain*. *J Biol Chem*, 2003. **278**(19): p. 16455-61.
50. Mitchell, P., *Coupling of phosphorylation to electron and hydrogen transfer by a chemi-osmotic type of mechanism*. *Nature*, 1961. **191**: p. 144-8.
51. Kayalar, C., J. Rosing, and P.D. Boyer, *An alternating site sequence for oxidative phosphorylation suggested by measurement of substrate binding patterns and exchange reaction inhibitions*. *J Biol Chem*, 1977. **252**(8): p. 2486-91.
52. Hilborn, D.A. and G.G. Hammes, *Equilibrium binding of nucleotides to beef heart mitochondrial adenosine triphosphatase*. *Biochemistry*, 1973. **12**(5): p. 983-90.
53. Boyer, P.D., *Energy, life, and ATP*. *Bioscience Reports*, 1998. **18**(3): p. 97-117.
54. Gresser, M.J., J.A. Myers, and P.D. Boyer, *Catalytic site cooperativity of beef heart mitochondrial F1 adenosine triphosphatase. Correlations of initial velocity, bound intermediate, and oxygen exchange measurements with an alternating three-site model*. *J Biol Chem*, 1982. **257**(20): p. 12030-8.
55. Gresser, M.J., J.A. Myers, and P.D. Boyer, *Catalytic Site Cooperativity of Beef-Heart Mitochondrial-F1 Adenosine-Triphosphatase - Correlations of Initial Velocity, Bound Intermediate and Oxygen-Exchange Measurements with an Alternating 3-Site Model*. *Journal of Biological Chemistry*, 1982. **257**(20): p. 2030-2038.
56. Penefsky, H.S., et al., *Partial resolution of the enzymes catalyzing oxidative phosphorylation. II. Participation of a soluble adenosine triphosphatase in oxidative phosphorylation*. *J Biol Chem*, 1960. **235**: p. 3330-6.
57. Pullman, M.E., et al., *Partial Resolution of the Enzymes Catalyzing Oxidative Phosphorylation .1. Purification and Properties of Soluble, Dinitrophenol-Stimulated Adenosine Triphosphatase*. *Journal of Biological Chemistry*, 1960. **235**(11): p. 3322-3329.
58. Racker, E., *Studies of Factors Involved in Oxidative Phosphorylation*. *Proceedings of the National Academy of Sciences of the United States of America*, 1962. **48**(9): p. 1659-&.

59. Kagawa, Y. and E. Racker, *Partial resolution of the enzymes catalyzing oxidative phosphorylation. 8. Properties of a factor conferring oligomycin sensitivity on mitochondrial adenosine triphosphatase.* J Biol Chem, 1966. **241**(10): p. 2461-6.
60. Summers, D.F., J.V. Maizel, and J.E. Darnell, *Evidence for Virus-Specific Noncapsid Proteins in Poliovirus-Infected Hela Cells.* Proceedings of the National Academy of Sciences of the United States of America, 1965. **54**(2): p. 505-&.
61. Tzagoloff, A. and P. Meagher, *Assembly of the mitochondrial membrane system. V. Properties of a dispersed preparation of the rutamycin-sensitive adenosine triphosphatase of yeast mitochondria.* J Biol Chem, 1971. **246**(23): p. 7328-36.
62. Nelson, N., et al., *Partial Resolution of Enzymes Catalyzing Photophosphorylation .13. Properties of Isolated Subunits of Coupling Factor-1 from Spinach-Chloroplasts.* Journal of Biological Chemistry, 1973. **248**(6): p. 2049-2055.
63. Kagawa, Y., et al., *Proton translocating ATPase of a thermophilic bacterium. Morphology, subunits, and chemical composition.* J Biochem, 1976. **80**(1): p. 141-51.
64. Bragg, P.D. and C. Hou, *Subunit composition, function, and spatial arrangement in the Ca²⁺-and Mg²⁺-activated adenosine triphosphatases of Escherichia coli and Salmonella typhimurium.* Arch Biochem Biophys, 1975. **167**(1): p. 311-21.
65. Foster, D.L. and R.H. Fillingame, *Energy-transducing H⁺-ATPase of Escherichia coli. Purification, reconstitution, and subunit composition.* J Biol Chem, 1979. **254**(17): p. 8230-6.
66. Brooks, J.C. and A.E. Senior, *Studies on the mitochondrial oligomycin-insensitive ATPase. II. The relationship of the specific protein inhibitor to the ATPase.* Arch Biochem Biophys, 1971. **147**(2): p. 467-70.
67. Senior, A.E. and J.C. Brooks, *The subunit composition of the mitochondrial oligomycin-insensitive ATPase.* FEBS Lett, 1971. **17**(2): p. 327-329.
68. Senior, A.E., *The structure of mitochondrial ATPase.* Biochim Biophys Acta, 1973. **301**(3): p. 249-77.
69. Deisinger, B., et al., *Purification of ATP synthase from beef heart mitochondria (FOF1) and co-reconstitution with monomeric bacteriorhodopsin into liposomes capable of light-driven ATP synthesis.* Eur J Biochem, 1993. **218**(2): p. 377-83.
70. Hekman, C. and Y. Hatefi, *The FO subunits of bovine mitochondrial ATP synthase complex: purification, antibody production, and interspecies cross-immunoreactivity.* Arch Biochem Biophys, 1991. **284**(1): p. 90-7.
71. Feng, Y. and R.E. McCarty, *Subunit interactions within the chloroplast ATP synthase (CF0-CF1) as deduced by specific depletion of CF0 polypeptides.* J Biol Chem, 1990. **265**(21): p. 12481-5.
72. Fernandez Moran, H., et al., *A Macromolecular Repeating Unit of Mitochondrial Structure and Function. Correlated Electron Microscopic and Biochemical Studies of Isolated Mitochondria and Submitochondrial Particles of Beef Heart Muscle.* J Cell Biol, 1964. **22**: p. 63-100.
73. Fernandez-Moran, H., *Cell-membrane ultrastructure. Low-temperature electron microscopy and x-ray diffraction studies of lipoprotein components in lamellar systems.* Circulation, 1962. **26**: p. 1039-65.

74. Kagawa, Y. and E. Racker, *Partial resolution of the enzymes catalyzing oxidative phosphorylation. X. Correlation of morphology and function in submitochondrial particles*. J Biol Chem, 1966. **241**(10): p. 2475-82.
75. Maclenna.Dh and J. Asai, *Studies on Mitochondrial Adenosine Triphosphatase System .V. Localization of Oligomycin-Sensitivity Conferring Protein*. Biochemical and Biophysical Research Communications, 1968. **33**(3): p. 441-&.
76. Walker, J.E. and I.R. Collinson, *The role of the stalk in the coupling mechanism of F1F0-ATPases*. FEBS Lett, 1994. **346**(1): p. 39-43.
77. Collinson, I.R., et al., *The F1F0-ATPase complex from bovine heart mitochondria: the molar ratio of the subunits in the stalk region linking the F1 and F0 domains*. Biochemistry, 1996. **35**(38): p. 12640-6.
78. Ogilvie, I., R. Aggeler, and R.A. Capaldi, *Cross-linking of the delta subunit to one of the three alpha subunits has no effect on functioning, as expected if delta is a part of the stator that links the F1 and F0 parts of the Escherichia coli ATP synthase*. J Biol Chem, 1997. **272**(26): p. 16652-6.
79. Wilkens, S., et al., *Solution structure of the N-terminal domain of the delta subunit of the E. coli ATPsynthase*. Nat Struct Biol, 1997. **4**(3): p. 198-201.
80. Gibbons, C., et al., *The structure of the central stalk in bovine F(1)-ATPase at 2.4 Å resolution*. Nat Struct Biol, 2000. **7**(11): p. 1055-61.
81. Menz, R.I., J.E. Walker, and A.G. Leslie, *Structure of bovine mitochondrial F(1)-ATPase with nucleotide bound to all three catalytic sites: implications for the mechanism of rotary catalysis*. Cell, 2001. **106**(3): p. 331-41.
82. Bowler, M.W., et al., *Ground state structure of F1-ATPase from bovine heart mitochondria at 1.9 Å resolution*. J Biol Chem, 2007. **282**(19): p. 14238-42.
83. Boyer, P.D., *A perspective of the binding change mechanism for ATP synthesis*. FASEB J, 1989. **3**(10): p. 2164-78.
84. Furuike, S., et al., *Axle-less F1-ATPase rotates in the correct direction*. Science, 2008. **319**(5865): p. 955-8.
85. Hossain, M.D., et al., *Neither helix in the coiled coil region of the axle of F1-ATPase plays a significant role in torque production*. Biophys J, 2008. **95**(10): p. 4837-44.
86. Hara, K.Y., et al., *The role of the DELSEED motif of the beta subunit in rotation of F1-ATPase*. J Biol Chem, 2000. **275**(19): p. 14260-3.
87. Nakamoto, R.K., et al., *Molecular mechanisms of rotational catalysis in the F(0)F(1) ATP synthase*. Biochim Biophys Acta, 2000. **1458**(2-3): p. 289-99.
88. Watts, S.D., C. Tang, and R.A. Capaldi, *The stalk region of the Escherichia coli ATP synthase. Tyrosine 205 of the gamma subunit is in the interface between the F1 and F0 parts and can interact with both the epsilon and c oligomer*. J Biol Chem, 1996. **271**(45): p. 28341-7.
89. Wilkens, S., et al., *Structural features of the epsilon subunit of the Escherichia coli ATP synthase determined by NMR spectroscopy*. Nat Struct Biol, 1995. **2**(11): p. 961-7.
90. Zhang, Y. and R.H. Fillingame, *Subunits coupling H⁺ transport and ATP synthesis in the Escherichia coli ATP synthase. Cys-Cys cross-linking of F1 subunit epsilon to the polar loop of F0 subunit c*. J Biol Chem, 1995. **270**(41): p. 24609-14.
91. Stock, D., A.G. Leslie, and J.E. Walker, *Molecular architecture of the rotary motor in ATP synthase*. Science, 1999. **286**(5445): p. 1700-5.

92. Aggeler, R., M.A. Haughton, and R.A. Capaldi, *Disulfide bond formation between the COOH-terminal domain of the beta subunits and the gamma and epsilon subunits of the Escherichia coli F1-ATPase. Structural implications and functional consequences.* J Biol Chem, 1995. **270**(16): p. 9185-91.
93. Aggeler, R. and R.A. Capaldi, *Nucleotide-dependent movement of the epsilon subunit between alpha and beta subunits in the Escherichia coli F1F0-type ATPase.* J Biol Chem, 1996. **271**(23): p. 13888-91.
94. Hausrath, A.C., R.A. Capaldi, and B.W. Matthews, *The conformation of the epsilon- and gamma-subunits within the Escherichia coli F(1) ATPase.* J Biol Chem, 2001. **276**(50): p. 47227-32.
95. Tsunoda, S.P., et al., *Large conformational changes of the epsilon subunit in the bacterial F1F0 ATP synthase provide a ratchet action to regulate this rotary motor enzyme.* Proc Natl Acad Sci U S A, 2001. **98**(12): p. 6560-4.
96. Iino, R., et al., *Mechanism of inhibition by C-terminal alpha-helices of the epsilon subunit of Escherichia coli FoF1-ATP synthase.* J Biol Chem, 2009. **284**(26): p. 17457-64.
97. Hara, K.Y., et al., *The role of the betaDELSEED motif of F1-ATPase: propagation of the inhibitory effect of the epsilon subunit.* J Biol Chem, 2001. **276**(26): p. 23969-73.
98. Sternweis, P.C., *The epsilon subunit of Escherichia coli coupling factor 1 is required for its binding to the cytoplasmic membrane.* J Biol Chem, 1978. **253**(9): p. 3123-8.
99. Yoshida, M., et al., *Reconstitution of thermostable ATPase capable of energy coupling from its purified subunits.* Proc Natl Acad Sci U S A, 1977. **74**(3): p. 936-40.
100. Giraud, M.F. and J. Velours, *The absence of the mitochondrial ATP synthase delta subunit promotes a slow growth phenotype of rho- yeast cells by a lack of assembly of the catalytic sector F1.* Eur J Biochem, 1997. **245**(3): p. 813-8.
101. Feniouk, B.A., T. Suzuki, and M. Yoshida, *The role of subunit epsilon in the catalysis and regulation of FOF1-ATP synthase.* Biochim Biophys Acta, 2006. **1757**(5-6): p. 326-38.
102. Kuki, M., et al., *Functional domains of epsilon subunit of Escherichia coli H+-ATPase (FOF1).* J Biol Chem, 1988. **263**(33): p. 17437-42.
103. Rondelez, Y., et al., *Highly coupled ATP synthesis by F1-ATPase single molecules.* Nature, 2005. **433**(7027): p. 773-7.
104. Cipriano, D.J. and S.D. Dunn, *The role of the epsilon subunit in the Escherichia coli ATP synthase. The C-terminal domain is required for efficient energy coupling.* J Biol Chem, 2006. **281**(1): p. 501-7.
105. Wilkens, S., et al., *Localization of the delta subunit in the Escherichia coli F(1)F(0)-ATP synthase by immuno electron microscopy: the delta subunit binds on top of the F(1).* J Mol Biol, 2000. **295**(3): p. 387-91.
106. Weber, J., et al., *F1F0-ATP synthase. Binding of delta subunit to a 22-residue peptide mimicking the N-terminal region of alpha subunit.* J Biol Chem, 2003. **278**(16): p. 13623-6.
107. McLachlin, D.T., J.A. Bestard, and S.D. Dunn, *The b and delta subunits of the Escherichia coli ATP synthase interact via residues in their C-terminal regions.* J Biol Chem, 1998. **273**(24): p. 15162-8.
108. Wilkens, S., et al., *Structural characterization of the interaction of the delta and alpha subunits of the Escherichia coli F1F0-ATP synthase by NMR spectroscopy.* Biochemistry, 2005. **44**(35): p. 11786-94.

109. Jounouchi, M., et al., *Escherichia coli H(+)-ATPase: role of the delta subunit in binding F1 to the Fo sector*. Arch Biochem Biophys, 1992. **292**(2): p. 376-81.
110. Joshi, S., et al., *Oligomycin sensitivity conferring protein of mitochondrial ATP synthase: deletions in the N-terminal end cause defects in interactions with F1, while deletions in the C-terminal end cause defects in interactions with F0*. Biochemistry, 1996. **35**(37): p. 12094-103.
111. Dimroth, P., C. von Ballmoos, and T. Meier, *Catalytic and mechanical cycles in F-ATP synthases. Fourth in the Cycles Review Series*. EMBO Rep, 2006. **7**(3): p. 276-82.
112. Dmitriev, O., et al., *Structure of the membrane domain of subunit b of the Escherichia coli F0F1 ATP synthase*. J Biol Chem, 1999. **274**(22): p. 15598-604.
113. Jiang, W., J. Hermolin, and R.H. Fillingame, *The preferred stoichiometry of c subunits in the rotary motor sector of Escherichia coli ATP synthase is 10*. Proc Natl Acad Sci U S A, 2001. **98**(9): p. 4966-71.
114. Fillingame, R.H., C.M. Angevine, and O.Y. Dmitriev, *Mechanics of coupling proton movements to c-ring rotation in ATP synthase*. FEBS Lett, 2003. **555**(1): p. 29-34.
115. Dunn, S.D., *The polar domain of the b subunit of Escherichia coli F1F0-ATPase forms an elongated dimer that interacts with the F1 sector*. J Biol Chem, 1992. **267**(11): p. 7630-6.
116. Rodgers, A.J. and R.A. Capaldi, *The second stalk composed of the b- and delta-subunits connects F0 to F1 via an alpha-subunit in the Escherichia coli ATP synthase*. J Biol Chem, 1998. **273**(45): p. 29406-10.
117. Del Rizzo, P.A., et al., *The "second stalk" of Escherichia coli ATP synthase: structure of the isolated dimerization domain*. Biochemistry, 2002. **41**(21): p. 6875-84.
118. Steigmiller, S., et al., *Distances between the b-subunits in the tether domain of F(0)F(1)-ATP synthase from E. coli*. Biochim Biophys Acta, 2005. **1708**(2): p. 143-53.
119. Del Rizzo, P.A., Y. Bi, and S.D. Dunn, *ATP synthase b subunit dimerization domain: a right-handed coiled coil with offset helices*. J Mol Biol, 2006. **364**(4): p. 735-46.
120. Hornung, T., et al., *Structure of the cytosolic part of the subunit b-dimer of Escherichia coli F0F1-ATP synthase*. Biophys J, 2008. **94**(12): p. 5053-64.
121. Walker, J.E. and V.K. Dickson, *The peripheral stalk of the mitochondrial ATP synthase*. Biochim Biophys Acta, 2006. **1757**(5-6): p. 286-96.
122. Sambongi, Y., et al., *Mechanical rotation of the c subunit oligomer in ATP synthase (F0F1): direct observation*. Science, 1999. **286**(5445): p. 1722-4.
123. Tsunoda, S.P., et al., *Rotation of the c subunit oligomer in fully functional F1Fo ATP synthase*. Proc Natl Acad Sci U S A, 2001. **98**(3): p. 898-902.
124. Hasler, K., O. Panke, and W. Junge, *On the stator of rotary ATP synthase: the binding strength of subunit delta to (alpha beta)3 as determined by fluorescence correlation spectroscopy*. Biochemistry, 1999. **38**(41): p. 13759-65.
125. Cherepanov, D.A., A.Y. Mulikidjanian, and W. Junge, *Transient accumulation of elastic energy in proton translocating ATP synthase*. FEBS Lett, 1999. **449**(1): p. 1-6.

126. Weber, J., S. Wilke-Mounts, and A.E. Senior, *Quantitative determination of binding affinity of delta-subunit in Escherichia coli F1-ATPase: effects of mutation, Mg²⁺, and pH on K_d*. J Biol Chem, 2002. **277**(21): p. 18390-6.
127. Weber, J., S. Wilke-Mounts, and A.E. Senior, *Identification of the F1-binding surface on the delta-subunit of ATP synthase*. J Biol Chem, 2003. **278**(15): p. 13409-16.
128. Dunn, S.D., D.T. McLachlin, and M. Revington, *The second stalk of Escherichia coli ATP synthase*. Biochim Biophys Acta, 2000. **1458**(2-3): p. 356-63.
129. Weber, J., et al., *Quantitative determination of direct binding of b subunit to F1 in Escherichia coli F1F0-ATP synthase*. J Biol Chem, 2004. **279**(12): p. 11253-8.
130. Krebstakies, T., et al., *Both rotor and stator subunits are necessary for efficient binding of F1 to F0 in functionally assembled Escherichia coli ATP synthase*. J Biol Chem, 2005. **280**(39): p. 33338-45.
131. Kinoshita, K., Jr., K. Adachi, and H. Itoh, *Rotation of F1-ATPase: how an ATP-driven molecular machine may work*. Annu Rev Biophys Biomol Struct, 2004. **33**: p. 245-68.
132. Nishizaka, T., et al., *Chemomechanical coupling in F1-ATPase revealed by simultaneous observation of nucleotide kinetics and rotation*. Nat Struct Mol Biol, 2004. **11**(2): p. 142-8.
133. Yasuda, R., et al., *Resolution of distinct rotational substeps by submillisecond kinetic analysis of F1-ATPase*. Nature, 2001. **410**(6831): p. 898-904.
134. Sielaff, H., et al., *Domain compliance and elastic power transmission in rotary F(O)F(1)-ATPase*. Proc Natl Acad Sci U S A, 2008. **105**(46): p. 17760-5.
135. Kersten, M.V., et al., *Site-directed spin-labeling of the catalytic sites yields insight into structural changes within the F0F1-ATP synthase of Escherichia coli*. Biochemistry, 2000. **39**(13): p. 3856-60.
136. Girvin, M.E., et al., *Solution structure of the transmembrane H⁺-transporting subunit c of the F1F0 ATP synthase*. Biochemistry, 1998. **37**(25): p. 8817-24.
137. Fillingame, R.H., *Coupling H⁺ transport and ATP synthesis in F1F0-ATP synthases: glimpses of interacting parts in a dynamic molecular machine*. J Exp Biol, 1997. **200**(Pt 2): p. 217-24.
138. Zhang, Y. and R.H. Fillingame, *Changing the ion binding specificity of the Escherichia coli H(+)-transporting ATP synthase by directed mutagenesis of subunit c*. J Biol Chem, 1995. **270**(1): p. 87-93.
139. Meier, T., et al., *Structure of the rotor ring of F-Type Na⁺-ATPase from Ilyobacter tartaricus*. Science, 2005. **308**(5722): p. 659-62.
140. von Ballmoos, C., *Alternative proton binding mode in ATP synthases*. J Bioenerg Biomembr, 2007. **39**(5-6): p. 441-5.
141. Mitome, N., et al., *Thermophilic ATP synthase has a decamer c-ring: indication of noninteger 10:3 H⁺/ATP ratio and permissive elastic coupling*. Proc Natl Acad Sci U S A, 2004. **101**(33): p. 12159-64.
142. Meier, T., et al., *Evidence for structural integrity in the undecameric c-rings isolated from sodium ATP synthases*. J Mol Biol, 2003. **325**(2): p. 389-97.
143. Stahlberg, H., et al., *Bacterial Na(+)-ATP synthase has an undecameric rotor*. EMBO Rep, 2001. **2**(3): p. 229-33.

144. Toei, M., et al., *Dodecamer rotor ring defines H⁺/ATP ratio for ATP synthesis of prokaryotic V-ATPase from Thermus thermophilus*. Proc Natl Acad Sci U S A, 2007. **104**(51): p. 20256-61.
145. Lolkema, J.S. and E.J. Boekema, *The A-type ATP synthase subunit K of Methanopyrus kandleri is deduced from its sequence to form a monomeric rotor comprising 13 hairpin domains*. FEBS Lett, 2003. **543**(1-3): p. 47-50.
146. Preiss, L., et al., *A New Type of Proton Coordination in an F1Fo-ATP Synthase Rotor Ring*. PLoS Biology, 2010. **8**(8): p. 1-10.
147. Seelert, H., et al., *Structural biology. Proton-powered turbine of a plant motor*. Nature, 2000. **405**(6785): p. 418-9.
148. Vollmar, M., et al., *Structure of the c14 rotor ring of the proton translocating chloroplast ATP synthase*. J Biol Chem, 2009. **284**(27): p. 18228-35.
149. Pogoryelov, D., et al., *The c15 ring of the Spirulina platensis F-ATP synthase: F1/F0 symmetry mismatch is not obligatory*. EMBO Rep, 2005. **6**(11): p. 1040-4.
150. Meier, T., et al., *Complete ion-coordination structure in the rotor ring of Na⁺-dependent F-ATP synthases*. J Mol Biol, 2009. **391**(2): p. 498-507.
151. Schwem, B.E. and R.H. Fillingame, *Cross-linking between helices within subunit a of Escherichia coli ATP synthase defines the transmembrane packing of a four-helix bundle*. J Biol Chem, 2006. **281**(49): p. 37861-7.
152. Hatch, L.P., G.B. Cox, and S.M. Howitt, *The essential arginine residue at position 210 in the alpha subunit of the Escherichia coli ATP synthase can be transferred to position 252 with partial retention of activity*. J Biol Chem, 1995. **270**(49): p. 29407-12.
153. Wada, T., et al., *A novel labeling approach supports the five-transmembrane model of subunit a of the Escherichia coli ATP synthase*. J Biol Chem, 1999. **274**(24): p. 17353-7.
154. Valiyaveetil, F.I. and R.H. Fillingame, *Transmembrane topography of subunit a in the Escherichia coli F1F0 ATP synthase*. J Biol Chem, 1998. **273**(26): p. 16241-7.
155. Long, J.C., S. Wang, and S.B. Vik, *Membrane topology of subunit a of the F1F0 ATP synthase as determined by labeling of unique cysteine residues*. J Biol Chem, 1998. **273**(26): p. 16235-40.
156. Zhang, D. and S.B. Vik, *Close proximity of a cytoplasmic loop of subunit a with c subunits of the ATP synthase from Escherichia coli*. J Biol Chem, 2003. **278**(14): p. 12319-24.
157. Rubinstein, J.L., J.E. Walker, and R. Henderson, *Structure of the mitochondrial ATP synthase by electron cryomicroscopy*. EMBO J, 2003. **22**(23): p. 6182-92.
158. Jiang, W. and R.H. Fillingame, *Interacting helical faces of subunits a and c in the F1Fo ATP synthase of Escherichia coli defined by disulfide cross-linking*. Proc Natl Acad Sci U S A, 1998. **95**(12): p. 6607-12.
159. Valiyaveetil, F.I. and R.H. Fillingame, *On the role of Arg-210 and Glu-219 of subunit a in proton translocation by the Escherichia coli F0F1-ATP synthase*. J Biol Chem, 1997. **272**(51): p. 32635-41.
160. Eya, S., M. Maeda, and M. Futai, *Role of the carboxyl terminal region of H(+)-ATPase (FOF1) a subunit from Escherichia coli*. Arch Biochem Biophys, 1991. **284**(1): p. 71-7.

161. Lightowers, R.N., et al., *The proton pore in the Escherichia coli F₀F₁-ATPase: a requirement for arginine at position 210 of the a-subunit*. Biochim Biophys Acta, 1987. **894**(3): p. 399-406.
162. Cain, B.D. and R.D. Simoni, *Proton translocation by the F₁F₀ATPase of Escherichia coli. Mutagenic analysis of the a subunit*. J Biol Chem, 1989. **264**(6): p. 3292-300.
163. Stalz, W.D., et al., *Direct interaction of subunits a and b of the F₀ complex of Escherichia coli ATP synthase by forming an ab₂ subcomplex*. J Biol Chem, 2003. **278**(29): p. 27068-71.
164. Angevine, C.M., et al., *Aqueous access pathways in ATP synthase subunit a. Reactivity of cysteine substituted into transmembrane helices 1, 3, and 5*. J Biol Chem, 2007. **282**(12): p. 9001-7.
165. Angevine, C.M. and R.H. Fillingame, *Aqueous access channels in subunit a of rotary ATP synthase*. J Biol Chem, 2003. **278**(8): p. 6066-74.
166. Angevine, C.M., K.A. Herold, and R.H. Fillingame, *Aqueous access pathways in subunit a of rotary ATP synthase extend to both sides of the membrane*. Proc Natl Acad Sci U S A, 2003. **100**(23): p. 13179-83.
167. Steed, P.R. and R.H. Fillingame, *Subunit a facilitates aqueous access to a membrane-embedded region of subunit c in Escherichia coli F₁F₀ ATP synthase*. J Biol Chem, 2008. **283**(18): p. 12365-72.
168. Mitome, N., et al., *Essential Arg of Fo-a subunit in FoF₁-ATP synthase has a role to prevent the proton shortcut without c-ring rotation in the Fo proton channel*. Biochem J, 2010.
169. Cross, R.L., C. Grubmeyer, and H.S. Penefsky, *Mechanism of ATP hydrolysis by beef heart mitochondrial ATPase. Rate enhancements resulting from cooperative interactions between multiple catalytic sites*. J Biol Chem, 1982. **257**(20): p. 12101-5.
170. Grubmeyer, C., R.L. Cross, and H.S. Penefsky, *Mechanism of ATP hydrolysis by beef heart mitochondrial ATPase. Rate constants for elementary steps in catalysis at a single site*. J Biol Chem, 1982. **257**(20): p. 12092-100.
171. Shimabukuro, K., et al., *Catalysis and rotation of F₁ motor: cleavage of ATP at the catalytic site occurs in 1 ms before 40 degree substep rotation*. Proc Natl Acad Sci U S A, 2003. **100**(25): p. 14731-6.
172. Adachi, K., et al., *Coupling of rotation and catalysis in F(1)-ATPase revealed by single-molecule imaging and manipulation*. Cell, 2007. **130**(2): p. 309-21.
173. Ariga, T., E. Muneyuki, and M. Yoshida, *F₁-ATPase rotates by an asymmetric, sequential mechanism using all three catalytic subunits*. Nat Struct Mol Biol, 2007. **14**(9): p. 841-6.
174. Shimo-Kon, R., et al., *Chemo-mechanical coupling in F(1)-ATPase revealed by catalytic site occupancy during catalysis*. Biophys J, 2010. **98**(7): p. 1227-36.
175. Oster, G. and H. Wang, *Reverse engineering a protein: the mechanochemistry of ATP synthase*. Biochim Biophys Acta, 2000. **1458**(2-3): p. 482-510.
176. Wang, H. and G. Oster, *Energy transduction in the F₁ motor of ATP synthase*. Nature, 1998. **396**(6708): p. 279-82.
177. Yasuda, R., et al., *F₁-ATPase is a highly efficient molecular motor that rotates with discrete 120 degree steps*. Cell, 1998. **93**(7): p. 1117-24.
178. Wang, H.Y. and G. Oster, *The Stokes efficiency for molecular motors and its applications*. Europhysics Letters, 2002. **57**(1): p. 134-140.
179. Schliwa, M., ed. *Molecular Motors*. 2003, Wiley-VCH.

180. Hirono-Hara, Y., et al., *Pause and rotation of F(1)-ATPase during catalysis*. Proc Natl Acad Sci U S A, 2001. **98**(24): p. 13649-54.
181. Hyndman, D.J., et al., *Nucleotide-binding sites on Escherichia coli F1-ATPase. Specificity of noncatalytic sites and inhibition at catalytic sites by MgADP*. J Biol Chem, 1994. **269**(46): p. 28871-7.
182. Okuno, D., et al., *Correlation between the conformational states of F1-ATPase as determined from its crystal structure and single-molecule rotation*. Proc Natl Acad Sci U S A, 2008. **105**(52): p. 20722-7.
183. Elston, T., H. Wang, and G. Oster, *Energy transduction in ATP synthase*. Nature, 1998. **391**(6666): p. 510-3.
184. Junge, W., H. Lill, and S. Engelbrecht, *ATP synthase: an electrochemical transducer with rotatory mechanics*. Trends Biochem Sci, 1997. **22**(11): p. 420-3.
185. Junge, W., *ATP synthase and other motor proteins*. Proc Natl Acad Sci U S A, 1999. **96**(9): p. 4735-7.
186. Xing, J., et al., *Torque generation by the Fo motor of the sodium ATPase*. Biophys J, 2004. **87**(4): p. 2148-63.
187. Feniouk, B.A., et al., *The of ATP synthase: ohmic conductance (10 fS), and absence of voltage gating*. Biophys J, 2004. **86**(6): p. 4094-109.
188. von Ballmoos, C., T. Meier, and P. Dimroth, *Membrane embedded location of Na+ or H+ binding sites on the rotor ring of F1F0 ATP synthases*. Eur J Biochem, 2002. **269**(22): p. 5581-9.
189. Dimroth, P., U. Matthey, and G. Kaim, *Critical evaluation of the one- versus the two-channel model for the operation of the ATP synthase's F(o) motor*. Biochim Biophys Acta, 2000. **1459**(2-3): p. 506-13.
190. Kaim, G., U. Matthey, and P. Dimroth, *Mode of interaction of the single a subunit with the multimeric c subunits during the translocation of the coupling ions by F1F0 ATPases*. EMBO J, 1998. **17**(3): p. 688-95.
191. Oster, G., H. Wang, and M. Grabe, *How Fo-ATPase generates rotary torque*. Philos Trans R Soc Lond B Biol Sci, 2000. **355**(1396): p. 523-8.
192. Dimroth, P., G. Kaim, and U. Matthey, *Crucial role of the membrane potential for ATP synthesis by F(1)F(o) ATP synthases*. J Exp Biol, 2000. **203**(Pt 1): p. 51-9.
193. Kaim, G. and P. Dimroth, *Voltage-generated torque drives the motor of the ATP synthase*. EMBO J, 1998. **17**(20): p. 5887-95.
194. Kaim, G. and P. Dimroth, *ATP synthesis by the F1Fo ATP synthase of Escherichia coli is obligatorily dependent on the electric potential*. FEBS Lett, 1998. **434**(1-2): p. 57-60.
195. Kaim, G. and P. Dimroth, *ATP synthesis by F-type ATP synthase is obligatorily dependent on the transmembrane voltage*. EMBO J, 1999. **18**(15): p. 4118-27.
196. Montal, M. and P. Mueller, *Formation of bimolecular membranes from lipid monolayers and a study of their electrical properties*. Proc Natl Acad Sci U S A, 1972. **69**(12): p. 3561-6.
197. Tsunoda, S.P., et al., *Observations of rotation within the F(o)F(1)-ATP synthase: deciding between rotation of the F(o)c subunit ring and artifact*. FEBS Lett, 2000. **470**(3): p. 244-8.
198. Nishio, K., et al., *Subunit rotation of ATP synthase embedded in membranes: a or beta subunit rotation relative to the c subunit ring*. Proc Natl Acad Sci U S A, 2002. **99**(21): p. 13448-52.

199. Ueno, H., et al., *ATP-driven stepwise rotation of FoF1-ATP synthase*. Proc Natl Acad Sci U S A, 2005. **102**(5): p. 1333-8.
200. Kaim, G., et al., *Coupled rotation within single FOF1 enzyme complexes during ATP synthesis or hydrolysis*. FEBS Lett, 2002. **525**(1-3): p. 156-63.
201. Borsch, M., et al., *Stepwise rotation of the gamma-subunit of EF(0)F(1)-ATP synthase observed by intramolecular single-molecule fluorescence resonance energy transfer*. FEBS Lett, 2002. **527**(1-3): p. 147-52.
202. Diez, M., et al., *Proton-powered subunit rotation in single membrane-bound FOF1-ATP synthase*. Nat Struct Mol Biol, 2004. **11**(2): p. 135-41.
203. Zimmermann, B., et al., *Subunit movements in membrane-integrated EF0F1 during ATP synthesis detected by single-molecule spectroscopy*. Biochim Biophys Acta, 2006. **1757**(5-6): p. 311-9.
204. Duser, M.G., et al., *36 degrees step size of proton-driven c-ring rotation in FoF1-ATP synthase*. EMBO J, 2009. **28**(18): p. 2689-96.
205. Zhang, Y.H., et al., *Rotary torque produced by proton motive force in FoF1 motor*. Biochem Biophys Res Commun, 2005. **331**(1): p. 370-4.
206. Hazard, A. and C. Montemagno, *Improved purification for thermophilic F1F0 ATP synthase using n-dodecyl beta-D-maltoside*. Archives of Biochemistry and Biophysics, 2002. **407**(1): p. 117-124.
207. Rigaud, J.L., B. Pitard, and D. Levy, *Reconstitution of Membrane-Proteins into Liposomes - Application to Energy-Transducing Membrane-Proteins*. Biochimica Et Biophysica Acta-Bioenergetics, 1995. **1231**(3): p. 223-246.
208. Pilizota, T., *A Programmable Optical Angle Clamp for Rotary Molecular Motors*, in *Physics*. 2006, University of Oxford: Oxford.
209. Fischer, S., et al., *Atp Synthase Catalyzed by the Atp Synthase of Escherichia-Coli Reconstituted into Liposomes*. European Journal of Biochemistry, 1994. **225**(1): p. 167-172.
210. Tanabe, M., et al., *Rotation of a complex of the gamma subunit and c ring of Escherichia coli ATP synthase - The rotor and stator are interchangeable*. Journal of Biological Chemistry, 2001. **276**(18): p. 15269-15274.
211. Senior, A.E., et al., *Unca Gene Codes for the Alpha-Subunit of the Adenosine-Triphosphatase of Escherichia-Coli - Electrophoretic Analysis of Unca Mutant Strains*. Biochemical Journal, 1979. **180**(1): p. 103-109.
212. Downie, J.A., et al., *Solubilization of Adenosine-Triphosphatase from Membranes of Escherichia-Coli - Effect of Para-Aminobenzamidine*. Journal of Bacteriology, 1979. **138**(1): p. 87-91.
213. Ishmukhametov, R.R., M.A. Galkin, and S.B. Vik, *Ultrafast purification and reconstitution of His-tagged cysteine-less Escherichia coli F1F0 ATP synthase*. Biochimica Et Biophysica Acta-Bioenergetics, 2005. **1706**(1-2): p. 110-116.
214. Deleij, L. and B. Witholt, *Structural Heterogeneity of Cytoplasmic and Outer Membranes of Escherichia-Coli*. Biochimica Et Biophysica Acta, 1977. **471**(1): p. 92-104.
215. Masamitsu Futai, Y.W., Jack H. Kaplan, ed. *Handbook of ATPases*. 2004, Wiley-VCH.
216. Taussky, H.H. and E. Shorr, *A Microcolorimetric Method for the Determination of Inorganic Phosphorus*. Journal of Biological Chemistry, 1953. **202**(2): p. 675-685.

217. Mirsky, R. and V. Barlow, *Purification and Properties of Atpase from Cytoplasmic Membrane of Bacillus-Megaterium Km*. *Biochimica Et Biophysica Acta*, 1971. **241**(3): p. 835-&.
218. Schneider, E. and K. Altendorf, *Bacterial adenosine 5'-triphosphate synthase (F1F0): purification and reconstitution of F0 complexes and biochemical and functional characterization of their subunits*. *Microbiol Rev*, 1987. **51**(4): p. 477-97.
219. Pitard, B., et al., *ATP synthesis by the F0F1 ATP synthase from thermophilic Bacillus PS3 reconstituted into liposomes with bacteriorhodopsin. 1. Factors defining the optimal reconstitution of ATP synthases with bacteriorhodopsin*. *Eur J Biochem*, 1996. **235**(3): p. 769-78.
220. Pick, U., *Liposomes with a Large Trapping Capacity Prepared by Freezing and Thawing of Sonicated Phospholipid Mixtures*. *Archives of Biochemistry and Biophysics*, 1981. **212**(1): p. 186-194.
221. Mayer, L.D., et al., *Solute distributions and trapping efficiencies observed in freeze-thawed multilamellar vesicles*. *Biochim Biophys Acta*, 1985. **817**(1): p. 193-6.
222. Kasahara, M. and P.C. Hinkle, *Reconstitution and Purification of D-Glucose Transporter from Human Erythrocytes*. *Journal of Biological Chemistry*, 1977. **252**(20): p. 7384-7390.
223. Hope, M.J., et al., *Production of Large Unilamellar Vesicles by a Rapid Extrusion Procedure - Characterization of Size Distribution, Trapped Volume and Ability to Maintain a Membrane-Potential*. *Biochimica Et Biophysica Acta*, 1985. **812**(1): p. 55-65.
224. Huang, C. and J.T. Mason, *Geometric packing constraints in egg phosphatidylcholine vesicles*. *Proc Natl Acad Sci U S A*, 1978. **75**(1): p. 308-10.
225. Richard, P., J.L. Rigaud, and P. Graber, *Reconstitution of CF0F1 into liposomes using a new reconstitution procedure*. *Eur J Biochem*, 1990. **193**(3): p. 921-5.
226. Levy, D., et al., *A Systematic Study of Liposome and Proteoliposome Reconstitution Involving Bio-Bead-Mediated Triton-X-100 Removal*. *Biochimica Et Biophysica Acta*, 1990. **1025**(2): p. 179-190.
227. Malvern. *Dynamic Light Scattering: An introduction in 30 Minutes*. 2010 [cited 2010 May]; Available from: <http://www.malvern.com/common/downloads/campaign/MRK656-01.pdf>.
228. Berne, B.J. and R. Pecora, *Dynamic Light Scattering With Applications to Chemistry, Biology, and Physics*. 2000: Dover Publications.
229. Wikipedia. *Rayleigh Scattering*. 2010 August 2010]; Available from: http://en.wikipedia.org/wiki/Rayleigh_scattering.
230. Dufour, J.P., A. Goffeau, and T.Y. Tsong, *Active proton uptake in lipid vesicles reconstituted with the purified yeast plasma membrane ATPase. Fluorescence quenching of 9-amino-6-chloro-2-methoxyacridine*. *J Biol Chem*, 1982. **257**(16): p. 9365-71.
231. Rottenberg, H. and R. Moreno-Sanchez, *The proton pumping activity of H(+)-ATPases: an improved fluorescence assay*. *Biochim Biophys Acta*, 1993. **1183**(1): p. 161-70.
232. Grzesiek, S. and N.A. Dencher, *The Delta-Ph-Probe 9-Aminoacridine - Response-Time, Binding Behavior and Dimerization at the Membrane*. *Biochimica Et Biophysica Acta*, 1988. **938**(3): p. 411-424.

233. Fiolet, J.W., E.P. Bakker, and K. van Dam, *The fluorescent properties of acridines in the presence of chloroplasts or liposomes. On the quantitative relationship between the fluorescence quenching and the transmembrane proton gradient.* Biochim Biophys Acta, 1974. **368**(3): p. 432-45.
234. Huang, C.S., S.J. Kopacz, and C.P. Lee, *Mechanistic differences in the energy-linked fluorescence decreases of 9-aminoacridine dyes associated with bovine heart submitochondrial membranes.* Biochim Biophys Acta, 1983. **722**(1): p. 107-15.
235. Downie, J.A., F. Gibson, and G.B. Cox, *Membrane Adenosine Triphosphatases of Prokaryotic Cells.* Annual Review of Biochemistry, 1979. **48**: p. 103-131.
236. Selvin, P.R. and T. Ha, eds. *Single-Molecule Techniques: A Laboratory Manual.* 1st ed. 2007, CSHL Press.
237. Kapanidis, A.N., et al., *Fluorescence-aided molecule sorting: analysis of structure and interactions by alternating-laser excitation of single molecules.* Proc Natl Acad Sci U S A, 2004. **101**(24): p. 8936-41.
238. Lakowicz, J.R., *Principles of Fluorescence Spectroscopy.* 3rd ed. 2006.
239. Schwille, P. and E. Haustein, *Fluorescence Correlation Spectroscopy: An Introduction to its Concepts and Applications,* Max-Planck-Institute for Biophysical Chemistry, Experimental Biophysics Group.
240. Ide, T., Y. Takeuchi, and T. Yanagida, *Development of an experimental apparatus for simultaneous observation of optical and electrical signals from single ion channels.* Single Molecules, 2002. **3**(1): p. 33-42.
241. Sandison, M.E., M. Zagnoni, and H. Morgan, *Air-exposure technique for the formation of artificial lipid bilayers in microsystems.* Langmuir, 2007. **23**(15): p. 8277-84.
242. Suzuki, H., et al., *Highly reproducible method of planar lipid bilayer reconstitution in polymethyl methacrylate microfluidic chip.* Langmuir, 2006. **22**(4): p. 1937-42.
243. Malmstadt, N., et al., *Automated formation of lipid-bilayer membranes in a microfluidic device.* Nano Lett, 2006. **6**(9): p. 1961-5.
244. de Planque, M.R., et al., *Controlled delivery of membrane proteins to artificial lipid bilayers by nystatin-ergosterol modulated vesicle fusion.* IEE Proc Nanobiotechnol, 2006. **153**(2): p. 21-30.
245. Funakoshi, K., H. Suzuki, and S. Takeuchi, *Lipid bilayer formation by contacting monolayers in a microfluidic device for membrane protein analysis.* Anal Chem, 2006. **78**(24): p. 8169-74.
246. Heron, A.J., et al., *Direct detection of membrane channels from gels using water-in-oil droplet bilayers.* J Am Chem Soc, 2007. **129**(51): p. 16042-7.
247. Holden, M.A., D. Needham, and H. Bayley, *Functional bionetworks from nanoliter water droplets.* J Am Chem Soc, 2007. **129**(27): p. 8650-5.
248. Bayley, H., et al., *Droplet interface bilayers.* Mol Biosyst, 2008. **4**(12): p. 1191-208.
249. Thompson, J.R., et al., *Enhanced stability and fluidity in droplet on hydrogel bilayers for measuring membrane protein diffusion.* Nano Lett, 2007. **7**(12): p. 3875-8.
250. Heron, A.J., et al., *Simultaneous measurement of ionic current and fluorescence from single protein pores.* J Am Chem Soc, 2009. **131**(5): p. 1652-3.

251. Pernodet, N., M. Maaloum, and B. Tinland, *Pore size of agarose gels by atomic force microscopy*. Electrophoresis, 1997. **18**(1): p. 55-8.
252. Maaloum, M., N. Pernodet, and B. Tinland, *Agarose gel structure using atomic force microscopy: gel concentration and ionic strength effects*. Electrophoresis, 1998. **19**(10): p. 1606-10.
253. Estes, D.J., et al., *Triggering and visualizing the aggregation and fusion of lipid membranes in microfluidic chambers*. Biophys J, 2006. **91**(1): p. 233-43.
254. Cohen, F.S., et al., *Parameters affecting the fusion of unilamellar phospholipid vesicles with planar bilayer membranes*. J Cell Biol, 1984. **98**(3): p. 1054-62.
255. Cohen, F.S., W.D. Niles, and M.H. Akabas, *Fusion of phospholipid vesicles with a planar membrane depends on the membrane permeability of the solute used to create the osmotic pressure*. J Gen Physiol, 1989. **93**(2): p. 201-10.
256. Rosenberg, P.A. and A. Finkelstein, *Interaction of ions and water in gramicidin A channels: streaming potentials across lipid bilayer membranes*. J Gen Physiol, 1978. **72**(3): p. 327-40.
257. Cullis, P.R., M.J. Hope, and C.P. Tilcock, *Lipid polymorphism and the roles of lipids in membranes*. Chem Phys Lipids, 1986. **40**(2-4): p. 127-44.
258. Mouritsen, O.G. and M.J. Zuckermann, *What's so special about cholesterol?* Lipids, 2004. **39**(11): p. 1101-13.
259. Qian, H., M.P. Sheetz, and E.L. Elson, *Single particle tracking. Analysis of diffusion and flow in two-dimensional systems*. Biophys J, 1991. **60**(4): p. 910-21.
260. Berg, H.C., *Random Walks in Biology*. Rev ed. 1993: Princeton University Press. 152.
261. Gupte, S.S., et al., *Two-dimensional diffusion of F1F0-ATP synthase and ADP/ATP translocator. Testing a hypothesis for ATP synthesis in the mitochondrial inner membrane*. Biochim Biophys Acta, 1991. **1069**(2): p. 131-8.
262. Vaz, W.L., et al., *Size dependence of the translational diffusion of large integral membrane proteins in liquid-crystalline phase lipid bilayers. A study using fluorescence recovery after photobleaching*. Biochemistry, 1982. **21**(22): p. 5608-12.
263. Aspinall, G.O., ed. *The Polysaccharides*. Molecular Biology An International Series of Monographs and Textbooks, ed. B. Horecker, et al. Vol. 1. 1982, Academic Press: London.
264. Luo, Y. and M.S. Shoichet, *Light-activated immobilization of biomolecules to agarose hydrogels for controlled cellular response*. Biomacromolecules, 2004. **5**(6): p. 2315-23.
265. Hermanson, G.T., *Bioconjugate Techniques*. 1996: Academic Press. 785.
266. Nicolas, F.L. and C.H. Gagnieu, *Denatured thiolated collagen .1. Synthesis and characterization*. Biomaterials, 1997. **18**(11): p. 807-813.
267. Serwer, P., *Agarose Gels - Properties and Use for Electrophoresis*. Electrophoresis, 1983. **4**(6): p. 375-382.
268. Hochuli, E., H. Dobeli, and A. Schacher, *New Metal Chelate Adsorbent Selective for Proteins and Peptides Containing Neighboring Histidine-Residues*. Journal of Chromatography, 1987. **411**: p. 177-184.
269. Lata, S., et al., *High-affinity adaptors for switchable recognition of histidine-tagged proteins*. J Am Chem Soc, 2005. **127**(29): p. 10205-15.

270. Goodman, R.P., et al., *A facile method for reversibly linking a recombinant protein to DNA*. *Chembiochem*, 2009. **10**(9): p. 1551-7.
271. Tanabe, M., et al., *Rotation of a complex of the gamma subunit and c ring of Escherichia coli ATP synthase. The rotor and stator are interchangeable*. *J Biol Chem*, 2001. **276**(18): p. 15269-74.
272. Nakanishi-Matsui, M., et al., *Stochastic high-speed rotation of Escherichia coli ATP synthase F1 sector: the epsilon subunit-sensitive rotation*. *J Biol Chem*, 2006. **281**(7): p. 4126-31.
273. Furuike, S., et al., *Temperature dependence of the rotation and hydrolysis activities of F-1-ATPase*. *Biophysical Journal*, 2008. **95**(2): p. 761-770.
274. Leake, M.C., et al., *Stoichiometry and turnover in single, functioning membrane protein complexes*. *Nature*, 2006. **443**(7109): p. 355-358.
275. Chung, S.H. and R.A. Kennedy, *Forward-backward non-linear filtering technique for extracting small biological signals from noise*. *J Neurosci Methods*, 1991. **40**(1): p. 71-86.
276. Hendrickson, W.A., et al., *Crystal structure of core streptavidin determined from multiwavelength anomalous diffraction of synchrotron radiation*. *Proc Natl Acad Sci U S A*, 1989. **86**(7): p. 2190-4.
277. Thompson, R.E., D.R. Larson, and W.W. Webb, *Precise nanometer localization analysis for individual fluorescent probes*. *Biophys J*, 2002. **82**(5): p. 2775-83.
278. Diez, M., et al., *Binding of the b-subunit in the ATP synthase from Escherichia coli*. *Biochemistry*, 2004. **43**(4): p. 1054-64.
279. Zimmermann, B., et al., *Movements of the epsilon-subunit during catalysis and activation in single membrane-bound H(+)-ATP synthase*. *EMBO J*, 2005. **24**(12): p. 2053-63.
280. Chourasia, M., G.M. Sastry, and G.N. Sastry, *Proton binding sites and conformational analysis of H+K(+)-ATPase*. *Biochem Biophys Res Commun*, 2005. **336**(3): p. 961-6.
281. Xing, J., J.C. Liao, and G. Oster, *Making ATP*. *Proc Natl Acad Sci U S A*, 2005. **102**(46): p. 16539-46.

Appendix 1 – Protocols for experiments

Appendix 1 contains the essential protocols that are used in this thesis. It comprises the procedure for protein purification, testing the activity of F_1F_0 ATPase, forming substrate supported planar bilayers and modifying agarose and gold nano-particles. It is meant to be a complete section by itself and has been designed to be as detailed as possible. For clarity and completeness, some of the diagrams and calculations used in the main text will be repeated in this section.

The first section contains the purification protocols, which is first adapted from Professor M. Futai's Laboratory by Dr Pilizota, and later modified by me. The second section contains the protocols for reconstituting the proteins onto vesicles and testing the activity of the reconstituted proteins. These protocols are obtained from publications and reproduced in this laboratory by me. The third section is about the protocol for the formation of the "Droplet on Hydrated support Bilayers" (DHB) [1]. It is adapted from Dr Mark Wallace and Dr Andrew Heron of the Chemistry Department, University of Oxford. Finally, the last section talks about the modification of agarose and gold nano-particles, Interleaving between these sections are also protocols for standard biochemistry assays and sample preparation.

Chemicals

DNase I (Cat No. 89835) is obtained from Perbio Science (UK). Nickel columns (Cat No. 11-0033-99) for the purification are from GE Healthcare (UK). SM2 Biobeads (Cat No. 152-8920) are obtained from Biorad Laboratories Ltd (UK). Fluorescence streptavidin (Cat No. S-32357, S11224) and dextrans (Cat No. D-22914) are obtained from Invitrogen (UK). Agarose is obtained from Sigma (UK) (Sigma Cat no. A9414) and Lonza Biologics (Nusieve GTG Cat no. 50081). Pyruvate kinase is purchased from Roche Diagnostics. Phospholipids used for vesicles reconstitution are obtained from Avanti Polar lipids (US). All other chemicals used for the purification are obtained from Sigma Aldrich (UK). Detailed description of the chemicals and buffers used can be found in Appendix 1.

Equipment

Standard equipments used for purification include centrifuges (Beckman Coulter Avanti J-26XP) and ultracentrifuges (Optima L-XP / Optima TLX), used primarily for sample separation and washing; French press (Sim Amanco, SLM Instruments) for lysing of bacteria; Spectrophotometer (Shimadzu UV-Vis mini-1240 / Varian Cary 50 UV-Vis) for absorbance measurement. A Spectrofluorometer (Photon Technology International) is used for bulk fluorescence measurement to determine the activity of reconstituted F_1F_0 ATP Synthase. Dynamic Light Scattering system (Viscotek 802DLS - Malvern Instruments Ltd) is used to measure the size of vesicles formed.

A1-1 Protocols For Purification Of F₁F₀ ATPase

BUFFERS TO PREPARE ON DAY 1:

Luria-Bertani medium:

To 200 mL of ddw, add:		
Final conc	Chemical	Mass Needed
1% (w/w)	Polypeptone	2 g
0.5% (w/w)	Yeast Extract	1 g
0.5% (w/w)	NaCl	1 g

Sterilize by autoclaving for 20 min at 15.7 psi (1.1 kg/cm²), 121°C on liquid cycle.
Store at 4°C.

10x Tanaka medium:

Part 1: in 500 mL Flask, add the chemicals + 300 mL DDW, Stir till dissolve, then top up to 500 mL			
Final conc	Chemical	MW	Mass / Vol Needed
640 mM	K ₂ HPO ₄	174.18	55.74 g
340 mM	KH ₂ PO ₄	136.09	23.14 g
200 mM	(NH ₄) ₂ SO ₄	132.14	13.21 g
Part 2: Added directly into part 1 and stir until precipitate dissolves			
10 μM	0.05M FeSO ₄	278.02	100 μL into Part 1
100 μM	1M CaCl ₂	110.98	50 μL into Part 1
10 μM	0.1M ZnCl ₂	136.30	50 μL into Part 1

Store at 4°C

**1x Tanaka (0,5% glycerol) medium with ampicillin:
Mix straight into 2L culture flasks**

In 703 mL of ddw, add		
Final conc	Buffer / chemical	Vol needed
1x	10x Tanaka mdium	80 mL
50 mg/l	5 mg/mL L(+)-Ile	8 mL
50 mg/l	5 mg/mL L-Val	8 mL
2 mg/l	2 mg/mL Thiamine-HCl	0.8 mL
0.3 mM	1M MgCl ₂	0.24 mL

Sterilize by autoclaving for 20 min at 15.7 psi (1.1 kgf/cm²), 121°C on liquid cycle.
Cool to room temperature.

Under an open flame, add:

Final Conc	Buffer / chemical	Vol needed	Note
0.5% (w/w)	50% (w/w) glycerol	8 mL	Autoclaved
100 µg/mL	100 mg/mL ampicillin	0.8 mL	0.2µm Filter sterilized
2µM	Biotin (1 mg in 20mL to get 200µM)	8 mL	<ul style="list-style-type: none"> • Stir to ensure fully dissolved. • Filter Sterilized • Only for specific strain with transcarboxylase PBMUS13-BetaTC-c-6-histag

Final pH= 6.7- 7.0

0.05M FeSO₄:

To 1 mL of ddw, add		
Chemical	MW	Mass needed
FeSO ₄	278.02	0.01391 g

Prepare fresh

1M CaCl₂:

To 10 mL of ddw, add		
Chemical	MW	Mass needed
CaCl ₂	110.98	1.11 g

0,1M ZnCl₂:

To 1 mL of ddw, add		
Chemical	MW	Mass needed
ZnCl ₂	136.30	0.0136 g

Prepare fresh

5 mg/mL L(+)-Ile (L-Leucine):

To 80 mL of ddw, add:		
Chemical	MW	Mass needed
L(+)-Ile	131.18	0.4 g

Store at room temp

5 mg/mL L-Val:

To 80 mL of ddw, add:		
Chemical	MW	Mass needed
L-Val	117.1	0.4 g

Store at room temp

2 mg/mL Thiamine-HCl:

To 80 mL of ddw, add:		
Chemical	MW	Mass needed
Thiamine-HCl	337.3	0.16 g

Store at room temp

1M MgCl₂:

To 40 mL of ddw, add:		
Chemical	MW	Mass needed
MgCl ₂	203.30	10.16 g

Adjust the volume of the solution to 50 mL with ddw.

Store at room temp

50% (w/w) glycerol:

To 250 mL of ddw, add:		
Chemical	MW	Vol needed
100% glycerol	92.09 Density=1.261g/mL	198 mL

Sterilize by autoclaving for 20 min at 15,7 psi (1,1 kg/cm²), 121°C on liquid cycle.

Store at 4°C

100 mg/mL Ampicillin:

To 10 mL of DDW, add:		
Chemical	MW	Mass needed
Ampicillin sodium		1.0 g

Sterilize by filtration through a 0.2 µm filter.

Dispense into 0.8 mL aliquots and store at -20°C.

2M KCl:

To 35 mL of DDW, add:		
Chemical	MW	Mass needed
KCl	74.55	7.455 g

Adjust the volume of the solution to 50 mL with ddw.

1M TRIS-HCl (pH 8,0 at 4°C):

To 600 mL ice cold ddw, add:		
Chemical	MW	Mass needed
Tris	121.1	121,1 g
Adjust the pH to 8.0 at 4°C by adding concentrated 2M HCl (Caution!!) Allow the solution to cool to 4°C before making final adjustments to the pH. Adjust the volume of the solution to 1L with ice cold ddw. Store at 4°C.		

If 1M solution has yellow colour, discard it and obtain Tris base of better quality.

The pH of Tris solution is temperature dependent and decrease ~0.03 pH units for each 1°C increase in temperature.

TKG buffer

To 355 mL ddw, add		
Final Conc	Buffer needed	Vol needed
20 mM	1M TRIS- HCl pH 8,0 at 4°C	10 mL
140 mM	2M KCl	35 mL
10% (w/w)	50% (w/w) glycerol	100 mL

Store at 4°C.

50 mM Tris-HCl (pH 8.0 at 4°C)

To 950 mL ddw, add		
Final Conc	Buffer	Vol needed
50 mM	1M Tris-HCl, pH 8.0 at 4°C	50 mL

Store at 4°C.

0.5M DTT

To 20 mL ddw, add		
Chemical	MW	Mass needed
Dithiothreitol	154.25	1.5425 g

Dispense into ~50 µL aliquots and store at -20°C.

10 mg/mL Leupeptin:

To newly opened 5 mg Leupeptin bottle, add:	
Chemical	Vol needed
EtOH	500 µL

Dispense into ~25 µL aliquots and store at -20°C.

10 mg/mL Pepstatin A:

To newly opened 5 mg PepstatinA bottle, add:	
Chemical	Vol needed
Anhydrous dimethylsulfoxide (DMSO)	500 µL

Dispense into ~25 µL aliquots and store at -20°C.

1 mg/mL DNase I (use straight from supplier)

Concentration provided: 10k units/mL or 0.05 mg/mL

0.25M PMSF

To 250 mg PMSF, add 5.75 mL EtOH			
Chemical	MW	Amount	Note
PMSF	174.2	250 mg	Prepare in fume hood. Toxic!!!
EtOH	100%	5.75 mL	

BUFFERS TO PREPARE ON DAY 2:

50 mM Aminohexanoic acid (for F1Fo pH adjusted):

Top up to 8 mL with 20 mM Tris Buffer and adjust pH with NaOH to ~ 8		
Description	MW	Amount
Aminohexanoic acid	131.2	0.0656g

50 mM Aminobenzamidine (for F1Fo pH adjusted):

Top up to 8 mL with 20 mM Tris buffer and adjust pH with NaOH to ~ 8		
Description	MW	Amount
Aminobenzamidine	208.1	0.104g

TKDG* buffer:

25 mL TKG buffer in 50 mL Falcon Tube		
Final Conc	Buffers / chemicals	Volume needed
20 mM	1M TRIS- HCl pH 8.0 at 4°C	25 mL of TKG buffer, 4°C
140 mM	2M KCl	
10% (w/w)	50% (w/w) Glycerol Autoclaved	
0.5 mM	0.5M DTT	25 µL
1 mM	50 mM Aminobenzamidine	0.5 mL
1 mM	50 mM Aminocaproic acid	0.5 mL

TKDG-a* buffer

50 mL TKG buffer in 50 mL Falcon tube			
Final Conc	Description	Amount	Note
20 mM	TRIS-HCL pH 8.0 at 4°C	TKG buffer 50 mL	
140 mM	KCl		
10% (w/w)	Glycerol		
0.5 mM	DTT	50 µL	*Represents half of PMSF needed, the other half is added just before French press (Final conc should be 0.5 mM)
0.25 mM	PMSF	50 µL*	
5 µg/mL	Leupeptin	25 µL	
5 µg/mL	Pepstatin	25 µL	
20 units/mL	DNAase I	100 µL	
1 mM	50 mM Aminobenzamidine	1 mL	
1 mM	50 mM Aminocaproic acid	1 mL	

TKDG*-b buffer

25 mL in 50 mL Falcon tube			
Original Conc	Description	Amount	Note
20 mM	TRIS-HCL pH 8.0 at 4°C	TKG buffer 25 mL	
140 mM	KCl		
10% (w/w)	Glycerol		
0.5 mM	DTT	25 µL	
0.5 mM	PMSF	50 µL	
5 µg/mL	Leupeptin	12.5 µL	
5 µg/mL	Pepstatin	12.5 µL	
1 mM	50 mM Aminobenzamidine	0.5 mL	
1 mM	50 mM Aminocaproic acid	0.5 mL	

BUFFERS TO PREPARE ON DAY 3:

Membrane wash buffer:

To 7.45 mL ice cold ddw, add			
Final Conc	Chemicals / buffer	Amount	Note
50 mM	1 M Tris-HCl (pH 8.0 at 4 ^o C)	0.5 mL	
2 mM	1 M MgCl ₂	0.02 mL	
10% (w/w)	50 % (w/w) glycerol	2 mL	
0.5 mM	0.5 M EDTA	0.01 mL	
1 mM	0.5 M DTT	0.02 mL	DTT added just before expt

Store at 4^oC.

200 mM Mes/Tricine buffer (pH 7.0)

To 100 mL of ice cold ddw, add		
Chemical	MW	Amount needed
MES	195.2 g/mol	7.81 g
Tricine	179.2 g/mol	7.17 g

Adjust pH at 4^oC using 5M NaOH. pH increases slightly when temp increases.

Top up with cold ddw to 200 mL

Buffer A (F₀F₁)

To 6.16 mL of ice cold ddw, add			
Final Conc	Buffer / Chemical	Amount needed	Note
25 mM	MES/Tricine (200 mM, pH 7 at 4 ^o C)	1.25 mL	A slightly higher concentration is used because there will subsequently be a dilution when detergent is added
6.25 mM	1M MgCl ₂	62.5 μL	
12.5%	50% Glycerol (w/w)	2.5 mL	
1.25 mM	0.5M DTT	0.025 mL	Only for Cysteine strain

Store at 4^oC

10% w/w C₁₂E₈

To 15 mL of ice cold ddw, add		
Chemical	Amount needed	Note
C ₁₂ E ₈	1.5 g	

Wash Buffer 1/2 (F₀F₁) for Ni Column

To 31.25 mL if ice cold ddw, add			
Final conc	Buffer / Chemicals	Amount needed	Note
20 mM	MES/Tricine (200 mM, pH 7 at 4 ^o C	5 mL	
5 mM	1M MgCl ₂	0.25mL	
10%	50% Glycerol (w/w)	10 mL	
80 mM	2M KCl	2 mL	
1 mM	0.5M DTT	0.1 mL	Only for strains with Cysteine
20 mM	1M Imidazole pH ~ 7 (balanced with 2M HCl)	1 mL	
0.05% w/w	C ₁₂ E ₈ 10% w/w	0.25 mL	
0.03% w/w	SoyPC 10% w/w	0.15 mL	Wash buffer 2 has no lipids

Elution Buffer (F₀F₁) for Ni Column

To 1.45 mL of ice cold ddw, add			
Final conc	Buffer / Chemicals	Amount needed	Note
20 mM	MES/Tricine (200 mM, pH 7 at 4 ^o C	1 mL	
5 mM	1M MgCl ₂	50 µL	
10%	50% Glycerol (w/w)	2 mL	
80 mM	2M KCl	0.4 mL	
1 mM	0.5M DTT	0.02 mL	Only for strains with Cysteine
500 mM	1M Imidazole pH ~ 7 (balanced with 2M HCl)	5 mL	
0.05% w/w	C ₁₂ E ₈ 10% w/w	0.05 mL	
0.03% w/w	Soy 10% w/w	0.03 mL	

Dialysis Buffer for Ni column

To 645 mL of ice cold ddw, add			
Final conc	Buffer / Chemicals	Amount needed	Note
20 mM	MES/Tricine (200 mM, pH 7 at 4 ^o C	100 mL	
5 mM	1M MgCl ₂	5 mL	
10%	50% Glycerol (w/w)	200 mL	
80 mM	2M KCl	40 mL	
1 mM	0.5M DTT	2 mL	Only for strains with Cysteine
0.05% w/w	C ₁₂ E ₈ 10% w/w	5 mL	
0.03% w/w	SoyPC 10% w/w	3 mL	

Glycerol gradient buffer (10%) with Leupeptin, Pepstatin A for Glycerol column only

To 5.936 mL of ddw, add:			
Final conc	Buffer / Chemicals	Amount needed	Note
10 mM	200 mM Mes/Tricine (pH 7.0)	0.4 mL	It may be possible to add a small amount of lipids e.g. 0.03% SoyPC or EColi Lipids as given in [2]. This has not been rigorously tested though it failed on the only time it was tested.
5 mM	1 M MgCl ₂	40 µL	
10% (w/w)	50%(w/w) Glycerol	1.6 mL	
0.01% (w/w)	10% (w/w) C ₁₂ E ₈	8 µL	
0.5 mM	0.5 M DTT	8 µL	
5 µg/mL	10 mg/mL Leupeptin	4 µL	
5 µg/mL	10 mg/mL Pepstatin A	4 µL	

Glycerol gradient buffer (30%) with Leupeptin, Pepstatin A:

To 2.736 mL of ddw, add:			
Final conc	Buffer / Chemicals	Amount needed	Note
10 mM	200 mM Mes/Tricine (pH 7.0)	0.4 mL	
5 mM	1 M MgCl ₂	40 µL	
30% (w/w)	50%(w/w) Glycerol	4.8 mL	
0.01% (w/w)	10% (w/w) C ₁₂ E ₈	8 µL	
0.5 mM	0.5 M DTT	8 µL	
5 µg/mL	10 mg/mL Leupeptin	4 µL	
5 µg/mL	10 mg/mL Pepstatin A	4 µL	

Glycerol gradient buffer (16.7%) with Leupeptin, Pepstatin A:

To mix 10% and 30% glycerol gradient buffer in the right proportion		
Buffer	Amount needed	Notes
Glycerol gradient buffer (10%)	2 mL	
Glycerol gradient buffer (30%)	1 mL	

Glycerol gradient buffer (20%) with Leupeptin, Pepstatin A:

To mix 10% and 30% glycerol gradient buffer in the right proportion		
Buffer	Amount needed	Notes
Glycerol gradient buffer (10%)	1.5 mL	
Glycerol gradient buffer (30%)	1.5 mL	

Glycerol gradient buffer (23.3%) with Leupeptin, Pepstatin A:

To mix 10% and 30% glycerol gradient buffer in the right proportion		
Buffer	Amount needed	Notes
Glycerol gradient buffer (10%) with Leupeptin and Pepstatin A	1 mL	
Glycerol gradient buffer (30%) with Leupeptin and Pepstatin A	2 mL	

2x Reaction Mix

To 44.8 mL of ddw, add:			
Final conc	Buffer / Chemicals	Amount needed	Note
20 mM	1M Tris-HCl (pH 8.0 at 37°C)	1 mL	
8 mM	100 mM ATP (pH 8.0)	4 mL	
4 mM	1M MgCl ₂	0.2 mL	

Divide into 10 mL aliquot

Store at -20°C

To 98 mL of ddw, add:			
Final conc	Buffer / Chemicals	Amount needed	Note
20 mM	1M Tris-HCl (pH 8.0 at 37°C)	2 mL	
2 µg/mL	50 mg/mL BSA	4 µL	

Store at 4°C

Pi colouring solution

To 9 mL of ddw, add			
Final conc	Buffer / Chemicals	Amount needed	Note
5% (w/w)	FeSO ₄ x 7 H ₂ O	0.5 g	
1% (w/w) (NH ₄) ₆ Mo ₇ O ₂₄ x 4 H ₂ O	10% (w/V) (NH ₄) ₆ Mo ₇ O ₂₄ x 4 H ₂ O / 5M H ₂ SO ₄	1.0 mL	
0.5M H ₂ SO ₄			

Store at 4°C

Protocol Day 1 - Start: 0700, End: 2000

- Remove the cover from a sterile 200 mL Erlenmeyer flask.
- Transfer 20 mL sterile LB medium into each flask with a sterile pipette.
- Add 20 μ L of 100 mg/mL ampicillin. (Final concentration 100 μ g/mL).
- Inoculate the medium with an aliquot of frozen *E. coli* cells.
- Cap the flask. Do not tighten fully.
- Place the flask in an incubator - Shaking speed 120 rpm; temperature 37°C.
- Grow at least for 12 hours.

START: 0700 hrs

END: 1900 hrs

- Prepare 1x Tanaka Media in 2L culture flasks.
- Autoclave the media - 2 flasks of 800 mL Tanaka Media + 1 bottle of 50% w/w glycerol.
- Allow to cool in room Temperature.
- Add the remaining chemicals into the 1x Tanaka Media.
- Take out some excess Media as blank for OD measurements.
- Inoculate 8 mL pre-culture per flask.
- Work in open flame during the inoculation and sterilise the surface with ethanol. Do not work with gloves for safety reasons.
- Place the Erlenmeyer flask in a shaker (shaking speed 140 - 180 rpm; temperature 37°C). Grow the culture until OD600 become about 1.0 – 1.5 ~ 12 hrs.

START: 2000 hrs

END: 0800 hrs

Bookings of centrifuges / equipment

Centrifuges and Rotors to book (Need to pre-cool all rotors):

- JLA 9.1000 / 8.100 rotor for Beckman Coulter centrifuge – Day 2 for 1½ hrs (2x 23 min) starting at T+1 to T+2 (T is the time which one start the day).
- JA 20 rotor for Beckman Coulter centrifuge – Day 2 for 30 mins starting at T+2 to T+3.
- French Press – Day 2 for 2 hrs. Remember to wait for the press to cool to 4°C. starting at T+3 to T+5.
- JA 20 rotor for Beckman Coulter centrifuge – Day 2 for 1 hr starting at T+5 to T+6.
- Type 70.1 TI rotor L-XP Beckman Coulter ultracentrifuge – Day 2 for 4 hrs starting at T+6 to T+10.
- Rotor TLA 100.2 ultracentrifuge – Day 3 for ½ hrs at T+1 to T+1.5.
- Rotor TLA 100.2 ultracentrifuge – Day 3 for ½ hrs at T+2.5 to T+3.
- Rotor SW 55 Ti rotor (Swing type rotor in Biochemistry) – Day 3 for 5 hrs at T+4 to T+9 (If glycerol column is used).

Protocol Day 2 - Start: 0800, End: 1900

Harvesting the bacteria (0800 – 1100 hrs)

- Pre-cool the centrifuge.
- Transfer the culture to 1L tubes for centrifuge - 1 flask per tube. Balance the volume by eye.
- Put sample in ice at all times from now on.
- Centrifuge for 23 min at ~ 6 000*g average, to 7 000*g max, 4°C
 - ❖ JLA 9.1000 rotor for Beckman Coulter centrifuge ~ 5800 rpm or
 - ❖ JLA 8.100 ~ 5100rpm.
- Discard the supernatant carefully by decantation.
- Use a paintbrush to resuspend the cell pellet with 50 mM Tris-HCl (pH 8.0 at 4°C) Use ~200 mL per 800 mL Tanaka medium. Balance the volume by eye.
- Centrifuge for 23 min with the same settings.
- Discard the supernatant carefully by decantation.
- Use a paintbrush to resuspend the pellet with TKDG* buffer (4°C) (~20 mL per 800 mL Tanaka medium).
- Transfer to 50 mL centrifuge tubes, for rotor JA 20.
- Weigh the empty tubes before transfer. (Remember to label top cap too)
- Centrifuge for **12 min at 9200rpm 4°C (JA 20 rotor for Beckman Coulter centrifuge)**.
- Discard supernatant carefully by decantation.
- Weigh the tube and calculate the cells wet weight.

Lysing the bacteria (1100 – 1400 hrs)

- Resuspend cells in TKDG-a* buffer at 4°C at the ratio of 7 mL of buffer /2 g cells wet weight. We should have at least ~ 14-15 mL of the bacteria suspension for the French press.
- Add 0.25M PMSF (~15 µL per 15 mL) immediately before French Press. See later for French press protocols.
- Disrupt the bacteria with French Press.
 - ❖ Set pressure gauge at 1800kg/cm², actual pressure is about 28 000 psi, when using 40k pressure cell.
 - ❖ Set pressure gauge to **1000 kg/cm² when using 20k pressure cell (Do not exceed 1100!!)**. Actual pressure will be ~19000 psi
 - ❖ (ALWAYS KEEP SAMPLE ON ICE).
- Do 3 passes through the French press.
- Transfer to 50 mL centrifuge tubes (JA20 tubes – small tubes with screw caps).
- Balance the tubes (Up to 0.0X g).
- Centrifuge for **13 min at 12 000*g average, Speed = 12500 rpm at 4°C (Use JA 20 rotor for Beckman Coulter centrifuge)**.
- Transfer the supernatant to new tubes.
- Centrifuge for 13 min with same settings.

Collecting membrane fragments – Ultracentrifuging (1400 – 1800 hrs)

- Pre-cool the next rotor 70.1 TI.
- Transfer the supernatant carefully to new tubes for ultracentrifuge - centrifuge tubes (Beckman part # 335630) - Capacity ~ 8 mL per tube.
- Balance the tubes (0.00X g).
- Centrifuge for 1.5 hr at 130 000*g average, 4°C.
 - ❖ For Type 70.1 TI rotor, Speed = 43500 rpm in L-XP Beckman Coulter ultracentrifuge or
 - ❖ Type 70TI at speed = 47600rpm for the same time.
- Discard supernatant carefully by decantation.
- Suspend the precipitate in 7 mL per 2g of TKDG-b* buffer (4°C) with a paintbrush on ice (use same tubes as before).
- Centrifuge again for 1.5 hr at 130 000*g average, 4°C (Type 70.1 TI rotor for 43,500rpm in L-XP Beckman Coulter ultracentrifuge).
- Discard supernatant carefully by decantation.
- Suspend the precipitate in TKDG* buffer (4°C) with a paintbrush on ice (approximately 200 µL/ 1 g cells wet weight).
- Transfer the milky suspension into aliquot of ~ 900 µL. Take 10 µL out and into a new microfuge tube for Lowry method (To be diluted by 20x for the test).
- Quickly freeze the aliquots in liquid nitrogen and store at -196°C.
- Store 1L of ddw in fridge for making buffer tomorrow.

Lowry method (1800 – 1900 hrs) using RC DC protein Assay Kit (Biorad)

- Prepare BSA with concentration 2 mg/mL to 0.25 mg/mL.
- Add 20 µL of each concentration of BSA into Eppendorf tubes.
- Dilute the membrane proteins in ratio of 1:10, 1:20, 1:40 and 1:80.
- Also prepare one sample with just TKDG buffer as blank.
- Add 20 µL of each concentration of protein into a test tube.
- Add 100 µL of Reagent A¹ into each Eppendorf tube.
- Immediately follow by 0.8 mL of Reagent B¹.
- Wait for 15 minutes and read absorbance at 750 nm.

Protocol for using the French Press

- Wash the tubing & rigs.
- Make sure the pressure dial is turned to the minimum (anticlockwise).
- Apply glycerol to the rubber sealant around the plunger and stopper.
- Change the plastic ball located at the tip of the turning knob that is used to control the outlet flow.
- Put the plunger (at the bottom) and the main cylinder on the stand.
- Load in the sample.
- Screw in the turning knob with the plastic ball facing up. Gravity will sit the ball in place and prevent it from misaligning while in the rig.
- Close the top of the main cylinder with the stopper cylinder.

¹ Reagent A and B are the standard reagent in the Protein Assay Kit (Catalog number. 500 0121)

- Mount the assembly onto the French press, making sure that the orientation of the plunger does not obstruct the screws that are used to hold the rig in place
- Secure the plastic tubing at the outlet and tighten a falcon tube at the other end. Keep the tube in an ice bath.
- Make sure that everything is tight and secure.
- Start the French press.
- Turn the operating handle to high.
- Turn the pressure knob clockwise slowly until the desired pressure of 1000kg/m^2 . Be careful when doing this as the pressure rating of the French press is 1200kg/m^2 .
- Once the pressure is set, it should remain constant until the turning knob (valve) is open to allow the sample to flow through.
- Release the sample through the tubing by opening the turning knob. Ideal flow rate should be dropwise at a fairly swift rate.
- Pass about 12 mL of the sample through the French press. **Do not attempt to pass all the sample (~14 mL) as this may damage the plunger permanently.**
- Turn the operating handle to down to stop the press.
- Do 3 good passes to ensure that most of the cells have been properly lysed.
- Clean the equipment with ethanol and put them back in the cold room when finished using the equipment.
- Switch off the system.

Equipment needed for the French Press:

- Jigs from the cold room
- Distill water
- Ethanol
- Eye protection
- Paper towel
- Beaker with ice
- Pipette 1 mL + 200 μL
- Pipette tips
- 100% Glycerol
- Ice box with empty falcon tubes. Quantity depending on the number of samples to be passed through the French Press.
- Samples
- PMSF

Protocol Day 3 - Start: 0800, End: 2000

Membrane washing and solubilisation (0800 – 1100 hrs)

- Add 500ul of Membrane Wash Buffer for every 12 mg of proteins. Re-suspend the membrane fragments with a paint brush.
- Centrifuge for **20 min at 370 000*g average at 4°C. Rotor: TLA 100.2, speed: 100 000 rpm, Tube 343778 – capacity 1 mL.**
- Balance the tube up to 0.00X. Also remember to press the button at the middle of the small rotor.
- Discard the supernatant carefully.
- Suspend the pellet in 0.4 mL of Buffer A, per 12 mg protein. (Note that this is not the same buffer A as F1 protocol)
- Add dropwise on top of a stirrer, 10% C₁₂E₈ to get a final concentration 2% & 2M KCl to final concentration = 100 mM.
- Incubate in cold room (at 4⁰C) for 30 minutes with constant stirring
- Centrifuge for **20 min at 180 000*g (average), temp: 4⁰C, Speed: 61000 rpm using rotor TLA 100.2.**
- (Prepare the glycerol gradient buffers at the time * if using glycerol col)
- Take the supernatant and place in a new Falcon tube. Discard the pellet.

Option 1: Purification with Glycerol Column (1100 – 1800 hrs)

- Hold the Ultraclear centrifuge tube (13 x 51 mm No. 344057) with a retort stand and add 800 µL of 30% (w/w) glycerol buffer.
- Place the next layer by carefully adding 800 µL of 23.3% (w/w) glycerol buffer. There should be a distinct border between the two glycerol layers.
- Repeat this for the remaining concentrations of glycerol buffer in descending order: 20% (w/w), 16.7% (w/w) and 10% (w/w).
- Finally add the sample on top of the last glycerol layer
- Place the column carefully into the metal housing of the swing rotor.
- Close the lid and balance the tube up to 0.00X
- It may be difficult to tighten the rotor housing when the centrifuge tube is inserted in. Make sure that this could be done before doing the weight balancing.
- All unused metal housing must remain on the rotor even though they are empty.
- Centrifuge for **5 hr at 250,000xg (average, in SW 55 Ti rotor, 51 300 rpm average), 4⁰C.** Make sure that the lids are tightened fully and the metal housing free to swivel on the rotor.
- Once finish, carefully take out the centrifuge tube and make a hole slightly above the bottom of the tube with a needle. Avoid disturbing the bottom of the tube.
- Fractionate the solution into microfuge tubes (~ 400 µL / tube). Do this in the cold room.
- Check the ATPase activity of the fractions.
- Determine the peak fraction to keep.
- Dispense 20 µL aliquots of the peak fraction into each Cryotube.
- Flash freeze aliquots in liquid nitrogen and store at –196°C.

Option 2: Purification with Nickel Column (1100 to 1900 hrs)

- Perform this part of the purification in the cold room
- Wash the column with 10 mL of ddw
- Rinse the column with 10 mL of wash buffer 2 (i.e. wash buffer 1 minus lipids)
- Adjust the flow rate using a stopper to get about 1 mL / 20 mins
- Insert the sample ~ 2 mL. Allow the sample to flow through the column till no more sample is above the resin. The resin should look yellowish brown now.
- Rinse the column with 10 mL of wash buffer 1, using the same flow rate
- Put in 4 mL of elution buffer and collect the fractions.
- Test the activity of each fraction using Pi colouring assay
- Chose the best 3 fractions and dialyse them (using 10 kDa membrane) using dialysis buffer (500x Excess Vol) over 24 hrs with 3 buffer exchanges.
- Flash freeze the sample in Liquid Ni and store at -196°C.

Measuring the hydrolysis activity of protein (1800 – 2000 hrs)

1. Calibration and activity measurement (This step is optional if calculation of specific activity is not required)
 - Add 1.5 µL of 10% C₁₂E₈ to 145.5 µL ATPase assay buffer. Vortex.
 - Pipette 3 µL F₁F₀ or 2-10 µL of 10 mM NaH₂PO₄. Adjust the amount of ATPase assay buffer accordingly to get a final volume of 150 µL.
 - Add 150 µL of 2x Reaction Mix A to test tube.
 - Vortex for few seconds.
 - Incubate at 37°C for about 10 min. (Final conc of detergent = 0.05%)
 - Place the test tubes on ice.
 - Add 150 µL of 1 M TCA (0°C)
 - Remove the excess detergent by incubating the sample in 40 mg of biobeads.
 - Stir continuously for 20 mins in cold room using small magnetic stirrer
 - Take 400 µL of the sample and add 250 µL of Pi colouring solution (0°C).
 - Vortex and incubate the tubes at 37°C for 30 sec.
 - Place the test tubes on ice.
 - Add 200 µL of ATP assay buffer (0°C).
 - Measure absorbance at 850 nm.

Compare the absorbance A₈₅₀ against standard curve and calculate the ATPase activity.

$$A_{850} = a * Pi + b$$

Where

A₈₅₀ is the absorbance at 850 nm

Pi is the amount of phosphate in mol

a and b are the parameters for the linear fit

$$\text{ACTIVITY (units/}\mu\text{L min)} = \text{Pi(mol)} / (\text{t(min)} * \text{Vol of ATPase})$$

Where

t = 10 min

Vol of ATPase = 3 μ L

SPECIFIC ACTIVITY ($\text{mol mg}^{-1} \text{min}^{-1}$) = ACTIVITY/ conc of protein ($\text{mg}/\mu\text{L}$)

Note1: The discrepancy in the absorbance between 10 μ L of 10 mM phosphate buffer treated with biobead and detergent, and untreated sample (no biobead / detergent), was found to be ~ 6 - 10%.

Note2: Detergent needs to be removed because excess of it would cause precipitation of the Ammonium Molybdenum. Such precipitation can lead to higher apparent absorbance because light is scattered by the particulates. This becomes evident when using the glycerol column to purify F_1F_0 . The later fractions, which have higher concentration of detergent, will give a high 'absorbance' reading. This is in fact due to the scattering of light by the precipitate.

For a quick activity test to choose the right fraction after the Ni column or Glycerol column, the following procedure is used.

- Pipette 3 μ L F_1F_0 from each fraction collected
- Add ATPase assay buffer accordingly to get a final volume of 150 μ L.
- Add 150 μ L of 2x Reaction Mix A to test tube.
- Vortex for few seconds.
- Incubate at 37°C for about 10 min.
- Place the test tubes on ice.
- Add 150 μ L of 1 M TCA (0°C)
- Vortex briefly
- Add 250 μ L of Pi colouring solution (0°C).
- Vortex and incubate the tubes at 37°C for 30 sec.
- Place the test tubes on ice.
- Choose the best fraction by visual inspection.

A1-2 Protocol For SDS Polyacrylamide Gel Electrophoresis [3]

Gel preparation

- Put the glass plate (Thick and Thin) together.
- Assemble them on a Mini gel holder and clip tightly.
- Make sure that the two glass plates are flushed at the bottom.
- Try putting some ddw to test whether it is leaky.
- Prepare a stack gel with 14% separating gel and 3.2% stacking gel. For F₁F₀.

14% (To be added in the sequence shown)

- ❖ 4.301 mL ddw
- ❖ 3.9 mL 40%, 37.5:1 Acrylamide
- ❖ 2.8 mL 1.5M Tris-HCl pH 8.8
- ❖ 0.113 mL 10% SDS – Sodium Dodecyl Sulfate
- ❖ 0.055 mL 10% APS – Ammonium PerSulfate
- ❖ 0.011 mL TEMED – Tetramethylethylenediamine

- Add about 3.5 mL of the acrylamide between the glass plate.
- Add a small quantity of isobutanol on top of the gel to remove any bubble that may be present
- Wait for the gel to solidify. This can be judged by the solidification of the excess gel in the falcon tube.
- Prepare the stacking gel with the following formula

3.2%

- ❖ 2.385 mL ddw
- ❖ 0.24 mL 40% 37.5:1 Acrylamide
- ❖ 0.375 mL 1M Tris-HCl pH 6.8
- ❖ 0.031 mL 10% SDS
- ❖ 0.015 mL 10% APS
- ❖ 0.004 mL TEMED

- Remove the isobutanol using tissue.
- Flow in the acrylamide for the stack gel.
- Carefully insert the comb on top of the stack gel.
- Tilt the gel holder back to minimise leaking.

Prepare gel loading buffer

- Use NanoSep 10k from flowgen to concentrate the sample. Spin at 5000xg for 20 mins
- To 10 µL of the sample, add
 - ❖ 3.3 uL 10% SDS
 - ❖ 3.3 uL 250 mM TrisHCl pH 6.8
 - ❖ 0.5 uL Loading dye

- Place the mixed solution in small test tubes and heat up to 55°C for 1 hr
- Load the protein and molecular ladder on the gel.
- Load in the bromophenol blue marker as well to see the lanes as the gel is run. The dyes need not be on the same lane as the proteins.

Gel running

- The mini gel system consists of an outer plastic container and a detachable inner housing.
- Slot the cast gel and the dummy plate into the inner housing and clamp them shut.
- Pour the electrophoresis running buffer into the inner housing.

Running buffer:

- ❖ 25 mM Tris-HCl pH 8.3
- ❖ 250 mM Glycine
- ❖ 0.1% w/v SDS

- Check that the buffer in the interior reservoir does not leak. If it does, try adjusting the plates again.
- Pour some of the running buffer into the outer plastic container until it is ~ 1/3 filled. The buffer should be well above the base of the inner housing.
- Place the inner housing into the outer container. Make sure that no bubbles are trapped at the bottom of the inner housing. This can be prevented by tilting the outer container to the side when placing the inner housing.
- Pull out the comb slowly and wash the interior of each well with a needle and syringe
- Pour the remaining running buffer into the inner housing until the brim.
- Run the gel at 100V for ~ 1 hr 45 mins
- Stop when the dye indicator is about 0.5cm away from the base of the gel.

Coomassie Staining

- Take out the gel gently, taking care not to break them when opening the glass plates.
- Use a razor if necessary and always keep the gel immerse in ddw water.
- Wash the gel a few times with ddw.
- Immerse gel in ddw for 5 mins to remove excess SDS (repeat 2 more times)
- Pour in the Coomassie Dye (EZblue gel staining – sigma).
- Put on rocker for 2 hrs
- Pour away the Coomassie stain and wash the gel a few times with ddw. Pour the Coomassie waste in designated waste jar.
- Destain the gel by rocking it in ddw, changing the water a few times in the process.

Silver staining from Biorad Silver Stain kit

- Prepare the Development Accelerator Solution by dissolving the 5g of developer accelerator powder in 95 mL of MilliQ water. Keep in refrigerator. The developer accelerator powder can be found in the chemical cabinet (dessicator box)
- Prepare the fixative enhancer solution in a 100 mL bottle:
 - ❖ 50 mL reagent grade Methanol, final conc - 50% v/v
 - ❖ 10 mL reagent grade Acetic acid, final conc – 10% v/v
 - ❖ 10 mL Fixative Enhancer Concentrate, final conc - 10% v/v
 - ❖ 30 mL ddw
- Wash the gel in ddw water.
- Fix the gel with the fixative enhancer solution for 20 min. (100 mL)
- Decant the fixative enhancer solution and wash the gels with ddw for 10 minutes. Repeat the wash again.
- Prepare the staining and development solution 5 min before the staining procedure.
- Prepare in a falcon tube the following
 - ❖ 17.5 mL ddw
 - ❖ 2.5 mL Silver Complex Solution
 - ❖ 2.5 mL Reduction Moderator Solution
 - ❖ 2.5 mL Image Development Reagent
- Add 25 mL of Development Accelerator Solution into the above just before the staining process.
- Decant the ddw from the gel and add the development solution prepared above. Wait for the desired intensity to form.
- Decant the development solution into a waste bottle and add 5% acetic acid to stop the staining reaction. Let the gel soak for 15 mins in the stopping solution.
- Pour the stopping solution away and rinse the gel with ddw for 5 mins.

A1-3 Protocols for F₁F₀ ATPase Vesicle Activity Test

Materials & Chemicals: Constituent of Lipid Mix

Lipid Mix

Final conc	Lipid / Chemicals	Amount needed	MW
7.7 mg/mL	E-Coli Polar Lipids @25 mg/mL	225 µL	~800
0.85 mg/mL	Diphythanoyl PC @ 10 mg/mL	62.5 µL	846
2.2 mM	Cholesterol @ 10 mM (in chloroform)	160 µL	387
7.8 mg/mL	Egg PC @ 25 mg/mL	228 µL	760
0.78 mg/mL	Egg PA @ 10 mg/mL	57 µL	697

Store at -20 °C

- All lipids are to be handled with glass Hamilton Syringe
- Total weight = 12.5 mg
- Total volume = 732.5 µL
- Total Concentration of lipids = 17.1 mg/mL
- Total amount of lipid (in mol) excluding cholesterol ~ 16 µmol
- 10% molar ratio cholesterol = 1.6 µmol => 160 µL of 0.01M
- Cholesterol molar ratio up to 30% was found to for enhanced TF₁F₀ and CF₁F₀ activity [4].
- Make aliquots of 188 µL (for vesicles formation in 200 µL buffer), 59 µL for making 1 mg/mL lipid in pentane (1 mL pentane) and 73 µL for making 5 mg/mL lipids in hexadecane (250 µL pentane).

Materials & Chemicals: Buffer used

MESs buffer

To 33.15 mL ddw, add:

Final conc	Chemicals	Amount needed	Notes
20 mM	200 mM Mes/Tricine (pH 7.0)	5 mL	
80 mM	4M NaCl	1 mL	
2 mM	1M MgCl ₂	100 µL	
10% w/w	50% (w/w) Glycerol	10 mL	

- Use MES/Tricine from purification so that the buffer / pH is consistent
- Filter the preparation with 0.2 µm filter

Materials & Chemicals: Biobeads

Biobeads washing:

- Rinse 3x with 100% Methanol
- Rinse 6x with water
- Vortex 30s for each wash

Preparation of vesicles

- To form 200 μL of 16 mg/mL lipids in MES buffer => Take out 188 μL from the lipid stock.
- Dry under Nitrogen gas in a fume hood.
- Dissolve in 200 μL of buffer to get 16 mg/mL lipid.
- Vortex for 1 min
- Sonicate in ice water for 10 mins. Make sure that most of the ice in the sonicator is melted as they tend to attenuate the sonication strength.
- Freeze-Thaw the sample 3x using liquid Nitrogen
- Extrude the sample using 0.2 μm membrane for 21 passes.
- Store the final vesicles in 4°C.

Reconstitution

- To 10 μL vesicles, add 10 μL of proteins (~ 0.3 mg/mL) to Eppendorf tube. Mix thoroughly.
- Slowly add 1.74 μL 10% Triton X (v/v)
- Mix thoroughly to ensure complete solubilisation of protein
- Final concentration of detergent ~ 0.8% was used.
- Incubate in ice for 1 hr
- Incubate in cleaned biobeads + constant stirring using small magnetic beads in cold room. Stirring is important as it will ensure efficient removal of detergent.
 - ❖ 3-4 mg first time for 1.5 hrs (2-3 mg)²
 - ❖ 5-6 mg second time for 1.5 hrs (2-3 mg)
 - ❖ 11-12 mg final time for 1 hr (try 5-6 mg)

Calculations (for diameter = 200 nm)

Approx area of 1 lipid = 0.6 nm ² [5]
Total surface area (inner and outer) of a 200 nm diameter vesicle = $4\pi(100)^2 \times 2 = 251 \times 10^3 \text{ nm}^2$
No. of molecules per vesicle = $251 \times 10^3 / 0.6 = 420 \times 10^3 \text{ molecules} = 7 \times 10^{-19} \text{ mol}$
No. of moles of lipid used (10 μL of 16 mg/mL) = $\frac{10 \times 16 \times 10^{-6}}{787.5} = 2 \times 10^{-7} \text{ mol}$ (M_r Lipid ~ 787.5)
No. of vesicles = $2 \times 10^{-7} / 7 \times 10^{-19} = 3 \times 10^{11} \text{ vesicles} = 5 \times 10^{-13} \text{ mol}$
No. of mol of protein @ 10 μL of 0.3 mg/mL = $6 \times 10^{-12} \text{ mol}$ (M_r Protein ~ 500KDa)
Ratio protein to vesicle = $6 \times 10^{-12} / 5 \times 10^{-13} = 12$
Concentration of vesicles = $5 \times 10^{-13} / 2 \times 10^{-5} = 2.5 \times 10^{-8} \text{ M}$

² Two different biobead amounts were tried. For the ACMA test, the protocol with less biobeads gave marginally better results. Lesser amount of biobeads will remove fewer lipid molecules and detergent more slowly. However, detergent not fully removed may destabilise the bilayer.

Calculations (for diameter = 80 nm)

Approx area of 1 lipid = 0.6 nm^2 [5]

Total surface area (inner and outer) of a 200 nm diameter vesicle = $4\pi(40)^2 \times 2 = 40 \times 10^3 \text{ nm}^2$

No. of molecules per vesicle = $40 \times 10^3 / 0.6 = 67 \times 10^3$ molecules = 1.1×10^{-19} mol

No. of moles of lipid used (10 μL of 16 mg/mL) = $\frac{10 \times 16 \times 10^{-6}}{787.5} = 2 \times 10^{-7}$ mol (M_r

Lipid ~ 787.5)

No. of vesicles = $2 \times 10^{-7} / 1.1 \times 10^{-19} = 1.8 \times 10^{12}$ vesicles = 3×10^{-12} mol

No. of mol of protein @ 10 μL of 0.3 mg/mL = 6×10^{-12} mol (M_r Protein ~ 500KDa)

Ratio protein to vesicle = $6 \times 10^{-12} / 3 \times 10^{-12} = 2$

Concentration of vesicles = $3 \times 10^{-12} / 2 \times 10^{-5} = 1.5 \times 10^{-7}$ M

Empirically, the number of rightly oriented F-ATPase per vesicle for a vesicle size of 80 nm is ~ 1 F-ATPase per vesicle (instead of 2 – see also chapter 3 of main text)

Activity test

- Dissolve 5 μL of F_1F_0 vesicles in 100 μL MES buffer.
- Let it stand for 5 min at room temperature.
- Add 5 μL of 25 μM ACMA (obtained from 1:20 dilution of 0.5 mM ACMA in ethanol). ACMA degrades once dissolve in buffer. So use fresh ACMA each time.
- Let it stand for 5 min at room temperature.
- Take 60 μL of the solution and placed it in a cuvette to record the fluorescence count.
- Take the fluorescence reading with the following settings on the fluorometer
 - Excitation wavelength = 410 nm
 - Emission wavelength = 480 nm
 - Slit width = 3 (1.5 nm) for all
- When the fluorescence counts steadied, add 2 μL of 50 mM ATP with pH adjusted to 7.

A1-4 Protocols for Trapping Fluorophores in Vesicles

Materials and Chemicals: Buffer

All buffer used in this section will be MOPs buffer

To 35 mL ddw, add:

Final conc	Chemicals	Amount needed	Notes
20 mM	1M MOPS	1 mL	
80 mM	4M NaCl	1 mL	
2 mM	1M MgCl ₂	100 µL	
10% w/w	50% (w/w) Glycerol	10 mL	

- Adjust with NaOH to pH (~ 7).
- To get pH 7, add ~ 500 µL 1M NaOH
- Top up with ddw until 50 mL
- Filter the preparation with 0.2 µm filter
- Store at 4°C

Preparation of vesicles for protein reconstitution (dextran inside and streptavidin outside)

- To form 200 µL of 16 mg/mL lipids in MES buffer => Take out 188 µL from the lipid stock.
- Dry under Nitrogen gas in a fume hood.
- Dissolve Dextran 647 in 200 µL of MOPs buffer to give a final concentration of **5 µM (High concentration because size of vesicles will decrease when treated with detergent)**.
- Mix the buffer with lipids to get 16 mg/mL.
- Vortex for 1 min.
- Sonicate in ice for 5 mins. Make sure that most of the ice in the sonicator is melted before sonication.
- Freeze-Thaw the sample 3x using liquid Nitrogen
- Extrude the sample using 0.2µm membrane for 21x.
- Store the final vesicles in 4°C.

- To 10 µL vesicles, add 10 µL of proteins (~ 0.3 mg/mL) to Eppendorf tube. (Mix thoroughly)
- Slowly add 1.74 µL 10% Triton X
- Mix thoroughly to ensure complete solubilisation of protein
- Final concentration of detergent ~ 0.8% was used.
- Incubate in ice for 1 hr
- Incubate in cleaned biobeads + constant stirring in cold room
 - ❖ 3-4 mg first time for 1.5 hrs (2-3 mg was added and appeared to work as well)
 - ❖ 5-6 mg second time for 1.5 hrs (2-3 mg)
 - ❖ 11-12 mg final time for 1 hr (try 5-6 mg)

- Add 20 μL of 2 μM Streptavidin Alexa 532 and incubate for $\frac{1}{2}$ hour. (This amount should be about 7x excess of the total amount of proteins added 0.3 mg/mL)

**An alternative method is to add the fluorescent dextran during the detergent incubation phase. This was done in the “Streptavidin in vesicle” control in chapter 3.

Preparation of vesicles with **no protein reconstitution**

- To form 200 μL of 16 mg/mL lipids in MES buffer => Take out 188 μL from the lipid stock.
- Dry under Nitrogen gas in a fume hood.
- Dissolve Dextran 647 (or streptavidin 647 / and streptavidin 532) in 200 μL of MOPs buffer to give a final concentration of 1 to 3 μM .
- Mix the buffer with lipids to get 16 mg/mL lipid.
- Vortex for 1 min
- Freeze-Thaw the sample 3x using liquid Nitrogen
- Extrude the sample using 0.2 μm membrane for 21x.
- Store the final vesicles in 4°C.

Removing dyes using ultracentrifuging

- Add 600 μL of MOPs buffer to 20 μL of proteoliposomes.
- Spin down @ 71000 rpm using TLA100.2 rotor for 20 min. There is a need to mark the outer side of the centrifuge tube relative to the rotor. This is because the spun down vesicles are not visible. We can only rely on the mark to determine where the vesicles have pellet.
- Remove excess buffer.
- Repeat 2 more times.
- Rehydrate the vesicle with 40 μL buffer + 0.1 mg/mL BSA

Removing dyes using biotin beads (only for fluorescence labelled Streptavidin)

- Take 100 μL of biotin agarose (Sigma), add 900 μL of MOPs buffer.
- Vortex for 10 s
- Spin down @ 13k RPM for 2 min
- Rehydrate biotin agarose to ~ 100 μL
- Dilute vesicles 10x using MOPs buffer to a final volume of 50 μL
- Add 10 μL of biotin agarose and incubate for 15 minutes under constant rotation in the cold room
- Repeat 2 more times

FCS and Alex measurements (Using El-Capitan from AK's group)

- The vesicle samples with trapped fluorophores is diluted 20x with MOPS buffer + 0.1 mg/mL BSA (Fluorescence grade), to give a final volume of ~ 50 μL .
- The entire sample is carefully placed onto a clean coverslip and put onto the microscope. One should see small droplet forming on top of the coverslip.

- Cover the sample.
- The laser power of the green and red laser **at alternating mode** is set at 75 μW and 35 μW respectively
- Focus is first set on the surface of the coverslip. This can be seen as a tight spot on the display.
- The focus is then shifted upwards by turning the z fine adjustment anticlockwise by 20 units.
- Data are recorded using ALEX at 50 μs switching time for 10 min per sample.
- Repeat for samples with different concentration of dyes trapped inside the vesicle. For each concentration, do at least 3 repetitions.
- While ALEX is taking the data, prepare new test samples of free streptavidin and dextran dyes without vesicles. Concentration of samples should be between 2 nM to 0.5 nM.
- Once all the vesicle samples are tested, we can start with the free dye samples.
- Place the samples on new coverslip and measure their intensity using ALEX for ~ 1 min.
- Switch to FCS, and remember to change the mode of operation of the red and green excitation to **CW** and modulate the intensity back to 35 μW and 75 μW respectively.
- Take the FCS data for 1 min using Flex02 program (Use Quad mode so that both green and red channels can be captured).
- From the FCS, one will be able to estimate the number of fluorophores in the detection volume. This number can then be plotted against the intensity measured using ALEX.

Calculations

Diameter of vesicles = 0.2 μm

\Rightarrow Vol of vesicles = $4.2 \times 10^{-21} \text{ m}^3 = 4.2 \times 10^{-18} \text{ dm}^3$

Final concentration of fluorophores = 1 to 3 μM

\Rightarrow Average number of fluorophores per vesicle = 2.5 to 7.5 molecules.

A1-5 Protocol for Making Droplet on Hydrogel

Material and Chemicals: Buffers

MOPs buffer

To 35 mL ddw, add:

Final conc	Chemicals	Amount needed	Notes
20 mM	1M MOPS	1 mL	
80 mM	4M NaCl	1 mL	
2 mM	1M MgCl ₂	100 µL	
10% w/w	50% (w/w) Glycerol	10 mL	

- Adjust with NaOH to pH (~ 7).
- To get pH 7, add ~ 500 µL 1M NaOH
- Top up with ddw until 50 mL
- Filter the preparation with 0.2 µm filter

Material and Chemicals: Agarose

1.5% w/v Agarose in ddw

- Dissolve 0.15 g of agarose (Nusieve GTG Cat no. 50081) in 10 mL ddw
- Microwave till all agarose dissolves

2% w/v Agarose in MOPS buffer

- Dissolve 0.2 g of agarose (Sigma Cat no. A9414) in 10 mL ddw
- Microwave till all agarose dissolves

Both the agaroses have low melting point. However, Nusieve GTG was chosen as the agarose to spread across the coverslip instead of Sigma A9414. This is because, by experience, there were more ‘good’ wells formed (i.e. wells that are not overfilled with hydrating agarose) when Nusieve agarose was used. On the contrary, when a high melting point agarose was used, formation of agarose tends to be inhibited, possibly because of the higher hydrophobicity.

Preparation of coverslips

- Place coverslips (22 mm x 64 mm) in coverslip holder and plasma etch them in O₂ for 3 mins
- Heat up both 1.5% Agarose and 2% Agarose.
- For TIRF application, add ~ 8µL of 1.5% agarose on the etched coverslip
- Place a second coverslip (22mm x 40mm) on top to spread the agarose.
- For darkfield application, add 10 µL of 1.5% agarose (10% NTA modified) on the etched coverslip
- Place the two coverslips on the heating block for 10 seconds or till the agarose is fully spreaded
- Quickly remove the top coverslip in a quick sliding action.
- Allow the bottom coverslip to dry

- Spread 10 μL NiCl_2 over coverslip and let it rest for 1 min.
- Wash the coverslip with DDW

Preparation of the setup

- Place the plastic chip on top of the coverslip.
- Put the electrode in the designated location, if electrode is used.
- Add the 2% hydrating agarose through the inlet until the channels of the bilayer chip are filled with agarose.
- Allow the agarose to solidify, remove excess agarose at the inlet / outlet.
- Dope each well with 1 mg/mL of lipid mix using a glass pipette / syringe.
- To form 1 mL of 1 mg/mL in Pentane, take out 59 μL of lipid from stock and mix with 941 μL of Pentane
- Leave for 2 minutes for the pentane to evaporate.
- Seal the inlet and outlet with tape to prevent the agarose from drying out.
- Cover the wells of the bilayer chip with about 30 μL of 5 mg/mL lipid in hexadecane.
- To form 250 μL of 5 mg /mL concentration in hexadecane, take out 73 μL from the lipid stock, dry and dissolve in 250 μL of hexadecane
- Remove bubbles that may be trapped in the well.
- Leave for at least 30 min.
- It is important to reduce the drying of the agarose to the minimum. This is because any drying will change the salt concentration of the agarose and hence the osmotic pressure between the bottom agarose and the droplet. Evaporation can be prevented by quickly sealing the inlets for the hydrating agarose and filling the wells with hexadecane.

Preparation of gold beads

- 5 μL of Streptavidin modified gold beads (60 nm) was taken from stock. (Remember to mix well by taping lightly, before pipetting)
- Spin down the sample with 10k RPM for 1 min.
- Remove the supernatant and resuspend the pellet with 10 μL HEPES pH 8.
- Spin down the suspension again and repeat the cleaning procedure for two more times. This should be sufficient to remove the unwanted chemicals in the gold suspension.
- Resuspend the gold in 5 μL proteoliposomes prepared.

Preparing the sample

- The protocol for making proteoliposomes has been described in the “Vesicle Activity Test” protocol.
- For Total Internal Reflection Fluorescence Microscopy (TIRFM) mode , sample will consist of
 - ❖ 7 μL MOPs Buffer with 15 mM CaCl_2
 - ❖ 1 μL of 2% BSA
 - ❖ 1 μL proteoliposomes

- ❖ 1 μL 10 nM Streptavidin Alexa 532
- For Darkfield microscopy mode, the sample will consist of (in sequence of addition)
 - ❖ 6.5 μL MOPs Buffer with 1 mM CaCl_2
 - ❖ 1 μL of preincubated proteoliposomes and 60 nm Au functionalised with streptavidin (conc as per A1-9 after wash)
 - ❖ 0.5 μL of 200 mM PEP (Phospho(enol) pyruvate, Sigma)
 - ❖ 0.5 μL of 10 mg/mL Pyruvate Kinase (Roche Diagnostics) 1:5 times dilution from stock.
 - ❖ 0.5 μL 50 mM ATP
 - ❖ 1 μL 50% glycerol
- Mix the sample and pipette about 0.2 μL out for brewing in 5 mg/mL lipids + hexadecane + (dried with 10% v/v – i.e. $\sim 7 \mu\text{L}$ DGS-NTA(Ni) lipids) for 3 min
- Transfer the small droplet to the well and observe under bright field until the bilayer is formed.
- Switch to either darkfield microscopy or TIRFM
- If electrode is used, to improve the insertion of electrode, the tip of the electrode can be doped with a small amount of agarose.

Settings of dark field microscope

- Power \sim low
- Frame rates = 1000 fps

A1-6 Protocol for Modifying Agarose with NTA:

Material and Chemicals: Buffers

PO₄ buffer (Na)

To 10 mL ddw, add:

Final conc	Chemicals	Amount needed	Notes
50 mM	100 mM Na ₂ HPO ₄	3.9 mL	
50 mM	100 mM NaH ₂ PO ₄	6.1 mL	

Method

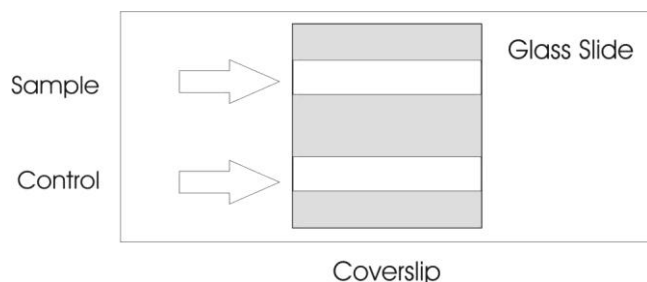
- Dissolve 0.068g of low melting point agarose (A9414 Sigma) in 1.5 mL anhydrous DMSO while stirring continuously to avoid clustering of agarose
- Heat the mixture with constant stirring using a water bath on top of the magnetic stirrer (temp ~ 80°C)
- Once fully dissolved, 0.5 mL of CDI at 60 mg/mL, pre-dissolved in anhydrous DMSO, was added drop-wise with constant stirring. **(Reactive Chemical, Be careful)**
- The solution is allowed to activate for 1hour.
- 0.34g of Cystamine was dissolved in 1 mL of Sodium Carbonate buffer (0.2M) to give a final concentration of 0.5M. The pH >10.
- The prepared Cystamine was mixed with the activated agarose solution dropwise and allow to react for 24hrs with constant mixing. It will eventually gellified.
- Dialyse the agarose gel using 12.4 kDa membrane in 500 mL of DDW for 24hrs with 3 changes of DDW.
- Place the agarose into a 50 mL Falcon Tube.
- Prepare 0.115g of TCEP (MW 286) in 4 mL 0.1M Sodium Phosphate buffer (pH 7) to give a final concentration of 0.1M.
- Mix the prepared TCEP with agarose and stir at high speed. Final volume ~ 10 mL. Leave the mixture to react for 2hrs. At the end, most of the agarose chunks should have broken down into small bits
- Dialyse the mixture in DDW (750 mL) + 1 mL HCl (1M) for 48 hrs with 6 changes in DDW. The slightly acidic condition stabilises the thiol group of the reduced cystamine.
- Take the agarose out from dialysis and spin it down in order to remove the excess water (13k rpm for 5 mins). Yield: ~ 2 mL of hydrated agarose.
- Prepare 500uL of 0.1M TCEP in 0.1M Sodium Phosphate buffer pH7. (TCEP needed ~ 14.3 mg)
- Add Sodium Hydroxide to get to a pH of ~ 7. (about 375uL of buffer to 125uL of 1M NaOH). Test using litmus paper.
- Mix 500uL of agarose with 125uL of the freshly prepared TCEP and incubate for 1 hours + shaking. To get a final concentration of 20 mM TCEP.
- Dissolve 3 mg of Maleimido NTA in 75uL Sodium Phosphate buffer pH 7 to get 40 mg/mL.
- Mix with the agarose. Check pH ~ 7. Incubate for 4hrs + shaking.
- Dialyse the mixture in 12.4 kDa membrane for 48 hours with 6 changes in DDW.

- Dry the agarose in dryer. Weigh the holding eppendorf tube before adding the agarose and after drying.
- Rehydrate the agarose in DDW to give 1.5% w/w. Heat to dissolve the agarose fully. There will some agarose that will not dissolve. This is thought to be due to crosslinking among the free thiol groups
- Dilute the agarose 1:10 times with normal agarose. Store for use.
- To use the agarose, take ~ 10 mg per coverslip and heat it on the heating block. The prevent continuous / repeated reheating of the agarose.

A1-7 Protocol for Testing the Affinity of NTA modified agarose to Histag proteins.

Method

- Plasma clean some 22x22 mm coverslips.
- Coat the surface with 5 uL of melted NTA agarose by sandwiching the agarose between 2 coverslips and quickly sliding them across in a quick sliding action.
- Allow the agarose to dry out.
- Make a double-channel tunnel slide using double sided tape.



- Flow in 10 uL of 10 mM NiCl₂ dissolved in MOPs buffer A³ into the first tunnel and 10 uL of MOPs buffer B⁴ into the second tunnel. Incubate in a humidity chamber for 10 mins
- Wash both tunnels with 20 uL of MOPs buffer A.
- Flow 10 uL of YFP-Histag ~ 0.05 mg/mL into each tunnel and allow to incubate in a humidity chamber for 10 mins
- Wash both tunnels with 20 uL of MOPs buffer A + 20 mM imidazole (pH 7), then with 80 µL MOPs buffer A.
- Seal the ends of the tunnels with nail polish and observe the fluorescence count under epifluorescence mode.

³ MOPs Buffer A – 10mM MOPS pH 7 + 80mM NaCl + 10% Glycerol

⁴ MOPs Buffer B – 10mM MOPS pH 7 + 80mM NaCl + 2mM Mg²⁺ + 10% Glycerol

A1-8 Protocol for Finding the K_d of Ni^{2+} NTA-DNA and Histag GFP

Material and Chemicals: Buffers

Buffer A

Final conc	Chemicals	Amount needed	Notes
0.1%	BSA		
140 mM	NaCl		
20 mM	KCl		
5%	Glycerol		
20 mM	Hepes pH 7.3		

Method

- Experiments to detect intensity changes at 504 nm and 558-564 nm were conducted using a standard Spectrofluorimeter (Photon Technology International).
- The excitation wavelength used was 395 nm and emission intensity was scanned from 470 nm to 650 nm.
- Histag-GFP was first diluted in buffer A to the desired concentration for titration (0.26 μ M and 0.11 μ M for Bis Ni^{2+} :NTA-DNA and Tris Ni^{2+} :NTA-DNA titration).
- The solution was then placed in a quartz cuvette and its emission spectrum scanned. Multiple scans were taken until the signals stabilised.
- This was then followed by addition of Nickel charged Bis Ni^{2+} :NTA-DNA (3.14 μ M) or Tris Ni^{2+} :NTA-DNA (1.22 μ M). The reactants were mixed thoroughly with the pipette tip.
- Two to three minutes intervals were allowed in between each titration point in order to give sufficient time for equilibrium to set in. This duration was chosen as there was no appreciable difference in the intensity from those obtained after waiting for a longer time.
- The intensities measured were normalised with the initial measured intensity at 504 nm and 558-564 nm respectively.
- Controls were done using non-Nickelated DNA samples to detect non specific interaction between GFP and NTA-DNA.
- Another set of controls were also conducted to ascertain the amount of direct excitation of Cy3, by 395 nm excitation.
- This was done by having only buffer A in the cuvette and repeating the titration with Ni^{2+} :NTA-DNA. The contribution of direct excitation of NTA-DNA was found to be insignificant.

A1-9 Protocol for Modifying GNP with Streptavidin

Material and Chemicals: Buffers

Buffer A

Final conc	Chemicals	Amount needed	Notes
10 mM	Hepes pH 8.0		

Buffer B

Final conc	Chemicals	Amount needed	Notes
10 mM	Hepes pH 8.0		
50 mM	KCl		

0.5 mM DSP

- 1 mg DSP (MW 404) dissolved in 247.2 μ L anhydrous DMSO to get 10 mM
- Dilute 20 times with Buffer B to get 0.5mM

10 mM TCEP

- 10 mg TCEP (MW 286.6) dissolved in 350 μ L buffer B to give 100 mM
- Take 30 μ L of 100 mM TCEP and add ~ 170 μ L KOH (500 mM) to pH 8
- Add 100 μ L of buffer B to give a final volume 10 mM

4 mM Cysteamine

- To 10 mg of cysteamine HCl (MW 113.61), add 1 mL buffer B to get 40 mM Cysteamine.
- Adjust pH to 8 with KOH (Note the vol of KOH added)
- Top up to final volume of 2.2 mL to give 40 mM
- To 50 μ L of 40 mM Cysteamine, add 450 μ L buffer B.

100 μ M Streptavidin

- Streptavidin (MW 52.8 kDa) is dissolved in Buffer B + MgCl₂ + Glycerol to give a final concentration of 100 μ M (5.28 mg/mL) and 2 mM MgCl₂ + 10% Glycerol (added as cyroprotectant)
- Save as aliquots of 10 μ L and store in -20°C freezer.

Method

- Premix 5 μ L of DSP with 5 μ L TCEP and 5 μ L Streptavidin and let them stand for 5 mins
- Add 1 mL of 100 nm Gold Nano Particles into the solution.
- Rotate the suspension in room temperature for 2 hours in room temperature
- Store in 4°C for use.

A1-10 Protocol for Counting Streptavidin in Gold NanoParticles

Materials and Chemicals

- Gold bead of size 100 nm, pre-modified with Streptavidin.
- 10 mM HEPES pH 7 (Low salt buffer – Buffer A).
- 20 mM MOPs + 80 mM NaCl + 2 mM MgCl₂ + 1% Glycerol (Buffer B) – Buffer B is design to have moderate amount of salt and is used as a general buffer in all F₁F₀ rotation / activity experiments.
- Buffer B + 0.1 mg/mL BSA – Buffer B*. BSA used should be of fluorescent grade. (i.e. suitable for fluorescent experiments)
- 100 nM Biotin Atto 565 predissolved in Buffer B*.
- 20 μM free Biotin dissolved in buffer B*.

Setup:

- Tunnel Slide made with plasma cleaned coverslips.

Procedure:

- Re-suspend the gold beads stock thoroughly and pipette 10 μL into a fresh Eppendorf tube.
- Spin down the gold beads once at 10k RPM for 1 min.
- Remove as much supernatant was possible.
- Re-suspend the gold in 20 μL buffer A.
- Spin down the gold beads once at 10k RPM for 1 min.
- Repeat 4 and 5 for two more times. Resuspend the gold in buffer A, to a final volume of 4 μL.
- Pipette 2 μL of gold bead into a fresh eppendorf tube.
- Add 2 μL of 100 nM biotin Atto 565 and 2 μL of buffer B*. For control, add 2 μL of 20 μM free biotin, incubate for 5 minutes, then add 2 μL of 100 nM biotin Atto 565.
- Incubate for 2-8 hours. Wrap the eppendorf with aluminium foil to prevent exposure to light.
- After incubation, add 16 μL of buffer A and mix thoroughly.
- Spin down the gold bead at 10k RPM for 1 min.
- Repeat step 10 and 11 for two more times, using 20 μL of buffer A instead.
- Re-suspend the gold beads in 20 μL of buffer B. Flow 10 μL into tunnel slide.

Setting of Epifluorescence

- Observe the gold bead in bright field. They should be easy to detect with most sticking to the plasma etched coverslip after a few minutes.
- Differentiate single gold beads from double. Centre a single to the centre of the field of view.
- Switch to epifluorescence mode.
- Excitation intensity is pre adjusted to 3.2 mW. If the intensity is too high such that saturation occurs, then intensity may be lowered.

- An exposure of 0.1 s is used with images taken at 1 second interval.
- Once the image is taken, move to another gold bead that's at least 50um away and repeat the process.

It is relatively easy to separate gold nano particles from the buffer as they are much denser and would sediment quickly. Equation 1 gives the theoretical sedimentation velocity (v) at 10k Rpm.

$$v = \frac{2}{9\eta}(\rho_{gold} - \rho_{water})r^2a$$

Where ρ_{gold} ($\sim 19\text{g/mL}$) and ρ_{water} are the density of gold and water respectively. r is the radius of the GNP, a is the net centrifugal acceleration due to the rotation and η is the viscosity of water.

A1-10 Protocol for F1Fo rotation on NTA agarose stabilised with lipids

Material and Chemicals: Buffers

Buffer A

Final conc	Chemicals	Amount needed	Notes
--	MOPs buffer (No MgCl ₂ , No Glycerol)	479 μ L	
0.5 mg/ml	Lipids (16 mg/ml)	16 μ L	
0.1 mg/ml	BSA (10 mg/ml)	5 μ L	

Buffer B

Final conc	Chemicals	Amount needed	Notes
--	MOPs buffer (2 mM MgCl ₂ , No Glycerol)	479 μ L	
0.5 mg/ml	Lipids (16 mg/ml)	16 μ L	
0.1 mg/ml	BSA (10 mg/ml)	5 μ L	

Buffer B*

Final conc	Chemicals	Amount needed	Notes
--	Buffer B	98 μ L	
20 mM	Imidazole 1M pH ~ 7	2 μ L	

Regeneration Solution

Final conc	Chemicals	Amount needed	Notes
	Buffer B	34.6 μ L	
0.1 mg/mL	Pyruvate Kinase 10 mg/ml	0.4 μ L	
5 mM	PEP 200 mM	1 μ L	
5 mM	ATP 50 mM	4 μ L	

Setup:

- Tunnel Slide made with plasma cleaned coverslips.

Procedure:

- Flow in 10 μ L of NiCl₂ and incubate for 5 to 10 min.
- Wash with 50 μ L buffer A.
- Flow in 10 μ L F1Fo ATPase, diluted 2x. If DCCD (MW: 206.33) is to be used, incubate the protein with 0.1 mM DCCD final concentration. DCCD is first dissolve in ethanol to ~ 10 mM, then diluted 100x with buffer B.
- Incubate the protein in humidity chamber for 10 min
- Wash the channel with 50 μ L of buffer B*.

- Flow in 10 μL of 60 nm gold beads. The gold has been washed 3x with HEPES and resuspend in buffer B.
- Incubate for 10 min.
- Wash out excess gold with 50 μL buffer B.
- Flow in 20 μL of regeneration solution.
- Seal the tunnel with nail polish and observe on dark field.

Microscope setting

- Power ~ low
- Frame rates = 1000 fps.
- Resolution = 256 x 256
- Exposure = 1/1000

1. Heron, A.J., et al., *Direct detection of membrane channels from gels using water-in-oil droplet bilayers*. J Am Chem Soc, 2007. **129**(51): p. 16042-7.
2. Foster, D.L. and R.H. Fillingame, *Energy-transducing H⁺-ATPase of Escherichia coli. Purification, reconstitution, and subunit composition*. J Biol Chem, 1979. **254**(17): p. 8230-6.
3. Sambrook, J. and D. Russell, *Molecular Cloning: A Laboratory Manual*. 3rd ed. Vol. 3. 2001: CSHLP.
4. Pitard, B., et al., *ATP synthesis by the F₀F₁ ATP synthase from thermophilic Bacillus PS3 reconstituted into liposomes with bacteriorhodopsin. 1. Factors defining the optimal reconstitution of ATP synthases with bacteriorhodopsin*. Eur J Biochem, 1996. **235**(3): p. 769-78.
5. Huang, C. and J.T. Mason, *Geometric packing constraints in egg phosphatidylcholine vesicles*. Proc Natl Acad Sci U S A, 1978. **75**(1): p. 308-10.

Appendix 2 – Derivations and Calculations

Scaling of the numerator and denominator of the Autocorrelation Function in FCS

By definition

$$g(\tau) = \frac{\langle F(t) \cdot F(\tau + t) \rangle}{\langle F(t) \rangle^2}$$

At $\tau = 0$ (complete correlation),

$$g(0) = \frac{\langle F(t) \cdot F(t) \rangle}{\langle F(t) \rangle^2} = \frac{\langle F(t)^2 \rangle}{\langle F(t) \rangle^2}$$

We know that $Var(F) = \langle F(t)^2 \rangle - \langle F(t) \rangle^2$. Dividing throughout by $\langle F \rangle^2$

$$\therefore \frac{Var(F)}{\langle F \rangle^2} = \frac{\langle F(t)^2 \rangle}{\langle F(t) \rangle^2} - 1$$

If N is the number of fluorophore in the detection volume and b is the brightness per fluorophore, then

$$Var(F) = Var(Nb) = b^2 Var(N), \text{ and } \langle F \rangle^2 = \langle bN \rangle^2 = b^2 \langle N \rangle^2$$

Since the number of fluorophore inside the detection follows a Poisson distribution,

$$\therefore Var(N) = \bar{N}, \text{ and } \langle N \rangle = \bar{N}$$

Hence

$$\frac{Var(F)}{\langle F \rangle^2} = \frac{\bar{N}b^2}{\bar{N}^2b^2} = \frac{1}{\bar{N}} = \frac{\langle F(t)^2 \rangle}{\langle F(t) \rangle^2} - 1$$

$$\therefore g(0) = \frac{1}{\bar{N}} + 1$$

Simple Linear Regression Derivation

For normal regression, the dependent variable Y is a linear function of the independent variable X :

$$\mathbf{y} = \boldsymbol{\beta}\mathbf{X}$$

Where

$$\mathbf{y} = (Y_1, Y_2, \dots, Y_n)$$

$$\mathbf{X} = \begin{pmatrix} X_{11} & \cdots & X_{1n} \\ \vdots & \ddots & \vdots \\ X_{n1} & \cdots & X_{nn} \end{pmatrix}$$

$$\boldsymbol{\beta} = (\beta_1, \beta_2, \dots, \beta_n)$$

However in actual case, $\mathbf{y} - \boldsymbol{\beta}\mathbf{X} = \boldsymbol{\varepsilon}$, where $\boldsymbol{\varepsilon}$ is the residue.

Expressing the square of total residue in Tensor notation:

$$\varepsilon^2 = (Y_i - X_{ij}\beta_j)(Y_k - X_{kj}\beta_j)\delta_{ik}$$

Where δ is the Kronecker delta

Minimising error

$$\frac{d\varepsilon^2}{d\beta} = -(Y_i - X_{ij}\beta_j)\frac{d}{d\beta_m}(X_{kj}\beta_j)\delta_{ik} - (Y_k - X_{kj}\beta_j)\frac{d}{d\beta_m}(X_{ij}\beta_j)\delta_{ik} = 0$$

$$= -[(Y_i - X_{ij}\beta_j)X_{kj}\frac{d}{d\beta_m}(\beta_j) + (Y_k - X_{kj}\beta_j)X_{ij}\frac{d}{d\beta_m}(\beta_j)]\delta_{ik}$$

$$= -[(Y_i - X_{ij}\beta_j)X_{km} + (Y_k - X_{kj}\beta_j)X_{im}]\delta_{ik}$$

Using the property of the Kronecker Delta $X_{km}\delta_{ik} = X_{im}$

$$= -2[(Y_i - X_{ij}\beta_j)X_{im}] = 0$$

Hence

$$X'_{mi}Y_i = X'_{mi}X_{ij}\beta_j$$

Where X' denotes the transpose of X

Finally reverting back to matrix notation

$$\mathbf{X}^T \mathbf{y} = \mathbf{X}^T \mathbf{X} \boldsymbol{\beta}$$

$$\boldsymbol{\beta} = (\mathbf{X}^T \mathbf{X})^{-1} \mathbf{X}^T \mathbf{y}$$

If a weighting function is used, w_{ik} replaces δ_{ik} . w_{ik} shares the property of the kronecker delta – i.e. it is zero elsewhere except for the leading diagonal. The diagonal however has different weighted values instead of ones.

Therefore

$$\frac{d\varepsilon^2}{d\beta} = -[(Y_i - X_{ij}\beta_j)X_{km} + (Y_k - X_{kj}\beta_j)X_{im}]w_{ik} = 0$$

Noting that w_{ik} is a diagonal matrix, then 1st term = 2nd term

$$(Y_k - X_{kj}\beta_j)X_{im}w_{ik} = 0$$

$$Y_k X_{im} w_{ik} = X_{kj} \beta_j X_{im} w_{ik}$$

Expressing in matrix notation

$$\mathbf{X}^T \mathbf{W} \mathbf{y} = \mathbf{X}^T \mathbf{W} \mathbf{X} \boldsymbol{\beta}$$

$$(\mathbf{X}^T \mathbf{W} \mathbf{X})^{-1} \mathbf{X}^T \mathbf{W} \mathbf{y} = \boldsymbol{\beta}$$

$\boldsymbol{\beta}$ can be solved using a simple MatLab code to obtain the gradient and y intercept.

Calculating the dissociation constant (Kd) between Ni²⁺:NTA-DNA and Histag YFP

It is assumed that the background corrected intensity at different titration points (I_i^{504}), can be expressed by the equation below

$$I_i^{504} = I_0^{504} * D_f - I_{complex} - I_{bleaching} - I_{free, Ni} - I_{non} \quad - \quad (A2-1)$$

Where I_0^{504} is the initial background-corrected intensity before titration, D_f is the dilution factor, $I_{complex}$ is the intensity reduction due to the formation of complexes, $I_{bleaching}$ is the intensity due to photo-bleaching of GFP, $I_{free, Ni}$ is the intensity drop due to quenching of unchelated Ni²⁺ in the solution and I_{non} is the intensity drop due to non specific binding.

It is however found that $I_{bleaching}$, $I_{free, Ni}$ and I_{non} do not contribute significantly to the reduction in intensity. Further assuming that the intensity due to the complexes is proportional to the concentration of complex formed:

$$k_c * I_{complex} = [complex] \quad - \quad (A2-2)$$

Where k_c is the proportionality constant relating the concentration of the complexes formed, to the intensity reduction due to the formation of the complexes.

Therefore, equation (A2-1) can be expressed simply as

$$(I_0^{504} * D_f - I_i^{504}) = [complex]_{504} / k_{c,(504)} \quad - \quad (A2-3)$$

Similarly, the average intensity increase at 558-564nm due to the formation of complexes ($I_{i,complex}^{558-564}$) is calculated as the increase in intensity after accounting for leakage of GFP emission at 558-564nm and direct excitation of Cy3 by 395nm excitation. Other factors like photo-bleaching and Cy3 interaction with Nickel and DNA are found to be negligible. Thus

$$I_{i,complex}^{558-564} = I_i^{558-564} - I_{leakage}^{558-564} - I_{direct}^{558-564} - I_{background}^{564} \quad - \quad (A2-4)$$

Where $I_{i,complex}^{558-564}$ is the average intensity increase due to the formation of complexes, $I_i^{558-564}$ is the measured intensity at i th titration point, $I_{leakage}^{558-564}$ is the average intensity at 558-564nm due to leakage of GFP emission into 558-564nm, $I_{direct}^{558-564}$ is the intensity due to direct excitation of Cy3 by 395nm excitation, and $I_{background}^{558-564}$ is the background intensity.

$I_{leakage}^{558-564}$ can be found by measuring the emission spectrum of GFP and taking the ratio (r) between the average emission at 558-564nm and the emission at 504nm. $I_{leakage}^{558-564}$ thus equals to $I_i^{504} * r$. $I_{direct}^{558-564}$ and $I_{background}^{564}$ can also be measured directly.

Further assuming that the intensity $I_{i,complex}^{558-564}$ is proportional to the amount of complex formed, we obtain:

$$(I_i^{558-564} - I_{leakage}^{558-564} - I_{direct}^{558-564} - I_{background}^{564}) = [complex]_{558-564} / k_{c,(558-564)} \quad - \quad (A2-5)$$

Curve fitting of experimental results to find the dissociation constants

The reaction scheme between $trisNi^{2+}$:NTA-DNA and GFP can be written as follows



For this equation, one can easily write the relation describing the dissociation constants Kd

$$\frac{([NTA] - U)([GFP] - U)}{U} = Kd \quad - \quad (A2-7)$$

Where $[NTA]$ is the total concentration of $tris Ni^{2+}$:NTA-DNA added, $[GFP]$ is the concentration of GFP added and U is the equilibrium concentration of $tris Ni^{2+}$:NTA-DNA-GFP

Solving equation (A2-7) for U allows us to express get an expression in terms of Kd , $[NTA]$ and $[GFP]$, i.e. $U = f(Kd, [NTA], [GFP])$.

Substituting U into equation (A2-3) and (A2-5), we get

$$\frac{f(Kd_1, NTA, GFP)}{k_{c,(NTA-DNA-GFP),(504)}} = I_0^{504} * D_f - I_i^{504} \quad - \quad (A2-8)$$

$$\frac{f(Kd_1, NTA, GFP)}{k_{c,(NTA-DNA-GFP),(558-564)}} = I_i^{558-564} - I_{leakage}^{558-564} - I_{direct}^{558-564} - I_{background}^{564} \quad - \quad (A2-9)$$

A two parameters curve fit was done to determine the best values for Kd and $k_{c,504}$ or Kd and $k_{c,558-564}$ in equation (A2-8) and (A2-9) respectively. The least square error was used to optimise the fitting. The average value of Kd could thus be computed.